# Investigating the fate of conjugated metabolites of the xenobiotic pollutant 2,4,6-trinitrotoluene within *Arabidopsis thaliana*

**Rhys Woodfin**

**Doctor of Philosophy**

**Biology**

**University of York**

**October 2023**

# Abstract

The explosive 2,4,6-trinitrotoluene (TNT) is a global pollutant, with its toxicity threatening both environmental and public health. The chemical properties of TNT enable its persistence, with natural degradative mechanisms being insufficient to address contamination. Phytoremediation is well-suited for addressing TNT-soil pollution, though it requires a thorough understanding of plant TNT-metabolism. Detoxification of TNT *in planta* is predicted to follow three steps: transformation, conjugation, and compartmentalisation. Currently, the TNT-detoxification pathways within *Arabidopsis thaliana* (Arabidopsis), reduction-initiated glucosylation and glutathionylation, are characterised up to conjugation. Glutathionylation of TNT generates 2-glutathionyl-4,6-dinitrotoluene (Conjugate 3), a metabolite offering potential for TNT-mineralization, due to the loss of a nitro-group. To understand the bioavailability of Conjugate 3, its fate *in planta* must be elucidated.

To confirm TNT-metabolite compartmentalisation, spatial metabolomic techniques were optimised for Arabidopsis root tissue. The successful optimisation of a benchtop non-aqueous fractionation (BNAF) technique confirmed the vacuolar association of the TNT metabolite hydroxaminodinitrotoluene-glucoside.

Following this, Conjugate 3 metabolic fate was characterised. The expression of a *Drosophila melanogaster* glutathione transferase released the bottleneck of TNT-glutathionylation, saturating Conjugate 3 metabolic pathways, thus allowing accumulation of downstream metabolites. Metabolite identification by mass spectrometry revealed malonylation to be a common fate for Conjugate 3 derivatives. Additionally, a dominant role for $\gamma$-glutamyl transpeptidases in initiating Conjugate 3 metabolism, and the vacuolar association of Conjugate 3 derivatives was confirmed.

Finally, to further characterise TNT and Conjugate 3 metabolism *in planta*, proteomic analysis of fractionated- and whole-root tissue was performed. Analysis of fractionated samples provided a spatial understanding of the root proteome. Whole-root tissue analysis identified biological processes and putative protein candidates involved in the response to TNT and Conjugate 3.

This research generates a testable model for TNT-metabolism within Arabidopsis which, alongside the demonstrated platform derived from BNAF and transgenic approaches, can further support characterisation of TNT detoxification *in planta*.

# List of Content

# List of Figures

# List of Tables

# Abbreviations

| | |
|---|---|
| **ADNT** | Aminodinitrotoluene |
| **AAAP** | Amino acid/auxin permease |
| **ABC** | ATP-binding cassette transporter |
| **ANOVA** | Analysis of variance |
| **APase** | Purple acid phosphatase |
| **APC** | Amino acid-polyamine-organocation transporter |
| **APPase** | Alkaline pyrophosphatase |
| **Arabidopsis** | *Arabidopsis thaliana* |
| **Basta** | Glufosinate-ammonium |
| **BCA** | Bicinchoninic acid |
| **BEH** | Ethylene bridged hybrid |
| **BNAF** | Benchtop non-aqueous fractionation |
| **BSO** | Buthionine sulfoximine |
| **CAT** | Cationic amino acid transporter |
| **CDNB** | 2-chloro-4,6-dinitrobenzene |
| **CND** | Cluster normalised distance |
| **CL-20** | Hexanitrohexaazaisowurtzitane |
| **Conjugate 3** | 2-glutathionyl-4,6-dinitrotoluene |
| **DDT** | Dichlorodiphenyltrichloroethane |
| ***Dm*GST** | *Drosophila melanogaster* glutathione transferase epsilon member 6 |

| | |
|---|---|
| ***Dm*GST.C** | *Dm*GST expressed within Col0 ecotype genetic background |
| ***Dm*GST-*ggt1ggt4*** | *Dm*GST expressed within *gg1ggt4* genetic background |
| ***Dm*GST.L** | *Dm*GST expressed within Ler ecotype genetic background |
| **DHAR** | Dehydroascorbate reductase |
| **$dH_2O$** | Distilled water |
| **DIA** | Data independent acquisition |
| **DMSO** | Dimethylsulfoxide |
| **DNAN** | 2,4-Dinitroaniline |
| **DNT** | 2,4-Dinitrotoluene/2,6-Dinitrotoluene |
| **DTT** | Dithiothreitol |
| **γ-ECS** | $\gamma$-glutamylcysteine synthase |
| **EGDN** | Ethylene glycol dinitrate |
| **FDR** | False discovery rate |
| **FOX7** | 1,1-diamino-2,2-dinitroethylene |
| **GST** | Glutathione transferase |
| **GGCT** | $\gamma$-glutamylcyclotransferase |
| **GGP** | $\gamma$-glutamylpeptidase |
| **GGT** | $\gamma$-glutamyltranspeptidase |
| **GPOX** | Glutathione peroxidase |
| **GO** | Gene ontology |
| **HADNT** | Hydroxyaminodinitrotoluene |
| **HADNT-Glc** | Hydroxyaminodinitrotoluene-glucoside |
| **HMX** | 1,3,5,7-tetranitro-1,3,5,7-tetrazocane |

| | |
|---|---|
| **HPLC** | High performance liquid chromatography |
| **IMS** | Imaging mass spectrometry |
| **LB** | Lysogeny broth |
| **LSC-MS** | Live single-cell mass spectrometry |
| **LC-MS/MS** | Liquid chromatography tandem mass spectrometry |
| **LMPA** | Low-melting point agarose |
| **LOPIT** | Localization of organelle proteins by isotope tagging |
| **KEGG** | Kyoto encyclopedia of genes and genomes |
| **KNIME** | Konstanz Information Mine |
| **MALDI-IMS** | Matrix-assisted laser desorption ionisation imaging mass spectrometry |
| **MAPEG** | Membrane associated proteins in eicosanoid and glutathione metabolism |
| **MATE** | Multidrug And toxic compound extrusion transporter |
| **MCL** | Markov clustering algorithm |
| **MDAR** | Monodehydroascorbate reductase |
| **MGL** | Methionine gamma lyase |
| **MS** | Mass spectrometry |
| **NAF** | Non-aqueous fractionation |
| **Nano-ESI** | Nanoelectrospray ionisation |
| **NanoSIMS** | Nano-secondary ion mass spectrometry |
| **NED** | N-(1-naphthyl)ethylenediamine |
| **NG** | Nitroglycerol |
| **NMI** | Normalized mutual information |

| | |
|---|---|
| **PCA** | Principle component analysis |
| **PCS** | Phytochelatin synthase |
| **PCR** | Polymerase chain reaction |
| **PETN** | Pentaerythritol tetranitrate |
| **PPM** | Parts per million |
| **OPR** | Oxyphytodienoate reductase |
| **OYE** | Old yellow enzyme |
| **RT** | Room temperature |
| **RDX** | 1,3,5-Trinitroperhydro-1,3,5-triazine |
| **RT-PCR** | Reverse transcription polymerase chain reaction |
| **SAGE** | Serial analysis of gene expression |
| **SD** | Standard deviation |
| **S-DNT** | 2-thiol-4,6-dinitrotoluene |
| **S-DNT-CG** | 2-cysteinylglycine-4,6-dinitrotoluene |
| **S-DNT-Cys** | 2-cysteine-4,6-dinitrotoluene |
| **S-DNT-$\gamma$EC** | 2-glutamylcysteine-4,6-dinitrotoluene |
| **S-DNT-Glc** | 2-thioglucose-4,6-dinitrotoluene |
| **S-DNT-(Mal)Cys** | 2-(N-malonyl)cysteine-4,6-dinitrotoluene |
| **S-DNT-(Mal)Glc** | 2-(O-malonyl)thioglucose-4,6-dinitrotoluene |
| **SRSM** | Stimulated Raman Scattering Microscopy |
| **STRING** | Search tool for the retrieval of interacting genes/proteins |
| **SUBA** | Subcellular localisation database for Arabidopsis proteins |
| **SVM** | Support vector machines |

| | |
|---|---|
| **TAT** | 2,4,6-triaminotoluene |
| **TCHQD** | Tetrachlorohydroquinone dehalogenases |
| **TEAB** | Tetraethylammonium bromide |
| **TNT** | 2,4,6-trinitrotoluene |
| **TNP** | 2,4,6-trinitrophenol |
| **T-test** | Student's t-statistic |
| **Tukey HSD** | Tukey's honest significance difference |
| **UGT** | UDP-glucosyltransferases |
| **UGPase** | UTP-glucose-1-phosphate uridylyltransferase |
| **uNASC** | Eurasian Arabidopsis Stock Centre |
| **UOX** | Unexploded ordinance |
| **UPW** | Ultrapure water |
| **WT** | Wild-type |
| **XTH** | Xyloglucan endotransglucosylase/hydrolase |
| **ZIFL** | Zinc induced facilitator-like protein |
| **2,4-D** | 2,4-dichlorophenoxyacetic |
| **½MS** | Half-strength Murashige-Skoog basal medium |
| $\boldsymbol{\rho}$ | Density (g $cm^{-3}$) |

# Acknowledgements

There are a number of people and organisations to whom I am indebted for completion of this PhD. Firstly, a massive thank you to Professor Neil C. Bruce, for offering me this opportunity and providing excellent and thoughtful supervision throughout. His faith in my ability to perform the research, even during the dark days of BNAF optimisation, was a great source of reassurance! I would also like to acknowledge the UKRI and the University of York White Rose DTP for funding this research and providing the various training events that have enhanced my professional and research skills.

Heartfelt thanks to Dr. Elizabeth L. Rylott, for providing her time, insight, and knowledge on all aspects of PhD life! Her dedication to aiding her colleagues has been an inspiration. Though involved in an inhuman amount of work, her door was always open, our chats never rushed, and the advice clear and thoughtful. For this I am extremely grateful.

A thank you to Professor Katherine J. Denby, for her valued supervision and input, and to whose keen analysis of chromatograms I owe for the comment that led to the identification of numerous metabolites. Also thank you to Professor Luke C.M. Mackinder, for his participation and valuable input in the thesis advisory panel. A very special thank you to Professor Lisa Fürtauer, for her generous offerings of advice and time in respect to all things relating to non-aqueous fractionation. A substantial portion of this research results from her willingness to provide this help. I aim to model her enthusiastic attitude towards collaboration in all future endeavors.

I would also like to thank all the members of M2 CNAP for generating such a positive and friendly environment! I will have fond memories of the lab socials, and special thanks to those of you who offered thoughtful solutions regarding my research, and the sympathetic nod during my BNAF rants! Big thanks to Dave for all his help in everything relating to lab-consumables, saved my bacon many-a-time!

To all my family, both immediate and extended, thank you for your support and belief in me during this endeavor! I would like to thank my parents for their unwavering enthusiasm for my research, and my brothers for keeping my ego in check by referring to me as a ‘glorified gardener’!

Finally, I would like to thank my partner and best friend Sioned Thomas to whom I am forever grateful for her love and support over the past four years. Her patience and compassion were invaluable during the difficult times of this research, and her belief in my capabilities greatly treasured.

# Authors Declaration

I declare that this thesis is a presentation of original work and I am the sole author. This work has not previously been presented for a degree or other qualification at this University or elsewhere. All sources are acknowledged as references.

**Signature:** 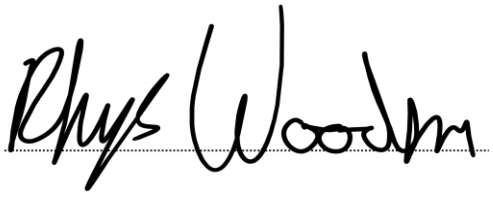

# Chapter 1: Introduction

## 1.1 Explosives

### 1.1.1 Explosive classifications

Energetic compounds were first documented in 9th Century China with the discovery of gunpowder [1]. Since then, the area of explosives chemistry has grown significantly, with the identification and development of more sophisticated compounds and mixtures to address different requirements. Energetic compounds can be categorised as low or high explosives. Low explosives undergo deflagration, generating explosive velocities below 100 m $s^{-1}$, and gas overpressures below 0.5 bar [1]. In comparison, high explosives undergo detonation which involves velocities of up to 6000 m $s^{-1}$, and gas overpressures up to 20 bars [1,2]. High explosives can be further categorised into either primary or secondary based on their sensitivity and performance. Primary explosives are characterised by high initiation sensitivity from stimuli such as impact, friction, heat, and electrostatic discharge [3]. Examples of primary explosives include lead azide, pentaerythritol tetranitrate (PETN) and diazodinitrophenol. Despite their high volatility, the energy released by primary explosives is low in comparison to secondary explosives. However, as secondary explosives have greater stability a preliminary detonation of a primary explosive is often required as a trigger. Examples of secondary explosives are 2,4,6-trinitrotoluene (TNT), 1,3,5-trinitroperhydro-1,3,5-triazine (RDX) and 2,4-dinitroaniline (DNAN). High explosives are used in a variety of sectors including but not limited to mining, demolition, and military activities [2], to prevent accidental detonation during transport and storage, explosives must be powerful whilst insensitive to weak/medium intensity stimuli. Military activities often use high explosive mixtures comprising nitro-organic compounds containing one or more nitro-groups (-$NO_2$). The reasons for this are two-fold. Firstly, the conversion of the nitrogen from its high-energy level, within the nitro-group, to its low-energy level, within inert nitrogen gas, is highly energetically favourable and thus releases a large amount of energy in the form of heat. Secondly, the high oxygen content of the nitro-group fuels the oxidation of the hydrocarbon backbone during combustion, thus allowing oxidation to occur in the absence of an external oxygen source. Nitro-organic explosives can be subdivided into four classes based on the atom to which the nitro-group is chemically bonded [2] (Figure 1.1.1.1). Within nitrate esters, this bond is to an oxygen atom, in nitramines it occurs on a nitrogen, and with nitroaliphatics and nitroaromatics it is to an aliphatic and aromatic carbon respectively.

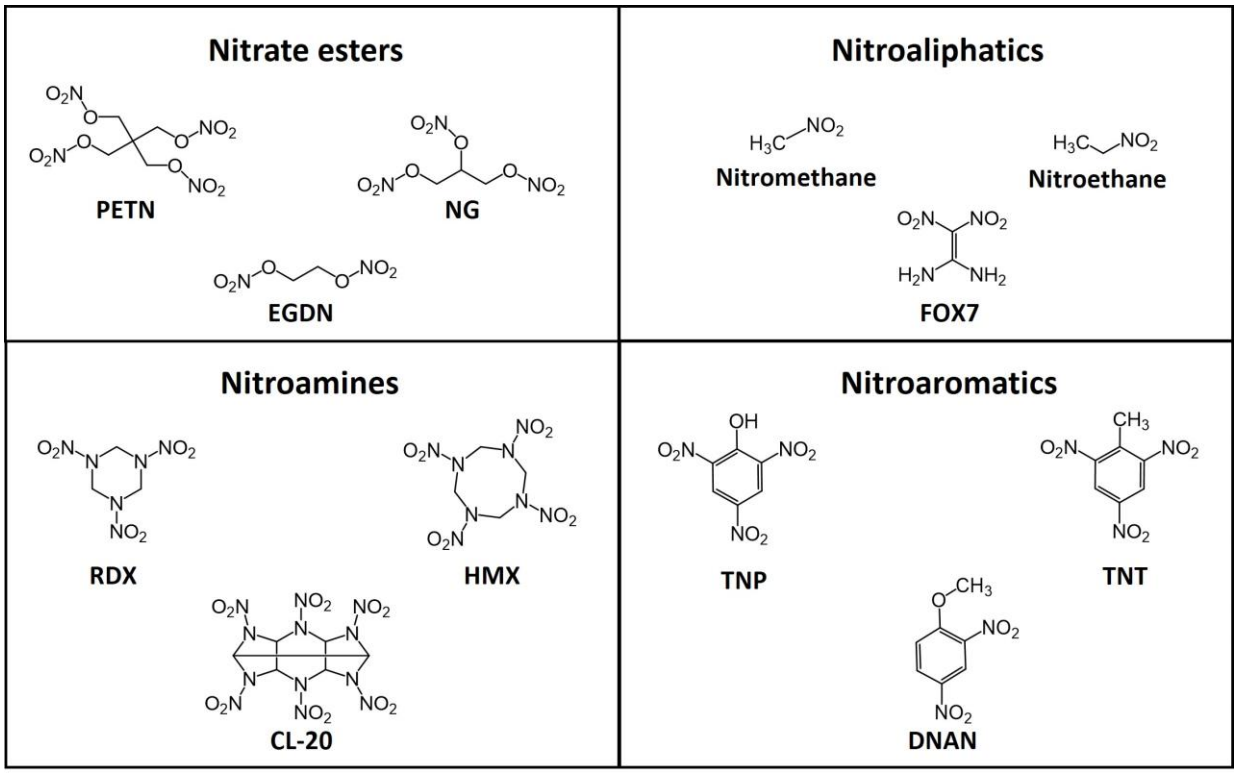


**Figure 1.1.1.1: Classes of nitro-organic compounds used in military activities.** Nitrate esters classified by the nitro-group bonded to an oxygen, examples include PETN, nitroglycerol (NG) and ethylene glycol dinitrate (EGDN). Nitroamines classified by nitro-group bonded to a nitrogen, examples include RDX, 1,3,5,7-tetranitro-1,3,5,7-tetrazocane (HMX) and hexanitrohexaazaisowurtzitane (CL-20). Nitroaliphatics are classified by nitro-group bonded to a carbon within an aliphatic structure, examples include nitromethane, nitroethane and 1,1-diamino-2,2-dinitroethylene (FOX7). Nitroaromatics are classified by the nitro-group bonded to a carbon within an aromatic structure, examples include 2,4,6-trinitrophenol (TNP), TNT, and DNAN.

### 1.1.2 Military nitroaromatics and TNT

The first nitroaromatic compound to be used for military purposes was 2,4,6-trinitrophenol (TNP), also referred to as picric acid, which was identified as a powerful explosive in 1873 [4]. However, due to the high corrosiveness of picric acid and its ability to form shock-sensitive salts with metals, it was replaced by TNT. First synthesised in 1863 through nitration of toulene, the explosive properties of TNT were identified in 1891 by German chemist Carl Haeussermann [5]. The relative insensitivity of TNT, compared to TNP, allowed artillery shells to pierce targets before detonation, therefore causing greater damage than comparative shells containing TNP, which detonated upon impact. This insensitivity of TNT also provided other benefits relating to its function within munitions. An important one is the melting point of TNT, 80 °C, which is far below its detonation temperature, 300 °C, thus allowing the compound

to be used as a melt-casting explosive that can be poured into artillery shells relatively safely. The ability to melt TNT, in addition to its relative stability, enables the use of the compound as an energetic binder, improving the integrity of composite explosive mixtures; an important trait for munitions handling, transportation and storage. These attributes, alongside the low manufacturing costs of TNT, have made it a staple part of military munitions from its first incorporation by the German army in 1902 through and into the 21st century. The use of TNT was expectedly high during World War II with over 150,000 tons generated per month [6]. This production resulted in extensive pollution at manufacturing and distribution sites [6]. Current explosive mixtures are replacing TNT with the nitroaromatic DNAN, as DNAN provides even greater shock stability providing in-field and transport benefits [7]. However, TNT is still a common ingredient within military munitions, with one assessment of the military market for TNT in 2017 being $714.79 million (U.S.), with further growth predicted in the coming decade [8].

## 1.2 The problems associated with TNT

### 1.2.1 TNT-toxicity

Whilst originally thought to be non-toxic, the high use of TNT during World War I revealed the falsehood of this assumption, with 17,000 cases of TNT poisoning resulting in 475 deaths in the US alone [9]. This exposure mainly occurred at manufacturing sites, either through inhalation of contaminated air and/or dermal exposure. Symptoms of TNT poisoning include dermatitis, cyanosis, aplastic anemia, and liver degeneration [10]. A case-controlled study of workers exposed to TNT in China, revealed the negative effects of the explosive on the reproductive system. Of the 104 workers, 50 exhibited significantly lower semen volumes, a reduction in motile spermatozoa, and a higher incidence of sperm malformation [11]. The United States Environmental Protection Agency has designated TNT as a Class C possible human carcinogen, with this classification supported by the development of urinary-bladder carcinoma within female rats following chronically high exposure to TNT, and by the presence of mutagenic compounds within the urine of TNT-exposed workers [12]. The harmful effects of TNT are not just limited to mammals, with exposure resulting in growth inhibition and toxicity in organisms from across the kingdoms of life [10]. In soil studies, TNT has been shown to reduce the biomass of a variety of plant species [13,14], and reduce earthworm populations [15] as well as decreasing the diversity and abundance of soil bacteria [16]. Chronic effects of TNT on aquatic life have also been observed with concentrations between 0.014 - 0.04 mg $L^{-1}$ impacting development and reproductive traits within fathead minnows [17,18] and high toxicity seen in algae and microcrustaceans [19]. The negative effects

of TNT on both human and environmental health have resulted in stricter controls in production and waste-management to reduce flux of this compound into ecosystems.

## 1.2.2 TNT within the environment

### 1.2.2.1 Environmental pollution and persistence

Due to its substantial use in military activities during the 20$^{th}$ and 21$^{st}$ centuries, TNT has become a significant global environmental pollutant. Entry of TNT into the environment can occur at the production, usage, and disposal stages of the munition's life cycle. During the production process of military-grade TNT, non-symmetric isomers that impact the solidification point are removed by treatment with aqueous sodium/ammonium sulphite [20]. The wastewater from this process, referred to as redwater, contains all the non-symmetric isomers of TNT. Whilst there are now tighter controls on the management of this waste, historical disposal practices commonly included release into unlined pits referred to as evaporation lagoons [21] (Figure 1.2.2.1.1A). This practice has resulted in high concentrations of nitroaromatics contaminating the surrounding soil such that the upper sediment of some lagoons now contains up to 40% explosive by weight [21,22]. The pollution of soil by TNT during munitions testing results from low order detonation, a term used to describe what happens when explosives are not entirely depleted during detonation, with the explosive released into the surrounding environment. Low-order detonations are also the entry point of TNT during disposal of excess, unserviceable and obsolete military munitions, as common practice for disposal is to perform open-air burning or open-air detonation [23]. Erosion of metal casings of unexploded ordinance (UOX) can also be an environmental entry point for TNT (Figure 1.2.2.1.1B). As military training sites are where munitions testing and disposal regularly occur, these areas are non-warzone sites where very high concentrations of TNT can be found within the soil [24]. There is currently an estimated 10 million hectares of such land within the US alone that has an associated cleanup cost estimate between $16-160 billion (U.S., estimates from 2004 and are not adjusted for inflation) [25] (Figure 1.2.2.1.1C).

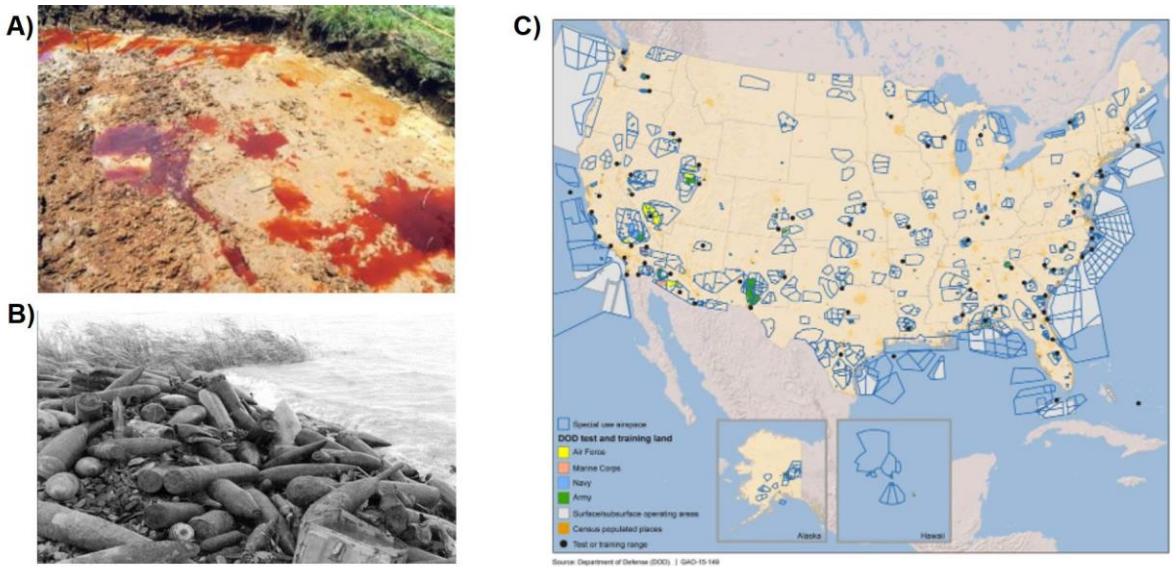


**Figure 1.2.2.1.1: Examples of TNT-pollution sources. A)** Redwater, a by-product of TNT production, contaminates land at manufacturing sites. Image taken from a report from Strategic Environmental Research and Development Program and Environmental Security Technology Certification Program on tackling red-water waste in TNT manufacturing [26]. **B)** UOX revealed at military training range by erosion. Image taken from a report by the United States General Accounting office [25]. **C)** Map of US Department of Defense owned-land, black dots present test or training ranges, and thus potential sites of explosive contamination. Image taken from report by the United States Government Accountability Office [27].

The persistence and accumulation of TNT in the environment results from the symmetrical layout of the three nitro-groups within its structure. The highly electronegative nature of these functional groups, through resonance effects, results in the $\pi$-system of the aromatic ring having a low electron density. This feature impacts TNT persistence and accumulation within the soil in two ways (Figure 1.2.2.1.2). Firstly, this attribute makes TNT highly recalcitrant to electrophilic attack by bacterial oxygenases, the main pathway within the soil for aromatic compound mineralization [28]. Secondly, it allows the explosive to bind strongly, but reversibly, to clays within the soil through electron donor-acceptor complex formation [29]. The formation of this complex reduces the mobility of TNT which provides a partial explanation, alongside unequal deposition of explosives during low-order detonation, for the heterogeneous nature of soil contamination by TNT [30]. However, as the formation of these complexes is reversible and competitive between nitro-aromatic compounds [31], TNT can leach from contaminated soil [32]. Therefore, the high concentrations of TNT within contaminated soil pose a credible threat to groundwater. Such contamination has been identified within groundwater found at both munitions manufacturing sites and at military training ranges, with TNT concentrations in the latter being significantly greater than EPA guidelines [33,34].

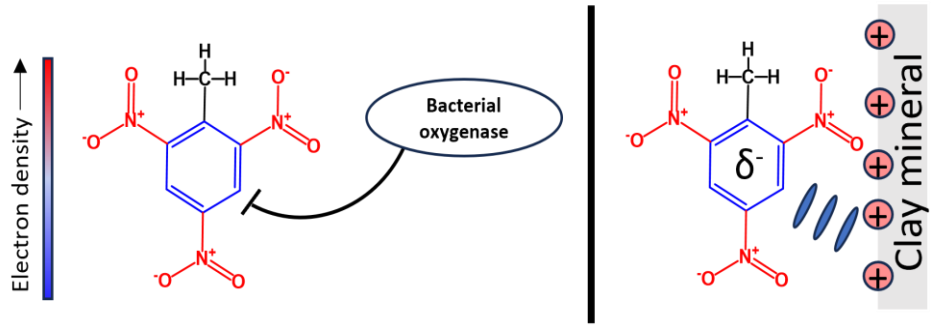


**Figure 1.2.2.1.2: Resonance effects contribute to accumulation and persistence of TNT within contaminated soil.** The three highly electronegative nitro-groups within the structure of TNT results in the $\pi$-system of the aromatic ring having a low electron density due to resonance effects. This prevents electrophilic attack of the aromatic ring by bacterial oxygenases and reduces mobility of the pollutant within the soil through electron-donor complex formation with cations in clay minerals.

### 1.2.2.2 Transformation of TNT within the soil

Though it persists within the soil environment, there are both abiotic and biotic mechanisms for the transformation of TNT. The degradation of TNT through photolysis is one such abiotic mechanism. Photolysis is the process in which TNT absorbs sunlight between the wavelengths of 315-400 nm with the ensuing increase in energy state causing the compound to spontaneously undergo both oxidation and reduction reactions, resulting in a variety of transformation products being generated. Using NMR analysis following photo-irradiation of TNT in both solid and aqueous states, 26 different breakdown products have been identified, including hydroxyaminodinitrotoluenes (HADNTs), aminodinitrotoluenes (ADNTs), nitriles, nitrones, azo and azoxy derivatives [35]. The production of these compounds is thought to be impacted by a range of different factors including but not limited to pH, exposure time and water content [35,36]. Photolysis can significantly reduce surface-levels of TNT within soil, for example a 35% reduction in TNT content of dry soil after 55 days [32]; however, as TNT contamination has been detected at depths of 15 cm below sites of low-order detonations [37], a considerable amount of the explosive remains unimpacted by photolysis. An abiotic process involved in sub-surface transformation of TNT is metal-catalysed reduction. This surface-mediated reaction requires aqueous iron (II) species to be adsorbed to iron (III) (hydr)oxides, or other mineral surfaces, to enable the sequential one-electron reduction of TNT to eventually form ADNT derivatives [38,39]. The absorption of the iron (II) species to a mineral surface is vital for this activity, with the reaction occurring very slowly with free iron (II) [38]. Within a reducing environment, such as anoxic subsurface soil, this chemical reaction can completely reduce TNT to generate 2,4,6-triaminotoluene (TAT) [39]. However, this process

is dependent upon the level of iron (II) within the soil, thus it may be limited in its ability to transform TNT in oxic-environments. Also, as the process requires TNT to be in an aqueous state, to allow access to the reactive surface sites, the ability of TNT to form electron-donor-acceptor complexes with clay minerals may further limit this reductive process. Evidence to support this hypothesis is the slower reduction rate of mono-nitroaromatics due to the formation of these complexes with the common clay mineral montmorilloniete [40].

Analysis of soil microbiota found at TNT-contaminated training ranges identified bacteria and fungi capable of transforming, and in some cases partially mineralizing, the explosive [41]. For the most part, aerobic transformation of TNT by bacteria is limited to the partial reduction of the explosive to form mono- and di-ADNT derivatives, through nitroso- and HADNT-intermediates. The very low reduction potential required to generate TAT from di-ADNT derivatives, between -0.629 and -0.712 V [42], makes the complete reduction of TNT chemically impossible for aerobic bacteria. Nitroreduction of TNT is catalysed by nitroreductases, an enzyme family which contains flavin-mononucleotide co-factors and use NADPH or NADH to perform sequential two-electron reduction of nitro-substituents. Several aerobic bacterial species capable of using TNT as a nitrogen source have been identified, these include members of the *Pseudomonas*, *Enterobacter* and *Rhodococcus* genera [41,43]. The *Pseudomonas* genus is particularly efficient in TNT transformation and is dominant in bacterial populations found within contaminated soil [44]. The use of TNT as a nitrogen source occurs via the condensation reaction between a HADNT and a Meisenheimer-complex, formed from central carbon ring reduction, the coupling of these TNT-derivatives releases nitrogen in the form of nitrite [45]. Enzymes that catalyse this reaction include the Old Yellow Enzyme (OYE) family, with homologs obtained from *Enterobacter cloacae* being capable of releasing nitrite from a variety of nitroaromatic compounds including TNT [46,47]. Whilst denitrification is believed to make the central carbon ring more accessible to oxygenase attack, there are currently no examples of aerobic bacteria using TNT as both a sole nitrogen and carbon source. However, this does not rule out the potential of co-metabolism by a bacterial consortium, as mineralization of dinitrotoluene (DNT) by aerobic bacterium has been shown [48]. In terms of anaerobic transformation of TNT, bacterial species within the *Clostridium* and *Desulfovibrio* genera have been shown to completely reduce TNT to TAT [43]. Within aqueous solutions, TAT is unstable and can be converted to *p*-cresol which bacteria can use as a carbon source [49,50]. However, evidence for TNT mineralization through TAT formation is weak, leading to suggestions that TAT may be a dead-end product biologically [51]. Fungal transformation of TNT within the soil environment also occurs through nitro-reduction, generating HADNT and ADNT products [52]. Some fungi within the Basidiomycota

phylum, which possess lignolytic capabilities, have potential roles in mineralizing TNT. This has been demonstrated for several white-rot fungi, including *Phanerochaete chysosporium*, which were able to mineralize TNT in both lignolytic (low nitrogen) and non-lignolytic (high nitrogen) conditions [53]. Under lignolytic conditions, these fungi were shown to release extracellular peroxidases that increased TNT mineralization. Interestingly, lignin peroxidases generated by *P.chysosporium* are inhibited by the presence of HADNTs [54]. Therefore, within the soil of munitions training ranges where high concentrations of TNT are converted to HADNTs by soil bacteria, inhibition of fungal-catalysed degradation could occur. Alongside Basidiomycetes, microscopic soil fungi are capable of mineralizing TNT, with strains of *Aspergillus niger*, *Mucor sp.* and *Trichoderma sp.*, isolated from TNT-contaminated soil, incorporating carbon from $^{14}$C-ring-labelled TNT into amino acids and organic acids [55]. However, the persistence of TNT within soils suggests these biotic transformation pathways may be limited by the biomass or metabolic activity of the microbial organisms that perform them.

Reduced derivatives of TNT, whether generated by abiotic or biotic processes, can undergo further reactions within the soil that impact upon subsequent bioavailability. The incorporation of ADNT derivatives into the organic matter of the soil is one such fate. Evidence for this fate was obtained through composting and soil-slurry studies within which, $^{14}$C-ring-labelled TNT was shown to be associated with the organic contents of the soil [56,57]. Liquid- and solid-state NMR has revealed all reduced derivatives of TNT could form covalent linkages via nucleophilic addition to quinone and other carbonyl groups found in soil humic acids and peat [59]. The formation of covalent linkages was also shown between di-ADNT and solid lignocellulosic material [59]. Interestingly, fungal laccases can catalyse the formation of these covalent linkages, suggesting incorporation into the organic matter can be facilitated by biotic mechanisms [60]. Reduced derivatives of TNT can also dimerise, in the presence of oxygen, to form azoxytetranitrotoluenes [61]. These compounds are highly recalcitrant to environmental degradation, and investigations using *Salmonella typhimurium* have shown azoxytetranitrotoluenes to be more genotoxic and mutagenic than TNT and its reduced derivatives [62]. The continued persistence of TNT at military training ranges, as well as at historical sites of munitions manufacturing during both World War I and II [63], indicate natural transformation processes are limited in their ability to remove the pollutant thus highlighting the need for external intervention.

## 1.3 Remediation methods for TNT contaminated soil

As TNT contamination of soil threatens public health through ground water contamination, and natural processes are limited in their ability to degrade the compound, remediation tactics to address this pollution issue are a necessity. However, the pollution found at munitions training ranges has unique challenges associated with it. These are:

- The vast area of contaminated land requiring treatment.
- The heterogeneous nature of contamination.
- The requirement to remediate active sites.
- The threat of UOX within the soil.

A suitable remediation method needs to overcome these challenges in a manner that is both cost efficient and sustainable.

### 1.3.1 Incineration

Incineration is one of the most common methods for dealing with a variety of organic wastes due to its efficiency. However, it has significant costs and environmental damage associated with it. Efficient incineration of organic contaminants requires extremely high temperatures, exceeding 648 °C, and oxygen quantities 100% to 200% greater than the amount required to combust the organic compounds [21]. Failure to achieve these requirements can result in the formation of reducing conditions that generate unwanted and toxic organic compounds within the resulting ash [21]. Meeting the temperature and oxygen-content requirements, alongside the removal and transport of contaminated soil, results in incineration having a high associated cost with estimates ranging from $200-1,000/ton (US; estimates are from 1992 and are not adjusted for inflation) [21]. Incineration also has a substantial negative environmental footprint, with the process destroying the structure and organic content of the contaminated soil. Due to the carbon sequestration capabilities of healthy soil, alongside the large amounts of $CO_2$ released during the process, the use of incineration to remediate large areas of explosives contaminated land does not fit with global aims of reducing atmospheric levels of $CO_2$.

### 1.3.2 Composting & Bioslurries

The earliest remediation alternatives to incineration exploited microbial activity towards TNT using composting and formation of bioslurries. The process of composting involves mixing the contaminated soil with an organic feedstock which provides a readily degradable source of nitrogen and carbon, such

as manure or food waste, as well as a bulking material that increases the aeration and moisture of the mix. The two main forms of composting are static pile and windrow composting, these approaches differ on the method of compost aeration. In static pile composting, the material is placed into piles and aerated using vacuum pumps. In comparison, windrow composting places the material in long piles, referred to as windrows, and periodically aerates the material through mixing with mobile equipment. Windrow composting is the favoured of the two approaches, as the combination of anaerobic and aerobic conditions is believed to enhance covalent incorporation of TNT into soil organic matter, whilst reducing the formation of recalcitrant azoxy-derivatives. Once TNT is incorporated into the organic content of the soil it is no longer bioavailable, thus is considered to be detoxified [56]. The detoxification of TNT by composting was demonstrated by the unperturbed growth of several plant species in soil, which prior to composting contained 100 g $kg^{-1}$ TNT [64]. Whilst effective, there are limitations to composting. One of these is the requirement of large volumes of additives, this results in a large space requirement for a comparatively small amount of contaminated soil being treated per composting batch.

A methodology generated to address the large space requirement of composting is the mixing of contaminated soil with large amounts of water and an inexpensive nutrient mixture, referred to as a bioslurry. On the whole, the fate of TNT within bioslurries is identical to composting with the explosive incorporated into the organic material within the mixture [57]. However, as bioslurries can be incubated within reactors, this provides greater control over the aeration condition such that highly reducing, anoxic conditions can be generated rapidly. The rapid generation of anoxic conditions aims to enhance TAT production, though results have been mixed [57]. Whilst allowing significantly more soil to be treated per batch, bioslurry is considerably more expensive than composting due to the energy requirements of running the reactor, and the nutrient feedstock required for rapid generation of anoxic conditions via the provision of carbon and nitrogen sources.

Both composting and bioslurries are highly effective methods of remediating TNT-contaminated soil and improve upon incineration as they do not degrade the soil substrate. However, the *ex situ* nature of these approaches makes them best suited for highly localised contamination, such as that found at munitions manufacturing sites. The scale and heterogeneous nature of TNT contamination at military training ranges make composting and bioslurry prohibitively expensive approaches, whilst the requirement of soil removal poses a safety risk due to UOX.

### 1.3.3 Alkaline hydrolysis

The use of *in situ* methods eliminates the requirement of soil excavation and transport, thus reducing the costs associated with remediation, one such method is alkaline hydrolysis. This approach takes advantage of the strong nucleophile nature of hydroxide ions to transform TNT through nucleophilic attack of the central carbon ring. The complete degradation of the aromatic structure has been shown to occur quickly at high pH, with TNT solutions of 25 mg $L^{-1}$ being completely degraded within six hours at pH 12 [65]. The products of TNT alkaline-hydrolysis have been shown to be predominantly polar [66] and are dependent upon the pH at which degradation occurs. This was demonstrated through the addition of neutralised solutions of $^{14}C$-ring-labelled TNT to soil following alkaline hydrolysis. The release of $^{14}C$-labelled $CO_2$ from the soil confirmed that alkaline hydrolysis can enable subsequent mineralization of TNT through both abiotic and biotic processes [67]. However, solutions treated at pH 11.5 showed a 13-16% higher mineralization than identical experiments using solutions treated at pH 10.5. The effectiveness of alkaline hydrolysis in treating explosives contaminated soil was shown in soil slurries, where an effective concentration of 0.1 % calcium peroxide reduced the TNT concentration by 97% within 24 hours [68]. The products of this reaction were shown to have undergone complete denitrification. However, the use of very high (>10) pHs is limited for *in situ* treatment, as such soils are considered hazardous waste. For this reason, investigations have assessed the use of calcitic/hydrated lime which can be applied to the soil in a land-farming approach. Laboratory microcosm studies using soil samples taken from contaminated sites, demonstrated that TNT concentration was reduced to non-detectable levels within 24 hours using 5% (w/w) lime treatment at 50% moisture content with agitation [69]. Bench-pan studies provided further evidence, showing an identical concentration of lime could reduce TNT within soil by 70% after 20-days at a 35 % soil moisture content [70].

Despite its effectiveness in reducing TNT content within contaminated soils, there are aspects of *in situ* alkaline hydrolysis that make it unsuitable for addressing the vast scale of contamination found at military training ranges. Firstly, the application of lime to contaminated land is a high input task, especially as lime has a limited solubility within water, 1.73 g $L^{-1}$, and thus cannot be sprayed onto soil but rather requires incorporation via ploughing; the presence of UOX within soils at training ranges makes this inherently risky. Secondly, this method is highly dependent upon soil water content and therefore would not be suitable for the large areas of contaminated land in relatively dry climates. Finally, there are high financial costs, and energy and emissions costs associated with the amount of lime required to treat the vast area of contaminated land, with 1.2 tonnes of $CO_2$ produced per tonne of lime [71].

### 1.3.4 Phytoremediation

Phytoremediation offers a potentially low cost, environmentally sustainable, and potentially low maintenance *in situ* approach to decontaminant soil located within active military training ranges. Phytoremediation is a broad term covering various methods that use plants to tackle pollution (Figure **1.3.4.1**).

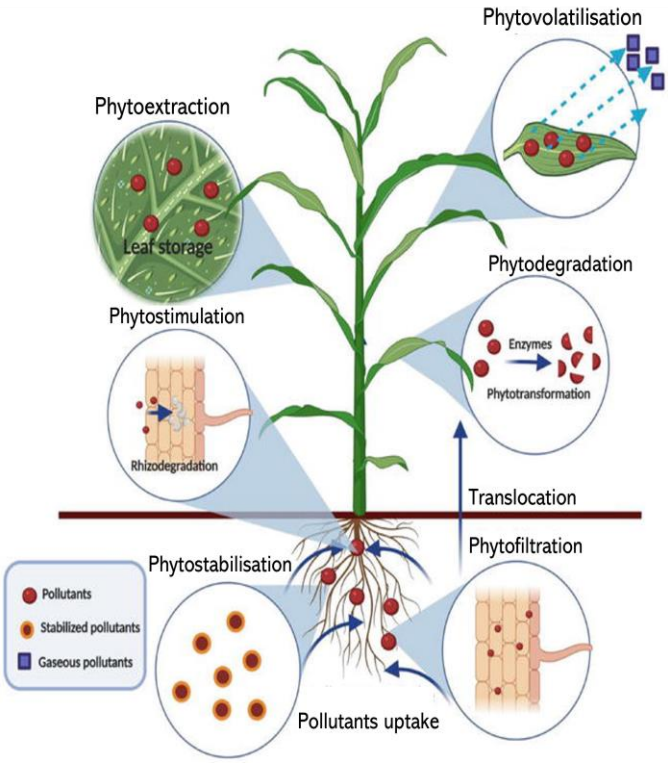


**Figure 1.3.4.1: Processes encapsulated under the umbrella term of phytoremediation.** Figure taken from Krishnasamy, Lakshmanan & Ravichandran (2021) [72], which itself was modified from Pilon-Smits (2005) [73].

**Phytovolatilisation** is an approach which allows pollutant concentrations to be dispersed from areas of high concentration within the soil to a much lower concentration within the atmosphere. Using the transpiration system, the pollutant is taken up from the surrounding soil and transported to the aerial tissue wherein it is released through gas exchange mechanisms. Depending on the volatility of the pollutant, metabolic modification may be required to allow its volatilisation. This process has been used for both organic and heavy metal pollutants. The remediation of overly selenium-rich soil being an example, with the members of the *Brassicaceae* family capable of releasing up to 40 g Se $ha^{-1}$ $day^{-1}$ as various gaseous compounds [74]. Due to the potential deposition of gaseous pollutants, the use of phytovolatilisation is controversial.

**Phytoextraction** is similar to phytovolatilisation, with pollutants being taken up via the root system and transported to the aerial tissue; however, in this case the compound accumulates rather than being expelled. The use of phytoextraction to obtain industrially important metals found at soil concentrations too low for conventional mining techniques is referred to as phytomining [75]. In respect to tackling pollution, phytoextraction is a technique of interest for remediating heavy metal contaminated soil, with a common example being arsenic whose presence in soil reduces crop yield and threatens consumer health [76,77].

**Phytodegradation** also requires the uptake of the pollutant by the plant, though in this case the compound is degraded through enzymatic activity either inherent within the plant or incorporated through transgenic techniques. An example of this, relating to explosive pollution, is the remediation of RDX-contaminated soil using plants expressing the XplAB enzyme system from *Rhodococcus rhodochrous*. Whilst RDX accumulates within the shoot tissue of unmodified plants [78], transgenic lines completely degraded the explosive [79–81]. Phytodegradation can also involve endophytic bacteria, with this demonstrated within hybrid poplar (*Populus deltoides* x *nigra*), where inoculation with *Enterobacter* bacterium enhanced trichloroethylene degradation capabilities, evidenced by 50 % more chloride ions being released into the rhizosphere [82].

**Phytostimulation** is also referred to as rhizodegradation. This method relies on the release of root exudates (e.g., enzymes, sugars, peptides etc.) to enhance the microbial activity within the rhizosphere. This enhanced activity is responsible for the degradation, or transformation, of the pollutant. The soil contaminants, that are often remediated through phytostimulation, have high hydrophobicity resulting in low mobility within the soil. Successful phytostimulation has been demonstrated with polyaromatic hydrocarbons (PAHs) [83].

**Phytostabilisation** reduces the bioavailability of the pollutants within the soil. This reduction can be through interactions with soil components and/or through stimulating rhizospheric bacteria as well as the incorporation into, or association with, the root tissue of the plant. Stabilisation of soil structure by the root system, limits erosion thus reducing pollutant bioavailability within leachate and runoff [73]. The prevention of downward leaching of contaminants through the soil has also been achieved using fast-transpiring trees, such as poplar, which prevents downward leaching of contaminants within the soil, as the fast-transpiration rate generates a powerful upward flow [73]. Additionally, plants can excrete carbon rich exudates that stimulate rhizospheric bacteria which themselves can sequester heavy metals within their cell-walls [84]. In the case of organic pollutants, phytostabilisation can be achieved

through the enhancement of pollutant assimilation into the organic content through rhizospheric interactions, alternatively it can be through plant uptake and transformation of the pollutant allowing its incorporated into the insoluble material of the cell wall [85–87].

**Phytofiltration** is a water-specific process that could be considered a sub-category of many of the processes described above. In phytofiltration, plant root tissue removes pollutants from water systems either through adsorption to the root surface or by pollutant uptake and transformation. This process is of growing interest in respect to wastewater treatment, with one example demonstrating the ability of a plantation of willow (*Salix miyabeana*) to remove nutrient contaminants from primary effluent wastewater at a rate of 19 million liters $ha^{-1}$ $yr^{-1}$ [88].

There are multiple aspects of phytoremediation that make it uniquely well suited to addressing the issue of TNT-contamination at military training ranges. Firstly, as an *in situ* method there are both cost and environmental savings due to the absence of soil excavation and transport. In fact, the presence of plants can increase the soil health and organic matter thus providing additional environmental benefits outside of pollutant remediation, such as carbon sequestration [89]. Unconventional methods for the sowing of plants, resulting from the robustness of seeds, eliminate the risk from UXO. An example of this is the dropping of seedballs over contaminated land by helicopters [90]. The relative robustness of some phytoremediation plant species, such as switchgrass (*Panicum virgatum*) and vetiver grass (*Chrysopogon zizanioides*), can allow them to grow in a variety of conditions with minimal maintenance. In respect to soil remediation, the large surface area of root systems, and the large biomass of plants make them efficient at removing soil contaminants. However, there are limitations to phytoremediation [91]. Firstly, this process is relatively slow, compared to e.g., excavation, and thus requires a timescale of years to see effective removal. The bioavailability of the pollutant is a significant factor impacting the timescale of phytoremediation. Secondly, the absence of *in planta* pollutant degradative biochemical pathways can lead to bioactivation and bioaccumulation of the xenobiotic. Finally, phytoremediation can only occur if the plant can survive the levels of pollution found at the contaminated site. In respect to this last limitation, the advancements in genetic techniques can now allow plant lines with enhanced tolerance to be developed. However, this requires a thorough understanding of the mechanisms by which plants uptake and metabolise pollutants.

## 1.4 Plant uptake and metabolism of TNT

### 1.4.1 Uptake

Plant uptake of pollutants is dependent upon several factors including plant species, soil and environmental conditions as well as the bioavailability of the compound. Bioavailability is dictated largely by the hydrophobicity of the molecule. The octonal: water partition co-efficient ($K_{OW}$), the ratio of chemical concentration within an octonal phase compared to the concentration in an aqueous phase when mixed in the two phase system, is a measure of molecule hydrophobicity. A Log $K_{OW}$ greater than 3.0 is considered high, with these molecules having a low bioavailability as they do not dissolve within water, and strongly associate with the organic fraction of the soil [73]. In contrast, a Log $K_{OW}$ less than 3.0 indicates that the molecule can diffuse into water to an extent that is inversely related to their log $K_{OW}$, thus allowing its transport and uptake by the plant. With TNT having a log $K_{OW}$ of 1.6, plant uptake of the explosive is possible. Currently no transporters have been identified that facilitate plant uptake of TNT or its transport between cells/organelles, and it is believed that the relative hydrophobicity of TNT allows it to passively diffuse across the lipid bilayers. Once within the plant, TNT is rapidly sequestered with most of the compound being retained within the roots. This finding has been confirmed in plants from angiosperm and gymnosperm lineages for which it has been investigated [78,85,86,92].

### 1.4.2 Phytotoxic mechanism of TNT

The toxicity of TNT in plants results from the activity of monodehydroascorbate reductase 6 (*MDAR6*) [93]. This is a dual-localised protein found within mitochondria and plastids [94]. Whilst this enzyme remains largely uncharacterised, it has been linked to protecting the function of photosystem 2 during high light exposure within leaves [95]. In respect to the phytotoxic mechanism of TNT, *MDAR6* facilitates a futile catalytic cycle (Figure 1.4.2.1A). In this cycle *MDAR6* uses NADH to catalyse a single electron reduction of TNT that generates a nitro-radical product that is highly unstable. This nitro-radical autooxidises in the presence of molecular oxygen, reforming TNT and producing superoxide. Therefore, this mechanism only requires a catalytic amount of TNT to significantly deplete cellular energy stores, through NADH consumption, whilst generating toxic levels of oxidative stress in the form of superoxide within the sensitive cellular locations of the mitochondria and plastids. Whilst the elimination of *MDAR6* activity did not improve plant uptake of TNT, it did significantly enhance tolerance to the explosive (Figure 1.4.2.1B).

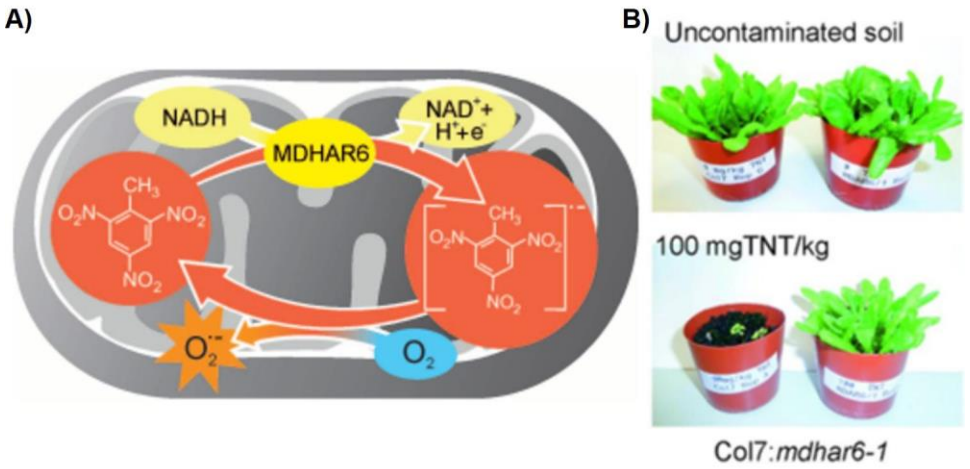


**Figure 1.4.2.1: Phytotoxicity of TNT within Arabidopsis. A)** *MDAR6* catalyses a single electron reduction of TNT within the mitochondria and plastids that generates a nitro-radical that in the presence of molecular oxygen spontaneously autooxidases to reform TNT and generate oxidative stress in the form of a superoxide free radical. **B)** Elimination of *MDAR6* activity within Arabidopsis provides significant tolerance to TNT. Both figures were taken from Johnston *et al*. (2015) [93].

### 1.4.3 Detoxification of TNT

As sessile organisms, in respect to geographical location, plants are unable to migrate from contaminated regions and have evolved a myriad of detoxification pathways to modify toxic compounds such as TNT. As a xenobiotic, a compound of synthetic origin, the process of TNT-detoxification within plants is predicted to follow the model described in Sandermann (1992) [96]. This model is comprised of three steps i) transformation, ii) conjugation and iii) compartmentalisation; though modern adjustments have added an additional step associated with metabolism post-compartmentalisation [97].

i) Transformation of the xenobiotic involves addition of, or allowing access to, a functional group. This step is catalysed by enzymes that perform redox and hydrolysis reactions. Hydroxyl (-OH), amino (-NH) and thiol (-SH) groups are functionalisations associated with this step. Transformation serves to increase xenobiotic reactivity, making the molecule more amenable to further chemical modification by conjugation. Whilst transformation is important for the conjugation of some xenobiotics, it is not required if a suitable functional group is already present within the molecule.

ii) Conjugation of transformed xenobiotics involves the covalent linkage to endogenous cellular compounds such as glucose or glutathione. Conjugation serves to increase the polarity of the xenobiotic, and thus provides greater control over movement and transport of the molecule.

Enzyme families that are associated with this step include glutathione transferases (GSTs), UDP-glucosyltransferases (UGTs), acyltransferases and methyltransferases. Whilst conjugation is thought to inactivate xenobiotics, this may not always be the case, as similar reactions within insects have been shown to be an important part of the toxic mechanism of haloalkenes [98].

iii) Compartmentalisation is the process in which the conjugated xenobiotic is removed from the sensitive biochemistry of the cytosol thus preventing any interference with primary metabolism. The cellular compartments believed to be important in this process are the vacuole and the cell wall, which are hypothesised to be important in the storage of soluble and insoluble xenobiotic metabolites respectively. Transport is believed to be facilitated through the action of membrane bound transporters, such as ATP Binding Cassette (ABC)-transporters, that show broad substrate specificity allowing them to transport a range of detoxified xenobiotics. The process of post-compartmentalisation metabolism involves the reclamation of metabolic components used in the detoxification process.

In respect to TNT, the plant metabolic pathways currently identified for the xenobiotic are reduction-initiated glucosylation and glutathionylation. Both pathways fit into the outlined model of xenobiotic metabolism, though currently only the steps up to conjugation have been elucidated *in planta*.

#### 1.4.3.1 Reduction-initiated glucosylation of TNT

Similar to bacteria and fungi, plants are also capable of reducing TNT. In this case reduction is catalysed by the oxyphytodienoate reductase (OPR) family of enzymes [99]. These proteins are plant OYE homologues, and like these enzymes, OPRs can catalyse the nitro-reduction of TNT at either the *ortho* or *para* positions to generate HADNT and ADNT derivatives. Currently only three functional OPRs have been identified within Arabidopsis, the cytosolic *OPR1* and *OPR2*, and the peroxisomal *OPR3* [99]. The endogenous function of *OPR1* and *OPR2* remains unknown; however, *OPR3* functions within jasmonate biosynthesis [100], with homologues in other plant species linked to a similar function [101,102]. Whilst *in vitro* analysis has confirmed that all three OPRs can reduce TNT, investigation using overexpression lines suggests that only *OPR1* and *OPR2* are involved in TNT-reduction *in planta* [99]. Alongside nitro-reduction, *OPR1* has the unique ability to reduce the aromatic ring of TNT to form a dihydride Meisenheimer complex [99], further metabolism of this metabolite has not been identified within plants. Nitroreduction of TNT in plants has been identified as rate-limiting in respect to detoxification, with the expression of a bacterial nitroreductase significantly enhancing plant uptake of TNT within liquid cultures [79,103].

The HADNT and ADNT derivatives generated by OPR activity with TNT are rapidly glucosylated via the activity of a UGT [104]. The UGT superfamily is very large within Arabidopsis, comprising 107 proteins. These enzymes are involved in glucosylating a variety of endogenous compounds within plants including alkaloids, flavonoids and glucosinolates. The mechanism of UGT activity involves transferring a nucleotide-diphosphate-activated sugar, commonly UDP-glucose within plants, to low-molecular weight aglycone substrates. This reaction can generate O-, N-, C- and S- linked glucosyl conjugates. In respect to TNT metabolism, microarray analysis of plants following 24-hour exposure to the xenobiotic identified eight induced UGTs [104] (Figure 1.4.3.1.1A). Seven of these proteins were capable of conjugating either HADNT or ADNT derivatives *in vitro* [104]. In respect to the conjugation of HADNTs, the glucosidic bond can occur either at the hydroxyl-group, O-linked, or via a C-linkage to the aromatic center of the molecule. The glucosylation of ADNT-derivatives occurs through N-linkages to the amine functional group (Figure 1.4.3.1.1B). The most induced UGT following TNT exposure was *UGT73B4*, which showed activity towards all isomers of HADNT and ADNT derivatives generated by OPR activity [104]. Overexpression of this enzyme within Arabidopsis lead to significant increases in the concentration of glucosylated-derivatives of TNT within plant tissue; however, it had no significant impact on TNT-uptake [104]. This result suggests that the glucosylation of HANDT and ADNT derivatives is not a rate limiting step in the detoxification of TNT *in planta*.

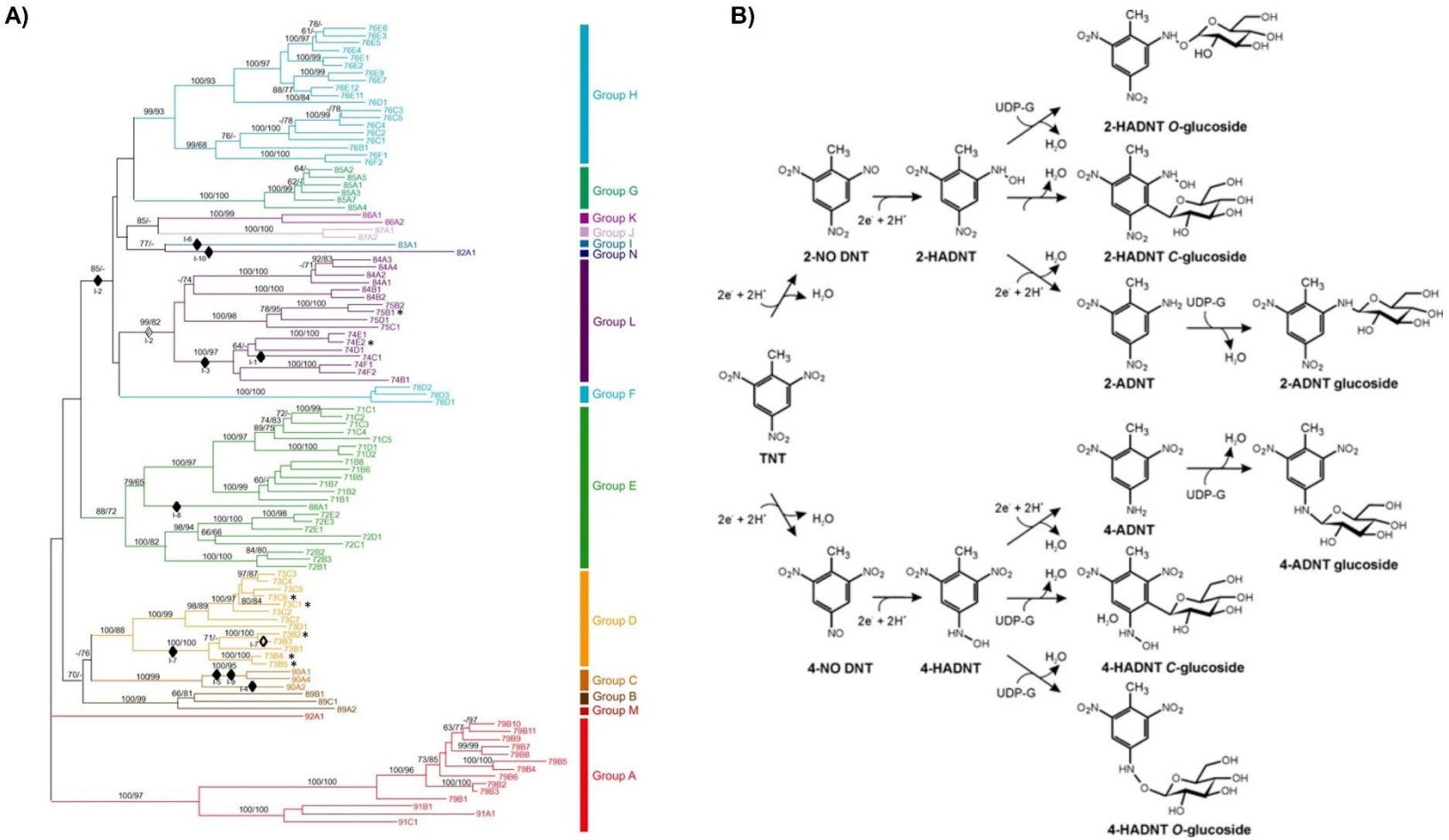


**Figure 1.4.3.1.1: Glucosylation of reduced TNT-derivatives *in planta*. A)** Phylogenetic analysis of 84, of the 107, UGTs within Arabidopsis, figure taken from Ross *et al*. (2001) [105]. Enzymes identified to be induced following TNT exposure are indicated (*). **B)** The reduction-initiated glucosylation pathway for TNT within Arabidopsis, figure taken from Gandia-Herrero *et al*. (2008) [104].

#### 1.4.3.2 Glutathionylation of TNT

Microarray analysis of Arabidopsis following TNT exposure also identified the upregulation of two GSTs, *GSTU24* and *GSTU25* [104]. Both enzymes were confirmed to have activity towards TNT *in vitro*, generating between them, three glutathione-conjugates (Figure 1.4.3.2.1) [106]. Conjugates 1 and 2 are isomeric products of glutathionylation of the methyl functional group, these metabolites are distinguished by the location of the hydroxylamino functional group, which is at the *para* position in Conjugate 1 and the *ortho* position in Conjugate 2. The nitro-reduction reaction is predicted to be a result of glutathionylation, as *in vitro* analysis of recombinant enzymes revealed no activity towards HADNTs [106]. Conjugate 3 is a product of a nitro-substitution reaction between TNT and glutathione which results in the release of free nitrite. Whilst *GSTU24* activity with TNT predominantly produces Conjugate 2, the conjugate profile of *GSTU25* has been shown to be pH-dependent with Conjugate 3 being the predominant product of enzymatic activity at pH 6-7 [106]. As the loss of a nitro-group is predicted to destablise the ring-structure of the molecule, it offers potential for the mineralization of TNT by rhizospheric bacteria [48]; therefore, the factors controlling Conjugate 3 production within plants are of interest for TNT-phytoremediation. The high sequence similarity between *GSTU24* and *GSTU25*, 79 % amino acid identity, indicates that the residues that differed within the catalytic domains of the enzymes are important for dictating the conjugate profiles. This was confirmed through site-directed mutagenesis, which discovered five key residues that impacted enzymatic activity towards TNT as well as the conjugate profile generated from the reaction [107]. The endogenous activity of *GSTU24* and *GSTU25* were also shown to be rate-limiting in the detoxification of TNT *in planta*, with plant lines overexpressing the enzymes showing enhanced uptake of the xenobiotic [106].

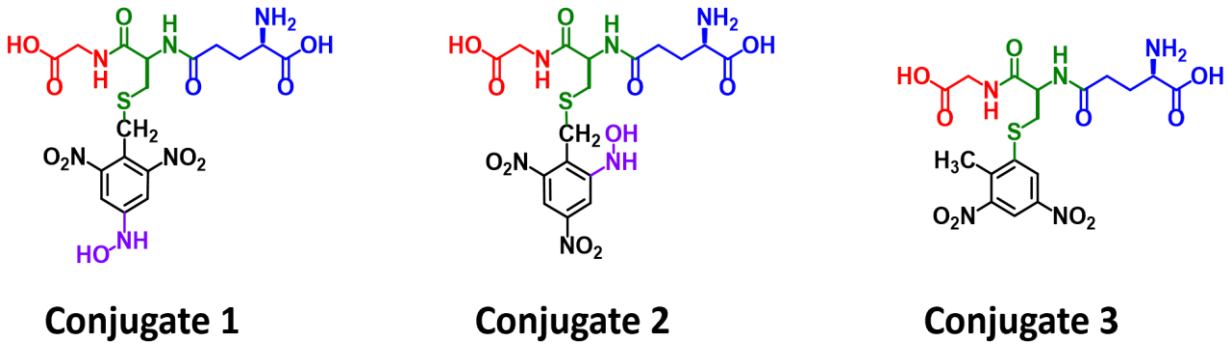


**Figure 1.4.3.2.1: Conjugate products of TNT glutathionylation.** *GSTU24* can generate Conjugates 2 and 3, whilst *GSTU25* can generate all three conjugates. At the physiological pH within the root cell *GSTU24* and *GSTU25* predominantly generate Conjugate 2 and Conjugate 3 respectively.

### 1.4.4 End-fate of TNT within plants

Following the model of xenobiotic detoxification, both glucosyl- and glutathione conjugates of TNT are predicted to be sequestered to the vacuole; however, evidence from $^{14}$C-labelling studies suggest this is not the end fate of TNT. The sequestration of xenobiotic glucosyl- and glutathione-conjugates to the vacuole has been indicated by *in vitro* transportation studies and isolation of intact vacuoles from plant cells [108–113]. In respect to glutathione-conjugates, vacuolar sequestration is believed to be important in their further metabolism [114,115]. Whilst the vacuole is believed to be an important intermediary store for TNT-conjugates, the organelle is not thought to be the end fate of TNT. Studies within both monocot and eudicot species using $^{14}$C-labelled TNT have identified that after a 14-day growth period, a substantial portion of radioactivity, 20-27%, was associated with the lignin fraction of the cell wall [85,86]. Similar results have been obtained with other xenobiotics that are predominantly detoxified within root tissue [87,116]. The use of gel-permeation chromatography confirmed that the association with lignin resulted from covalent linkages [116]. Whilst incorporation of TNT into the lignocellulosic material has not been confirmed within Arabidopsis, microarray analysis of plants following 24-hour exposure to TNT supports this fate, with multiple lignin synthesis genes induced [104]. The incorporation of xenobiotics into the lignin offers a route for their mineralization within the environment through the action of actinomycetes or white-rot fungi. This route has been demonstrated with $^{14}$C-labelled lignin-associated metabolites of chloroanilines fed to *Phanerochaete chrysosporium*, 65 % of the radiolabel was captured as $CO^2$ suggesting substantial mineralization [116]. Currently, the metabolic pathways that occur between the identified conjugation reactions of TNT and the incorporation of the xenobiotic into the lignocellulosic material of the cell wall are currently uncharacterised.

## 1.5 Glutathione in plants

Glutathione is a tripeptide comprising glycine, glutamate, and cysteine (Figure 1.5.1). Due to glutathione being readily oxidised and reduced, the molecule is the predominant redox regulator within eukaryotes, reaching millimolar concentrations within some plant tissues [117]. Due to this function in redox regulation, glutathione is involved in various cellular and developmental processes. These include but are not limited to cell-cycle regulation, root meristem development, pollen germination and defense responses to biotic and abiotic stressors [117]. Alongside its active functions within metabolism, the incredibly high concentrations of glutathione found within plant tissue make it a key reservoir for sulfur within plants [118].

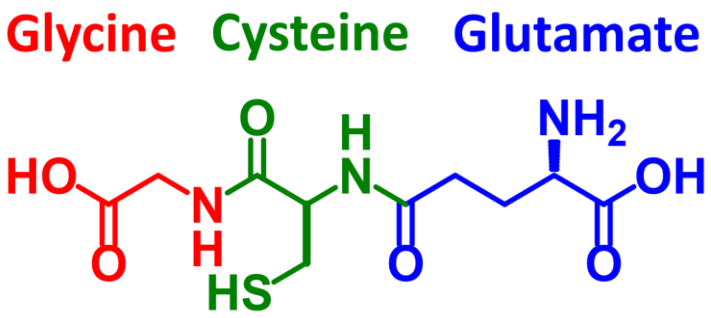


**Figure 1.5.1: The chemical structure of glutathione.**

### 1.5.1 The $\gamma$-glutamyl cycle

The plethora of roles for glutathione require mechanisms within plants to maintain the cellular glutathione pool, this is achieved through the $\gamma$-glutamyl cycle. This cycle encompasses the biosynthetic and degradative processes associated with glutathione metabolism (Figure 1.5.1.1). Synthesis of glutathione from its constitutive amino acids is a two-step process, catalysed by the sequential activity of the enzymes $\gamma$-glutamylcysteine synthase ($\gamma$-ECS) and glutathione synthase. Within Arabidopsis these steps are hypothesised to be separated spatially, with $\gamma$-ECS active within the plastid and the majority of glutathione synthase activity located to the cytosol [117]. Whilst glutathione synthase does have a plastid-targeted isoform, it comprises less than 9% of the total transcript population of the protein [119]. The main control point for glutathione synthesis has been identified as $\gamma$-ECS, with the activity of the enzyme regulated via glutathione feedback inhibition, this inhibition is competitive in respect to glutamate [120]. When used in a reaction, glutathione can either be conjugated to itself to form a disulphide, referred to as oxidised glutathione, or to an electrophilic compound to form a glutathione conjugate. The recycling of glutathione requires specialised enzymes capable of hydrolysing the unique

$\gamma$-glutamyl bond present within the tripeptide. Within Arabidopsis several such protein families have been identified. The first are the $\gamma$-glutamyltranspeptidases (GGTs), of which there are four, with the apoplastic GGT1 and the vacuolar GGT4 comprising the majority of activity throughout the plant [115]. These enzymes transfer the glutamate residue from glutathione to an acceptor residue, such as alanine, forming a $\gamma$-glutamyl peptide [115,121]. In respect to their cellular functions, GGT1 has been shown to be important in the recycling of oxidised glutathione [121], whilst GGT4* has been indicated to be primarily responsible for the hydrolysis of glutathione conjugates [114,115,122]. Glutathione and the resulting $\gamma$-glutamyl peptides released from GGT activity, or from other enzymatic reactions, are hydrolysed by cytosolic $\gamma$-glutamylcyclotransferases (GGCTs) in a pathway important in glutamate recycling [123–125]. The final group of proteins capable of hydrolysing $\gamma$-glutamyl bonds are the $\gamma$-glutamylpeptidases (GGPs). The cytosolic GGP1 and GGP3 have been identified to function in glutathione-recycling [126], as well as in glucosinolate biosynthesis [125]. The activity of the enzymes within the $\gamma$-glutamyl cycle is important in maintaining cellular glutathione levels, with perturbations impacting both glutathione and sulfur homeostasis [121,125].

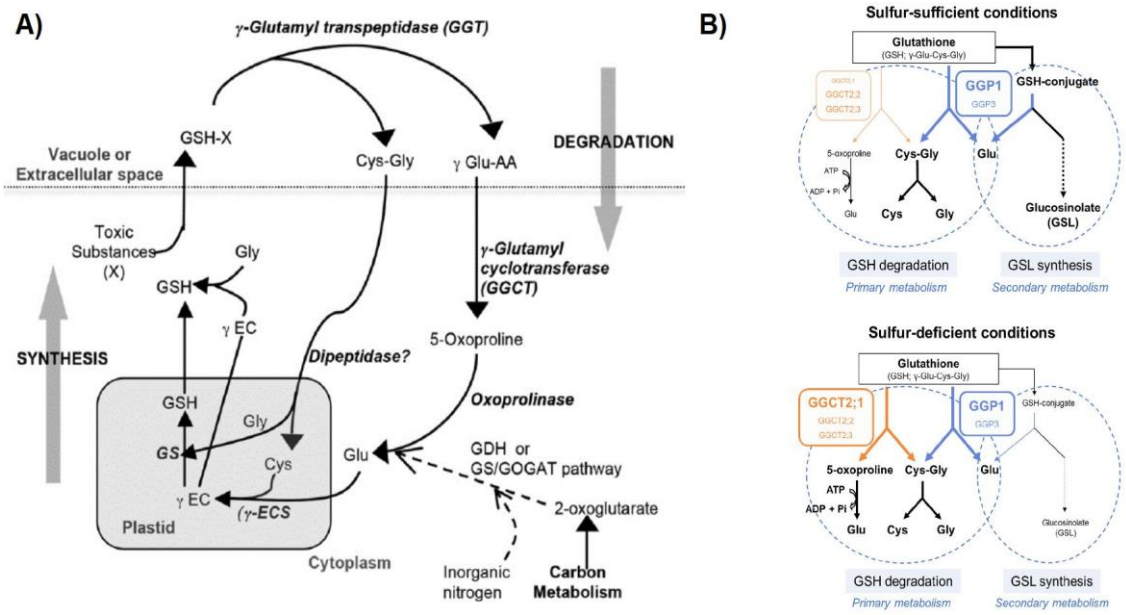


**Figure 1.5.1.1: The $\gamma$-glutamyl cycle within Arabidopsis. A)** Biosynthesis and recycling mechanisms involved in glutathione metabolism showing the function of $\gamma$-*ECS*, glutathione synthase, GGTs and GGCTs. Figure taken from Kumar *et al*. (2015) [124]. **B)** Function of GGCTs and GGPs in glutathione recycling and its links to sulfur availability. Figure taken from Ito *et al*. (2022) [125].

### 1.5.2 Glutathione in detoxification responses

Glutathione is involved in several mechanisms important in the plant response to abiotic stress. One of these is the response to reactive oxygen species, for this glutathione can be used in both a direct and indirect manner. The direct use of glutathione to detoxify reactive species, generated during oxidative stress, is achieved through the activity of glutathione peroxidases (GPOXs) [127]. The indirect mechanism in which glutathione controls reactive oxygen species levels is through the ascorbate-glutathione cycle, this is the main hydrogen peroxide detoxification mechanism operating in the cytosol, plastids and mitochondria within plant cells [128]. Within this cycle, ascorbate is used to detoxify hydrogen peroxide generating a monodehydroascorbate radical, this radical undergoes non-enzymatic disproportionation to ascorbic acid and dehydroascorbate. Glutathione is used to reduce dehydroascorbate, via the activity of a dehydroascorbate reductase (DHAR), thus maintaining the cellular ascorbate pool. The activity of both GPOXs and DHARs generates oxidised glutathione, it is for this reason that during oxidative stress within plants, the ratio between reduced and oxidised forms of glutathione can drop from 20:1 to 1:1 [117]. Another function of glutathione, in responding to abiotic stresses, is the chelation of heavy metals. Chelation of heavy metals *in planta* is achieved via phytochelatins, which are polymers of $\gamma$-glutamylcysteine generated from glutathione via the activity of a phytochelatin synthase (PCS) [129]. The chelation of heavy metals aids in their sequestration to the vacuole, a step important in their detoxification [130]. The importance of glutathione in heavy metal chelation *in planta* was demonstrated using the $\gamma$-ECS inhibitor buthionine sulfoximine (BSO), with plants co-exposed to BSO showing a significant reduction in cadmium tolerance [131]. The detoxification of electrophilic toxins is another important role for glutathione in responding to abiotic stress. The ability of glutathione to conjugate weak electrophiles results from its ready conversion to a thionate anion, which can perform nucleophilic attack. Glutathione conjugation is important in the detoxification of endogenous metabolites, an example being the conversion of genotoxic methylglyoxal, a reactive aldehyde generated during threonine metabolism, to lactic acid [132]. In respect to abiotic stress, glutathione conjugation is important in xenobiotic detoxification, having a significant role in herbicide tolerance [133]. Other xenobiotics that have been shown to be detoxified by glutathione conjugation *in planta*, include pharmaceutical drugs [134] and antibiotics [135]. Once formed, glutathione conjugates of xenobiotics are predicted to be sequestered to the vacuole, where GGT4 activity initiates their metabolism. However, *in planta* evidence for this is limited to the xenobiotic bimane [114,115].

### 1.5.3 The GST superfamily

The roles of glutathione within cellular metabolism are facilitated through the action of GSTs, a family of enzymes found throughout the kingdoms of life, though is particularly large within plants. Crystal structure comparison indicates that protein structure is highly similar across the GST family, with the length of component peptide loops and helices, as well as the presence, or absence, of N- and C-terminal extensions being the primary areas of difference [136]. Each soluble GST is a homodimer, which possesses a central cleft between its monomers, with enzymatic activity dependent upon this dimerisation [136]. The key regions of GSTs are the glutathione domain (G-site), located at the N-terminal, and the alpha-helical domain (H-site), located at the C-terminal, which contains the majority of the hydrophobic co-substrate binding site. As expected, these domains are adjacent to each other in correctly folded proteins, facilitating the reaction between the two co-substrates. The G-site contains the critical residue for stabilising glutathione as the reactive thiolate, in plants this residue is predominantly serine, though in some cases it is cysteine, with this change impacting enzymatic function (examples are provided later). Within plants, there are eight classes of GST within Arabidopsis, comprising 55 proteins. (Figure 1.5.3.1). The function of GST classes varies, reflecting the diversity of roles glutathione performs within the plant. A brief overview of the GST superfamily within Arabidopsis is provided below, for an in-depth review please see Dixon & Edwards (2010) [136].

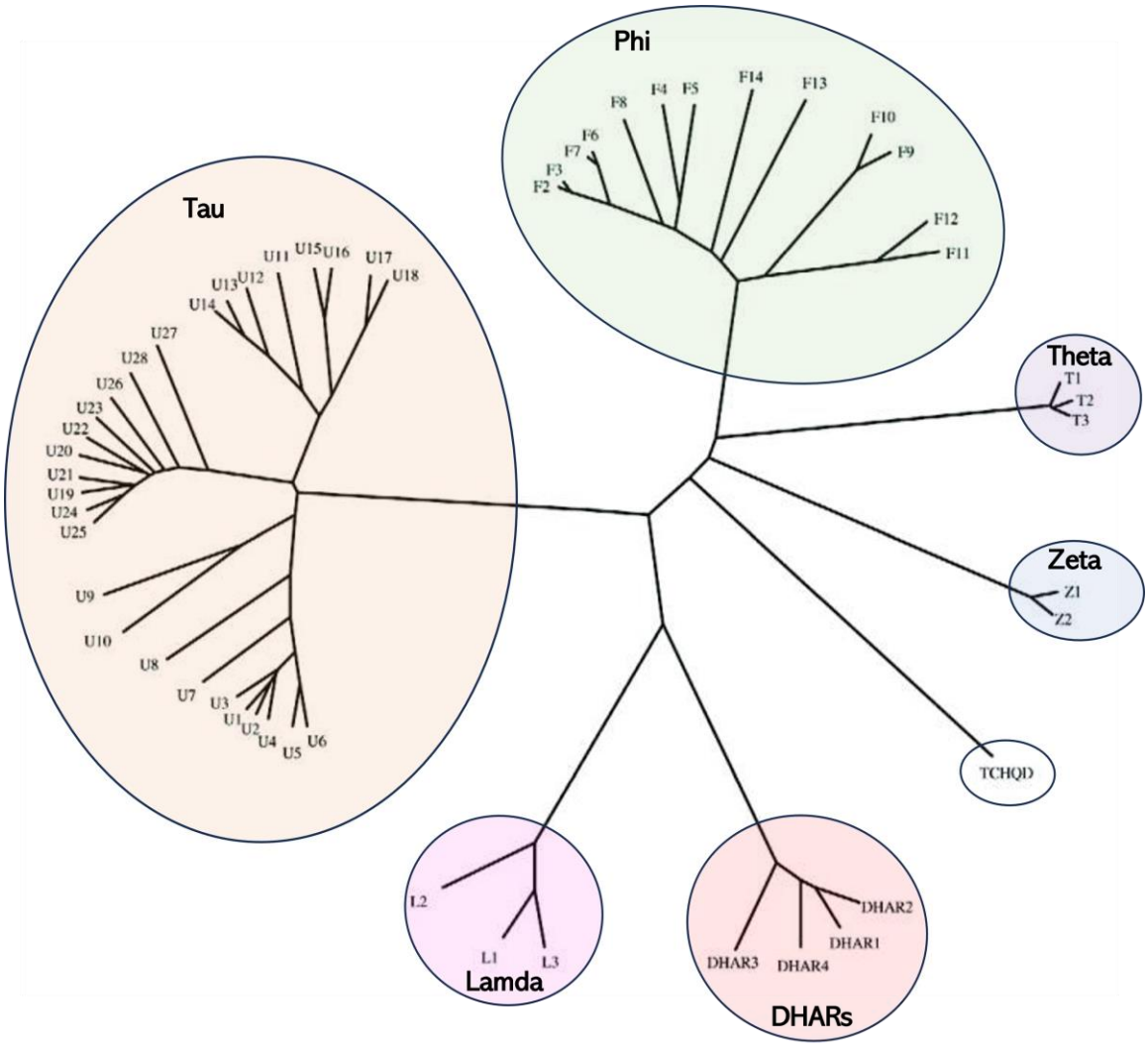


**Figure 1.5.3.1: The Arabidopsis GST superfamily.** Phylogenetic tree showing the seven related GST classes. Modified figure taken from Dixon & Edwards., (2010) [136]

**Membrane associated proteins in eicosanoid and glutathione metabolism (MAPEG)** are a phylogenetically unrelated GST family, found within eukaryotes and prokaryotes, that form membrane-bound trimers capable of GST and GPOX activity [137]. There is a single MAPEG-like protein within Arabidopsis, At1g65820, which is currently uncharacterised.

**Tetrachlorohydroquinone dehalogenases (TCHQD)** are a GST class consisting of a single protein, At1g77290, which was identified by sequence homology to prokaryotic proteins capable of metabolising chlorinated xenobiotics [138]. Aside from the presence of the catalytic G-site serine being confirmed, and the protein being localised to the plasma membrane [139], this protein remains largely uncharacterised.

**Zeta** GSTs are a highly conserved class across all eukaryotes, these proteins catalyse the isomerisation of maleylacetoacetate to fumarylacetoacetate within tyrosine catabolism in fungi. This metabolic activity has been confirmed for Arabidopsis GSTZ1 [140,141]. Alongside this activity, GSTZ1 also catalyses the glutathione-dependent dehalogenation of dichloroacetic acid to glyoxylic acid [140]. As glyoxylic acid can enter primary metabolism, this is a unique example of a plant GST enabling complete xenobiotic mineralization. Of the two Zeta class GSTs within the Arabidopsis, only *GSTZ1* is transcribed at any significant level with the adjacent *GSTZ2* believed to be a pseudogene.

**Theta** GSTs are a class that is found in both plants and animals. Within the Arabidopsis genome, the three theta GSTs are clustered and show constitutive expression. Whilst members of this family have shown activity towards the xenobiotic and model GST-substrate 2-chloro-4,6-dinitrobenzene (CDNB) [139], they are predicted to function as GPOXs within the plant, due to being particularly efficient at reducing organic hydroperoxides to alcohol derivatives [139]. In agreement with this activity, all three theta GSTs contain a C-terminal peroxisome targeting signal and have been localised in both GFP-tagging and proteomic analysis of isolated peroxisomes [139]. These findings imply a function for theta GSTs in responding to oxidative damage of peroxisomal components, caused by the high levels of hydrogen peroxide within the organelle. Interestingly, GSTT2 and GSTT3 have been shown to have alternative splicing, this produces much larger proteins which contain a C-terminal myb-like transcription factor domain. In respect to GSTT2, alternative splicing masks the peroxisomal targeting signal, resulting in the exclusive nuclear localisation of the protein [139], a finding that explains its important function in systemic acquired resistance through the epigenetic modifier FLD [142].

**Lambda** GSTs are one of the unique classes in which the catalytic G-site serine is replaced by a cysteine. This substitution results in the formation of a mixed disulfide with the glutathione substrate, resulting in Lamba GSTs being unable to catalyse typical GST-associated conjugation reactions [143]. The formation of a mixed disulfide is important in the activity of this class of enzyme to bind flavonoids [144]. Of the three lambda GSTs encoded within the Arabidopsis genome, only *GSTL1* is strongly induced by stress responses, with *GSTL2* and *GSTL3* showing more modest, constitutive expression.

**Dehydroascorbate Reductases (DHARs)** are a plant-specific class of protein that also contains a cysteine in place of a serine within the G-site. These proteins catalyse the reduction of dehydroascorbate within the ascorbate-glutathione cycle [145]. The Arabidopsis genome encodes three functional DHARs, *DHAR1-3*. Investigations crossing DHAR knockout lines with a catalyse-deficient line, *cat2*, that has enhanced intracellular hydrogen peroxide, revealed DHAR1 is responsible for the majority of DHAR

activity induced by oxidative stress [146]. This was evidenced by *in vitro* assays of leaf extract, in which an increase in DHAR activity was detected in *cat2* single knockout lines but was absent in *cat2dhar1* double knockouts [146]. This effect was also seen in *cat2dhar3* lines but to a much lesser extent. This same study identified that both DHAR1 and DHAR2 are localised to the cytosol in both root and leaf tissue, whilst DHAR3 was localised to the plastids of these tissues [146].

**Phi** GSTs are another plant-specific class of proteins, the functions of these proteins within plant metabolism remains largely uncharacterised. A high level of redundancy between phi GSTS has been demonstrated, with quadruple knockout lines showing no visual changes in plant growth even under stress [147]. Members of this family have been linked with redox state regulation within Arabidopsis, with *gstf8* knockout lines showing accumulation of singlet oxygen within root tissue during salt stress [148], whilst *gstf9* knockout lines accumulate greater levels of ascorbate and glutathione in control conditions [149]. The proteins GSTF11, GSTF12, and GSTF14 do not contain the catalytic serine within their G-Sites, leading to suggestions these proteins may act in facilitating metabolite transport. This hypothesis is evidenced in respect to *GSTF12*, with knockout lines presenting the *transparent testa* phenotype indicative of an inability to accumulate anthocyanins within the vacuole [150]. Structural investigation of GSTF2 identified the presence of non-catalytic ligand-binding sites, these regions allowed the protein to bind molecules such as indole-3-aldehyde and the flavonoid quercetrin, with the authors suggesting a potential role for GSTF2 in transporting these metabolites [151]; however, this remains to experimentally confirmed.

**Tau** GSTs are the largest class within Arabidopsis and are also specific to plants. This class of GST has the unique capability to bind fatty acid derivatives that are either oxidised or glutathionylated [152]. This ability has led to suggestions that an endogenous function of tau GSTs is to stabilise oxidised fatty-acids, generated by oxidative stress and hormone biosynthesis [152]. The 28 proteins within the tau class can be split into three clades. Clade 1 is comprised of GSTU1-10, these proteins are mainly expressed within the roots. Members of this clade have a strong affinity to fatty acid-glutathione thioesters of chain length $C_{12}$-$C_{16}$ [152]. The second clade contains GSTU11-18. The protein GSTU13, is an indispensable member of the PENETRATION2-pathway for indole glucosinolate metabolism, with knockout lines defective in 4-O-$\beta$-D-glucosyl-indol-3-yl formamide, indole-3-ylmethyl amine, and raphanusamic acid biosynthesis, in response to pathogen infection [153]. The final clade comprises GSTU19-28, members of this clade have functions in general stress tolerance [154] and aliphatic glucosinolate synthesis [155].

The crystal structure has been obtained for GSTU25, which confirmed the formation of a complex with oxidised glutathione [107], providing structural evidence for the GPOX activity of this enzyme [139].

## 1.6 Project aims

This project aimed to further characterise TNT metabolism within Arabidopsis, focusing on the metabolic steps that occur following conjugation and before incorporation into lignocellulosic material. To achieve these aims a methodology that could reliably confirm the compartmentalisation of xenobiotic metabolites was required. The identification and optimisation of such a methodology was the aim of the work described in Chapter 3. Focusing on two techniques, Live Single Cell Mass Spectrometry (LCS-MS) and Benchtop Non-aqueous Fractionation (BNAF), the latter was successfully optimised and applied to identify the relative association of a glucosylated TNT-derivative with the plastidial, cytosolic, and vacuolar compartments within Arabidopsis root tissue. Following on from this, research described in Chapter 4 aimed to use the optimised BNAF technique, alongside other methods, to characterise the metabolism of the nitro-substituted product of TNT-glutathionylation, Conjugate 3. Through enhancement of Conjugate 3 formation, via transgenic expression of *Drosophila melanogaster* GST, several downstream metabolites were identified, alongside a protein activity important in their formation, and their compartmentalisation in root tissue was confirmed. Finally, Chapter 5 details proteomic investigations which aimed to generate resources to support the formation of models relating to Conjugate 3 metabolism. These investigations used the approaches developed in Chapters 3 and 4 to provide an understanding of the compartmentalised root proteome and its response to enhanced Conjugate 3 production. The findings of this research are compiled in Chapter 6 through the presentation of an expanded model for TNT metabolism within Arabidopsis. Through contextualising the findings of this research with those of the broader literature, this chapter outlines several hypothesised metabolic steps and suggests approaches through which to validate and further expand the model.

# Chapter 2: General Materials and Methods

## 2.1 Consumables and Reagents

Consumables and reagents were obtained from the following suppliers, unless stated otherwise in the text: Fisher Scientific Ltd (Loughborough, UK), Formedium (Hunstanton, UK), Honeywell (Leigh-on-sea, UK), Invitrogen (Paisley, UK), Insight Biotechnology (London, UK), New England Biolabs Ltd. (Hitchin, UK), Promega (Southampton, UK), Qiagen (West Sussex, UK), Sigma - Aldrich Company Ltd. (Poole, UK), Scientific Laboratory Supplies Ltd. (Nottingham, UK), Thermo Fisher Scientific (Loughborough, UK).

Primers were synthesised by Sigma - Aldrich and DNA gel markers were obtained from Thermo Fisher Scientific and Promega. TNT was kindly provided by the Defense Science and Technology Laboratory (DSTL) (Fort Halstead, Kent, UK). Ultrapure water (UPW) was generated using a Suez Ultrapure water unit (Sartorius, Epsom UK).

## 2.2 Molecular Biology techniques

### 2.2.1 Polymerase Chain Reaction (PCR) amplification of DNA fragments

Stock primer solutions (100 µM) were generated from lyophilised primers using UPW, 10 µM working solutions were used for all reactions.

Genomic DNA and cDNA, ≤ 1000 ng, was diluted 1/5 in PCR master mix. The master mix component quantities for a single 20 µL reaction are shown in Table 2.2.1.1 . A DNA engine thermocycler (BioRad, Watford UK) was used for PCR amplification, cycle conditions are described in Table 2.2.1.2. Details regarding the individual PCR primers can be found in the relevant sections.

**Table 2.2.1.1: PCR master mix recipe for 20 µL reaction.**

| Component | Volume |
|---|---|
| Gotaq Green Master Mix (Promega, UK) | 12 µL |
| 10 µM Forward Primer | 0.8 µL |
| 10 µM Reverse Primer | 0.8 µL |
| Nuclease-free water | 5.4 µL |

**Table 2.2.1.2: PCR conditions used for genotyping.**

| Temperature | | Time |
|---|---|---|
| Step 1: | 95 °C | 2 minutes |
| Step 2: | 94 °C | 15 seconds |
| Step 3: | 60 °C | 30 seconds |
| Step 4: | 72 °C | 1 minute |
| Step 5: Repeat from step 2 for 35 cycles | | |
| Step 6: | 72 °C | 10 minutes |

## 2.2.2 Reverse transcription PCR (RT-PCR).

A 20 µL reaction volume was used for reverse transcription of total RNA. Initially 1 µL of Oligo(dT)$_{12-18}$ (500 µg mL$^{-1}$) (Thermo Fisher Scientific), 1 µL of dNTP mix (10 mM) (Thermo Fisher Scientific), and 1 ug of total RNA were mixed and volume made up to 12 µL using nuclease-free UPW. The solution was heated at 65 °C for five minutes and quickly chilled on ice. To the chilled solution, 4 µL of 5X first strand buffer (Thermo Fisher Scientific), 2 µL 0.1M dithiothreitol (DTT) and 1 µL of RNAseOUT (Thermo Fisher Scientific) were added and mixed by gently tapping. Following a two-minute incubation at 42 °C, 1 µL of Superscript II reverse transcriptase (Thermo Fisher Scientific) was added, the solution was then incubated at 42 °C for 50 minutes with a subsequent inactivation step of 70 °C for 15 minutes. The purified cDNA concentration was quantified using a Nanodrop 8000 (Thermo Fisher Scientific) and used for subsequent semi-quantitative PCR reactions. Semi-quantitative PCR reactions were carried out as described in Section 2.2.1.

## 2.2.3 Agarose gel electrophoresis

DNA fragments were separated according to size in a 1.2% (w/v) agarose gel containing 0.7 µM ethidium bromide (Sigma - Aldrich) in 1x Tris-acetate-EDTA buffer. Recipe for 50x Tris-acetate-ethylenediaminetetraacetic acid (EDTA) stock buffer is provided in Table 2.2.3.1. Samples were run and separated at 130 V alongside a DNA gel marker which provided a reference for molecular weight. Ethidium-bromide-stained DNA was visualised using a Uvitec Essential V6 UV visualiser (Uvitec, Cambridge UK)

**Table 2.2.3.1: Recipe for 50x Tris-acetate-EDTA stock buffer**. Stock buffer was diluted to 1x in distilled water ($dH_2O$) for gel electrophoresis.

| Reagent | Quantity |
|---|---|
| Tris | 242 g |
| Glacial Acetic acid | 57.1 mL |
| 0.5M EDTA solution (pH 8) | 100 mL |
| $dH_2O$ | Make up to 1 L |

### 2.2.4 Purification of PCR amplicon

Amplicons of target DNA were purified from PCR reaction using Wizard® SV Gel and PCR Clean-Up system (Promega). Briefly, PCR reaction was diluted 1:1 in membrane binding solution. The solution was applied to a minicolumn and centrifuged at 16,000 xg for one minute. Flowthrough was discarded and 700 µL of membrane wash solution (with ethanol) was added and the column centrifuged again. This step was repeated with 500 µL of membrane wash solution, after which the flowthrough was discarded and the column re-centrifuged to dry the membrane. Bound DNA was eluted from minicolumn by incubation at room temperature (RT) with 50 µL of Nuclease-free water followed by a final centrifugation step.

### 2.2.5 Plasmid purification

Propagated plasmid was purified from overnight culture using QIAprep® Spin Miniprep Kit (Qiagen, West Sussex UK) according to the manufacturer's instructions. The concentration of purified plasmid was quantified using a Nanodrop 8000 (Thermo Fisher Scientific).

### 2.2.6 Nucleotide sequencing and analysis

Sequencing was performed by Eurofins (Konstanz, Germany). Purified DNA was diluted to 5 ng $\mu L^{-1}$ and mixed in a ratio of 1:1 with 5 µM forward or reverse primer stock to a final volume of 10 µL. Analysis of the sequencing results was performed using SnapGene (v7.0).

## 2.3 Plasmids, bacteria and growth conditions

### 2.3.1 Plasmids

**Table 2.3.1.1: Plasmids used within this research**. The plasmid, the antibiotic resistance conferred by the plasmid, the antibiotic concentration required for efficient selection, and the source of the plasmid.

| Plasmid | Antibiotic Resistance | Antibiotic Concentration | Source |
|---|---|---|---|
| pMLBART-*Dm*GST | Spectinomycin | 50 µg $mL^{-1}$ | Bruce group stocks |

### 2.3.2 Bacterial strains

**Table 2.3.2.1: Bacterial strains used within this research**. The bacterial species, the respective strain, the inherent antibiotic resistance within the strain, the use of the bacterial strain within the research, and the source of the bacterial strain.

| Bacteria | Strain | Known Resistance | Purpose | Source |
|---|---|---|---|---|
| *Escherichia coli* | DH5$\alpha$ | None | Plasmid preparation and long term storage as glycerol stock (-70 °C) | Bruce group stocks |
| *Agrobacterium tumefaciens* | GV3101 | Gentamycin (50 µg $mL^{-1}$)<br>Rifampicin (15 µg $mL^{-1}$) | Transformation of Arabidopsis by floral dipping | Denby group stocks |

### 2.3.3 Plasmid propagation

The *Escherichia coli* strain DH5$\alpha$ was used to propagate the pMLBART-*Dm*GST binary vector. Glycerol-stocks of transformed cells were inoculated onto lysogeny-broth (LB; Invitrogen) solid agar containing the appropriate antibiotic for plasmid selection and incubated overnight at 37 °C. Single colonies were streaked onto new LB solid agar for colony PCR confirmation of pMLBART-*Dm*GST binary vector. Colonies positive for pMLBART-*Dm*GST plasmid were transferred to 5 mL of LB media, containing the appropriate antibiotic for plasmid selection, and incubated overnight. Propagated pMLBART-*Dm*GST binary vector was purified from overnight culture as described in Section 2.2.5.

### 2.3.4 Preparation of electrocompetent *Agrobacterium tumefaciens*

Agrobacterium strain GV3101 glycerol stock was inoculated onto LB agar containing 50 µg $mL^{-1}$ of gentamycin and incubated at 28 °C for three days. A single colony was inoculated into 5 mL of LB media containing 50 µg $mL^{-1}$ gentamycin and incubated overnight (28 °C, 180 rpm agitation). The entire overnight culture was used to inoculate 500 mL of LB media containing 50 µg $mL^{-1}$ gentamycin, the culture was incubated until an OD between 0.8-1 was reached (28 °C, 180 rpm agitation). The culture

was chilled on ice for 20 minutes, then subsequently aliquoted into ten 50 mL pre-chilled centrifuge tubes. Bacterial suspension underwent centrifugation at 4000 xg for 20 minutes at 4 °C, the resulting cell pellet was washed via resuspension in 50 mL of ice-cold $dH_2O$, followed by centrifugation. The resulting cell pellets were resuspended in 10 mL of ice-cold $dH_2O$ and pooled into four, pre-chilled 50 mL falcon tubes. The suspensions were made up to 50 mL with ice-cold $dH_2O$, centrifuged, and pairs of cellular pellets were pooled into two, pre-chilled 50 mL falcon tubes. This process was repeated, so that all bacteria was contained within a single pellet. This pellet was re-suspended in 4.5 mL ice-cold 10% glycerol and 80 µL of suspension aliquoted into pre-chilled 1.5 mL tubes. Aliquots were snap frozen in liquid nitrogen and stored at -70 °C.

### 2.3.5 Transformation of electrocompetent *Agrobacterium tumefaciens*

A single 80 µL aliquot of *A.tumefaciens* was thawed and mixed, by gentle tapping, with 1 µL of 100 ng $\mu L^{-1}$ pMLBART-*Dm*GST binary vector. The mixture was incubated on ice for two minutes then transferred to a pre-chilled, 2 mm electroporation cuvette (Flowgen Bioscience Ltd., London UK). A brief pulse of 1.8 kV was applied to the suspension using a micropulser (BioRad, Watford UK), as per the manufacturer's instructions, and 800 µL of LB media pre-warmed to 28 °C was immediately added to the cuvette. The cell suspension was transferred to a 1.5 mL microcentrifuge tube and incubated for 3 hours (28 °C with 180 rpm agitation). Following incubation, 30 µL of cells were inoculated onto LB agar plates containing the respective antibiotics for plasmid selection. After a three-day incubation at 28 °C, colony PCR was performed to confirm the presence of the pMLBART-*Dm*GST binary vector.

## 2.4 Plant Methods

### 2.4.1 Preparation of growth media

For all investigations plants were grown on half-strength Murashige-Skoog basal medium (½MS). Generation of liquid and solid ½MS media are provided in Table **2.4.1.1**.

**Table 2.4.1.1: Recipe for ½MS liquid and solid medium**.

| **Instructions** | |
|---|---|
| Step 1: | Dissolve 2.15 g Murashige-Skoog basal medium (Sigma - Aldrich) in 800 mL of distilled $H_2O$ |
| Step 2: | pH to 5.7 using 0.1M potassium hydroxide |
| Step 3: | Make up to 1 L using distilled $H_2O$ |
| Optional step for solid media: | Add 8 g of agarose (Sigma - Aldrich) |

| Instructions | |
|---|---|
| Step 4: | Autoclave at 121 °C for 15 minutes |

### 2.4.2 Preparation of glufosinate-ammonium (Basta) soil

Finale 150 (Bayer Crop Science, Cambridge UK), 1 mL containing 150 g $L^{-1}$ of Basta, was mixed with 1.5 L of tap water and poured into the bottom of a tray. Following this, the solution was absorbed by the addition of ~3 L Levington Seed & Modular F2+S soil to the tray.

### 2.4.3 Seed sterilisation

Seeds were surface-sterilised using vapour-phase sterilisation in which seeds were incubated for three hours in a sealed container containing chlorine gas. Chlorine gas was generated by the reaction of 3 mL concentrated HCl with 100 mL sodium hypochlorite. Residual chlorine gas was removed post-sterilisation by venting the container in a fume-hood for ten minutes.

### 2.4.4 Stratification

Sterilised seeds were placed onto half strength Murashige and Skoog basal medium (½ MS; Sigma-Aldrich) agar and were stratified for 2 days at 4 °C in the dark (wrapped in aluminium foil).

### 2.4.5 Growth conditions for soil

The following conditions refer to plants grown on soil for the purpose of floral dipping or seed-propagation. For these aims, non-sterile seed was sown in trays of Levington Seed & Modular F2+S (with sand) compost (ICL, Suffolk UK). Plants were propagated at the Biology glasshouse facilities with regular application of an all-purpose fertiliser. Pests were controlled with foliar application of entomopathogenic nematode *Steinernema feltiae* (Koppert B.V., Berkel en Rodenrijs Netherlands) for the control of the larvae of the *Frankliniella occidentalis* and sciarid flies (*Lycoriella* spp., *Bradysia* spp). The wetting agent 'Addit' (Koppert B.V., Netherlands) 0.2% (v/v) was applied with nematodes for increased leaf coverage and adherence. The further daily operation (2 hours) of Sulfume sulphur vapourisers (HotBox International, Hull UK), and the fungicide Systhane 20EW (Corteva Agriscience, Cambridge UK) containing 200 g $L^{-1}$ (20% w/w) myclobutanil and 103 g $L^{-1}$ cyclohexanone was used to stop growth of powdery mildew (*Erysiphe cruciferarum*).

### 2.4.6 Growth conditions in hydroponic systems

Stratified seedlings were germinated and then grown on ½ MS solid agar within a growth room (16-hour day/8-hour night photoperiod, light intensity: 100 µmoles $m^{-2}$ $sec^{-1}$, day/night temperatures: 24 °C/20

°C). At 14-days post-germination seedlings were transferred to hydroponic cultures. Hydroponic cultures contained ½ MS media within a Tipone™ micropipette tip box with 5-6 plants placed in foam bungs within polystyrene rafts (Figure 2.4.6.1). The boxes were placed in a Sanyo MLR Growth Cabinet (12-hour day/night photoperiod, light intensity: 180 µmoles $m^{-2}$ $sec^{-1}$, day/night temperatures: 21 °C/18 °C), for a further 21 days, replacement of liquid media every seven days.

**Figure 2.4.6.1: Hydroponic system used for investigations.**

### 2.4.7 Genomic DNA extraction from plant material

The DNA was extracted from plant material using a DNeasy Plant Pro kit (Qiagen) according to manufacturer's instructions. Briefly, 100 mg of plant tissue was homogenised in 500 µL of lysis buffer (CD1) using a TissueLyser II (Qiagen, Manchester UK) with a 2x 24 adapter. TissueLyser settings were two one-minute rounds at 25 Hz, with position of samples switched between rounds. Samples were centrifuged at 12,000 xg for 2 minutes with the resulting supernatant being retained. Proteins were precipitated from the solution via the addition of solution CD2, which was followed by a second

centrifugation with the resulting supernatant being retained. DNA was isolated from supernatant via column purification in which the supernatant was loaded onto a DNA-binding column followed by two-washing steps using wash buffers AW1 and AW2 respectively. Each of these steps was separated by a round of centrifugation after which the supernatant was discarded. Bound DNA was eluted from the column through the addition of 100 µL of elution buffer.

Eluted DNA was quantified using a Nanodrop 8000 (Thermo Fisher Scientific) and stored at -20 °C until required.

### 2.4.8 Total RNA extraction from plant material

Total RNA was extracted from plant material using a RNeasy Plant Kit (Qiagen), according to manufacturer's instructions. To summarise, 100 mg of plant material was ground to a fine powder in liquid nitrogen within a pre-chilled pestle and mortar. Powder was transferred to a pre-chilled 2 ml microcentrifuge tube. Before the powder could thaw, 450 µL of lysis buffer (Buffer RLT) containing 1% $\beta$-mercaptoethanol was added and the suspension mixed using a vortex mixer. The suspension was then passed through a QIAshredder column to remove tissue debris and the resulting flowthrough mixed, via pipetting, with 0.5 volumes of ethanol. The solution was then applied to a RNeasy mini spin column and centrifuged at 12,000 xg for 15 seconds. Flowthrough was discarded and column was washed three times, once with 700 µL of buffer RW1 and twice with 500 µL of buffer RPE. The bound RNA was eluted by incubating 50 µL of RNAse-free water on the membrane, followed by centrifugation (12,000 xg for 1 min). The eluate was then passed over the membrane again to obtain greater yield. No DNase treatments were required during this process.

Eluted RNA was quantified using a Nanodrop 8000 and stored at -70 °C until required.

## 2.5 Statistical analysis and data visualisation

Unless stated otherwise statistical analysis was performed using R statistical software (v4.2.2) [156] and Rstudio [157]. Students test-statistic (T-test) [158], Analysis of Variance (ANOVA) [159] and Tukey's Honest Significance Difference (Tukey HSD) [160] were performed utilising the rstatix package(v0.7.2) [161].

Raw data was processed and figures generated utilising the tidyverse package (v2.0.0) [162]

# Chapter 3: Compartmentalisation of TNT metabolites within Arabidopsis root tissue: methodology optimisation

## 3.1 Introduction

Compartmentalisation is an important aspect of eukaryotic organisms that allows a variety of chemical environments to exist within a single cell. The separation of these chemical environments enables multiple, conflicting, metabolic processes to occur simultaneously and at a high efficiency. Compartmentalisation also provides a method of controlling the impact of endogenous compounds. An example of this is the glycosylation of plant hormones which inactivate and target these signaling molecules for vacuole sequestration, allowing their physiological impact to be tightly controlled [163–165]. Enhancing the understanding of the compartmentalised metabolome, and the mechanisms involved in its generation, will aid in the development of more productive plant lines through synthetic biology techniques.

### 3.1.1 Compartmentalisation of detoxified xenobiotics

Compartmentalisation is important in plant detoxification responses, such as those for xenobiotic compounds. The vacuole and the cell wall are believed to be the subcellular compartments to which metabolites are sequestered [96]. Channeling metabolites into these locations prevents them from interfering with important cellular processes or being bioactivated within the cytosol [166]. Multiple lines of evidence suggest that vacuole sequestration is a vital mechanism in detoxification. Firstly, in the absence of the required tonoplastic transporters, plants show an increased susceptibility to arsenic and cadmium, despite chelating mechanisms within the plant being functional and active [130,167]. Secondly, in respect to xenobiotic conjugate sequestration, knockout lines of the tonoplastic transporter ABCC2 show decreased tolerance to CDNB [168]. As GST-conjugation of CDNB was not indicated to be impaired within knockout lines, it suggests sequestration of conjugated-xenobiotics is important in detoxification. However, it is crucial to note in this case a direct link between lower CDNB tolerance and an inability to sequester conjugated derivatives was not made.

Most evidence for the sequestration of xenobiotic-conjugates to the vacuole has been obtained *in vitro*. Isolated vacuoles have been shown to uptake a variety of conjugated-products generated during xenobiotic metabolism which include glucosyl-, malonyl and glutathione-conjugates [111,112,169,170].

This approach, alongside the use of vacuole membrane-enriched vesicles, has also allowed the specific transport activity of several tonoplastic transporters to be identified [109,171–174]. Whilst these various *in vitro* studies have confirmed the xenobiotic-conjugate transport capability within the tonoplast, *in planta* confirmation of sequestration is needed to understand its significance within cellular metabolism.

### 3.1.2 Confocal microscopy

Currently, the only evidence for rapid compartmentalisation of conjugated xenobiotics *in planta* has been obtained using derivatives of the xenobiotic bimane. The fluorescent nature of thiol-conjugated derivatives of bimane allowed the use of confocal microscopy to follow metabolite movement [175]. This revealed that following a brief accumulation in the cytosol, the majority of glutathione-conjugates of bimane were sequestered to the vacuole of Arabidopsis root tissue after 30 minutes. However, as most conjugates generated from xenobiotic detoxification do not fluoresce, including derivatives of TNT, other techniques are required to confirm the significance of conjugate compartmentalisation within the plant cell.

### 3.1.3 Approaches for spatial metabolomics

Until recently spatial metabolomics has been achieved primarily through the isolation of organelles however, this methodology has limitations. Firstly, metabolism is not arrested during the isolation process. Continuation of metabolism may prevent metabolites of interest from being detected within isolated organelles, despite their presence *in vivo*. Secondly, the high mobility of metabolites can limit the strength of conclusions. Finally, analysing isolated organelles only confirms metabolite presence within that organelle and does not provide context within the broader cellular metabolism. Newly developed techniques that build on the advancements in Raman spectroscopy and mass spectrometry are avoiding the requirement of organelle isolation and allowing investigation of compartmentalised metabolism *in planta*.

#### 3.1.3.1 Stimulated Raman Scattering Microscropy

A label-free alternative to confocal microscopy that can obtain below micrometer resolution is Stimulated Raman Scattering Microscopy (SRSM). Raman scattering is the scattering of photons, following contact with a molecule, with the energy of photons either increasing, decreasing or staying the same depending on the molecular bonds present within the compound. The change in energy resulting from Raman scattering is referred to as a Raman shift and can be quantified by comparing the frequency of scattered light to that of the original light source. By rastering laser-scanning microscopes

across a biological specimen, and measuring the Raman shifts, SRSM can map the distribution of chemical bonds within the sample across three-dimensional space and in real time at lateral resolutions of 300-400 nm (for a detailed description of this analytical technique see Hue, Shi and Min, 2019 [176]). The absence of chemical fixation is a particular strength of SRSM as it avoids metabolomic perturbations that can result from this process. Further to this, by obtaining a hyperspectral image, in which each pixel contains a Raman spectrum containing multiple Raman shifts, SRSM can distinguish between different chemical constituents within a single sample [177]. This capability has allowed the use of SRSM to investigate the compartmentalisation of differing metabolites within a variety of plant tissues including Arabidopsis root and leaf tissue [178]. However, due to the overlapping nature of peaks within Raman shifts, SRSM can lack the specificity required to distinguish between molecules with high structural similarity within the complex matrix of the plant cell [179], such as what could be expected with xenobiotic conjugates and their metabolites generated during the detoxification process.

#### 3.1.3.2 Imaging Mass Spectrometry

Imaging mass spectrometry (IMS) is a non-targeted metabolomic approach which can detect thousands of metabolites across a range of metabolic species i.e., lipids, proteins and glycans. The variations of IMS, which differ on the type of ionisation method used, each have their respective strengths and weaknesses in areas such as resolution, *m/z* ranges and the variety of molecular species detected (for a comprehensive review, see Buchberger *et al*. (2018) [180]). The most used variation of IMS is matrix assisted laser desorption ionisation-IMS (MALDI-IMS), due to the wide range of molecular weights and species that can be detected [180]. Tissue analysed by MALDI-IMS is flash frozen, lyophilised, and sectioned before being coated in a crystalline matrix that extracts metabolites enabling their ionisation by a focused laser. By rastering the laser across the tissue surface, a spatial map of metabolite distribution can be obtained. This information can be superimposed onto an image of the tissue section as a heat map, the resultant model allows intuitive understanding of results in the context of the sample. In comparison to organelle isolation, the rapid freezing and subsequent lyophilisation involved in MALDI-IMS reduces metabolite diffusion and degradation, thus providing a more representative understanding of endogenous metabolism. Improvements in the methodology such as secondary ionisation steps, MALDI-2 [181], are allowing a greater breadth of molecules to be detected during analysis. However, a current limitation of MALDI-IMS is the resolution that be obtained with most experiments being within 10-20 µm [182]. Whilst this is sufficient to gain a comprehensive understanding across tissue sections, limited conclusions can be obtained at the subcellular level.

### 3.1.3.3 Live Single-Cell Mass Spectrometry

An alternative to IMS, designed for the high-resolution investigation of cellular and sub-cellular metabolism is live single-cell mass spectrometry (LSC-MS). This technique directly obtains extract from a single cell, using a nanospray capillary, and analyses it using nanoelectrospray-ionisation (Nano-ESI) mass spectrometry [183] (Figure 3.1.3.3.1). Direct extraction has confirmed metabolic differences between cell types [184], as well as allowing the analysis of organelle metabolomes [185], without the requirement of extensive isolation procedures. As no prior treatment of tissue is required and there are no experimental steps between extraction and analysis, the risk of metabolic profile perturbations is reduced. Whilst there will be a metabolic response to the insertion of a capillary into the cell, the speed at which extract is obtained should mitigate against severe changes. The inclusion of fluorescent markers has aided the use of LSC-MS to extract from specific cell types [186], with multiple organelle dyes now commercially available [187] this approach can aid the accuracy of LSC-MS in subcellular sampling. A weakness of LSC-MS, like organelle isolation, is that extraction from single organelles only confirms metabolite presence within the extracted organelle; therefore, it does not provide context with regards to cellular metabolism. Extraction from various sub-cellular compartments offers a method to mitigate this issue though requires substantial technical skill [188].

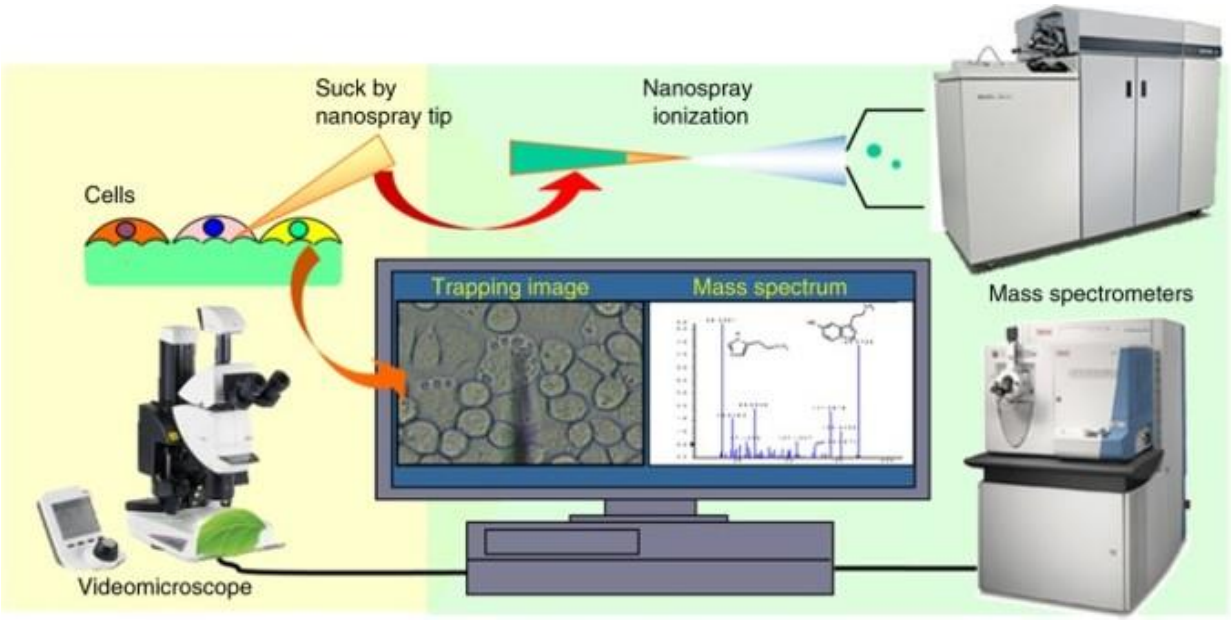


**Figure 3.1.3.3.1: Overview of the LSC-MS technique.** Organelles or extract from a single cell are obtained by insertion of a nanospray-tip into a target cell using a micromanipulator. The manipulation of the nanospray-tip in respect to the cell is achieved using a microscope. Once obtained the extract can be analysed by Nano-ESI MS, either immediately or after cold-storage. Figure was taken from Fujii *et al.* (2015) [183].

### 3.1.3.4 Non-Aqueous Fractionation

Another technique that provides subcellular resolution, in the context of metabolism at the tissue level, is non-aqueous fractionation (NAF). Using a density gradient comprising the organic solvents heptane and tetrachloroethylene, NAF separates subcellular compartments within a tissue sample. As the use of organic solvents prevents polar metabolite diffusion and inhibits enzymatic activity, metabolites remain associated with their compartment of origin at levels proportional to what is present *in vivo*. Degradation of metabolites is further reduced by performing all experimental steps on ice or at 4 °C. Marker enzyme and metabolite assays are used to calculate the compartmental distributions across the density gradient, which is then used to localise other metabolites through distribution comparisons. The result of this analysis is a relative-subcellular distribution of detected metabolites within plant tissue. First applied to plant material in the 1980s [189], NAF has gained renewed interest within the past decade due to the advancements in MS allowing for large scale metabolic analysis of obtained fractions. Classical NAF protocols generate a linear density gradient and achieve separation through ultracentrifugation. The use of a linear gradient and ultracentrifugation requires large amounts of starting material, >4 g fresh weight, which limits the types of tissue that this technique has been applied to. Examples include Arabidopsis leaf tissue, potato tubers and apple fruits [190–192]. However, an adapted protocol which uses an iterative fractionation process with a benchtop microcentrifuge, benchtop non-aqueous fractionation (BNAF), has been described which generates distinct compartmental distribution patterns using lyophilised material roughly equivalent to 200-400 mg fresh weight [193] (Figure 3.1.3.4.1). Through reduction in sample requirement, BNAF can allow metabolite compartmentalisation to be investigated within a variety of tissues including Arabidopsis roots, the location of TNT-detoxification. A limitation of NAF techniques is the compartmental resolution that can be achieved, with distinction between particular subcellular compartments being difficult due to their similar density profiles, examples being the vacuole and apoplast [191,194]. However, the ability to distinguish between cytosol and vacuole or apoplast makes NAF techniques well suited to confirm the compartmentalisation of xenobiotic conjugates *in planta*.

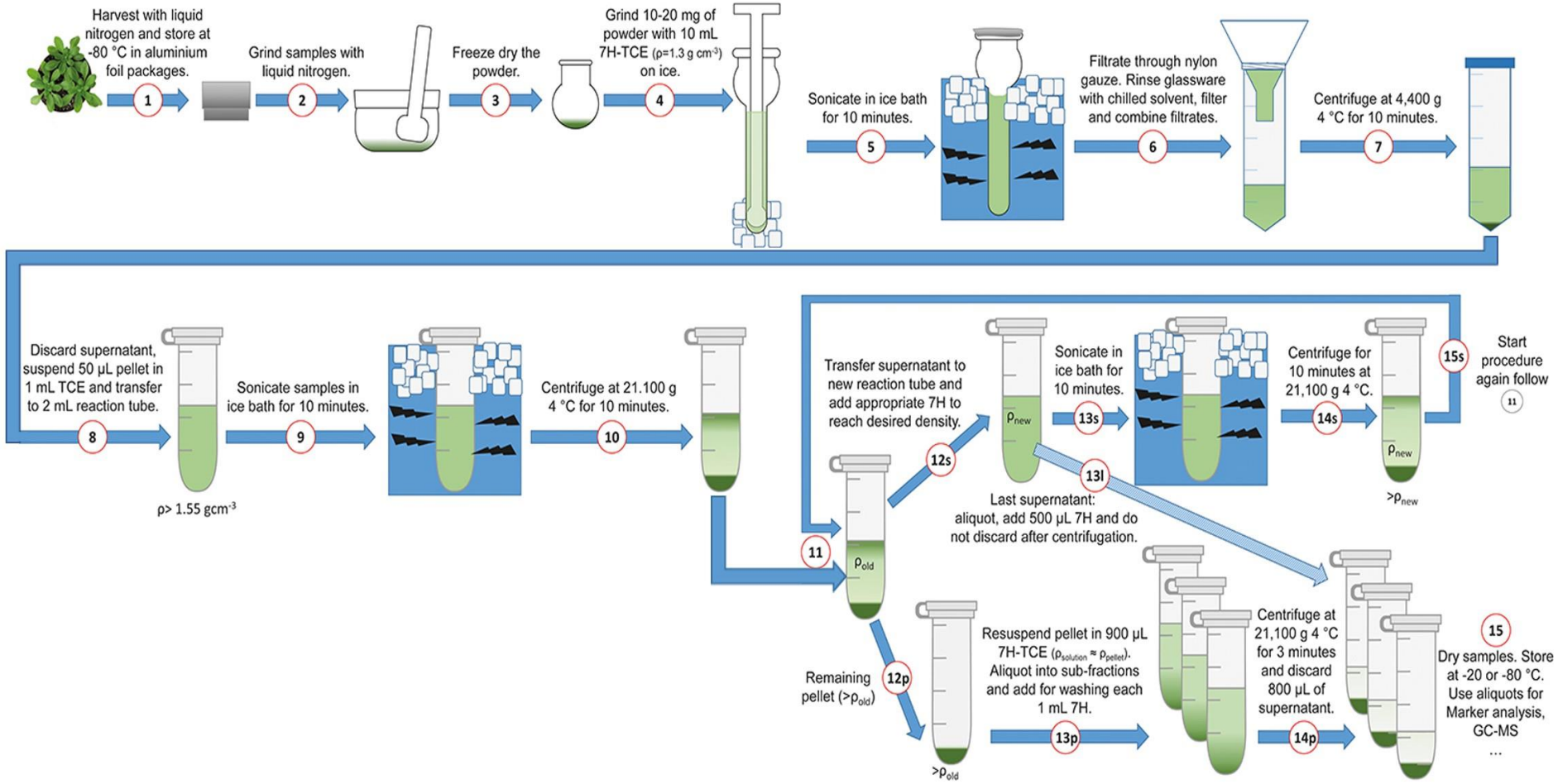


**Figure 3.1.3.4.1: Overview of the BNAF technique.** Figure was taken and modified from Fürtauer *et al*. (2016) [193]. In this 7H refers to heptane and TCE refers to tetrachloroethylene.

Chapter 5: Compartmentalisation of TNT metabolites within Arabidopsis root tissue: methodology optimisation

This chapter describes the work undertaken to identify, and optimise, a technique that will test the compartmentalisation of conjugates generated by metabolism of TNT within Arabidopsis root tissue. This work focused on two methodologies i) LSC-MS and ii) BNAF. Investigations identified BNAF as the most suitable and the technique described within the literature was optimised for use with Arabidopsis root tissue. Success in this endeavour has provided the first *in planta* evidence for dominance of compartmentalisation in the metabolism of xenobiotic glucosyl-conjugates, within root tissue.

## 3.2 Materials and Methods

### 3.2.1 Plant material

Arabidopsis (Col0) obtained from the Eurasian Arabidopsis Stock Centre (uNASC) was used for all investigations.

### 3.2.2 Plant preparation for LSC-MS

Four-day-old seedlings were transferred to ½MS liquid culture containing 500 µM TNT and incubated for 24 hours (120 rpm agitation, 20 µmol m−2 s−1 light intensity, 16-hour day/8-hour night photoperiod, 21/18 °C day/night temperature). Prior to extraction, dosed plants were washed in ½MS liquid culture (10 minutes, 120 rpm agitation) to reduce background levels of TNT originating from the root surface. For extraction, the seedling root tissue was immobilized on a microscope slide using low-melting point agarose (LMPA). Borosilicate glass 100 mm capillaries (World Precision Instruments, Hitchin UK) were used to generate nanospray-tips using a Sutter model 97 micropipette puller (Sutter Instrument, Novato CA) and an Inject man N12 micro-manipulator (Eppendorf, Stevenage UK) was used for micromanipulation. Nanospray-tips containing cellular extract were kept at -70 °C until required for downstream analysis.

### 3.2.3 LSC-MS analysis of plant extract

Metabolite analysis of plant extracts obtained within nanospray-tips was performed on an Orbitrap Fusion Trihyrbid Mass Spectrometer (Thermo Fisher Scientific, Oxford UK) following published guidance [183] with minor modifications. Firstly, 4 µL of ionisation solvent (acetonitrile: 0.1 % formic acid $dH_2O$, (60: 40 v/v)) was pipetted into the nanospray-tip, after which a clean copper electrode was inserted into the tip. The nanospray-tip was placed within the ion source, and the source set to MS mode. An ion source voltage of 1.4 kV was used for both positive and negative ionisation mode. Xcalibur Qual browser software (Thermo Fisher Scientific, Oxford UK) was used to manually inspect the raw data, the criteria

for peak identification were ion intensity of >$10^3$, 5 parts per million (ppm) mass accuracy and the presence of isotope peaks.

### 3.2.4 Dosing of hydroponic plants with TNT

Plants were grown as described in Chapter 2 section 4.5. Once plants were 5-week-old plants, spent media was replaced with fresh media containing 250 µM TNT in dimethylsulfoxide (DMSO) or equivalent volumes of DMSO only. After a 20-hour incubation, the root tissue was washed in tap water, to reduce background levels of TNT and DMSO originating from the root surface, momentarily blotted to remove excess surface water, then flash-frozen in liquid nitrogen.

### 3.2.5 Benchtop non-aqueous fractionation

The BNAF methodology described in Fürtauer *et al*. (2016) [193] was followed for the fractionation of plant material. Plant tissue, 200-600 mg, was flash frozen using liquid nitrogen and ground to a fine powder in a pestle and mortar pre-chilled using dry-ice. Ground samples were then lyophilised for 4-days (-108 °C, <0.06 mbar). Lyophilised powder, 7-10 mg, was suspended in an ice-cold solvent mixture comprised of heptane and tetrachloroethylene (density ($\rho$) =1.3 g $cm^{-3}$) within a 15 mL borosilicate glass test tube. Both solvents were stored over 0.3Å molecular sieves (Sigma-Aldrich) prior to use, ensuring the solvents had sufficiently low water content (<10 ppm). Suspended plant material was sonicated (45 KHz) in an ice-bath for a total of 20 minutes, after which it was filtered through a 25 µm nylon gauze and centrifuged at 4400 xg for 20 minutes at 4 °C. The resulting supernatant was discarded, leaving 50 µL, and the pellet was resuspended in 1 mL of ice-cold tetrachloroethylene and transferred to a 2 mL microcentrifuge tube. Thus started an iterative process where the solution was sonicated in an ice-bath for a total of ten minutes and then centrifuged at 21,100 xg for ten minutes at 4 °C. The resulting supernatant was transferred to a new microcentrifuge tube and ice-cold heptane was added to obtain the required density. The amount of heptane required was calculated using Equation 1, within which $V_{heptane}$ is the volume of heptane, $V_{solution}$ is the volume of the supernatant, $\rho_i$ is the density of the supernatant, $\rho_j$ is the desired density and 0.68 is the density of heptane.

**Equation 1**

$$V_{heptane} = \frac{V_{solution}(\rho_i - \rho_j)}{0.68 - \rho_j}$$

The resulting pellet, obtained from centrifugation, was re-suspended in 450 µL of an ice-cold heptane-tetrachloroethylene mixture for which $\rho_{solution}$ is equal to $\rho_{pellet}$. To enhance the concentration of

conjugates within final fractionated material, pellets obtained at the same density from two separate fractionations were pooled together before being aliquoted into three 300 µL sub-fractions. A washing step was performed, within which 1 mL of heptane was added to each sub-fraction and the samples centrifuged at 21,100 xg for three minutes. Of the resulting supernatant, 800 µL was discarded, and the remainder concentrated *in vacuo* using a Genevac EZ-2 Elite (Scientific Products, Ipswich UK). Concentrated sub-fractions were stored at -70°C until required for enzyme assays and metabolite analysis.

### 3.2.6 Measurement of compartmental marker enzyme activity

Initial assay conditions were as described in Fürtauer *et al*. (2016) [193]. Concentrated sub-fractions were re-suspended in 1 mL extraction buffer (50 mM Tris-HCl (pH 7.3), 10 mM magnesium chloride hexahydrate, 1 mM DTT). Following a 15-minute incubation on ice, which included vortexing every five minutes, the suspension was centrifuged at 13,000 rpm for five minutes at 4 °C using a FA-45-24-11 rotor (Eppendorf, Stevenage UK). The resulting supernatant was used for subsequent marker enzyme assays, performed in microplate format with absorbance measured on a CLARIOstar$^{Plus}$ plate reader (BMG Labtech, Aylesbury UK).

For the vacuolar marker, Acid phosphatase (APase), enzyme activity was measured following a modified protocol originally outlined in Boller *et al*. (1979) [195] (Figure 3.2.6.1A). Briefly, protein extract was incubated with reaction buffer (0.125 M sodium acetate (pH 4.8), 0.125 % (v/v) Triton-X100) at 37 °C for five minutes. The reaction was initiated through the addition of 100 µL sodium phenylphosphate solution (1 mg mL$^{-1}$ in reaction buffer) and incubated in the dark at 37 °C for 25 minutes with agitation. The reaction was stopped by the addition of 400 µL 1M sodium carbonate. The release of 4-nitrophenol by APase was quantified by measuring absorbance at 405 nm. Absorbance values obtained from samples quenched with sodium carbonate, prior to sodium phenylphosphate addition, were used for blank correction.

For the plastid marker, Alkaline pyrophosphatase (APPase), enzymatic activity was measured following a modified protocol originally outlined in Jelitto *et al*. (1992) [196] (Figure 3.2.6.1B) 12 µL of protein extract was mixed with 800 µL reaction buffer (43 mM Tris-HCl, (pH 8), 8.6 mM magnesium chloride hexahydrate, 1.1 mM tetrasodium pyrophosphate decahydrate) and incubated at RT for ten minutes. When analysing fractions obtained from root tissue, 24 µL of protein extract was incubated at RT for 30 minutes due to lower activity of APPase in this tissue. Reaction was stopped by a five-minute incubation at 95 °C. The release of inorganic phosphate by APPase was quantified by measuring absorbance of

solution at 760 nm following a four-minute RT incubation with a molybdenum solution (1.25 M $H_2SO_4$, 4.86 mM ammonium molybdate, 30 mM ascorbic acid, 0.205 mM antimony potassium tartrate). Values were blank corrected against extraction buffer controls.

For the cytosolic marker, UTP-glucose-1-phosphate uridylyltransferase (UGPase), enzymatic activity was measured following a modified protocol originally outlined in Zrenner *et al*. (1993) [197] (Figure 3.2.6.1C). Protein extract, 70 µL, was mixed with 140 µL reaction buffer (0.1 M Tris-HCl (pH 8), 2 mM magnesium chloride hexahydrate, 0.25 mM NADP, 2 mM sodium fluoride, 20 µM glucose-1,6-phosphate, 2 mM UDP-glucose, 3.4 $U.mL^{-1}$ phosphoglucomutase, 6.65 $U.mL^{-1}$ glucose-6-phosphate dehydrogenase), within a Greiner UV-Star® flat bottom 96-well microplate, and the reaction was initiated through the addition of 6 µL 100 mM tetrasodium pyrophosphate decahydrate. NADPH release resulting from UGPase activity was quantified by measuring change in absorbance at 340 nm over six minutes. Values were blank corrected against extraction buffer controls.

Two technical replicates were performed for each sample. Enzyme activity within fractions was normalised as a relative percentage of the total activity measured across all fractions.

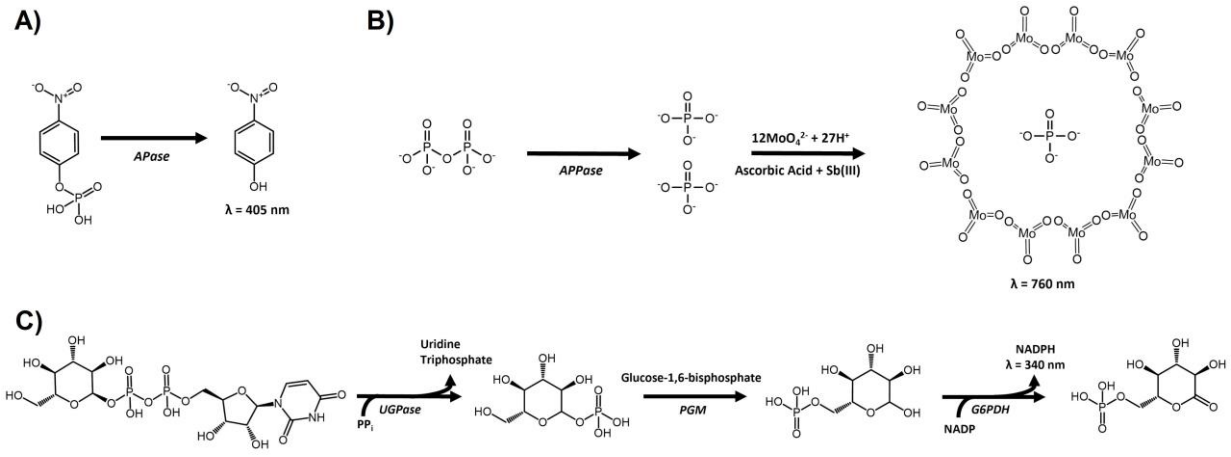


**Figure 3.2.6.1: Spectrophotometric marker enzyme assays used in BNAF. A)** Assay for vacuole marker enzyme APase measures the release of release of *p*-nitrophenol from *p*-nitrophenyl phosphate. **B)** Assay for plastid marker enzyme APPase was quantified by measuring the enzymatic release of inorganic phosphate from pyrophosphate. Formation of molybdenum inorganic phosphate levels were quantified using the molybdenum blue method [198]. **C)** Assay for cytosol marker enzyme UGPase was quantified by measuring the release of NADPH from the conversion of UDP-glucose to 6-phospho-D-gluconolactone. Pyrophosphate is represented by $PP_i$.

### 3.2.7 Quantification of TNT-conjugate relative distribution

Metabolites were extracted from sub-fractions by resuspending the pellet in 1 mL of methanol. Following a 15-minute incubation on ice, which included vortexing every five-minutes, the suspension was centrifuged at 13,000 rpm for five-minutes at 4 °C. The resulting supernatant was transferred to a fresh microcentrifuge tube and concentrated *in vacuo*. Concentrated material was resuspended in 200 µL of 20 % methanol solution (v/v). Reverse-phase high performance liquid chromatography (HPLC) analysis was performed using 40 µL of extract and a HPLC system (Waters 2695 separator and Waters Photodiode array detector) with an Ethylene Bridged Hybrid (BEH) C18 column (5 µm; 4.6 x 250 mm) at a flow rate of 1 mL $min^{-1}$. Elution gradient was comprised of 0.1 % formic acid (Solvent A) and acetonitrile (Solvent B). The HPLC conditions used for analysis of TNT-metabolite content are described in Table 3.2.7.1.Peak area at 250 nm was measured for known metabolites within each fraction and normalised as a relative percentage of the total area measured for that respective peak across all fractions within a sample batch.

**Table 3.2.7.1: HPLC conditions optimised for Waters X-bridge C18 column.**

| | | | |
|---|---|---|---|
| Sample temperature: 25 °C | | | |
| Column temperature: 25 °C | | | |
| Injection volume: 40 µL | | | |
| Mobile phase A: acetonitrile | | | |
| Mobile phase B: $H_2O$ (UPW) + 0.1 % formic acid | | | |
| HPLC gradient: | | A | B |
| | 0 | 5 % | 95 % |
| | 5 min | 5 % | 95 % |
| | 25 min | 40 % | 60 % |
| | 30 min | 100 % | 0 % |
| | 35 min | 5 % | 95 % |

## 3.2.8 Determination of metabolite compartmental associations

Metabolite associations with subcellular compartments were identified using a pairwise comparison algorithm originally described in Fürtauer *et al*. (2016) [193]. The process is summarised in Figure 3.2.8.1 and is described here. This analysis used relative distributions of metabolites and marker enzymes across a density gradient (Step 1). Marker enzyme distribution was assumed to be representative of the respectively assigned subcellular compartments distribution. Analysis was comprised of *m* Metabolites (x =1:m) and *f* fractions (*i,j* = 1:f, *i<j*). Slopes for the change of relative distribution for each metabolite and marker enzyme between each fraction were generated. For each metabolite, slopes were compared in a pairwise fashion to respective slopes obtained for each marker enzyme, and the absolute difference from each comparison was calculated (Step 2). The marker enzyme slope that generated the minimum absolute difference when compared to the metabolite slope was identified as a compartmental hit for that set of comparisons (Step 3). Minimum absolute difference was then subtracted from absolute

differences obtained for the other compartmental comparisons (Step 4). If values from these calculations were within the 5 % error-bound, then the corresponding compartment was also considered a hit for that slope comparison. Metabolites that were only detected within a single fraction were labelled special cases, and only the marker enzyme with the highest activity in that fraction was considered (Step 5). The number of hits for each compartment across all comparisons for each metabolite is summed and calculated as a percentage of the total number of compartmental hits to provide a final relative compartmental association for each metabolite (Step 6).

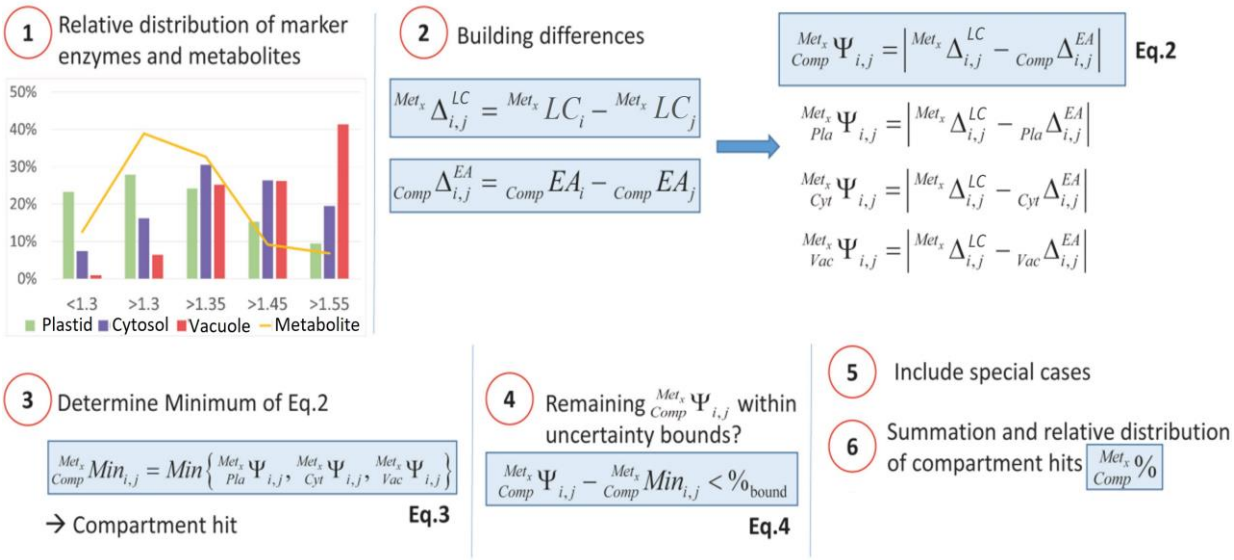


**Figure 3.2.8.1: Outline of algorithm used to calculate compartmental association of metabolites.** Abbreviations: Metabolite - *Met*, Compartment - *Comp*, Relative metabolite distribution - *LC*, Relative marker enzyme distribution - *EA*, Plastid - *Pla*, Cytosol - *Cyt*, Vacuole - *Vac*, Minimum Absolute difference - *Min*. Figure was taken and modified from Fürtauer *et al*. (2016) [193].

### 3.2.9 Statistical analysis

Two-way ANOVA followed by a Tukey HSD test was performed to calculate the significance of metabolites association between subcellular compartments.

## 3.3 Results

### 3.3.1 Live Single Cell Mass Spectrometry

#### 3.3.1.1 Optimisation of microextraction protocol to obtain viable extract

Preliminary work focused on developing a microextraction protocol that could reproducibly obtain cell extract from Arabidopsis root tissue. The fragility of Arabidopsis root tissue made extraction difficult as the tissue moved with the force of the nanospray-tip. Prior published protocols had utilised double-sided tape to prevent sample movement [183]. However, in practice this was unsuitable as root hairs became embedded within the adhesive. The fragility of root tissue also resulted in immediate desiccation (Figure 3.3.1.1.1A), which invalidated any obtained extract. To overcome these issues, embedding agents were investigated for their ability both to provide suitable resistance to tissue movement as well as prevent tissue desiccation. Two agents were investigated, Cygel™ (Biostatus, Loughborough UK) and LMPA (Sigma - Aldrich). Both Cygel™ and LMPA have a gelling point within 5 °C of RT, 21 °C and 24-28 °C respectively, allowing microscopy investigations into living organisms with minimal stress-induced perturbations to endogenous metabolism [199,200]. Cygel™ was shown to be unsuitable as, in the absence of a coverslip, it rapidly desiccated under observation (Figure 3.3.1.1.1B). In contrast, LMPA retained the viability of the root tissue (Figure 3.3.1.1.1C) whilst its viscosity provided suitable resistance to tissue movement. Therefore, root tissue was embedded within LMPA for subsequent extractions.

Extractions were initially attempted using a system built around an Axiovert 200 inverted microscope (Zeiss, Cambridge UK) (Figure 3.3.1.1.1D). This system provided a high total magnification, 630x total, which allowed clear visualisation of individual root hair cells. Incorporation of a camera attachment to the microscope also aided nanospray-tip manipulation. However, the inverted viewpoint made extractions highly laborious and error prone, with breakage of the nanospray-tip on the viewing slide being a common problem which resulted from difficulty in gauging distance. For this reason extraction equipment was transferred to a Leica MZ 16 F stereomicroscope (Leica Microsystems, Milton Keynes UK; Figure 3.3.1.1.1E). This microscope system still provided a suitable level of magnification, 460x total magnification, however the viewpoint of observation allowed for more intuitive manipulation of nanospray-tip thus reducing extraction error rate.

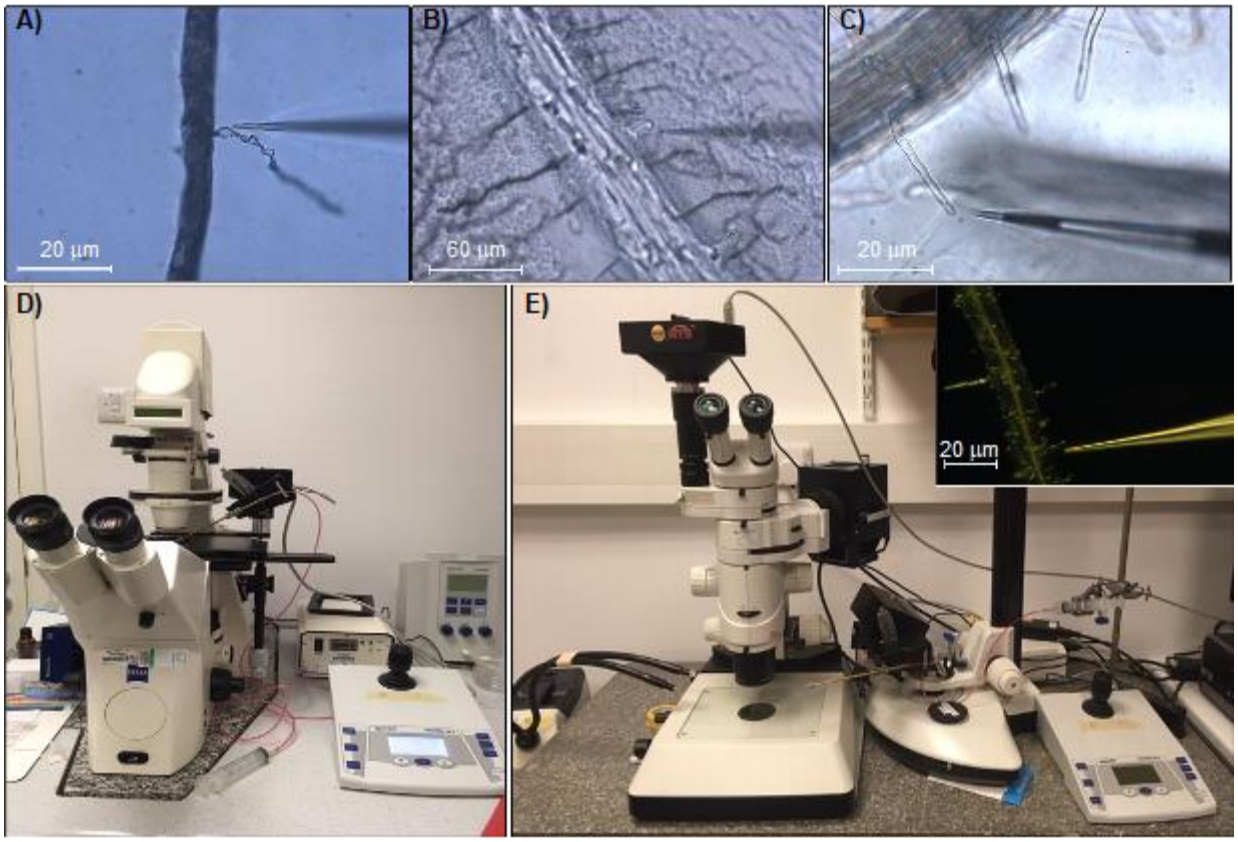


**Figure 3.3.1.1.1: Optimisation of micro-extraction system used in LSC-MS. A)** Non-embedded Arabidopsis root tissue, rapid desiccation occurs whilst under observation. Image taken at 630x total magnification. **B)** Cygel™ embedded root tissue, both Cygel™ and root tissue rapidly desiccate. Image taken at 200x total magnification. **C)** LMPA embedded root tissue, tissue integrity was retained. Image taken at 630x total magnification. **D)** Micro-extraction system using an Axiovert 200 inverted microscope. Images **A-C** were obtained using this system. **E)** Micro-extraction system using a Leica MZ 16 F stereomicroscope. Inset image shows the improved viewpoint for extraction this system provided.

### 3.3.1.2 Unsuitability of LSC-MS for detection of TNT-metabolites within plant extracts

Optimisation of the microscopy system and embedding of root tissue with LMPA allowed extract to be obtained from individual Arabidopsis root hair cells (Figure 3.3.1.2.1A). Nano-ESI analysis confirmed successful extraction of cellular material as ion peaks corresponding to $[M-H]^-$ adducts of fumarate (*m/z* = 117.02), malate (*m/z* = 135.02), $\alpha$-ketoglutarate (*m/z* = 147.03), and citrate (*m/z* = 193.03) were detected during extract analysis, these ion peaks were absent within ionisation solvent controls (Figure 3.3.1.2.1B). However, metabolites of TNT were not detected within extract obtained from dosed plants. A possible cause for the inability to detect TNT-metabolites was interference by other compounds

within the cellular extract. To investigate this, all three TNT-glutathione conjugates, at a final concentration of 100 µM, were analysed by Nano-ESI in the presence or absence of plant extracts. For this analysis whole tissue methanol extracts were used due to a limited number of single cell-extracts available. Conjugate standards diluted in 20 % methanol were used as corresponding controls. The TNT-glutathione conjugate standards ionised efficiently when diluted in 20 % methanol; however, when diluted within plant extract conjugates were not detected (Figure 3.3.1.2.1C). These results confirmed that TNT-glutathione conjugates, and most likely other TNT conjugates, were not ionising efficiently when analysed in the presence of endogenous plant compounds. As conjugate concentration used in this analysis was far greater than that expected within a single cell, it was concluded LSC-MS was not a suitable technique for investigating TNT-conjugate compartmentalisation. Therefore, further work on the optimisation of the technique was stopped.

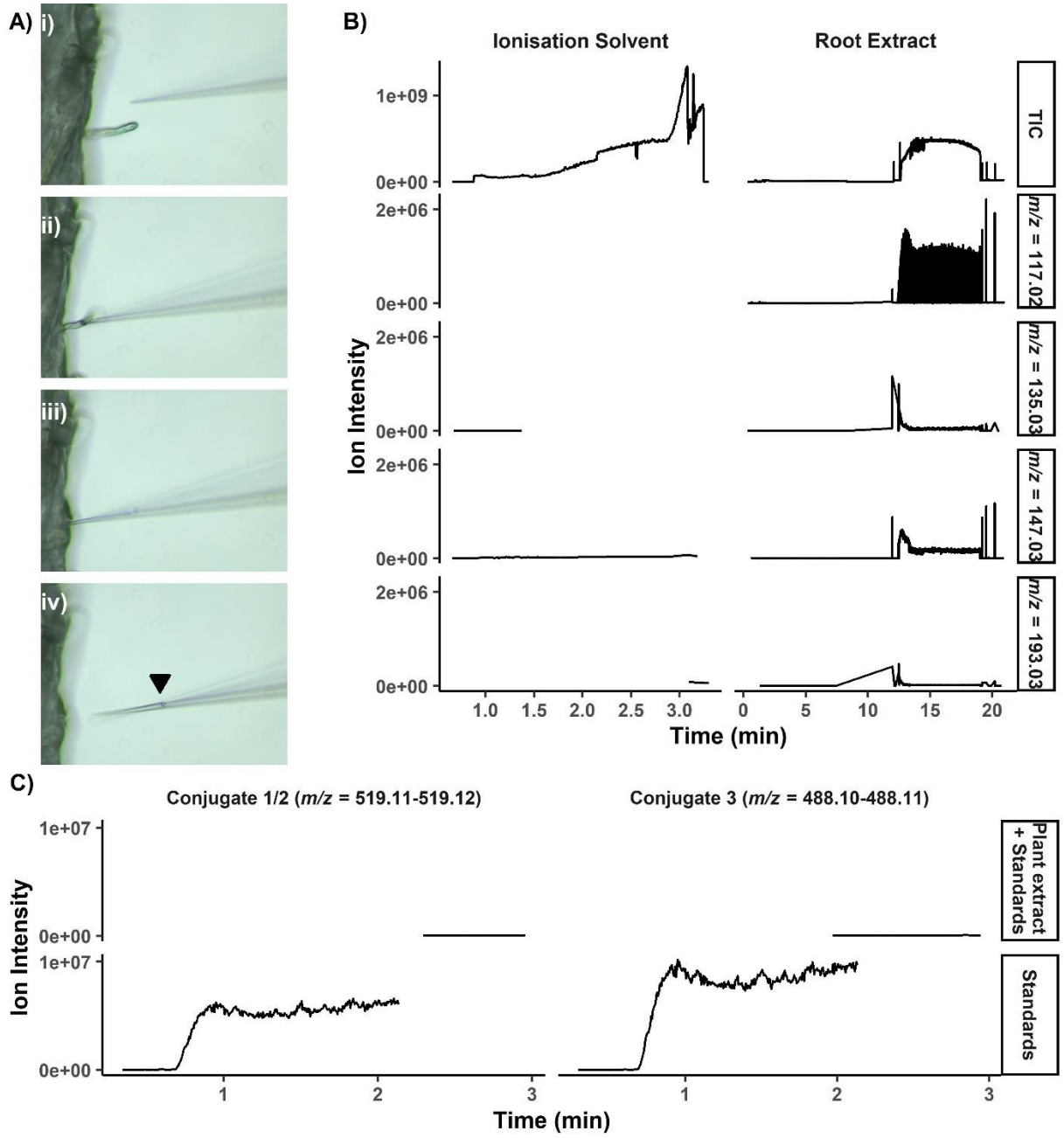


**Figure 3.3.1.2.1: Optimised LCS-MS microextraction protocol can obtain and analyse extract from a single cell but is unable to detect TNT-glutathione conjugates. A)** Sequential images showing the acquisition of root cell extract using developed micro-extraction system. The arrow indicates meniscus of extract within nanospray-tip. **B)** Ion chromatograms obtained by Nano-ESI analysis of plant extract and ionisation solvent control. Total Ion Chromatogram (TIC) shows timespan in which active sample analysis occurred. Extracted ion chromatograms for fumarate ($[M-H]^+$ = 117.02), malate ($[M-H]^+$ = 135.03), $\alpha$-ketoglutarate ($[M-H]^+$ = 147.03) and citrate ($[M-H]^+$ =193.03) confirm successful extraction of cellular contents. Analysis was performed in positive mode. **C)** Extracted Ion chromatograms of TNT-glutathione conjugate standards in the presence or absence of plant extract following Nano-ESI analysis In the presence of plant

extract, TNT-glutathione conjugates do not ionise. The *m/z* ranges used to generate these chromatograms were 519.11-519.12 and 448.1-488.11 for Conjugates 1 & 2 and Conjugate 3 respectively. Analysis was performed in positive mode.

## 3.3.2 Benchtop Non-aqueous Fractionation

### 3.3.2.1 Confirming ability of BNAF to fractionate subcellular compartments

Conventional, non-benchtop, NAF methods specify that several grams of fresh tissue is required per fractionation [191], this would be a substantial task to perform with Arabidopsis root tissue. It was for this reason that the BNAF technique described in Fürtauer *et al*. (2016) [193] was used. The BNAF technique was developed to remove the requirement of long periods of ultracentrifugation, transferring the process to a benchtop centrifuge, this increased the throughput capacity of the technique and reduced its tissue requirements. Whilst the developers of BNAF highlighted that the changes allowed a greater range of tissues to be investigated, currently only Arabidopsis leaf tissue has been analysed with the technique [193,201,202]. Initial experiments in this thesis focused on repeating published work of Fürtauer *et al*. using leaf tissue obtained from three-week-old Arabidopsis. Enzymatic assays for the vacuolar (APase), cytosolic (UGPase) and plastidial (APPase) marker enzymes confirmed subcellular compartments were successfully differentially fractionated across a gradient comprising five densities between $\rho$ = 1.59 g cm$^{-3}$ and $\rho$ = 1.3 g cm$^{-3}$ with the sixth fraction, $\rho$ < 1.3 g cm$^{-3}$, showing no enzymatic activity (Figure 3.3.2.1.1).

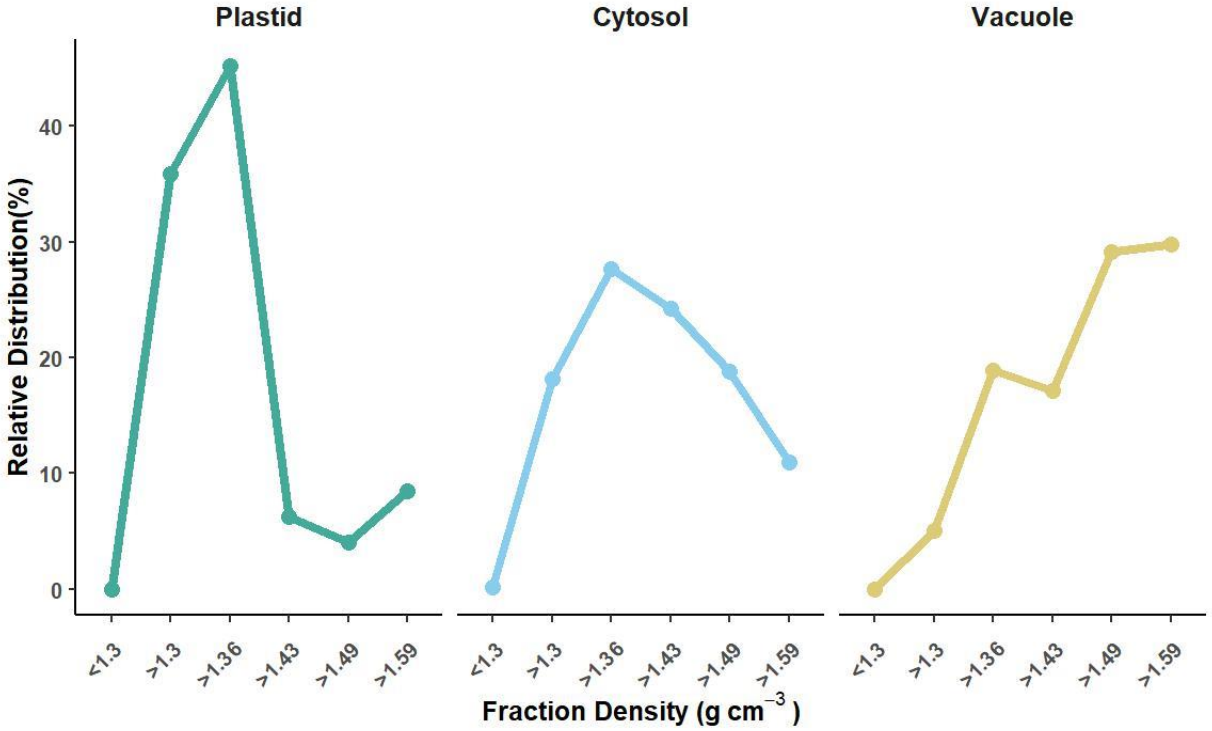


**Figure 3.3.2.1.1: Successful fractionation of Arabidopsis leaf tissue using BNAF.** Leaf tissue from three-week-old Arabidopsis grown on solid agar was analysed. Differential distribution patterns for plastid (APPase), cytosol (UGPase) and vacuole (APase) compartmental marker enzymes confirm successful fractionation. Solid lines represent the mean of two technical replicates.

### 3.3.2.2 Optimisation of BNAF technique for use with hydroponically-grown root material

Successful application of BNAF with leaf tissue allowed for progression onto optimizing the technique for hydroponically grown root tissue. A hydroponic system was used to expose roots to TNT as the faster diffusion of TNT within liquid culture, compared to solid agar, allowed TNT-metabolites to reach detectable concentrations within fractionated material. The hydroponic system also allowed for relatively quick and efficient harvesting of root material without damage. As there are no examples within the literature of NAF being used with media-grown plant tissue, troubleshooting of the fractionation procedure was required.

The use of organic solvents in BNAF to generate the density gradient makes the method extremely sensitive to compounds that can form polar interactions with plant material. Introduction of such compounds during the process results in plant material aggregating, presenting as a mass at the top of the solvent solution with a plate-like consistency (Figure 3.3.2.2.1A). This issue is acknowledged in the

current literature with recommendations to ensure all equipment is kept dry and solvents stored over molecular sieves [204]. The optimisation of this protocol has identified further precautions that need to be followed for successful BNAF. Firstly, liquid nitrogen was substituted for dry ice in the preparation of plant material for lyophilisation. This substitution allowed effective lyophilisation, which is seen in the cloudy consistency of non-pelleted material during the iterative fractionation process (Figure 3.3.2.2.1B). Residual detergents on the surface of glassware also prevented successful BNAF due to their leaching into the solvent mixture during sonication of plant material. Washing glassware in distilled water prior to use removed detergents preventing this issue. Incorporation of these changes allowed successful BNAF to be reliably achieved. Key observations that identify successful fractionation along the process are described in Table **3.3.2.2.1**.

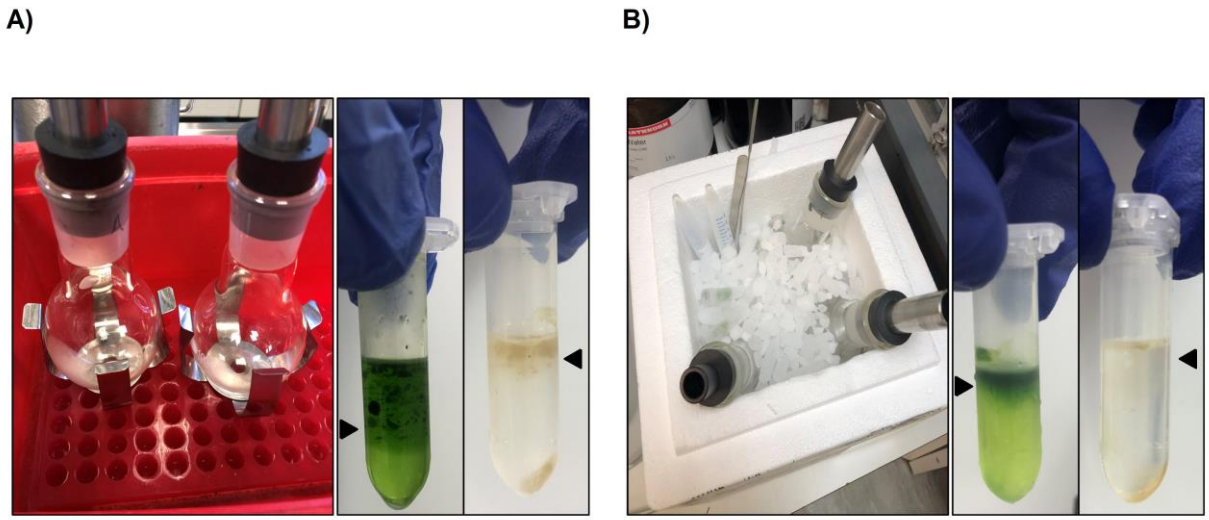


**Figure 3.3.2.2.1: Exposure of powdered plant material to liquid nitrogen prior to lyophilisation prevents successful BNAF. A)** Plant material fails to fractionate when liquid nitrogen is used to pre-chill lyophilisation equipment and to powder plant material. i) Set-up used to pre-chill lyophilisation vessels. ii) Failure to fractionate leaf tissue confirmed by plate-like aggregates at the top of the solvent solution. **B)** Plant material successfully fractionates when dry ice is used to pre-chill lyophilisation equipment and to powder plant material. i) Set-up used to pre-chill lyophilisation vessels. ii) Successful fractionation of leaf tissue confirmed by the fine cloud-like consistency of plant material at the top of solvent mixture. iii) Successful fractionation of root tissue.

**Table 3.3.2.2.1: Observations that identify successful BNAF**. Listed are the experimental points which provide visual confirmation on the success or failure of the fractionation process.

| Observation | Indication of successful fractionation | Indicator of failed fractionation |
|---|---|---|
| Appearance of plant material after lyophilisation | Lyophilised powder should be easily electrostatically charged under agitation, resembling iron filings under a magnetic field. | Lyophilised powder does not become electrostatically charged under agitation, remains in a mound |
| Homogenisation of lyophilised material in solvent mixture | Visibly large particles of material are broken down after a total of 20 minutes sonication | Extensive sonication is required to break down particles of material with many remaining after the 20 minutes of sonication |
| Resuspension of pellet following 4400 x g centrifugation | Pellet should immediately be resuspended upon addition of 1 mL tetrachloroethylene | Pellet does not resuspend easily, showing a plate-like consistency that requires micropipette aspiration to homogenise |
| Appearance of non-pelleted material during iterative fractionation process | Non-pelleted material should display a cloud-like appearance/consistency that is easily taken up by pipetting | Non-pelleted material has a plate-like appearance/consistency |
| Resuspension of fractions in 100 % methanol for metabolomic analysis | Pellet suspends easily with minimal aspirations | Pellet displays a plate-like consistency that does not resuspend |

Compartmental separation across the density-gradient during BNAF requires compartmental integrity to be maintained in the harvested tissue. Exposing plants to TNT generates oxidative stress which can damage membrane integrity [93]. To test if compartmental integrity was disrupted by TNT, root tissue was grown in a hydroponic system with and without TNT exposure, then analysed by BNAF. All tissue was blotted for 60 seconds prior to flash-freezing to remove excess water. Resulting analysis of the compartmental distribution revealed an inability to differentially fractionate the subcellular compartments irrespective of TNT-exposure (Figure 3.3.2.2.2A). These results suggested compartmental integrity was severely compromised; however, hydroponically-grown plants did not show any signs of stress. It was therefore hypothesised, that perturbation to compartmental integrity occurred after harvesting of the root material. As extensive blotting of tissue may cause desiccation and mechanical damage, both resulting in cell lysis and mixing of organelle contents, this was the first factor to be investigated. Blotting time of harvested root tissue was reduced from 1 minute to a momentary placement (1-2 seconds) onto an absorbent surface prior to flash-freezing. Subsequent BNAF analysis confirmed that reduction of blotting time enabled successful differential distributions of subcellular compartments (Figure 3.3.2.2.2B). However, the degree of compartmental separation was not sufficient for subcellular localisation of metabolites. Therefore, these results confirmed organelle integrity was not impacted by TNT exposure but was damaged by extensive blotting; it also revealed that optimisation of the density gradient was required for effective BNAF analysis of root tissue.

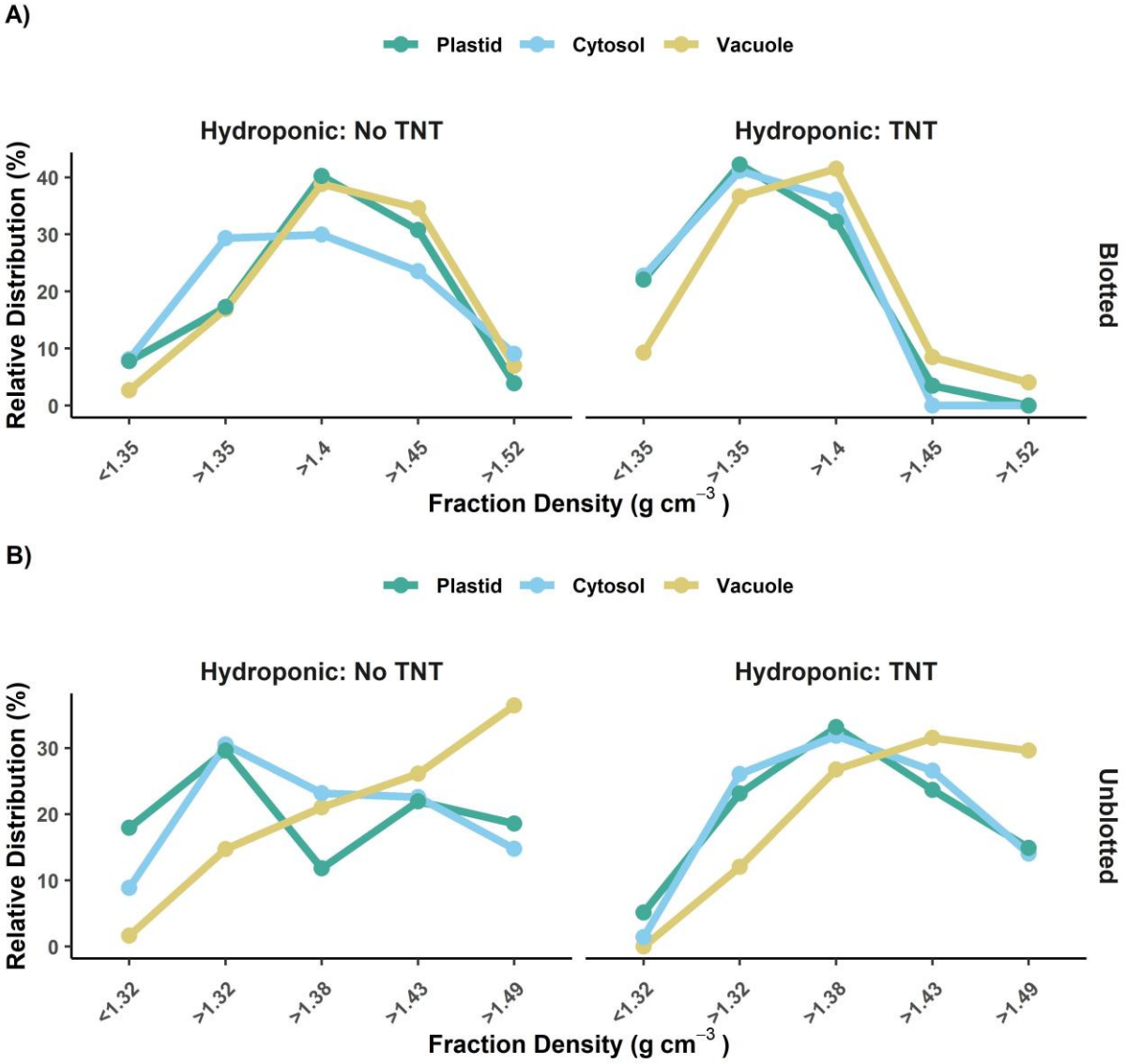


**Figure 3.3.2.2.2: Excessive blotting of hydroponically-grown tissue prevents successful BNAF. A)** The distribution of plastid (APPase), cytosol (UGPase), and vacuole (APase) compartments from root tissue that was blotted for 60 seconds. All three subcellular compartments showed similar distribution patterns, the effect was independent of TNT-exposure. **B)** Distribution of compartments for root tissue that was momentarily blotted, referred to as unblotted. Samples showed trends towards differential distribution of compartments confirming successful fractionation.

Gradient optimisation focused on obtaining distinct distribution profiles for the vacuole and cytosol as conjugated xenobiotics are hypothesised to move between these compartments. Prior investigations during trouble shooting had shown that a starting density below 1.5 g cm$^{-3}$ was required for vacuole enrichment, and that no enzymatic activity was pelleted below a density of 1.3 g cm$^{-3}$. Therefore, all

density gradients investigated comprised either 5 or 6 density steps that ranged between 1.3 g $cm^{-3}$ and 1.5 g $cm^{-3}$. Four gradients were investigated to identify compartmental distribution patterns so as to discern suitable density steps for an optimised gradient (Figure 3.3.2.2.3). In respect to the vacuole, the majority of marker enzyme activity pelleted between densities of 1.4-1.49 g $cm^{-3}$. Utilising a starting density between 1.45-1.48 g $cm^{-3}$, a second density of 1.42-1.45 g $cm^{-3}$ and a third density of 1.4 g $cm^{-3}$ provided suitably distinguishable vacuole and cytosol distribution patterns as seen in gradients 1 and 4. Within these gradients, the vacuole was enriched within the first fraction and abundance decreased with density, whilst the cytosol distribution behaved in the inverse manner. Analysis of gradient 1 indicated that incorporation of equally distributed gradient steps between 1.4 g $cm^{-3}$ and 1.3 $cm^{-3}$ could enrich the plastid without enriching the cytosol and vacuole; however, the inclusion of more than two steps between these densities prevented plastid enrichment, as shown in gradient 2. Therefore, an optimised gradient incorporating these findings was hypothesised to enrich the vacuole within the densest fraction, enrich the plastid in fractions of lower densities whilst maintaining a more equal distribution for the cytosol across all fractions.

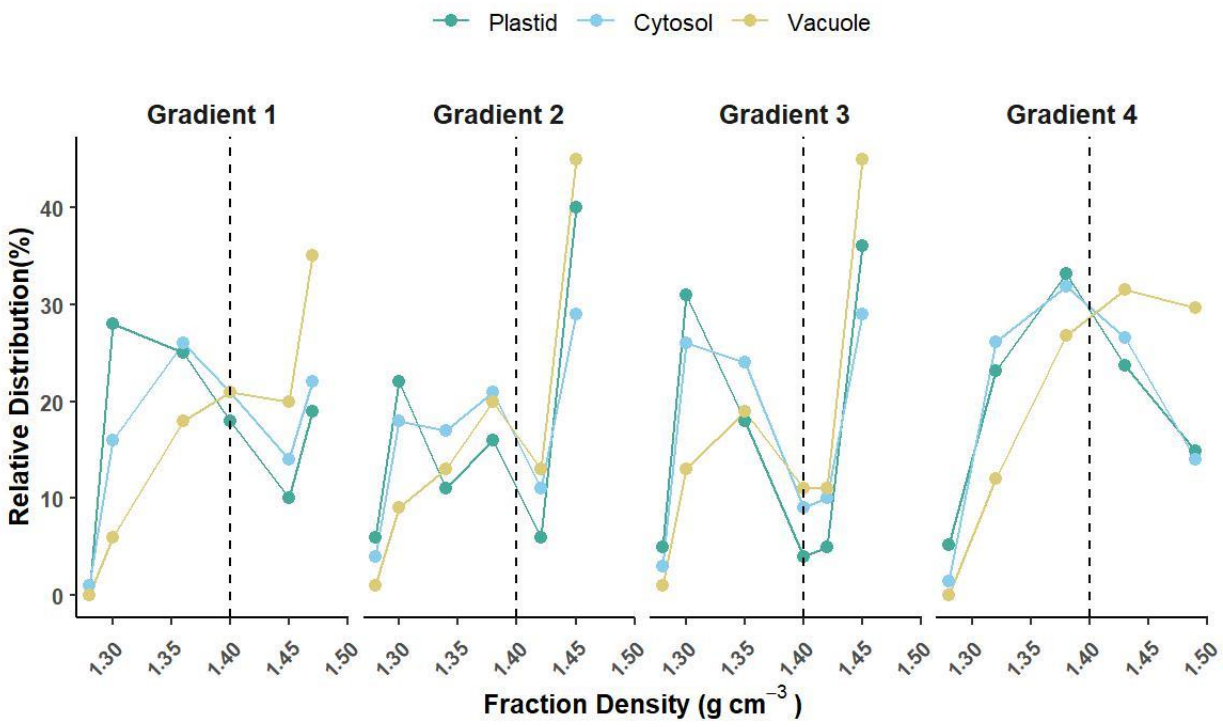


**Figure 3.3.2.2.3: Optimisation of BNAF gradient for root tissue.** Vacuole enrichment is achieved if gradient starts between 1.45-1.48 g $cm^{-3}$ (Gradients 1 and 4). Plastid enrichment is achieved if gradient starting density is greater than 1.45 $cm^{-3}$ and no more than two gradient steps are incorporated below density of 1.4 g $cm^{-3}$ (Gradients 1,2 and 3). With

these parameters the cytosol shows a more dispersed distribution across the gradient (Gradient 1). Compartmental distributions inferred from enzymatic analysis of vacuolar (APase), cytosolic (UGPase) and plastidial (APPase) marker enzymes.

A six-step, optimised gradient with density steps of <1.3, 1.3, 1.35, 1.4, 1.43, 1.47 g $cm^{-3}$ was chosen for analysis of metabolite distribution within TNT-dosed hydroponically grown root-tissue. Using this range, a plastid enriched fraction was obtained at 1.35 g $cm^{-3}$ (Figure 3.3.2.2.4A), and a vacuole enriched fraction at 1.47 g $cm^{-3}$ (Figure 3.3.2.2.4C) whilst the cytosol distribution showed little change between densities of 1.35-1.47 g $cm^{-3}$(Figure 3.3.2.2.4B). When overlaying compartmental distributions with the distribution of the known product of TNT metabolism HADNT-glucoside (HADNT-Glc) [104], obtained by HPLC analysis of BNAF-derived fractions, a striking similarity in metabolite and vacuole distributions is clearly seen. Compartmental association analysis confirmed that HADNT-Glc had a significant association with the vacuole (Tukey HSD, $p.adj < 0.0001$) (Figure 3.3.2.2.4D).

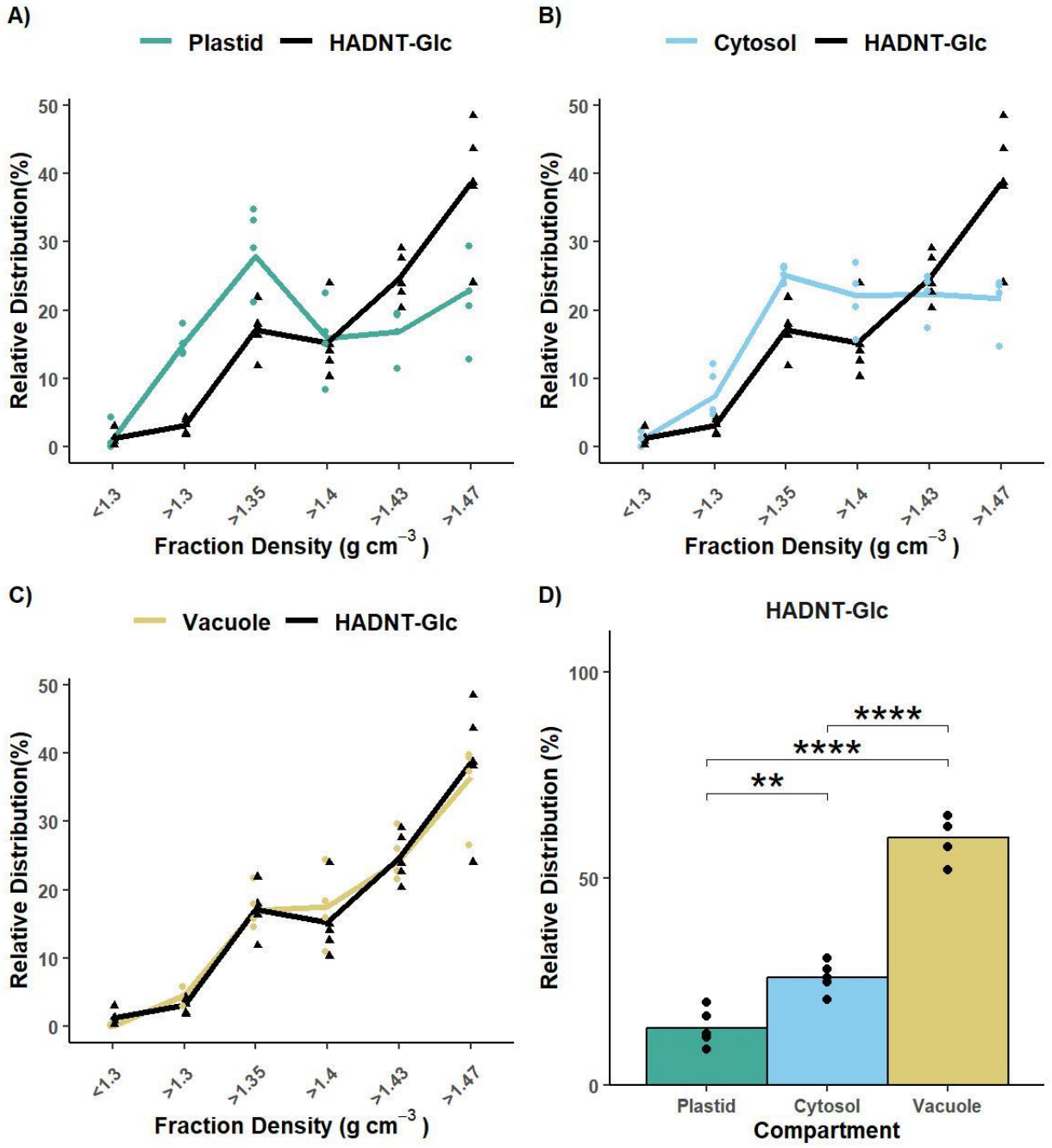


**Figure 3.3.2.2.4: Optimised BNAF density gradient confirms significant association of TNT-metabolite HADNT-Glc with the vacuole. A)** Distribution profile of the plastid (APPase) and HADNT-Glc across the density gradient. Relative distribution of HADNT-Glc inferred from peak area measured in each fraction at 250 nm as a proportion of peak area measured across all fractions at 250 nm. **B)** Distribution profile of the cytosol (UGPase) and HADNT-Glc. **C)** Distribution profile of the vacuole (APase) and HADNT-Glc, striking similarities are seen. **D)** Pairwise-comparison of metabolite and compartmental distributions across the density gradient confirm highly significant association of HADNT-Glc with the vacuole compartment (Tukey HSD, $p < 0.0001$). n = 5, bar representative of biological mean, points representative of

individual biological replicates. Statistically significant differences between compartmental associations: ***, $p < 0.001$; ****, $p < 0.0001$.

## 3.4 Discussion

The research presented within this chapter has demonstrated the successful application of the BNAF technique to confirm the compartmental fate of TNT metabolites within Arabidopsis root tissue. Pairwise analysis of marker enzyme and metabolite distributions has established the dominance of glucosyl-conjugate sequestration during xenobiotic metabolism *in planta* for the first time. These results are the first example of utilising BNAF with Arabidopsis root tissue, demonstrating that it can be a powerful platform for investigating the compartmentalised metabolome within this tissue.

### 3.4.1 Practicalities relating to successful use of LSC-MS

This research has presented the first demonstration, to the author's knowledge, of harvesting and analyzing Arabidopsis root cell extracts via LSC-MS, with these results demonstrating the technique to be unsuitable for TNT-conjugate measurement. Desiccation of root tissue was a problem that had to be overcome to achieve successful extraction. Whilst drying of samples is mentioned in published protocols [183], speed of extraction was the only stated mitigation method. This advice is limited, as it assumes a certain level of efficiency in both the practitioner and extraction system, as well as the assumption that tissue used for extraction can remain hydrated for several minutes during observation. The use of LMPA to embed Arabidopsis seedlings was shown to be an effective alternative that maintained tissue viability for extended periods of time, >20 minutes, thus allowing less-experienced practitioners to harvest cell extract. Embedding within LMPA also provided sufficient resistance to tissue movement allowing the nanospray-tip to pierce the cell wall. However, an issue identified with LMPA embedding was the uptake of agar into the nanospray-tip during extraction, which subsequently blocked the tip preventing effective sample spraying during Nano-ESI. The diameter and taper of the nanospray-tip affected agar uptake, therefore future LSC-MS studies using LMPA as an embedding agent should allocate time for optimising nanospray-tip design parameters. This work also confirmed that the use of a stereomicroscope provided more intuitive control of the nanospray-tip in respect to the target cell. These informative findings will be of benefit for research utilising LSC-MS for tissue types in which sectioning via microtome is not suitable.

Whilst LSC-MS was successful in detecting several organic acids within root cell extract, it was unable to detect TNT metabolites. In respect to TNT-glutathione conjugates, there was a reduction in ionisation

efficiency in the presence of co-eluting endogenous plant compounds, a phenomenon referred to as matrix effects. Conventional tactics for eliminating or limiting matrix effects is the altering of chromatography separation parameters to reduce co-elution of compounds [205]. Due to the nature of LSC-MS this option is not possible. A potential route to overcome this issue, that was not thoroughly investigated due to resource restraints, is optimisation of the ionisation solvent and ionisation mode used during analysis. Altering these parameters could impact the ionisation efficiencies of compounds; however, preliminary analysis performed in negative ionisation mode failed to detect TNT metabolites. Identifying matrix effects as an inherent weakness within LSC-MS should encourage future studies to check for this issue using plant extracts and authentic standards prior to optimising the microextraction set-up.

### 3.4.2 Successful BNAF is dependent on several parameters

Optimisation of the BNAF protocol for hydroponically-grown root tissue identified multiple factors that were important for successful implementation of the technique. The first, and most important, was preventing interference from compounds that can form polar interactions with plant material. This research has identified the presence of residual detergents on glassware and the contact of ground plant material with liquid nitrogen as two potential sources of polar compounds. Residual detergents weakly bound to glassware are hypothesised to be released during the sonication step of BNAF, which is used to homogenise lyophilised material in organic solvents. Performing multiple hand-washes with distilled water, rather than using machine-washing systems, enabled the use of detergents as it ensured sufficient removal of the compounds prior to drying. The presence of residual detergents on washed glassware can be accessed via the use of a pH meter, an increase of wash solution pH by more than 0.2, following washing of glassware, indicates insufficient detergent removal [206]. The inability to achieve successful fractionation when liquid nitrogen was used to pre-chill equipment, as well as grind plant material, prior to lyophilisation is an interesting finding that is difficult to explain. Inefficient lyophilisation results in greater retention of moisture within samples [207]. As the use of dry ice enabled successful fractionation, it indicates the temperature achieved by liquid nitrogen, -196 °C compared to the -78.5 °C achieved by dry ice, prevents effective lyophilisation of plant material. As this phenomenon has not been reported for conventional NAF protocols, it may result from the smaller quantities of tissue used for BNAF which results in the effect impacting a greater proportion of the sample. Electron-microscopy analysis into the macrostructure of lyophilised material prepared using dry ice vs liquid nitrogen may provide insight into possible explanations for this phenomenon.

Another factor critical for BNAF success is the time taken to blot the harvested tissue prior to cryo-preservation. Blotting of harvested tissue was initially included within the protocol to remove excess water, so a more accurate fresh weight could be obtained. However, this step resulted in a loss of compartmental integrity preventing successful fractionation. This result was most likely due to tissue desiccation during blotting which led to organelle lysis. The sensitivity of hydroponically-grown tissue to gentle blotting could be a result of growth within a static hydroponic system. Hyperhydricity is a common effect associated with submersion of plant tissue and is a common issue during *in vitro* culturing of cuttings for plant propagation [208]. Anatomical alterations association with hyperhydricity is hypolignification, reduction in cell wall thickness and damaged membranes and cell structures [209,210]. Weaker structural integrity of hydroponically-grown root tissue may have resulted in greater susceptibility to desiccation during the blotting process. This is supported by findings that root tissue grown on solid medium did not show similar loss of compartmental integrity, despite undergoing identical blotting (data not shown). However, this hypothesis was not investigated, as obtaining fresh weight was not critical for analysis of results and removal of surface water was shown not to be important prior to lyophilisation. Microscopic visualisation of cellular and subcellular structures, within hydroponically-grown tissue and tissue grown on agar, is one way in which this hypothesis could be investigated.

Optimisation of the density gradient was also required to obtain distinct distributions for the three subcellular compartments of interest. The need for optimisation resulted from the starting density of published gradients [193], optimised for leaf tissue, being too high to enrich the vacuole compartment of root tissue, requiring a drop from ~1.55 g $cm^{-3}$ to ~1.47 g $cm^{-3}$. The decrease in vacuole density between Arabidopsis leaf and root tissue suggests the composition of the tonoplast differs significantly between these organs. This is likely to reflect the different demands placed on vacuoles within photosynthetic and non-photosynthetic tissues. Whilst compositional analysis of both the lipid and protein profiles of tonoplasts have been performed within Arabidopsis [211,212], a comparison of profiles between tissues is currently missing within the literature. Identifying how compartmental membranes differ between tissues would deepen the understanding surrounding specification within tissue types down to the sub-cellular level.

### 3.4.3 BNAF confirms sequestration of xenobiotic conjugates from the cytosol

The successful application of BNAF on Arabidopsis root tissue has confirmed the sequestration of xenobiotic glucosyl-conjugates from the cytosol *in planta*, most likely to the vacuole, and shown it to be

the dominant fate for these metabolites in the context of the compartmentalised metabolome. These findings build on the discovery of tribromophenol-glucosyl conjugates within the vacuole and as bound elements of the cell-wall fraction within rice cells [87], providing much needed *in planta* evidence for this fate. There are multiple, related explanations for the dominance of xenobiotic glucoside compartmentalisation in cellular metabolism. The first is to prevent uncontrolled bioactivation by cellular glucosidases; enzymes that have been referred to as 'detonators of plant chemical defense' [213]. Arabidopsis is within the phylogenetic order *Capparales*, members of which generate glucosinolates. These compounds are strongly associated with defence responses, being activated though hydrolysis of the glycosidic bond by $\beta$-glucosidases which releases an unstable aglycone that spontaneously decomposes to form compounds of varying toxicity [213]. Compartmentalisation is used to separate glucosinolates and $\beta$-glucosidases spatially, so that the toxic compounds are only released when the plant is mechanically damaged i.e., through herbivory. A similar rationale could explain the rapid compartmentalisation of xenobiotic-glucosides, as the aglycones formed from the release of the glucosyl moieties could be highly cytotoxic. The indefinite sequestration of glucosyl-conjugates to the vacuole is unlikely due to the evidence supporting TNT incorporation into the lignocellulosic material of the cell wall [85,86,104]. Feasible mechanisms for the incorporation of monolignol glucosides into lignin polymers have been proposed [214] and glycosylated lignin oligomers have been detected within isolated vacuoles obtained from Arabidopsis leaves [113]. These findings support a role for glucosylation in lignocellulosic incorporation, though the mechanisms for this remain to be elucidated. Taken together, these findings provide a hypothesis that the vacuole acts as an intermediate storage compartment which protects the sensitive biochemistry of the cytosol whilst also ensuring the controlled incorporation of glucosyl-conjugate into the cell wall.

An identified limitation of NAF is the inability to distinguish between the vacuole and apoplastic compartments, due to their similar density profiles [191,194]. Therefore, in which of these two compartments glucosyl-conjugates are localised cannot be identified from the current experiment. However, prior experiments were solely within leaf tissue of Arabidopsis [191,194]. The findings from the current work show that vacuole material within the root is pelleted at lower densities, than that of leaves, offering a possibility that apoplast and vacuole density profiles could be distinguishable within this tissue. This possibility could be investigated through proteomic methods as it would allow multiple protein markers to be utilised thus increasing the confidence in the distribution profiles of the two compartments [215].

### 3.4.4 Applications of BNAF in characterising xenobiotic detoxification *in planta*

The platform that BNAF provides when combined with transgenic and knockout plant populations offers a methodology for elucidating the importance of compartmentalization in cellular functions. Current uses of NAF have primarily focused on describing the compartmentalised metabolome and how it changes in response to abiotic or developmental states [190,191,193,194,203,216,217]. Only in recent years has this powerful technique been used with knockout and overexpression lines to investigate protein function within the wider context of cellular metabolism [194,201,202,217]. Using BNAF to investigate knockout lines of putative transporters involved in xenobiotic-glucoside sequestration could provide functional characterisation of transporters *in planta*. This approach could also provide important evidence to link the inability to compartmentalise xenobiotic-conjugated derivatives with any unique physiological response specific to knockout lines. As glucoside transport across the tonoplast is driven by transporters directly energised by ATP-hydrolysis or proton gradients [112,218], protein families likely involved are ABC- and Multidrug and toxic compound extrusion (MATE)-transporters. Several members of these protein families are upregulated in response to TNT [104] and thus would be suitable candidates to start investigations. Alongside xenobiotics, a variety of endogenous compounds are also glucosylated, examples being monolignols and plant hormones [163–165]. Compartmentalisation is assumed to have an important role in the physiological impact of these compounds but *in vivo* compartmentalization within whole tissue has yet to be confirmed; the BNAF technique provides a means with which to investigate the importance of this process in a variety of tissues.

### 3.4.5 Conclusions

In conclusion, this chapter has demonstrated that the BNAF technique offers substantial promise in characterising the compartmental metabolome of root tissue. The results presented here have built on existing evidence of glucosyl-conjugate compartmentalisation, obtained *in vitro*, by confirming this compartmentalisation *in planta* and establishing it to be the dominant fate of TNT glucosyl-conjugates in the context of cellular metabolism. Future research can build on these results by investigating the transporters responsible for conjugate sequestration, using BNAF to link the inability to compartmentalise conjugates with physiological responses seen in respective knockout lines. As BNAF is a highly versatile technique, it can aid in elucidating the role of compartmentalisation in areas such as hormonal regulation, biosynthetic pathways, and xenobiotic metabolism.

# Chapter 4: Characterising *in planta* metabolism of TNT glutathionylation product Conjugate 3

## 4.1 Introduction

Glutathione conjugation during xenobiotic detoxification is a significant commitment due to the variety of roles glutathione has in cellular processes [117,219]. To prevent dangerous depletion of the glutathione pool, mechanisms have evolved to reclaim the component glutathione residues post-conjugation. Reclaimed residues can then be recycled to replenish the glutathione pool. As the major redox regulator within eukaryotic cells, an efficient glutathione recycling system may provide benefits relating to stress tolerance within organisms. Whilst the characterisation of glutathione conjugate metabolism within mammals has progressed substantially, for a review see Cooper & Hannigan. (2018) [220], the understanding of the analogous pathway within plants is far less comprehensive with only a few enzymes identified as being involved and the metabolic end-fate remaining unknown [221] (Figure 4.1.1). Obtaining a greater knowledge of the molecular mechanisms involved in glutathione conjugate metabolism could aid the generation of plants with greater tolerance to xenobiotic stress.

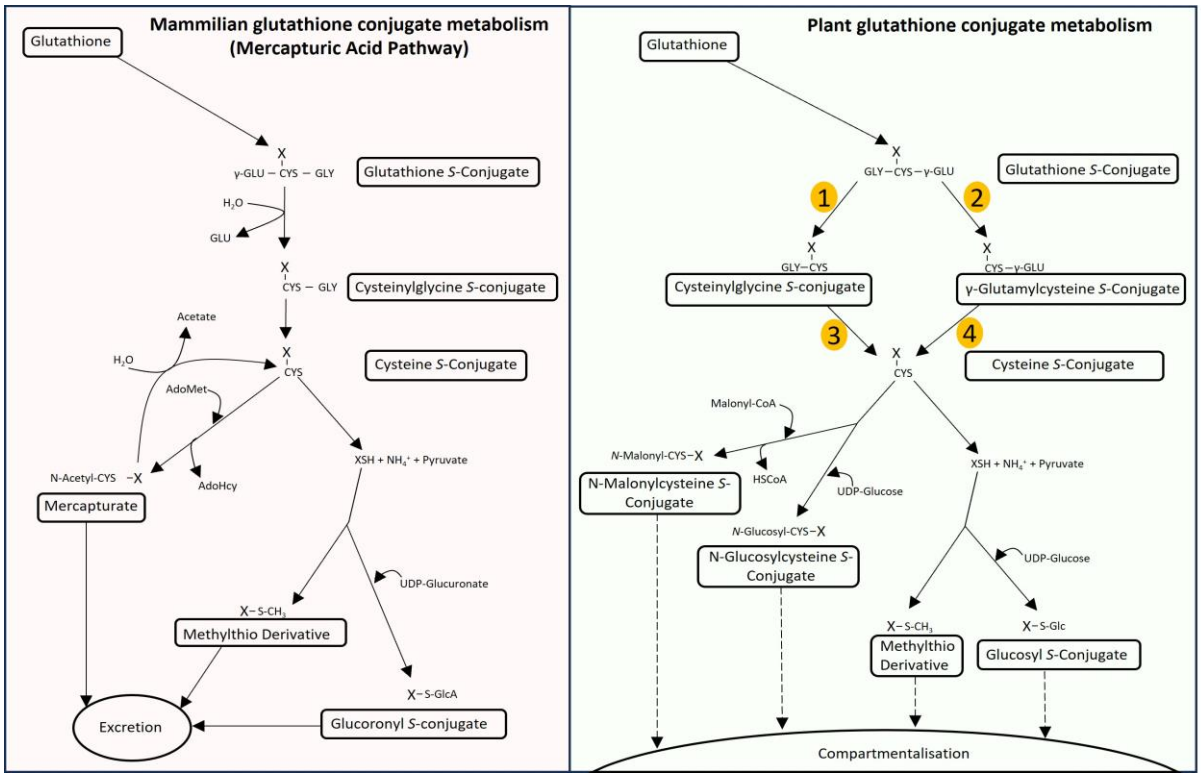


**Figure 4.1.1: Models for glutathione conjugate metabolism within mammalian and plant systems.** Within the mammalian system, the sequential action of a GGT and a carboxypeptidase metabolises the glutathione conjugate to a cysteinyl conjugate. Cysteinyl conjugates can then be acetylated to form a mercapturate derivative or metabolised by a cysteine conjugate $\beta$-lyase to form a thiol-derivative. Thiol-derivatives can then be methylated or conjugated to glucoronic acid. All cysteinyl conjugate derivatives are excreted from the organism. Within the plant system, glutathione conjugate metabolism to a cysteinyl conjugate can be initiated either by a GGT or a carboxypeptidase. Plants have been shown to either directly glucosylate or malonylate the cysteinyl-conjugate, generating N-linked derivatives, or generate thiol intermediates through an unknown cysteine $\beta$-lyase. Thiol-intermediates can be methylated or glucosylated. All cysteinyl conjugate derivatives are hypothesised to be sequestered to the vacuole or apoplast. Solid arrows represent experimentally confirmed pathway, dashed arrows indicate hypothesised pathway. The figure was taken and modified from Cooper & Hannigan. (2018) [220].

The model for xenobiotic-glutathione conjugate metabolism within plants predicts sequestration to the vacuole where conversion to a cysteinyl conjugate occurs [221]. Metabolism within the vacuole is initiated through the GGT-catalysed removal of glutamate in a process analogous to that which occurs within the mercapturic acid pathway within mammals and insects [114,121,220,222] (Figure 4.1.1, reaction 1). However, a plant-specific secondary pathway initiated by a carboxypeptidase, which removes the glycine residue generating $\gamma$-glutamylcysteine derivatives, has also been identified [170] (Figure 4.1.1, reaction 2). Intermediates of both pathways have been detected for a variety of

xenobiotics in a range of plant species suggesting that glutathione-conjugate fate may not be as uniform as the model predicts [121,170,223,224,225,226]. Within Arabidopsis, both pathways are active, and the initiating enzymes have been identified as the vacuolar GGT4 (GGT-initiated pathway) [115,222] and the cytosolic PCS1 (carboxypeptidase-initiated pathway) [114,227,228]. The function of these enzymes in conjugate metabolism was elucidated using derivatives of the xenobiotic bimane, a compound that fluoresces when conjugated to a thiol-functional group. The fluorescence of conjugates allowed their movement to be tracked by confocal microscopy within Arabidopsis leaf tissue and cell suspension cultures, this confirmed the dominance of vacuole sequestration over cystosolic metabolism [114,175,228]. These results were further supported by findings within Arabidopsis seedlings and root tissue, in which the absence of *GGT4* expression significantly reduced bimane-conjugate metabolism [115,222,228]. However, the detection of only $\gamma$-glutamylcysteine conjugates within cell extract, obtained from cell-suspensions cultures exposed to herbicide-safener fenclorim, questions the universality of GGT4-initiated metabolism being the dominant pathway [224]. The rapid metabolism of cysteinylglycine derivatives, preventing their accumulation, could explains these results and is supported by cysteinylglycine-derivatives of bimane comprising a smaller portion of the conjugate pool despite GGT-initiated metabolism being identified as the dominant pathway [121,228]. However, the results could also reflect a flexibility between the dominance of the GGT- and PCS-initiated pathways either in response to plant developmental state or the xenobiotic parent structure of the conjugate. Characterising the role of the GGT-initiated pathway in TNT-glutathione conjugate metabolism *in planta* will provide important information on this area, confirming whether this pathway is dominant in the metabolism of glutathione conjugates derived from xenobiotics other than bimane.

Cysteinyl conjugates are the common product of both xenobiotic-glutathione conjugate metabolic pathways within plants (Figure 4.1.1, reactions 3 & 4), and these compounds can undergo a variety of metabolic reactions. Cysteinyl conjugate metabolism within both mammalian and plant systems can be separated into two categories: i) conjugation of the cysteine residue ii) further metabolised by a cysteine conjugate $\beta$-lyase to a thiol-conjugate(X-SH) which is subsequently conjugated [97,220]. Within mammals cysteinyl-conjugates undergo N-acetylation to generate mercapturic acids whilst thiol-conjugates undergo methylation and glucoronylation [220]. All of these conjugates are readily excreted through the urinary system [229–231]. Similar reactions occur within plants with cysteinyl-conjugates undergoing either N-malonylation or N-glucosylation with the former being the most common for a variety of xenobiotics [224,225,232]. Similar to mammalian systems, within plants thiol-conjugates also undergo methylation, though glucosylation can also occur [224,226,233,234]. However, unlike in

mammals the fate of these metabolites within plants is not well understood. All are hypothesised to be the terminal metabolites of xenobiotic-glutathione conjugate metabolism, due to the inability to detect further downstream products, and are believed to be compartmentalised to either the vacuole or apoplast. However, *in vivo* evidence for this remains to be presented. Characterising the metabolism of TNT-cysteinyl conjugates within Arabidopsis would provide a greater understanding of their bioavailability within plants.

The conjugate products of TNT-glutathionylation are not detectable within wild-type (WT) root tissue, thus their fate within the plant is also unknown as respective down-stream metabolite concentrations are also below the threshold of detection. The low-concentrations of TNT-glutathione conjugates is most likely due to the dispersal of TNT across two detoxification pathways, reduction-initiated glucosylation and glutathionylation. The flux of TNT into glutathionylation has been enhanced through the near-constitutive overexpression of the endogenous *GSTU24* and *GSTU25* by the CaMV35S promoter [106]. Despite overexpression lines showing enhanced TNT uptake and tolerance, only Conjugate 3 accumulated to detectable levels within root tissue of lines with enhanced *GSTU25* expression; however, this did not lead to detection of downstream derivatives of the metabolite. This result demonstrated that glutathione-conjugate metabolism was unsaturated in the conditions tested; highlighting that further increases in GST activity are required for the accumulation and detection of downstream metabolites. Two *Drosophila melanogaster* GSTs from within the epsilon subfamily have TNT-specific activity that is magnitudes greater than GSTU24 and GSTU25 [235]. One of these enzymes, DmGSTE6 (*Dm*GST), specifically generates Conjugate 3 *in vitro*, and when expressed within plants enhances both TNT uptake and tolerance [236]. The effects of *Dm*GST expression on TNT-related plant traits is assumed to be a result of enhanced Conjugate 3 production, though this remains to be confirmed through analysis of the molecules concentration within plant tissue following TNT-exposure. However, the increased flux of TNT into Conjugate 3 production provided by *Dm*GST expression provides a platform from which to characterise the metabolism of this conjugate *in planta*.

The work in this chapter utilises *Dm*GST expression lines to characterise the fate of Conjugate 3 in Arabidopsis. This novel approach allowed the identification of several downstream metabolites, including previously undescribed products of malonylation. It also describes the work performed to confirm the dominant role of GGTs in initiating Conjugate 3 metabolism, and the level of redundancy for this step in Arabidopsis. Finally, this chapter describes the first use of BNAF to confirm compartmentalisation of Conjugate 3 and downstream metabolites *in planta*.

## 4.2 Materials and Methods

### 4.2.1 Plant lines

The *Dm*GST plants lines, derived from the Col0 genetic background, were obtained from T3 seed-stock originally generated by Tzafestas *et al*. (2017) [236].

The *ggt1ggt4* double-knockout line was originally described in Ohkama-Ohtsu *et al*. (2007) [115], it is the product of crossing *ggt1* and *ggt4* single knockout lines obtained from the *Ds* transposon insertion population [237].

### 4.2.2 CDNB assay

Fresh tissue, 50 mg, was homogenised in 500 µL of ice-cold extraction buffer (100 mM Tris-HCl (pH 8), 2 mM EDTA, 1 mM DTT and 5 % PVPP-40) using a Tissuelyser II, then centrifuged for five minutes (10,000 xg, 4 °C) with the resulting supernatant used for enzymatic assays. Detectable GST activity was measured by mixing 50 µl of plant extract with 445 µl of reaction buffer (100 mM Potassium Phosphate buffer (pH 6.5), 5 mM reduced glutathione) within a UV transparent-microcuvette (Brand GMBH, Wertheim Germany). Reactions were initiated through the addition of 5 µl CDNB (1 mM final concentration). The change in absorbance at 340 nm was measured over five minutes. The extinction coefficient of CDNB at 340 nm, 0.0095 $\mu M^{-1}$ $cm^{-1}$, was used to calculate enzymatic activity per mg of freshweight from the change in absorbance.

### 4.2.3 Liquid culture

Two-days post-germination, seedlings were transferred to 20 mL of sterilised ½MS (pH 5.7) plus 20 mM sucrose and incubated for a period of 18-days on a rotary shaker (120 rpm, 20 µmol $m^{-2}$ $s^{-1}$ light intensity, 16-hour day/ 8-hour night photoperiod, 21 °C /18 °C day/night temperature). At 20-days-old plants were dosed with ½MS plus 20 mM sucrose containing either 250 µM TNT in DMSO or a corresponding volume of DMSO only. Media samples were taken, under sterile conditions, every four hours. After 24 hours whole-plant tissue was washed in tap-water to reduce background TNT and DMSO originating from the plant surface, blotted to remove surface water and the fresh mass recorded. Tissue was flash frozen in liquid nitrogen and stored at -70 °C until required for downstream analysis.

### 4.2.4 Dosing and harvesting of hydroponically-grown root tissue

Dosing of hydroponically-grown root tissue with TNT was performed in an identical manner to that described in Chapter 3 Section 2.4.

In respect to the investigation of GGT-activity in Conjugate 3 metabolism, after the initial 20-hour dosing period, the root tissue of all samples was washed in tap water to remove surface bound TNT. For half of the samples, the root tissue was harvested, blotted and the fresh mass recorded prior to flash-freezing. Non-harvested samples were placed in fresh ½MS media absent TNT and incubated for a further 24 hours after which root tissue was harvested in an identical manner.

### 4.2.5 TNT quantification

The TNT content of media was quantified via reversed-phase HPLC system (Waters 2695 separator and Waters Photodiode array detector) with a XBridge BEH C18 column (5 µm; 4.6 x 250 mm) (Waters$^{TM}$,Ireland). Media samples, 10 µL, were eluted over ten minutes at 1 ml $min^{-1}$ using an isocratic mobile phase comprised of acetonitrile and 0.1 % formic acid (60: 40, v: v). Sample and column temperatures for analysis were set to RT. The concentration of TNT within media samples was quantified from peak area absorption at 230 nm through linear regression against TNT standards.

### 4.2.6 TNT-conjugate quantification

Frozen tissue was ground in liquid nitrogen using a pre-chilled pestle and mortar. Powder was suspended in 15 mL ice-cold methanol and incubated for 40 minutes in the dark, to prevent any potential photodegradation of metabolites, with two rounds of vortexing. Insoluble material was removed using a 0.45 µm filter and the solution concentrated *in vacuo* using a Genevac EZ2. Concentrated material was re-suspended in 1 mL 20 % methanol (v/v) per gram of fresh weight. For metabolic investigations using *ggt1ggt4-Dm*GST transformants and respective controls, concentrated material was resuspended in a ratio of 2 mL per gram of fresh weight.

Initial HPLC analysis of metabolite profile used conditions identical to what is described in Chapter 3 section 2.7. A Conjugate 3 standard, verified using MS, was used to identify its retention time and thus calculate its concentration within extracts using linear regression.

For metabolite identification plant extract, 10 µL, was analysed by liquid chromatography tandem mass spectrometry (LC-MS/MS) data-dependent acquisition analysis using a Waters Acquity UPLC I-Class with a BEH C18 column (5 µM; 4.6 x 250 mm). The elution gradient was identical to the gradient used for HPLC analysis. The eluent was analysed using a Orbitrap Fusion™ Tribrid™ (Thermo Fisher Scientific); after electrospray ionisation (Negative ionisation mode, ionisation energy: 2.5 kV. Collision energy was set to 40 % to ensure fragmentation.

Metabolite identification was initially achieved through manual inspection of spectral traces. Proteowizard [238] was used to process raw data to mzML format which was subsequently analysed with Sirius 4 [239] to predict chemical formulas from MS1 and MS2 spectra. Relative abundance of metabolites for the investigation of GGT function in Conjugate 3 metabolism were obtained using CompoundDiscoverer™ software (Thermo Fisher Scientific).

### 4.2.7 $\gamma$-gluytamyl *p*-nitroaniline assay for GGT activity

Investigation of GGT activity in root tissue was achieved using a spectrophotometric assay outlined in Ohkama-Ohtsu *et al.* (2007) [121]. Briefly, 200 mg of tissue was ground in a pre-chilled pestle and mortar and the resulting powder was then suspended and incubated in 500 µl ice-cold extraction buffer (100 mM Tris-HCl (pH 8), 1M sodium chloride, 0.1 % Triton X-100, 0.25 % polyvinylpolypyrrolidone-40) for ten minutes. Homogenised samples were centrifuged for five minutes (10,000 xg, 4 °C) and the resulting supernatant was used for enzymatic assays. GGT activity was measured by mixing 100 µl of extract with 400 µl of reaction buffer (100 mM Tris-HCl, 100 mM diglycine, 5 mM $\gamma$-glutamyl-4-nitroanilide) and measuring production of 4-nitroaniline at 410 nm for ten minutes. The protein content of extracts was quantified using the bicinchoninic acid (BCA) method (Thermo Fisher Scientific) following the manufacturers protocol.

### 4.2.8 Agrobacterium-mediated transformation of Arabidopsis lines

Agrobacterium strain GV3101 transformed with the pMLBART-*Dm*GST binary vector was generated as described in Chapter 2 section 3.4. Colonies containing the *Dm*GST gene were identified by colony PCR and grown overnight in 5 mL of LB broth (28 °C, 180 rpm agitation). Pre-culture was transferred to 500 mL of LB broth and incubated overnight. Bacterial suspensions were centrifuged and resulting pellets were resuspended in 5 % sucrose solution plus 0.05 % Silwet® L-77 (Generon, Slough UK). The 5-week-old plants were dipped in Agrobacterium suspension, ensuring all inflorescence were submerged, after which plants were transferred to the growth room. The heterozygous T1 transformants were identified by selection on Basta-soaked soil prepared as described in Chapter 2 Section 4.2. Multiple-transgene insertion events introduce variation in transgene expression, and thus activity, as well as leading to greater likelihood of transgene-silencing in subsequent generations. For this reason, T2 lines with segregation ratios indicative of a single insertion event, and the resulting T3 homozygous progeny, were identified by segregation ratios on agar plates containing 10 µg $mL^{-1}$ Basta (Figure 4.2.8.1). In respect to *Dm*GST transformants derived from the WT(Ler) genetic background, no T2 lines showed segregation ratios indicative of a single insertion event (all seedlings were Basta resistant); therefore, to prevent risk

of gene-silencing in subsequent T3 populations and due to time-restraints, three independent lines from the T2 population were used in described investigations.

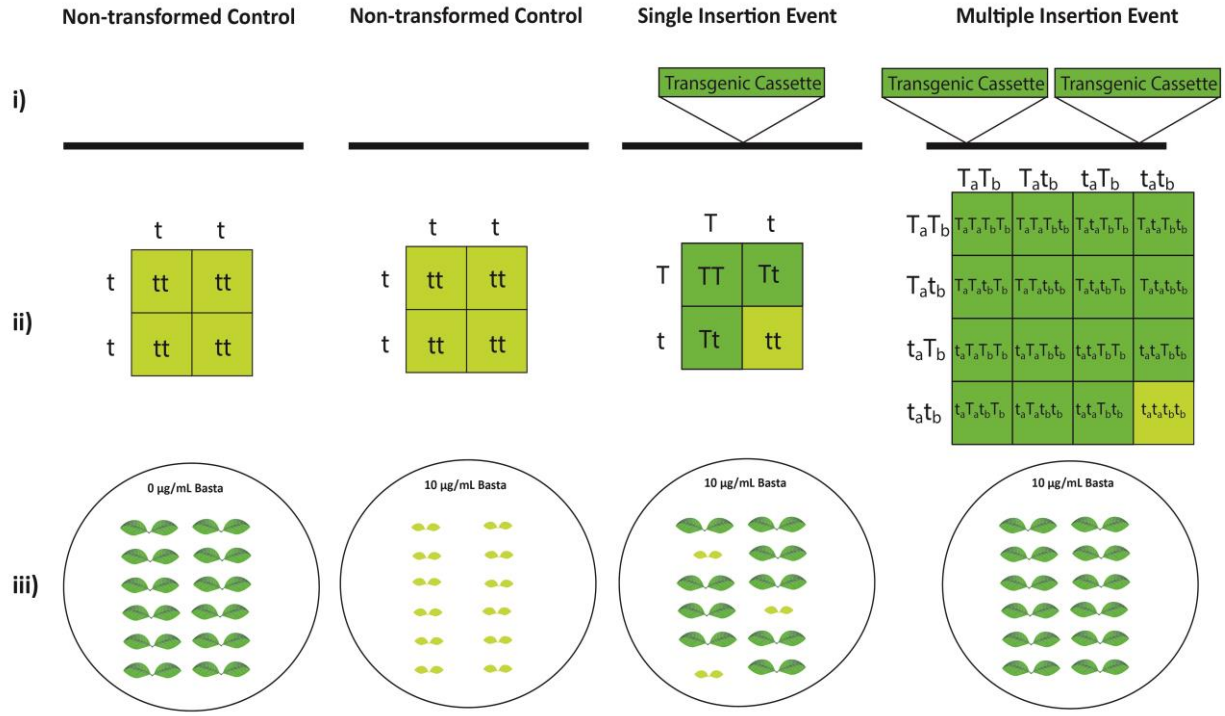


**Figure 4.2.8.1: Identifying single transformation events using segregation ratios**. i) Gene cassette containing transgene and selectable marker (BAR gene from *Streptomyces hygroscopicus* [240], conferring Basta-resistance) insert into the plant genome during Agrobacterium-mediated transformation. ii) Selfing of T1 population results in transgene segregation within T2 according to Mendelian genetics. Single insertion events produce offspring either homozygous for transgene (TT), heterozygous for transgene (Tt) or homozygous for no transgene (tt), which segregate in classical Mendelian ratios (1:2:1). Multiple insertion events generate complex segregation pattern e.g., double insertion events generate one T2 line homozygous for no transgene insertions ($t_at_at_bt_b$) per 16 offspring. $T_a/t_a$ represents the first transgenic allele and $T_b/t_b$ represents the second. iii) Growth on solid agar containing Basta allows identification of segregation ratios, and thus genotypes, in T2 population. Seedlings absent the BAR gene (tt or $t_at_at_bt_b$), have a small chlorotic phenotype as Basta inhibits glutamine synthesis.

## 4.2.9 PCR genotyping

The presence of T-DNA insertions within *ggt1ggt4* knockout lines and *Dm*GST transformants was confirmed by PCR genotyping. In respect to *ggt1ggt4* knockout lines, the sequences for gene specific primers and the T-DNA specific primer (Ds5-1a) were obtained from Ohkama-Ohtsu *et al*. (2007) [115]. PCR amplicons from the reaction between Ds5-1a and gene specific reverse strand primers

(GGT1_reverse and GGT4_reverse) were sequenced to confirm correct localisation of T-DNA in *GGT1* and *GGT4* coding regions.

In respect to *Dm*GST transformants, the presence of the *Dm*GST transgene within the genome was confirmed using gene-specific primers obtained from Tzafestas *et al*. 2017 [236].

Primer sequences are provided in Table 4.2.9.1.

**Table 4.2.9.1: Primers used for genotyping of plants lines.** Amplification of GGT1 with gene specific primers, gives a product of 716 bp. Amplification of GGT4 with gene specific primers, gives a product of 500 bp. Amplification using GGT1 and GGT4 gene specific reverse primers with the T-DNA specific primer Ds5-1a, gives products of ~750 bp and ~500 bp respectively. Amplification of the *Dm*GST transgene with gene specific primers gives a product of 500 bp.

| Primer name | Sequence (5'-3') |
|---|---|
| GGT1_forward | ATGTCGCTGGTTCGAACAGTGA |
| GGT1_reverse | CGCTTCTAGTCGCGTTCATCT |
| GGT4_forward | CGGACAGGTTTTGAAAACCG |
| GGT4_reverse | AGTACTCAGGTGGGAATGTCGTGT |
| Ds5-1a | ACGGTCGGGAAACTAGCTCTAC |
| DmGST_forward | ACCTATGAGTATGTTAACGTGGATATTGT |
| DmGST_reverse | TGTTCCAGCTTCTTGATCCAC |

## 4.2.10 Semi-quantitative PCR of *Dm*GST expression.

Purified total RNA, 1 µg, obtained from *Dm*GST transformants was used to assess successful transgene expression *in planta*. Duplicate 20 µL PCR reactions were performed for both reactions using primers specific to the *Dm*GST gene and the loading control Actin 2 gene. Primer sequences are provided in Tabel 4.2.10.1.

**Table 4.2.10.1: Primers used for semi-quantitative PCR analysis of *Dm*GST expression.** Amplification of cDNA using *Dm*GST primer pair, give a product of 139 bp; whilst amplification of cDNA with ACT2 primer pair, give a product of 79 bp.

| Primer name | Sequence (5'-3') |
|---|---|
| qDmGST_forward | GGACGACGGTCACTACATCT |
| qDmGST_reverse | GCCGCTTTCAAAATGCAGAC |
| qActin2_forward | TACAGTGTCTGGATCGGTGGTT |
| qActin2_reverse | CGGCCTTGGAGATCCACAT |

### 4.2.11 Nitrite production by plant extract

Fresh tissue, 50 mg, was homogenised in 500 µl ice-cold extraction buffer (100 mM Tris-HCl (pH 8), 2 mM EDTA, 1 mM DTT and 5% PVPP-40). Following centrifugation, 10,000 xg for five minutes at 4 °C, the resulting supernatant was used for enzymatic assays. To measure *Dm*GST activity 125 µL of plant extract was mixed with 325 µL of reaction buffer (0.1 M potassium phosphate (pH 8), 5 mM reduced glutathione and 500 µM TNT) and incubated for five hours at RT under agitation. Nitrite production was quantified using the Griess assay described in French et al. (1998) [241]. Briefly, 1.13 µL of 10 mM 1-methoxyphenazine methosulfate is added to each sample and incubated for ten-minutes at RT. This step oxidises any remaining reduced glutathione that can interfere with the assay [242]. Following this, 150 µL of 10 mg $mL^{-1}$ sulfanilamide in 0.68 M HCl and 30 µL of 10 mg $mL^{-1}$ N-(1-naphthyl)ethylenediamine (NED) was added to each sample and incubated for ten minutes at RT. In acidic conditions, free nitrite reacts with sulfanilamide to form a diazonium cation which couples with aromatic amine NED to form a red–violet coloured, water-soluble azo dye that has an absorbance maxima of 540 nm (Figure 4.2.11.1). As azo dye concentration is directly proportional to nitrite concentration, and thus Conjugate 3 concentration, this provides a spectrophotometric assay for quantifying *Dm*GST activity. Free-nitrite concentrations were quantified by linear regression of values obtained from serial dilution of sodium nitrite standard.

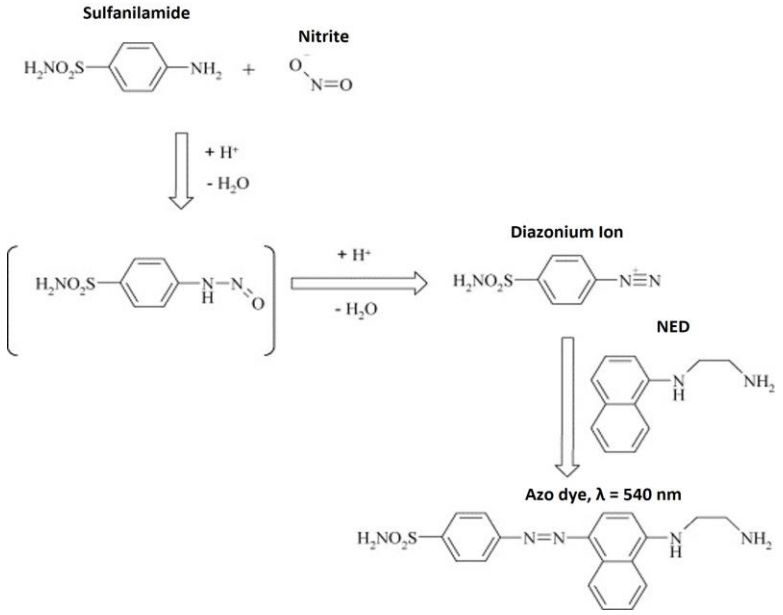


**Figure 4.2.11.1: Chemistry of Griess assay.** Diazonium cation is formed from the reaction of free nitrite and the amine group of sulfanilamide under acidic conditions. Azo dye formed from the subsequent coupling of the Diazonium cation in the *para* position to NED. Modified figure taken from Tsikas. (2007) [243].

### 4.2.12 Compartmental analysis of metabolite localisation

Compartmental association of metabolites was identified using the BNAF methodology developed and described in Chapter 3 section 2.4 - 2.6.

### 4.2.13 Statistical analysis

Two-sample T-test with a Bonferroni multiple comparison correction [244] was used to confirm the statistical difference in media concentration of TNT between conditions within liquid culture studies. Two-sample T-test was also used to confirm statistical differences in the relative abundance of Conjugate 3 metabolites detected by LC-MS/MS between *Dm*GST transformants and respective controls. The difference in nitrite production measured by the Griess assay was analysed using ANOVA with a Tukey HSD test. The significance of association between identified metabolites and subcellular compartments was measured using a Two-way ANOVA with a Tukey HSD test.

## 4.3 Results

### 4.3.1 Investigating the impact of *Dm*GST on TNT metabolism within Arabidopsis

The plant lines used in this investigation were T4 populations obtained from T3 seed-stock generated for previously published work [236], thus transgene activity within these plant lines needed to be confirmed. The model GST substrate CDNB was used to detect enhanced GST activity, resulting from transgene expression, within shoot- and root-tissue extract. Of the 24 lines investigated five showed a significantly greater GST activity compared to the WT controls (Two-sample T-test, $p < 0.05$; Figure 4.3.1.1A), only lines 2b-1a and 3a-5a showed significantly greater activity within both shoot and root tissue. Three independent lines were taken forward for further investigation, and for clarification purposes renamed as follows: 2b-1a (*Dm*GST.C1), 3a-2a (*Dm*GST.C2) and 12c-5a (*Dm*GST.C3). Selection criteria for these lines was predominantly based on seed-availability; however, level of variance between replicates, and detected GST activity was also taken into consideration. Liquid-culture based investigations were then used to test the ability of *Dm*GST expression to enhance plant uptake of TNT, an effect seen in the previously published work [236]. All three transgenic lines showed an increased uptake of TNT over 24 hours compared to the WT control with this being significant at T=10 hours for *Dm*GST.C3 (Two-sample T-test, $p.adj < 0.05$) and at T=15 hours for *Dm*GST.C1 and *Dm*GST.C3 (Two-sample T-test, $p.adj < 0.05$) (Figure 4.3.1.1B). These results confirmed successful enhancement of TNT-detoxification within transgenic plants, thus the impact of *Dm*GST activity on metabolite profile following TNT-exposure was subsequently investigated.

The HPLC analysis of extract obtained from whole plant tissue exposed to TNT in a liquid culture system revealed *Dm*GST expression alters the metabolic profile following TNT-exposure (Figure 4.3.1.1C). In particular a substantial accumulation of Conjugate 3, shown by the novel peak at ~21.8 min, as well as the accumulation of multiple unknown metabolites which were present only in *Dm*GST lines following TNT exposure. These unidentified metabolites were presumed to be downstream products of Conjugate 3 metabolism.

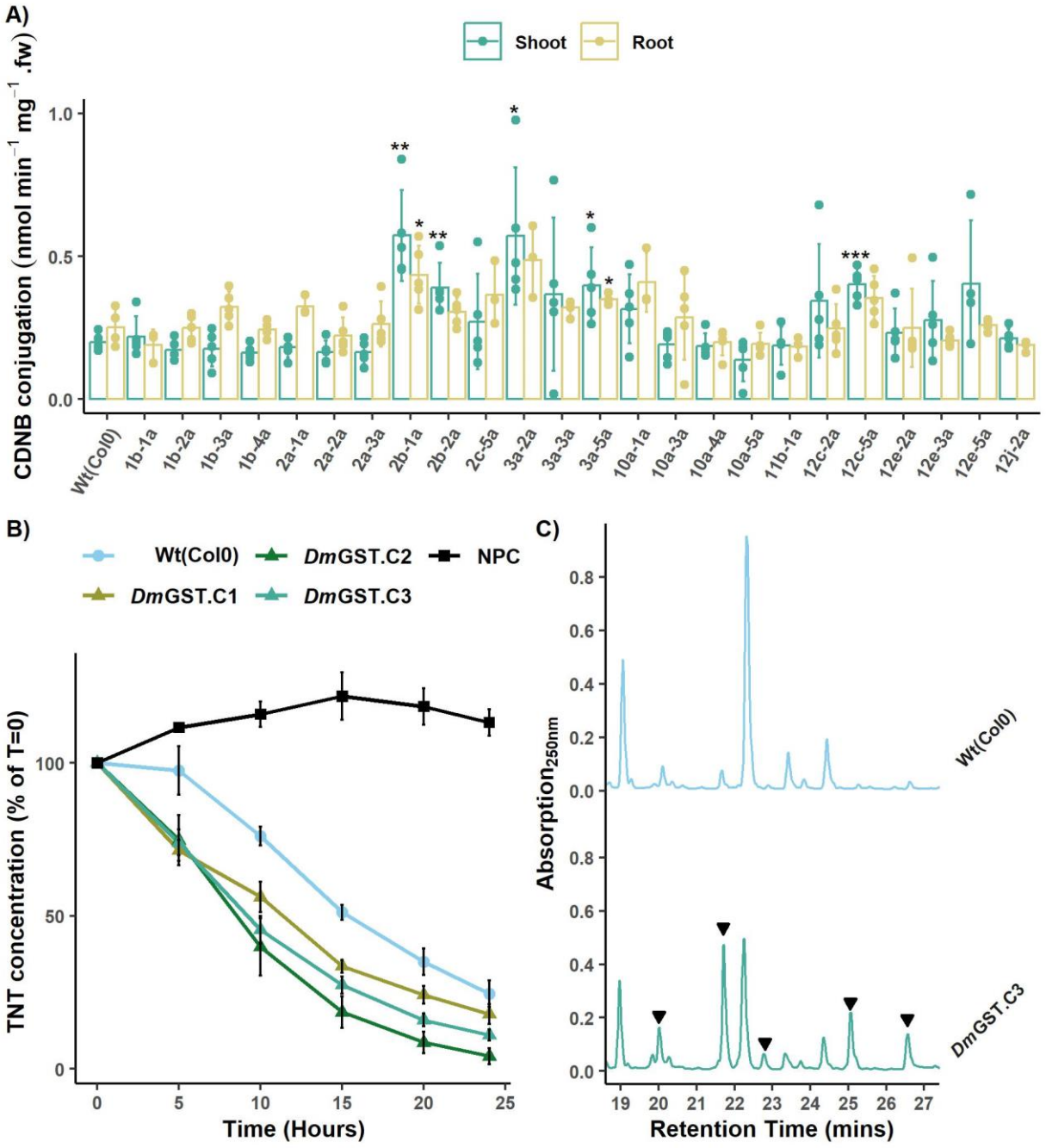


**Figure 4.3.1.1: Expression of *Dm*GST removes the bottleneck for Conjugate 3 production resulting in significantly enhanced TNT-uptake and accumulation of novel metabolites. A)** Detectable GST activity in shoot and root extract of T4 transgenic lines expressing *Dm*GST enzyme measured using the CDNB assay. Tissue was obtained from three-week-old plants grown on ½MS solid agar. Points are representative of biological replicates, bars representative of biological mean. n = 4 ± standard deviation (SD). Statistically significant differences from wild type: *, $p < 0.05$; **, $p < 0.01$. **B)** Rates of TNT depletion from liquid-culture over a 24-hour period by selected transgenic plant lines. *Dm*GST expression lines 2b-1a (*Dm*GST.C1), 3a-2a (*Dm*GST.C2) and 12C-5a (*Dm*GST.C3) were included alongside the Wt(Col0) genetic

background and no plant control (NPC). Concentrations of TNT were normalised to a percentage of concentration at 0 hours (T=0) for each replicate. Statistical differences from wild type were observed at T=10 hours for line *Dm*GST.C3 (FDR < 0.05) and T=15 hours for lines *Dm*GST.C1 and *Dm*GST.C3 (FDR < 0.05). Points representative of biological mean, n=5 ± standard error. **C)** HPLC analysis of methanol extracts obtained from whole-plant tissue following 24 h exposure to TNT. Arrows indicate retention times of novel peaks within *Dm*GST-lines that are absent in Wt(Col0). Novel peaks were confirmed to be absent in no-TNT controls. Results are representative of five biological replicates.

### 4.3.2 Identification of metabolites produced from Conjugate 3 metabolism

To identify the unknown metabolites detected in HPLC analysis, methanol extract from *Dm*GST.C3 whole plant tissue was analysed by LC-MS/MS. Previously published work had shown that Conjugate 3 had a unique fragmentation pattern that generated a DNT-sulphur fragment (*m/z* = 212.9987) [106]. Current understanding of glutathione conjugate metabolism within plants suggested that this core-structure would be retained within metabolic products of Conjugate 3 [221], thus allowing their identification. Generation of an extracted-ion chromatogram confirmed that the DNT-sulfur fragment was detected at ten different retention times during analysis (Figure 4.3.2.1A). The distribution of these retention times corresponded strongly to the pattern observed for the novel peaks detected by HPLC analysis. This result supported the hypothesis that these peaks represented products of Conjugate 3 metabolism. The ion peaks containing the DNT-sulfur fragment within their MS2 spectra were identified by manual inspection. Chemical formulas for these ions were generated based on their MS1 and MS2 spectra which was used, alongside the current literature of glutathione-conjugate metabolism within plants, to generate putative metabolite identifications within two ppm mass accuracy (Figure 4.3.2.1B). This process identified the cysteine-conjugate metabolite (S-DNT-Cys) of Conjugate 3, alongside both the $\gamma$-glutamylcysteine- and cysteinylglycine-conjugate precursors (S-DNT-$\gamma$EC and S-DNT-CG respectively). Two fates for S-DNT-Cys within Arabidopsis were also identified. The first being N-malonylation to form a malonylcysteine conjugate(S-DNT-(Mal)Cys) whilst the second was a O-malonylglucose conjugate (S-DNT-(Mal)Glc) generated from an S-glucose conjugate (S-DNT-Glc). The MS2 spectra for the $[M-H]^-$ adducts of these putative metabolites are presented in Figure 4.3.2.2A-E. Whilst a $[M-H]^-$ adduct for the putative S-DNT-(Mal)Glc was not detected, the identification was generated from the presence of corresponding $[2M-H]^-$ and $[M-COOH]^-$ adducts(Figure 4.3.2.2F). The loss of -COOH was a fragmentation pattern that was also identified for the $[M-H]^-$ adducts of S-DNT-(Mal)Cys (Figure 4.3.2.2G). The thiol-intermediate between S-DNT-Cys and S-DNT-Glc was not identified. Alongside malonyl-conjugates generated within Conjugate 3 metabolism, putative HADNT-O-(O-malonyl)glucoside (HADNT-(Mal)Glc) and ADNT-O-(O-malonyl)glucoside (ADNT-(Mal)Glc) were detected at ~22.38 and ~23.28 minutes

respectively, with both peaks generating an $[M\text{-}COOH]^-$ fragment in their MS2 spectra. Adducts detected for each metabolite, the detected *m/z* value and the accuracy to the predicted *m/z* value are presented in Table 4.3.2.1.

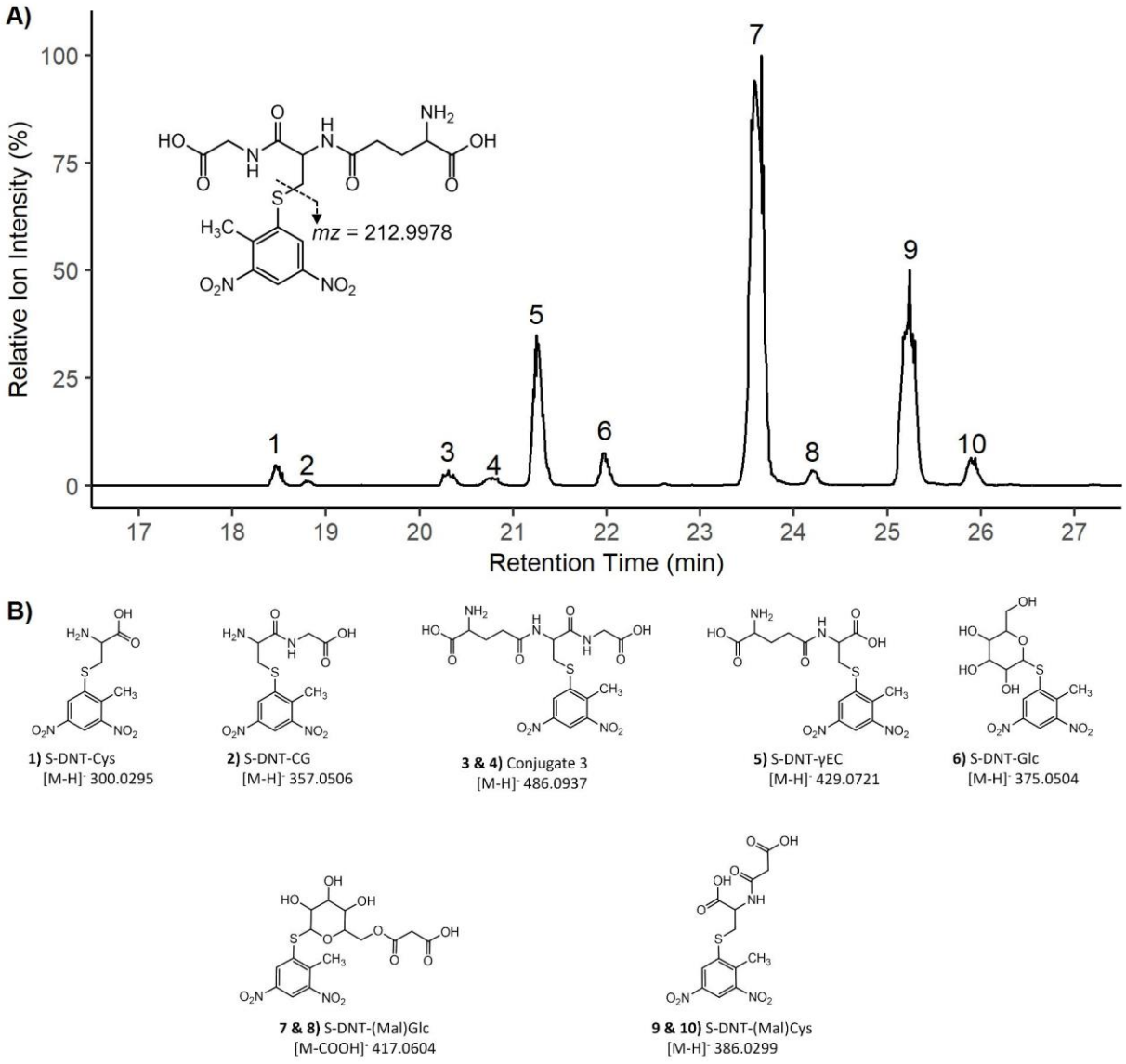


**Figure 4.3.2.1: Metabolites derived from the metabolism of Conjugate 3 within Arabidopsis. A).** Extracted ion chromatogram for the Conjugate 3 specific DNT-sulfur fragment, *m/z* = 212.99 -213.00. The chromatogram was generated from the LC-MS/MS analysis of DmGST.C3 whole plant tissue methanol extract. The fragment was detected at 10 separate retention times. **B)** Identities, chemical structures and the detected adducts *m/z* values of putative metabolites generated from Conjugate 3 metabolism are shown alongside their corresponding peak numbers.

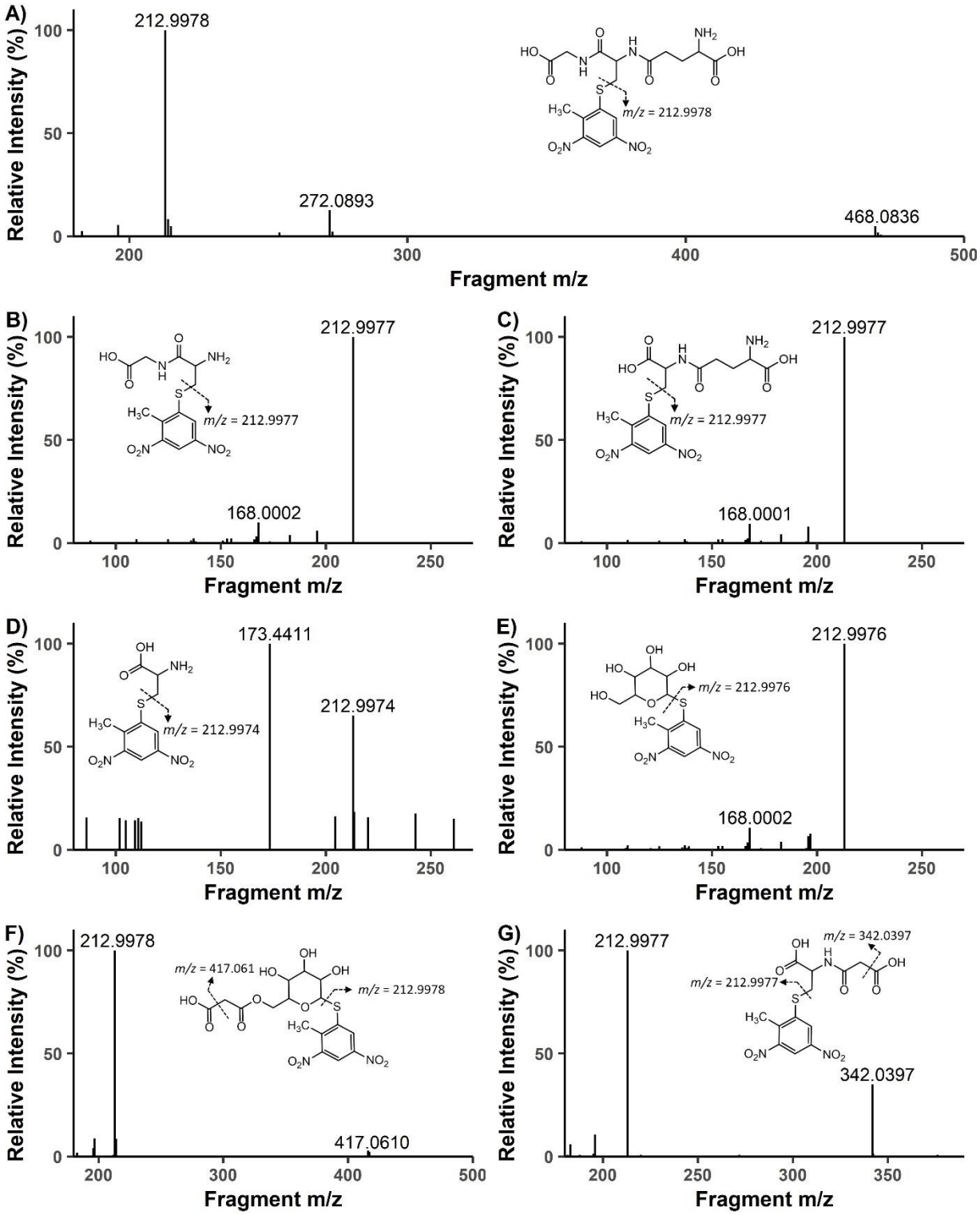


**Figure 4.3.2.2: MS2 spectra of Conjugate 3 and respective downstream metabolites. A)** MS2 spectra of $[M-H]^-$ adduct for Conjugate 3, precursor ion *m/z* = 486.0938. **B)** MS2 spectra of $[M-H]^-$ adduct for S-DNT-CG, precursor ion *m/z* = 357.0505. **C)** MS2 spectra of $[M-H]^-$ adduct for S-DNT-γEC, precursor ion *m/z* = 429.0721. **D)** MS2 spectra of $[M-H]^-$

adduct for S-DNT-Cys, precursor ion *m/z* = 300.0294. **E)** MS2 spectra of $[M-H]^-$ adduct for S-DNT-Glc, precursor ion *m/z* = 375.0498. **F)** $[2M-H]^-$ adduct for S-DNT-(Mal)Glc, precursor ion *m/z* = 923.11. **G)** MS2 spectra of $[M-H]^-$ adduct for S-DNT-(Mal)Cys, precursor ion *m/z* = 386.0296.

**Table 4.3.2.1: The majority of isotope peaks for adducts of Conjugate 3 and putative downstream metabolites were detected to within 2 ppm of the calculated *m/z* values.**

| Metabolite | Adduct | Predicted *m/z* value | Detected *m/z* value | Accuracy (ppm) |
|---|---|---|---|---|
| Conjugate 3 | $[M-H]^-$ | $^{32}S$ = 486.0936 | 486.0937 | 0.21 |
| | | $^{33}S$ = 487.097 | 487.0952 | -3.7 |
| | | $^{34}S$ = 488.0894 | 488.0925 | 6.35 |
| | | $^{36}S$ = 490.0937 | 490.0937 | 0 |
| | $[2M-H]^-$ | $^{32}S$ = 973.1951 | 973.195 | 0.47 |
| | | $^{33}S$ = 974.1979 | 974.1976 | -0.31 |
| | | $^{34}S$ = 975.1903 | 975.196 | 5.85 |
| | | $^{36}S$ = 977.1971 | 977.198 | 0.92 |
| S-DNT-Cys | $[M-H]^-$ | $^{32}S$ = 300.0295 | 300.0295 | -0.33 |
| | | $^{33}S$ = 301.0329 | 301.0328 | -0.33 |
| | | $^{34}S$ = 302.0254 | 302.0251 | -0.99 |
| | | $^{36}S$ = 304.0296 | 304.0606 | 10 |
| | $[2M-H]^-$ | $^{32}S$ = 601.0664 | 601.0673 | 1.26 |
| | | $^{33}S$ = 602.0698 | 602.0697 | -0.17 |
| | | $^{34}S$ = 603.0622 | 603.0660 | 6.3 |
| | | $^{36}S$ = 605.0665 | 605.0662 | -0.5 |
| S-DNT-CG | $[M-H]^-$ | $^{32}S$ = 357.051 | 357.0506 | 1.19 |
| | | $^{33}S$ = 358.0544 | 358.0538 | -1.68 |
| | | $^{34}S$ = 359.0468 | 359.0463 | -1.39 |
| | | $^{36}S$ = 361.0511 | 361.0536 | 6.92 |
| | $[2M-H]^-$ | $^{32}S$ = 715.1094 | 715.1093 | 0 |
| | | $^{33}S$ = 716.1127 | 716.1125 | -0.28 |
| | | $^{34}S$ = 717.1052 | 717.1045 | -0.98 |
| | | $^{36}S$ = 719.1119 | 719.1105 | -1.95 |
| S-DNT-γEC | $[M-H]^-$ | $^{32}S$ = 429.0722 | 429.0721 | -0.06 |

| Metabolite | Adduct | Predicted *m/z* value | Detected *m/z* value | Accuracy (ppm) |
|---|---|---|---|---|
| | | $^{33}$S = 430.0755 | 430.0749 | -1.4 |
| | | $^{34}$S = 431.068 | 431.068 | 0 |
| | | $^{36}$S = 433.0722 | 433.0483 | -10 |
| | $[2M-H]^-$ | $^{32}$S = 859.1516 | 859.152 | 0.55 |
| | | $^{33}$S = 860.1550 | 860.1562 | 1.4 |
| | | $^{34}$S = 861.1474 | 861.1474 | 0 |
| | | $^{36}$S = 863.1541 | 863.1693 | 10 |
| S-DNT-Glc | $[M-H]^-$ | $^{32}$S = 375.0504 | 375.0499 | -1.33 |
| | | $^{33}$S = 376.0537 | 376.0529 | -2.13 |
| | | $^{34}$S = 377.0462 | 377.0458 | -1.06 |
| | | $^{36}$S = 379.0504 | 379.051 | 1.58 |
| | $[M+Cl]^-$ | $^{32}$S = 411.0265 | 411.0268 | -0.68 |
| | | $^{33}$S = 412.0299 | 412.0302 | 0.73 |
| | | $^{34}$S = 413.0236 | 413.0241 | 1.21 |
| | | $^{36}$S = 415.0193 | 415.02 | 1.69 |
| | $[2M-H]^-$ | $^{32}$S = 751.1080 | 751.1084 | 0.43 |
| | | $^{33}$S = 752.1114 | 752.1112 | -0.27 |
| | | $^{34}$S = 753.1038 | 753.1086 | 6.37 |
| | | $^{36}$S = 755.1105 | 755.1047 | -7.68 |
| S-DNT-(Mal)Glc | $[M-COOH]^-$ | $^{32}$S = 417.0609 | 417.0607 | 0.48 |
| | | $^{33}$S = 418.0643 | 418.0638 | -1.2 |
| | | $^{34}$S = 419.0567 | 419.0563 | -0.95 |
| | | $^{36}$S = 421.0610 | 421.0577 | -7.84 |
| | $[2M-H]^-$ | $^{32}$S = 923.1088 | 923.109 | 0.324 |
| | | $^{33}$S = 924.1122 | 924.1122 | -0.97 |
| | | $^{34}$S = 925.1046 | 925.109 | 4.76 |
| | | $^{36}$S = 927.1113 | 927.1114 | 0.11 |
| S-DNT-(Mal)Cys | $[M-H]^-$ | $^{32}$S = 386.03 | 386.0295 | -1 |
| | | $^{33}$S = 387.0333 | 387.0328 | -1.29 |
| | | $^{34}$S = 388.0258 | 388.0256 | -0.52 |

| Metabolite | Adduct | Predicted *m/z* value | Detected *m/z* value | Accuracy (ppm) |
|---|---|---|---|---|
| | | $^{36}$S = 390.03 | 390.0294 | -1.54 |
| | [M-COOH]$^-$ | $^{32}$S = 342.0401 | 342.0397 | 0 |
| | | $^{33}$S = 343.0435 | 343.0427 | -2.33 |
| | | $^{34}$S = 344.0359 | 344.0354 | -1.45 |
| | | $^{36}$S = 346.0402 | 346.0393 | -2.6 |
| | [2M-H]$^-$ | $^{32}$S = 773.0672 | 773.0674 | -1 |
| | | $^{33}$S = 774.0706 | 774.0706 | 0 |
| | | $^{34}$S = 775.0630 | 775.0667 | 4.77 |
| | | $^{36}$S = 777.0697 | 777.0697 | 0 |
| HADNT-(Mal)Glc | [M-H]$^-$ | 460.0843 | 460.0843 | 0 |
| | [M-COOH]$^-$ | 416.0945 | 416.0943 | -0.48 |
| | [2M-H]$^-$ | 921.1763 | 921.1767 | 0.98 |
| ADNT-(Mal)Glc | [M-COOH]$^-$ | 400.0992 | 400.0996 | 1 |
| | [2M-H]$^-$ | 889.1865 | 889.1872 | 0.76 |

### 4.3.3 Investigating the role of GGTs in Conjugate 3 metabolism

The currently accepted model for the metabolism of xenobiotic glutathione-conjugates predicts their metabolism to be initiated by a GGT, specifically the vacuolar GGT4 [221]. Whilst metabolic analysis of *Dm*GST plant extract detected the product of this reaction, S-DNT-CG, it has also detected S-DNT-$\gamma$EC which is an intermediate of the competing PCS1-initiated pathway. To test if GGTs are the dominant route for Conjugate 3 metabolism, a *ggt1ggt4* double-knockout line was transformed with *DmGST*. This double-knockout line was used to prevent potential redundancy between GGT1 and GGT4, both active within Arabidopsis root tissue [115], which could mask effects on conjugate metabolism. Genotyping PCR and subsequent amplicon sequencing confirmed the *ggt1ggt4* line to have the T-DNA insertions within the 1st and 3rd exon of *GGT1* and *GGT4* respectively, as identified by Ohkama-Ohtsu *et al*. (2007) [115]. Enzymatic investigation established the absence of detectable GGT activity within *ggt1ggt4* root tissue, prior to Agrobacterium-mediated transformation (Figure 4.3.3.1A). Following transformation, transgenic lines that demonstrated suitable segregation ratios for BASTA resistance were assessed for *Dm*GST activity *in planta* by measuring nitrite release from the plant-extract catalysed nitro-substitution reaction between TNT and glutathione. Within both the Wt (Ler) (*Dm*GST.L) and *ggt1ggt4* (*Dm*GST-

*ggt1ggt4*) transformation populations all plant lines assessed showed substantially greater nitrite release (Figure 4.3.3.1B), compared to untransformed controls, with three independent lines for which this difference was significant being selected from both populations (Tukey HSD, *p.adj* < 0.05; Figure 4.3.3.1B inset figure). Enhanced Conjugate 3 production was further validated by HPLC analysis on plant lines exposed to TNT within a liquid culture system. This analysis revealed that all transgenic lines accumulated significantly greater levels of Conjugate 3 compared to untransformed controls, confirmed by presence of the peak at ~21.8 minutes (Figure 4.3.3.1C). However, both S-DNT-(Mal)Glc and S-DNT-(Mal)Cys were detected within the *Dm*GST-ggt1ggt4 lines, peaks at ~25.2 and ~26.8 minutes respectively, confirming Conjugate 3 metabolism to putative end-point metabolites can occur in the absence of GGT-activity.

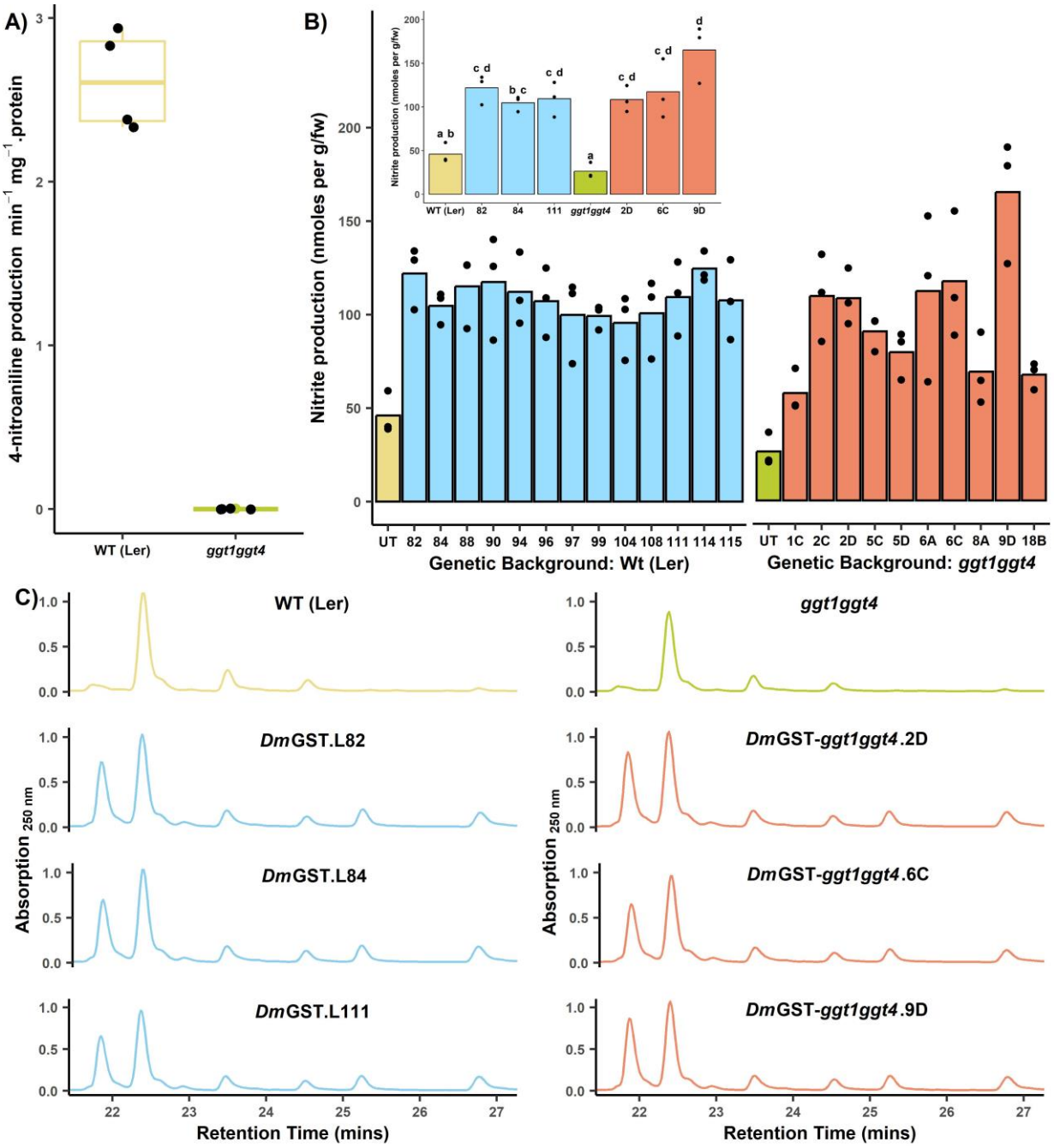


**Figure 4.3.3.1: Absence of GGT activity within plant lines expressing *Dm*GST transgene does not arrest Conjugate 3 metabolism. A)** GGT activity of root protein extracts obtained from 3-week-old plants grown on agar-plates assayed using the model GGT substrate $\gamma$-glutamyl-*p*-nitroanilide. Results confirm the *ggt1ggt4* genetic background does not contain any detectable GGT activity, n=4. **B)** *Dm*GST activity within plant extract inferred from measuring nitrite release, via the Griess assay, from the enzyme-catalysed reaction between glutathione and TNT. Plant extract was obtained from 14-day-old seedlings. *Dm*GST phenotype was confirmed by the release of significantly more nitrite, n =3. Inset figure shows statistical analysis results for three independent lines from each genetic population selected for further analysis,

letters identify which lines differed significantly in nitrite production, plant lines sharing the same letter showing no statistical difference. **C)** HPLC analysis of methanol extracts obtained from whole plant methanol extract of liquid culture grown plants exposed to 250 μM TNT for 24 hours. Peaks corresponding to Conjugate 3 and downstream derivatives metabolites, ~21.8, ~25.2 and 26.8 minutes, are present in *Dm*GST lines but absent in untransformed controls. Chromatograms were generated from absorption at 250 nm.

The detection of Conjugate 3 metabolites within *Dm*GST-*ggt1ggt4* lines confirmed a level of redundancy in the role of GGTs in glutathione-conjugate metabolism. To test the currently existing model of GGT dominance, turnover of Conjugate 3 within root tissue of transgenic lines was investigated. Hydroponically-grown *Dm*GST.L111 and *Dm*GST-*ggt1ggt4*.2D lines were dosed with TNT for 20 hours and then incubated for a further 24 hours in fresh ½ MS without TNT. Enzymatic assays had shown these plant lines to have no statistical difference in *Dm*GST activity (Figure 4.3.3.1B), thus any differences in Conjugate 3 concentration will be a result of the *Dm*GST-*ggt1ggt4*.2D line being unable to initiate conjugate metabolism through GGT activity (Figure 4.3.3.2A). Levels of Conjugate 3 within *Dm*GST.L111 and *Dm*GST-*ggt1ggt4*.2D were compared at both the 20-hour and 44-hour time point. There was no difference in Conjugate 3 content after the initial 20-hour dosing, confirming these plant lines to have similar capabilities in the *Dm*GST-catalysed formation of the metabolite. However, after the further 24 hour incubation in which the TNT-flux into Conjugate 3 production was stopped, Conjugate 3 concentration was significantly greater within *Dm*GST-*ggt1ggt4*.2D compared to *Dm*GST.L111 (Tukey HSD, $p.adj < 0.001$; Figure 4.3.3.2B). As these results indicated a significant role of GGTs in Conjugate 3 metabolism within root tissue, relative levels of downstream metabolites within *Dm*GST.L111 and *Dm*GST-*ggt1ggt4*.2D were compared via LC-MS/MS analysis. For this analysis, root extract was harvested at the end of the 20-hour dosing to ensure downstream metabolites were at detectable concentrations. Relative to *Dm*GST.L111, concentrations of Conjugate 3 downstream metabolites were significantly lower in *Dm*GST-*ggt1ggt4*.2D (Two-sample T-test, $p < 0.05$; Figure 4.3.3.2C), with S-DNT-Cys being undetectable. These results confirm the dominance of GGTs in Conjugate 3 metabolism within Arabidopsis root tissue.

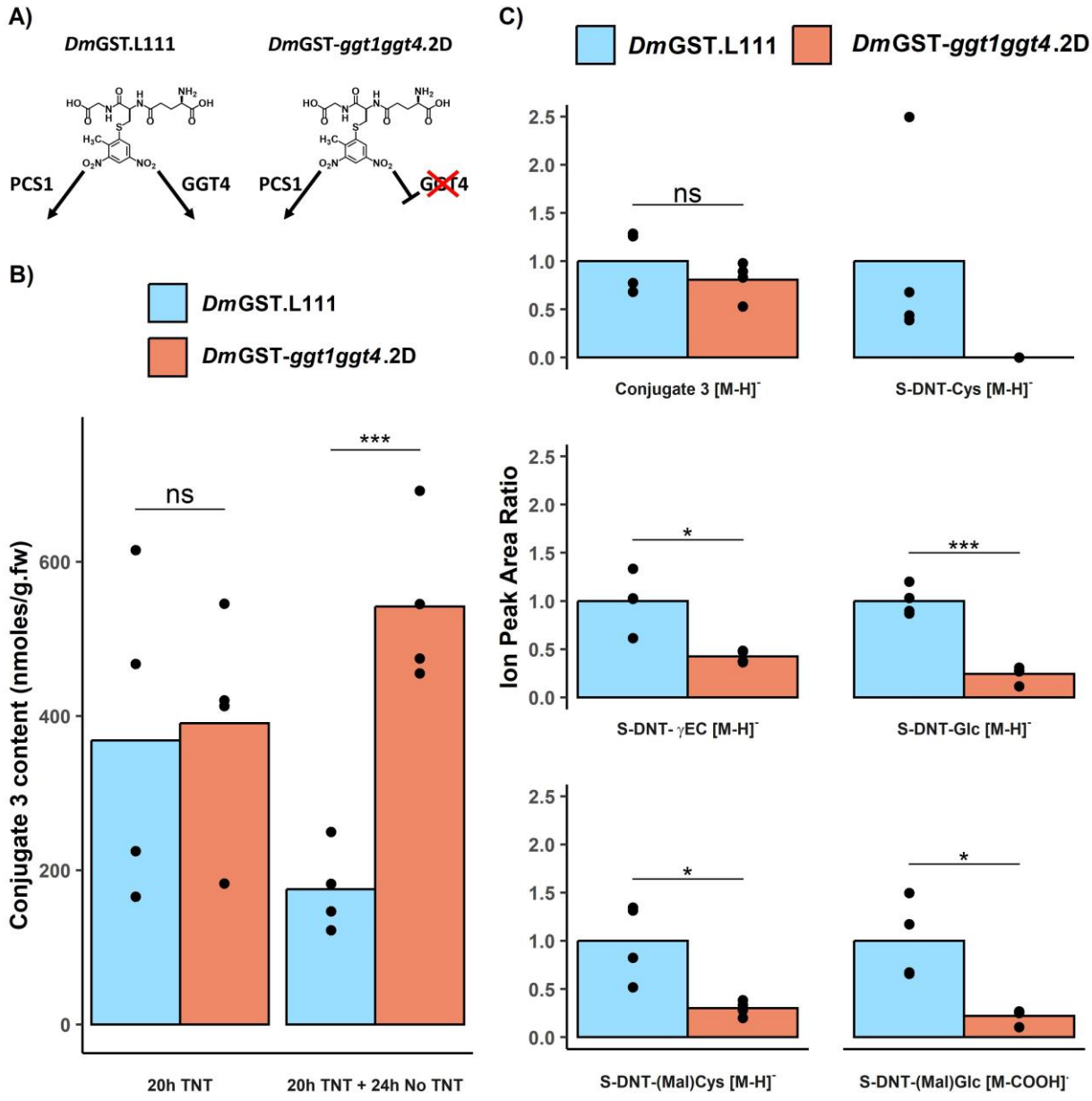


**Figure 4.3.3.2: GGTs have a significant but partially redundant role in initiating Conjugate 3 metabolism. A)** *Dm*GST.L111 lines metabolise Conjugate 3 through the activity of either PCS1 or GGT4; in comparison, *Dm*GST-*ggt1ggt4*.2D lines can only initiate Conjugate 3 metabolism via PCS1 activity. **B)** Quantification of Conjugate 3 content within root tissue of plants after the initial 20-hour dosing period and after the further 24-hour incubation in ½ MS media. **C)** Relative quantification of metabolites within root tissue of plants following initial 20-hour dosing period. Extracts were normalised according to fresh mass of tissue and ion peak areas, relative to *Dm*GST.L111 values, were calculated for indicated adducts. Points are representative of biological replicates, n=4, and bars representative of biological means. Statistically significant difference between transgenic lines: *, $p < 0.05$; ***, $p < 0.001$.

### 4.3.4 Confirming the Compartmentalisation of Conjugate 3 and downstream metabolites.

The dominant role of GGTs in the metabolism of Conjugate 3 supports the hypothesis that the metabolite is sequestered from the cytosol, as neither GGT1 nor GGT4 are localised to that compartment [121,222]. To further test this, BNAF was used to analyse compartmental association of metabolites. Alongside confirming Conjugate 3 sequestration, BNAF analysis would also provide information on where down-stream metabolites are localised within the cell. Root tissue from *Dm*GST.C3, following 20-hour exposure to TNT, was used for this investigation. Examination of marker enzyme distributions confirmed a suitable differential distribution of subcellular compartments (Figure 4.3.4.1A). The compartmental associations for Conjugate 3, and related downstream metabolites, were investigated following HPLC analysis of BNAF-derived fractions. This analysis revealed that all investigated metabolites showed strikingly similar distribution patterns to the vacuole (Figure 4.3.4.1B-F). Pair-wise comparison analysis of marker enzyme and metabolite distributions confirmed the vacuolar association of Conjugate 3, and related downstream metabolites, was highly significant (Tukey HSD, *p.adj* <0.001; Figure 4.3.4.1G). These results confirm the compartmentalisation of Conjugate 3, and related metabolites.

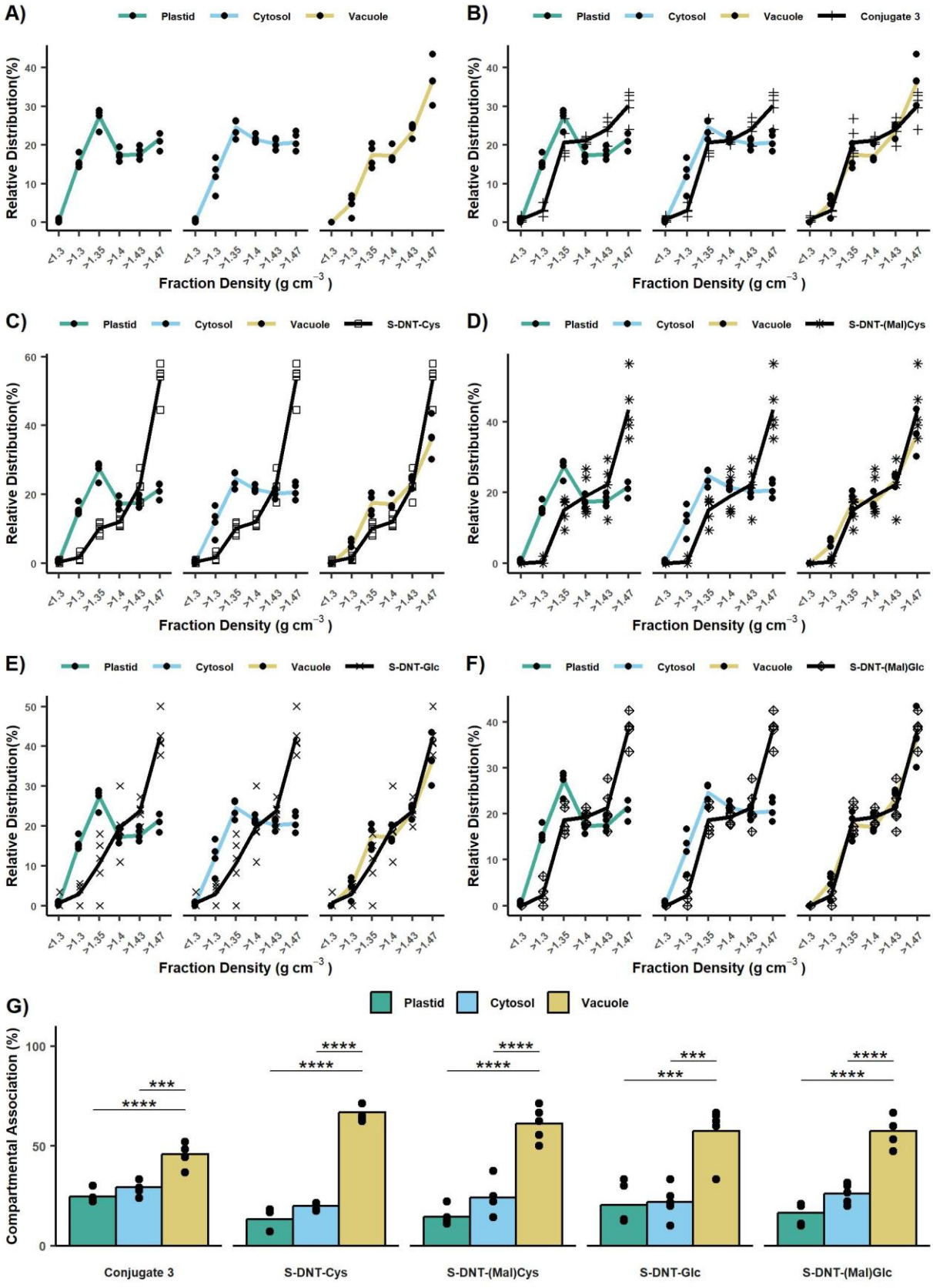
A)
Plastid
Cytosol
Vacuole
Relative Distribution(%)
Fraction Density (g cm$^{-3}$)
B)
Conjugate 3
C)
S-DNT-Cys
D)
S-DNT-(Mal)Cys
E)
S-DNT-Glc
F)
S-DNT-(Mal)Glc
G)
Compartmental Association (%)
Conjugate 3
S-DNT-Cys
S-DNT-(Mal)Cys
S-DNT-Glc
S-DNT-(Mal)Glc

**Figure 4.3.4.1: Conjugate 3 and related downstream metabolites have a significant association with the vacuole. A)** Relative distribution of plastid (APPase), cytosol (UGPase), and vacuole (APase) marker enzymes across density gradient. Points are representative of individual biological reps and the line represents the biological mean, n=5. **B)** Relative distribution of organelle marker enzymes and Conjugate 3 across density gradient. Metabolite relative distribution inferred from peak area measured in each fraction by HPLC analysis at 250 nm as a proportion of peak area measured across all fractions at 250 nm. **C)** Relative distribution of organelle marker enzymes and S-DNT-Cys across density gradient, metabolite relative distribution inferred from HPLC analysis at 250 nm. **D)** Relative distribution of organelle marker enzymes and S-DNT-(Mal)Cys across density gradient, metabolite relative distribution inferred from HPLC analysis at 250 nm **E)** Relative distribution of organelle marker enzymes and S-DNT-(Mal)Cys across density gradient, metabolite relative distribution inferred from HPLC analysis at 250 nm, **F)** Relative distribution of organelle marker enzymes and S-DNT-Glc across density gradient, metabolite relative distribution inferred from HPLC analysis at 250 nm. **G)** Compartmental association of Conjugate 3 and downstream metabolites. Points are representative of individual biological reps and bars are representative of biological means. Statistically significant differences between compartmental associations: ***, $p < 0.001$; ****, $p < 0.0001$.

## 4.4 Discussion

The research presented within this chapter has provided a greater understanding of the glutathione detoxification pathway for TNT, specifically for Conjugate 3. The enhanced flux of TNT into Conjugate 3 formation, via *Dm*GST expression, provides plants with significant enhancements in respect to TNT-uptake, as well as allowing down-stream metabolites to accumulate to concentrations above the threshold of detection. Putative identification of these downstream metabolites has provided further evidence for the prominence of malonylation within plant detoxification pathways. Alongside this finding, the production of these metabolites from Conjugate 3 within roots was shown to be controlled predominantly by a GGT-catalysed enzymatic reaction. Finally, these findings provide strong evidence that compartmentalisation from the cytosol is a fate shared for xenobiotic conjugates, as predicted by the current model for xenobiotic detoxification within plants.

### 4.4.1 Malonylation is a common fate in Conjugate 3 metabolism

Enhancing TNT-flux into Conjugate 3 formation, via *Dm*GST expression, allowed putative terminal metabolites to accumulate to detectable concentrations within plant tissue. Detection of N-malonylcysteine and S-glucoside derivatives of Conjugate 3 supports previous findings that cysteinyl-conjugate metabolism within Arabidopsis can occur either through direct conjugation, or via the activity of a cysteine conjugate $\beta$-lyase [224]. This is only the second documented case, to the author's knowledge, of a S-glucoside being generated during glutathione conjugate metabolism in plants [233]

and the first within Arabidopsis. The inability to detect a thiol-intermediate of the S-glucoside could be explained by its co-elution from the HPLC column with other products of Conjugate 3 metabolism. This co-elution would result in an inability to distinguish the $[M-H]^-$ adduct of the thiol-conjugate from the DNT-sulfur fragment generated by Conjugate 3 related metabolites. Rapid glycoslyation of the thiol-conjugate in response to acute toxicity could also explain its absence from the detectable metabolome, as thiol-compounds have been shown to inhibit aerobic and oxidative enzymes [245].

The first documented identification of a S-(O-malonyl)glucoside confirms the commonality of malonylation in S-DNT-Cys metabolism, suggesting an important role in xenobiotic detoxification, and warranting further investigation. Whilst N-malonylated conjugates are commonly described xenobiotic metabolites within plants [224,225,232], the enzymes that catalyse this reaction have not been identified. Two potential acyl-CoA N-acyltransferases candidates, adjacently encoded, are *At2g32020* & *At2g32030*. Gene expression response within whole-plant tissue has identified upregulation of *At2g32020* and *At2g32030* in response to TNT exposure [104], 12- and 17-fold respectively, with these genes also upregulated in response to other stressors [246,247]. However, it is important to note that *At2g32020* and *At2g32030* have only been identified as TNT-inducible genes within this one study, with other investigations using lower TNT concentrations or specifically investigating the gene-expression response within Arabidopsis root tissue, failing to detect upregulation of these genes [248–250]. This may indicate that the sole example of TNT-induced upregulation of these genes could be an artifact of the system in which plants were exposed to TNT. Gene-expression analysis of *At2g32020* and *At2g32030* in leaf and root tissue, following exposure to a variety of TNT concentrations, would clarify whether these genes are viable candidates for further investigation. As *At2g32020* and *At2g32030* are hypothesised to be products of tandem duplication, sharing 69.6 % amino acid sequence similarity, *in vivo* investigations of their activity would need to mitigate against functional redundancy; the generation of double-knockout lines through CRISPR methods would be the best approach to address redundancy concerns. These lines could then be transformed with *Dm*GST allowing the effects of S-DNT-(Mal)Cys production to be investigated. An enzymatic candidate for the O-malonylation of S-DNT-Glc is PMAT1 which is also upregulated over 10-fold in response to TNT [104]. Unlike N-malonytransferase candidates, a non-redundant function for PMAT1 in the O-malonylation of glucosides, including conjugates of the xenobiotic naphthol, has been identified *in planta* [251,252]. Therefore, preliminary studies into the function of PMAT1 in HADNT metabolism could be investigated by measuring HADNT-(Mal)Glc and ADNT-(Mal)Glc production within *pmat1* knockout lines following TNT exposure. Identical studies could be performed within knockout lines transformed with the *Dm*GST transgene to investigate

the role of PMAT1 in S-DNT-(Mal)Glc production during Conjugate 3 metabolism. The inability to detect products of malonyl conjugate metabolism supports the hypothesis that these are terminal metabolites [253]. However, within chickpea (*Cicer arietinum* L.) a malonylestererase regulates the active isoflavone pool through the release of glucosides from malonyl-glucoside derivatives [254]. This opens the possibility that malonylglucosides are intermediaries in the detoxification response from which glucosyl-conjugates are produced as end-products.

### 4.4.2 Redundancy in the initiation of Conjugate 3 metabolism

Upstream intermediates of S-DNT-Cys were detected alongside downstream metabolites within *Dm*GST transformants derived from both Col0 and Ler ecotype genetic backgrounds. The detection of both S-DNT-CG and S-DNT-$\gamma$EC confirms that Conjugate 3 metabolism can be initiated by either of the competing pathways identified for glutathione conjugates, vacuolar catalysed by GGT4 [115] and cytosolic catalysed by PCS1 [227]. Expression of *Dm*GST within *ggt1ggt4* knockout lines confirmed the dominance of GGT-initiated metabolism, with depletion of Conjugate 3 over 24 hours significantly impaired within these plant lines. This result was further supported by the strong association of Conjugate 3 with the vacuole in BNAF analysis. Replicating the findings of this investigation with the inclusion of *Dm*GST-*ggt4* lines would be a useful addition as it would allow the identified effect to be allocated to a single protein.

The finding that *Dm*GST-*ggt1ggt4* lines had significantly lower levels of S-DNT-$\gamma$EC after the 20-hour exposure to TNT was surprising, due to S-DNT-$\gamma$EC being generated independently of GGT activity. No significant difference in Conjugate 3 content measured by HPLC and LC-MS/MS confirms that this is not a result of differences in *Dm*GST enzyme activity between *Dm*GST.L and *Dm*GST-*ggt1ggt4* lines. One possible explanation could be the difference in the vacuole sequestration rate of Conjugate 3. Greater sequestration would reduce substrate availability for the generation of S-DNT-$\gamma$EC within the cytosol. This hypothesis could be investigated by measuring Conjugate 3 uptake by isolated vacuoles obtained from both plant lines [255,256].

The detection of both S-DNT-(Mal)Glc and S-DNT-(Mal)Cys within *Dm*GST-*ggt1ggt4* plants indicates that Conjugate 3 is able to be fully metabolised in the absence of GGT activity. This finding disproves prior assumptions that GGT1 was involved in metabolism of $\gamma$-glutamylcysteine derivatives generated from PCS1 activity [224]. Possible candidates for the metabolism of the S-DNT-$\gamma$EC is the GGP family. Whilst GGP activity toward $\gamma$-glutamylcysteine conjugates has not been investigated, their cytosolic localisation, and role in metabolising glutathione-conjugates within glucosinolate and camalexin

biosynthesis [126] makes them strong candidates. The detection of S-DNT-(Mal)Glc and S-DNT-(Mal)Cys also confirms that the end-fate of cysteinyl-conjugates within plants is not dictated by the pathway that initiates glutathione-conjugate metabolism. This discovery implies overlap between the pathways occurs at some point, most likely the cysteinyl-conjugate pool. However, depletion of downstream metabolites within *Dm*GST-*ggt1ggt4* knockout lines does confirm that initiation of Conjugate 3 metabolism by GGTs is the rate-limiting-step for this pathway in endogenous metabolism. Understanding the physiological importance of the GGT-catalysed step in glutathione homeostasis during xenobiotic stress, could identify factors that limit glutathionylation in the phytoremediation of TNT.

Prior investigations have shown the absence of GGT4 activity does not impact seedling tolerance to the herbicide 2,4-dichlorophenoxyacetic (2,4-D), despite a significant increase in gene expression [115], a finding supported by unpublished results that found no phenotypic response in GGT knockout lines grown on agar, or in soil, contaminated with TNT (Dr Liz Rylott, University of York, pers comm). A possible explanation for these results is the redundancy between glutathionylation and other plant detoxification pathways. The involvement of multiple pathways in detoxifying xenobiotics limits the depletion of cellular glutathione, whilst redundancy within glutathione-conjugate metabolism pathways ensures continued recycling even in the absence of GGT4 activity. Straining the recycling pathways for xenobiotic glutathione-conjugates could generate a phenotypic response in *ggt4* knockout lines, *Dm*GST expression in combination with TNT exposure offers a method to achieve this. The measurement of TNT uptake, total-glutathione content, and the accumulation of stress markers within *Dm*GST-*ggt4* lines in comparison to *Dm*GST lines, following prolonged TNT exposure, is one example of how the physiological importance of GGT4 within xenobiotic tolerance could be discerned. This experiment could also be complemented by assessing the impact of *GGT4* overexpression within *Dm*GST expression lines, identifying whether this is sufficient to generate an enhanced recycling pathway or whether downstream enzymatic reactions become rate-limiting. These investigations would make valuable contributions to the understanding of the glutathione detoxification pathway, for the purpose of generating enhanced plants for phytoremediation of TNT.

### 4.4.3 Compartmentalisation of Conjugate 3 and related metabolites

The combination of BNAF and *Dm*GST expression lines has provided the first evidence that xenobiotic conjugates derived from a variety of conjugation reactions are compartmentalised, most likely to the vacuole, *in planta*. The confirmation of this fate for Conjugate 3, supports the model of vacuole sequestration as the dominant pathway for glutathione conjugates [114,115,222]. Vacuole import of

glutathione-conjugates is thought to be carried out by ABC-transporters, with multiple members of the C-subfamily being shown to have activity *in vitro* [110]. Gene-expression analysis has identified two members of this subfamily, *ABCC1* and *ABCC2*, as potential candidates for this transport with both being tonoplastic transporters upregulated in response to TNT [104]. As previously mentioned, ABCC2 has been linked to glutathione-conjugate transport *in planta* with knockout lines showing reduced tolerance to CDNB; however, a direct link between lower tolerance and failure to sequester glutathione conjugates was not established [168]. The combination of *Dm*GST expression within *abcc2* lines and BNAF offers a platform to provide this evidence for TNT-glutathione conjugates.

The strong association of the S-DNT-Cys conjugate with the vacuole supports the hypothesis that the metabolism of glutathione-conjugate to cysteinyl-conjugate occurs within this compartment [221]. However, no enzymes capable of generating the glucosylated and malonylated products of S-DNT-Cys have been identified within the vacuole. Whilst the existence of such proteins cannot be ruled out, the formation of malonyl and glucosyl derivatives indicates that cysteinyl-conjugates can be transported out of the vacuole. However, no such activity has been described for a plant tonoplastic transporter. Transport of cysteinyl conjugates has been identified within mammalian cells with a L-type large neutral amino acid transporter (LAT1) being responsible for transporting methylmercury-cysteine conjugates across the plasma membrane [257]. Tonoplastic amino-acid transporters within plants that could potentially perform this function are members of the amino acid/auxin permease (AAAP), PQloop and amino acid-polyamine-organocation (APC) superfamilies. The AAAP family has been shown to function predominately as amino acid exporters within *Saccharomyces cerevisiae* [258], the mammalian PQloop protein cystinosin is the primary exporter of lysosomal oxidised cysteine into the cytosol [259] whilst the APC family contains several tonoplast-localised cationic amino acid transporters (CATs) [260,261]. As cysteinyl-conjugates are indicated to be generated by GGT4 in endogenous metabolism [122], understanding the transport mechanisms for these conjugates out of the compartment would translate to research beyond xenobiotic metabolism.

The strong association of malonyl-conjugates with the vacuole provides the first *in planta* evidence that these conjugates are compartmentalised within plants. A functional role of malonylation to aid in glucosyl-conjugate vacuole sequestration has been suggested, with a tonoplast-localised transporter within *Medicago truncatula* preferentially transporting malonlyglucoside conjugates over the parent-glucosides [174]. This hypothesis is also supported by evidence from Arabidopsis, wherein the elimination of PMAT1 activity resulted in greater release of naphthol-glucosides into the culture

medium, compared to WT controls. The use of BNAF with *Dm*GST-*pmat1* transgenic lines would allow the mechanistic function of malonyation within compartmentalisation to be investigated within plant tissue.

### 4.4.4 Conclusions

In conclusion this chapter has provided a greater understanding of the glutathione-detoxification of TNT, specifically relating to Conjugate 3, which is of high interest to phytoremediation studies due to the further degradation and mineralization potential of the molecule in the environment. The work has supported the currently accepted model of glutathione detoxification, confirming the dominance of GGT activity in initiating metabolism of glutathionylated xenobiotics. It has also provided the first *in planta* evidence for compartmentalisation of conjugated xenobiotics, as predicted by the accepted model for xenobiotic detoxification. Future research can build on the platform that the combination of TNT, *Dm*GST expression and BNAF provides to gain a greater understanding of the physiological role of compartmentalisation within xenobiotic detoxification, and to aid in the development of enhanced plant lines for phytoremediation purposes.

# Chapter 5: Characterising the endogenous and *Dm*GST-enhanced proteomic response to TNT within Arabidopsis roots

## 5.1 Introduction

The end-fate of TNT within plants is incorporation into the lignocellulosic material of the root tissue [85,86]. However, the proteins involved in this metabolic pathway, starting at transformation, and ending at lignocellulosic incorporation, remain for the most part unknown. The work described in previous chapters has provided further information on this area through the identification of new metabolic intermediates and their subcellular localisation. Combining this information with an understanding of the proteomic response to TNT can provide a more targeted approach for identifying putative proteins involved in its metabolism. At the time of writing, there have been several studies investigating the response to TNT within Arabidopsis; however, these have all been at the transcriptomic level [104,248–250]. Whilst transcriptomic profiles are valuable tools for investigating the response to stimuli, these datasets can contain false positives in respect to functionality at the protein level due to post-transcriptional and translational regulation. Another limitation of existing studies is their sole focus on the response to TNT within WT lines. The focus on WT lines limits the further characterisation of Conjugate 3 metabolism, as the significance of glutathionylation in endogenous metabolism of TNT is poorly understood. Due to the potential of Conjugate 3 to be subsequently mineralized, identifying the proteins involved in its metabolism is important. Towards this aim, the proteomic response to TNT within endogenous and *Dm*GST-enhanced systems is of high interest.

Alongside differential expression analysis, proteomics can be used to identify the spatial localisation of putative candidates, allowing detailed metabolic models to be developed. Classical approaches to identify protein localisation include GFP-tagging and immunoblotting. These methods, though precise, are highly laborious and thus are often only used to investigate a few proteins within a single study. High-throughput alternatives to these techniques utilize mass spectrometry (MS), due to its capabilities in detecting thousands of proteins within a single analysis. Organelle isolation is a common approach often combined with MS analysis and has provided an understanding of the proteomic profile of individual subcellular compartments [211,262–264]. Whilst analysis of isolated organelles theoretically provides the greatest confidence in compartmental localisation, it is reliant on high organelle purity and

thus can be a laborious process. Analysis of isolated organelles also only acquires information on a single compartment, which can limit conclusions if investigating multi-compartmental, xenobiotic detoxification pathways. Improvements in instrument precision and accuracy, in combination with advancements in machine learning techniques, are now allowing centrifugation-based proteomics to provide a multi-compartmental understanding of cellular proteomes. Examples of such techniques are Localization of Organelle Proteins by Isotope Tagging (LOPIT) and the label-free Protein Correlation Profiling [265,266]. These approaches separate cellular extract, via density gradients or differential centrifugation, and then use machine learning algorithms to allocate spatial identity to proteins through comparative analysis against distribution profiles of known organelle marker proteins. As with all proteomic techniques, these methods have benefited from advancements in MS resolution and acquisition rates, which have allowed greater numbers of proteins to be used in compartmental analysis, thus increasing the resolution and confidence of spatial allocations [267]. The growing capabilities of these techniques have also spurred the development of versatile, computational packages that reduce the knowledge/skills required to perform the associated complex spatial allocation analysis [215]. These centrifugation-based proteomic techniques have been applied to Arabidopsis whole root tissue [268], and root-tissue-derived callus cells [269], to provide an understanding of the organelle proteome within this tissue. However, as the aqueous gradient used in these studies could not prevent diffusion of soluble organelle proteins during centrifugation, only the membrane-associated proteins were investigated. Therefore, there is still substantial information to be acquired on the organelle proteome within Arabidopsis root tissue.

Proteomic analysis of BNAF fractions offers the potential to allocate organelle identity to both membrane-associated and free proteins, whilst also potentially improving resolution in respect to TNT-metabolite localisation. The use of organic solvents within NAF-techniques prevents the diffusion of polar species, which includes free proteins, from their compartment. Therefore, the use of NAF-techniques, theoretically, offers an ability to provide spatial identity to a greater variety of root proteins than what has previously been described [268,269]. Prior studies have used proteomic analysis of NAF-derived fractions to detect a greater number of marker proteins, than is available for spectrophotometric marker enzyme assays, thus improving the compartmental resolution of the analysis [191,194]. The combination of enhanced compartmental resolution, provided by proteomic analysis, with the co-fractionation of metabolites and proteins in NAF-based techniques, allows for a more integrated approach in studying subcellular metabolism. This was demonstrated in Arabidopsis leaf tissue, with proteins and metabolites within different aspects of central carbon metabolism forming

distinct compartmental clusters [191]. The improved compartmental resolution provided by proteomic analysis of BNAF fractions may also allow the distinction between vacuole and extracellular/apoplastic localisation of TNT-derived metabolites. Whilst a distinction between these compartments was not achieved within published examples [191,194], these results were obtained from analysing leaf tissue with a linear density gradient. As BNAF uses a non-linear gradient, and the density profiles between leaf and root tissue have been shown to differ (see Chapter 3 Section 3.2), the distinction between apoplast and vacuole may be achieved.

This chapter describes the work performed to characterise the proteomic response to TNT within Arabidopsis root tissue. The proteomic analysis of BNAF fractions identified that the currently optimised technique can provide spatial information to a large number of proteins, ~2389, based on a five compartmental-cluster model. The use of this model to investigate TNT-metabolite compartmentalisation validated sequestration of these metabolites from the cytosol as identified by colorimetric assays within previous chapters. The proteomic response to TNT and *in planta Dm*GST presence was investigated through the analysis of whole-root tissue. This analysis revealed key biological processes induced in response to TNT, as well as putative protein candidates involved in the metabolism of TNT and Conjugate 3. The combination of these two proteomic datasets provides a resource to develop detailed models on the pathways involved in TNT detoxification based on protein's response to TNT, molecular function, and localisation within the root cell.

## 5.2 Materials and Methods

### 5.2.1 Plant material

*Dm*GST.C3 root tissue was used for proteomic analysis of fractionated tissue. Whole root tissue from WT and *Dm*GST.C3 plant lines was used for investigation of differential protein response to TNT.

Plant material used in proteomic analysis was obtained in a manner identical to that described in Chapter 3 section 2.4.

### 5.2.2 Total protein extraction and LC-MS/MS analysis

A modified version of the protocol outlined in Fürtauer *et al*. (2018) [217] was used for total protein extraction and preparation from both whole and fractionated tissue. In respect to whole root tissue, this required frozen material to be ground into a fine powder over dry ice and lyophilised overnight (-50 °C, ~0.05 mbar). Lyophilised material was homogenised in 8.5 mL extraction buffer (50 mM

Hepes/potassium hydroxide (pH 7.8), 8M urea) via 30 minutes sonication, broken into five-minute batches, within a chilled ultrasonication bath (45 KHz). The suspension was then passed through a 25 µm nylon gauze and centrifuged for ten minutes (4400 xg at 4 °C). Soluble protein was then precipitated by mixing the resulting supernatant with pre-chilled acetone plus 0.5 % $\beta$-mercaptoethanol (1:4 v/v) and leaving at -20 °C overnight. The precipitated protein was then pelleted by a five-minute centrifugation (4400 xg at 4 °C), and the supernatant discarded. The protein pellet was washed three times using 10 ml of ice-cold methanol after which the pellet was resuspended in 5 mL of ice-cold acetone and allowed to dry at RT within a fume hood. The dried protein pellet was then resolubilised in 1 mL of extraction buffer, and the protein content of the solution was quantified using a microplate format of the Bradford assay according to the manufacturer's instructions (BioRad, Watford UK).

Total protein was extracted from fractionated material in a similar process with some minor modifications. Firstly, fractionated material was resuspended in 1 mL of extraction buffer and incubated on ice for 20 minutes with vortexing every five minutes. Insoluble material was pelleted by a five-minute centrifugation (10,000 xg at 4 °C), and 800 µL of the resulting supernatant was mixed with pre-chilled acetone plus 0.5 % $\beta$-mercaptoethanol (1:4 v/v). Following overnight incubation at -20 °C, the protein pellet underwent three washing steps using 1 ml of ice-cold methanol before being resuspended in 500 µL ice-cold acetone. Dried protein pellets were dissolved in 400 µL of extraction buffer. Samples were normalised by volume for digestion and loading steps to retain relative distributions of proteins within fraction batches.

Purified proteins were digested by S-trap digestion procedure (PROTIFI, NY USA) then normalised by solution volume for BNAF fraction analysis and protein content, equivalent to 50 µg total protein, for whole tissue analysis. The manufacturers protocol for digestion was followed and is briefly described. Protein sample, 20 µL, was reduced by the addition of 1 µL of 120 mM Tris(2-carboxyethyl)phosphine (aqueous) and incubated at 55 °C for 15 minutes. Samples were then cooled for five minutes, then alklyated by addition of 1 µL of 500 mM methyl methanethiosulfonate in isopropanol. Solution was incubated for ten minutes at RT after which 2.5 µL of 27.5 % phosphoric acid (aqueous) and 165 µL 100 mM tetraethylammonium bromide (TEAB) in 90 % methanol was added. The solution was vortexed briefly and loaded onto S-trap micro-spin column held within a 2 mL collection tube. Samples were centrifuged for 30 seconds (4000 xg at 20 °C), the resulting flow through was discarded, and 165 µL TEAB in 90% methanol added to the column. The samples were centrifuged again, and this step was repeated a further five times. Upon completion of the final iteration, samples were centrifuged for one

minute (4000 xg at 20 °) to remove liquid residue, and each minicolumn was transferred to a new 2 mL collection tube. To each sample, 20 µL of trypsin/Lys-C protease mixture was added (0.1 µg $\mu L^{-1}$ in 50 mM TEAB buffer (aqueous)) (Promega), and the samples were incubated at 47 °C for two hours. Following incubation, 40 µL 50 mM TEAB (aqueous) was added to each sample and eluted by centrifugation for one minute (4000 xg at 20 °C). The elutant was retained and the elution step repeated twice more, first with 0.2 % formic acid (aqueous) and secondly with 50 % acetonitrile (aqueous). The resulting elutants from all three samples were combined and transferred to a LoBind tube (Eppendorf, Stevenage UK). Peptide solutions were dried and then dissolved in 100 µL 0.1 % trifluoroacetic acid (aqueous). Samples were centrifuged for one minute (4000 xg at 20 °) and the resulting supernatant analysed using LC-MS/MS.

Post-digestion, 2 µg equivalent aliquotes of peptides were used for analysis of whole tissue samples whilst equal volumes of peptide solution were used for analysis of the fractionated sample. Introduction to LC-MS/MS system was achieved via a EvoSep Pure tip (EvoSep Biosystems, Denmark) and separation of peptides was achieved using an EvoSep One UPLC (EvoSep Biosystems, Denmark) with an 8 cm Endurance C18 column and a 60 samples-per-day elution method. Eluted peptides were detected using a TimsTOF HT mass spectrometer (Bruker, Coventry UK) operated in data independent acquisition (DIA) parallel accumulation-serial fragmentation mode. A 50 *m/z* window between 400-1200 *m/z* was used with a total 1.1 s cycle time.

### 5.2.3 Protein identification and quantification

Proteins were identified from raw data using the *Arabidopsis thaliana* subset of UniProt using the DIA-NN software [270]. The resulting *in silico* spectral library was iterated against the acquired DIA data. The target false discovery rate (FDR) set for peptide spectral matches was 1%. To allow statistical comparison of relative protein abundance, processed results were transformed to a protein-centric format using an in-house Konstanz Information Mine (KNIME) pipeline (Technology Facility, University of York). A minimum requirement of two unique peptides was applied for accepted proteins whilst missing quantification values were filled using a minimum value imputation.

### 5.2.4 Compartmental allocation of Arabidopsis root proteome

For the compartmental allocation of proteins, a bioinformatic workflow designed for hyperLOPIT experiments was used [271]. This analysis used relative distribution of marker proteins as labelled input for machine-learning classification of compartmental identity using the Support Vector Machines (SVM)

method. Marker enzymes were identified using the subcellular localisation database for Arabidopsis proteins (SUBA, v5.0) [272]. Criterium for marker protein selection was the confirmed localisation of the candidate to a specific compartment within a plant cell system using fluorescence assays i.e., GFP-tagging. Generated marker enzyme lists were verified manually. The marker protein set comprised 93 nuclear, 92 plastid, 28 endoplasmic reticulum (ER), 32 plasma-membrane, 38 mitochondrial,30 peroxisomal, 54 cytosolic, 15 extracellular, 20 golgi and 14 vacuolar. The full lists of marker enzymes can be found in Table 5.2.4.1. For analysis at the five-cluster resolution these marker enzymes were labelled with their respective cluster rather than their respective compartment.

The SVM method of compartmental/cluster prediction of unknown protein is briefly described. Each set of marker protein profiles were separated into training and validation groups. The training group was obtained by stratified sampling of 80 % of the profile of each compartment without replacement, the remainder became the validation group. Each training group underwent five-fold cross-validation to identify optimised SVM regularisation parameter (cost) and Gaussian kernel width (sigma) pairs. Performance of all cost and sigma pairs was assessed by testing their ability to train a classifier using training groups and correctly allocate test groups. The output of this analysis gave macro F1 estimate generalisation performance values. This process was iterated 500 times, and mean macro F1 scores for each cost: sigma combination calculated. The cost: sigma pair that gave the highest F1 score was used to develop the model for allocation of compartmental or cluster association. For both the ten-compartment and five-cluster analysis, the best performing cost: sigma pair was 16 and 0.1 respectively.

**Table 5.2.4.1: Subcellular compartments and their respective marker proteins used as inputs for SVM allocation of compartmental identity.**

| Subcellular Compartment | Marker Proteins |
|---|---|
| Cytosol | NBR1, GSTU9, DHAR2, EXO70F1, CPK6, URH2, LSG1-1, PYD3, MS2, AAO3, REP, ASP2, ATEXO70D2, ABA2, UXS3, MAP1A, GSTF2, ACBP4, SAT5, UGE1, GLYR1, PIMT1, DPE2, LSM1B, TRX3, TPK1, LSM1A, ACT7, SDH, PRS4, MIOX2, ACBP6, SOT16, GSTU7, RH6, STR18, MAP2B, BOB1, SH3P2, SOT18, GGP3, GRXC2, TFCB, SOT17, ELF5A-2, TCTP1, UXS5, UXS6, BCAT4, GSTF9, ENGASE1, BCAT6, HPD, XK2 |
| Endoplasmic Reticulum | ABCI20, DPL1, CYTB5-D, CK1, BIP3, SAC8, CYP73A5, BGLU23, CNX1, PDIL2-3, PDIL2-2, SAC7, STL2P, CYP98A3, CYP51G1, PSD3, PYD2, PDIL1-3, KCR1, CRT2, CYTB5-B, BIP1, ABCI21, ACA2, ACBP1, CYP83B1, SQS1, CYP83A1 |
| Extracellular | PME3, CRRSP1, CYS5, PER39, PER4, CuAOgamma1, PER62, PER71, AGP31, FUC95A, PR1, SRPP, XTH4, SCPL24, GGT1 |
| Golgi | HLB1, GC6, COG6, UXS2, KEG, AGD7, AGD9, GC5, MTV1, AGD5, CASP, APY1, GC1, AGD8, GMII, TMN1, GAUT1, RABA4B, VPS52, GUX3 |

| Subcellular Compartment | Marker Proteins |
|---|---|
| Mitochondrion | ELM1, ETFQO, NDB2, D2HGDH, ISU1, ABCB25, HXK1, AAC1, PHB1, CYSC1, ICP55, CLPP2, FRO1, IVD, PHB4, HCC1, NDT2, VDAC1, MFDX2, PHB2, ORRM2, ADNT1, FUM1, SAT3, PHB6, GRXS15, VDAC2, EMB1467, VDAC4, WHY2, TIM17-2, PECT1, PPR336, GFA2, NTR1, TIM23-2, KPHMT1, PPT1 |
| Nucleus | SPX2, CENH3, NUP107, XLG2, XLG3, TCP8, CAMTA5, PHYE, PP7, HDA19, CPL1, RH37, XPO1, XRN3, NUP96, NUP85, NUP1, VAL1, MOS1, ARP6, ALY3, AHL1, EMB3142, RAP74, HDC1, NUP133, LUG, NUA, RPA1A, AGO4, NUP155, CBP20, LUH, VIP2, MBD4, STIPL1, NUP160, MBD2, CRWN1, SE, NUP54, MOS4, PES, SR45, STA1, ALY4, SMU2, HMGA, RBR1, EMB514, HIT4, HDT3, FIB2, NSN1, FIB1, NOP56, SUVH1, NRPB4, ESD4, MBD1, HDT2, PRORP3, SCL30, TGA1, TFIIS, ASIL1, FIE, HEN1, GRP23, DIM1A, NUP58, MAIL1, FEN1, NUP43, SR30, MBD11, RH36, DOT2, VRN1, HDA15, HMGB5, HMGB1, SKIP, YAO, APC1, RH5, SC35, HDT4, NRPB3, HDT1, RS31, SR34, SCL30A |
| Peroxisome | NADK3, CuAOzeta, APX3, OPR3, UP3, KAT1, AAE1, SDRA, ICL, ALDH10A9, PUMY, PGD2, SOX, AAE7, CPK1, CAT3, MFP2, PED1, AAE5, GSTT1, LACS7, ECH2, ICDH, SCP2, GGAT1, ECI2, HINT4, DHNAT1, LACS6, ECHIA |
| Plasma Membrane | CSI1, LYK4, At2g39360, ABCG37, AT1G51840, AHA2, ABCG34, HPCA1, ACA8, PSY1R, AMT1-3, BSK1, SULTR1;2, SYP122, BCA4, GPA1, IOS1, RBOHD, ABCC4, MSL9, CPK21, HIR1, TTL, MSL10, ABCG40, FLOT1, ABCG36, GDPDL3, ABCB19, BIR2, CPK9, NHL3 |
| Plastid | PAP2, ATHX, NHL10, PAP1, ADT3, STR16, HISN7, PAA2, GPX1, RIBA1, SFR2, FC1, FSD1, KIN11, CIPK23, QPT, ABC1, PUR5, APS2, PYD1, CLPD, SIRB, DHAR3, PAA1, THF1, KEA2, PSAT1, CRB, ICS1, PSB33, PSP, UKL2, CLPP4, GGPPS1, HO1, HON5, CYP74A, ISPD, WHY3, ISA3, DJA5, GWD1, ADT2, TAAC, ASP5, DXR, BAM2, CBSX2, ADK, CLPR4, ABCI8, FBA3, CLPR1, KAS1, TPS08, QS, BCA5, APS4, MS3, PKP1, FD3, ADT5, ASE1, RIBA2, OMR1, EMB2360, PPA6, CCH, SUFE1, BCAT3, WHY1, APS1, HSK, PKP2, OASB, LHCB5, SHM3, WIN1, GA2, LTO1, FZL, TGD3, PSBO1, ADT1, GWD3, DEGP1, FTSZ2-2, FLN2, YLMG1-1, ARC6, AO, FTSZ2-1 |
| Vacuole | VCL1, ALEU, RD19C, SCPL49, TIP1-2, At4g32940, ABCC1, GGT3, ABCC2, ACA11, ACA4, TPC1, BFRUCT3, AVP1 |

### 5.2.5 Assessment of compartmental/cluster resolution

The separation of clusters, the clustering resolution, was quantified using the QSep function and visualised through PCA analysis via the pRoloc R package [271].

### 5.2.6 Differential protein analysis in whole-root tissue

Relative abundance of proteins within total protein extract obtained from whole root tissue was compared using a pair-wise T-test followed by a Benjamini-Hochberg procedure for multiple test correction [273] to obtain an FDR value. Selection criteria for significantly altered abundance were an FDR value below 0.05 and a $Log_2$ fold change > |1|. This analysis was achieved using the FragPipe analyst package [274]. Principle component analysis (PCA) was performed on centered and scaled protein abundance data.

### 5.2.7 Hierarchical analysis

Hierarchical clustering of BNAF fractions considered the similarities in proteomic distribution profiles between individual fractions, this analysis was performed within R. Normalized Mutual Information

(NMI) scores for measuring quality of clustering were calculated using the dendextend [275] and aricode [276] R packages. Dendrograms were visualised using the ggdendro R package [277].

Hierarchical clustering of subcellular compartments considered the similarities in marker enzyme distribution profiles and was achieved using pRoloc R package [271].

Hierarchical clustering of logarithmic changes in protein abundance within whole tissue extracts compared to WT(-TNT) control was performed and visualised using the HeatmapR package [278].

### 5.2.8 Network analysis of whole root proteome

Network analysis of differentially-expressed proteins was performed within Cytoscape (v3.10) [279] using the clusterMaker2 package application [280]. Protein-protein interaction networks were imported from the Search Tool for the Retrieval of Interacting Genes/Proteins (STRING) database (v12.0) [281], with a STRING score of 0.4 being the threshold for interaction. Markov Clustering Algorithm (MCL) [282] was used for clustering differentially-expressed proteins. Clustering parameters were an inflation value of 2 and 1.8 and an edge-cut-off score of 0.5.

### 5.2.9 Biological pathway enrichment and molecular function analysis

The molecular function Gene Ontology (GO) terminology for each differentially expressed protein was obtained using the AnnotationDbi package [283]. Molecular functions were binned according to broad enzymatic activity terms.

Biological process GO terminology and Kyoto Encyclopedia of Genes and Genomes (KEGG) pathway enrichment was performed using the stringAPP application for Cytoscape [284] with enrichment analysis have a 0.05 FDR threshold.

# 5.3 Results

## 5.3.1 Compartmental analysis of root proteome

### 5.3.1.1 Confirming reproducibility of BNAF methodology

To enable machine learning techniques to be used to allocate compartmental identity to Conjugate 3 metabolites, BNAF fractions used in the proteomic analysis were generated from *Dm*GST-expression-line root tissue exposed to TNT. Using DIA-analysis, 5182 proteins were detected within all analysed fractions. The ability of BNAF to reproducibly generate fractions with unique compositions was assessed by hierarchical cluster analysis of relative protein distributions, with clustering efficiency assessed using NMI. The NMI score is a measurement of the efficiency in which labelled data can be grouped based on a designated number of clusters. In respect to this analysis, samples were labelled according to the density from which they were obtained, and the number of clusters reflected the number of fractions comprising the density gradient, which was six. An NMI score of 1 indicates perfect clustering of samples into six clusters, with each cluster corresponding to a different fraction of the density gradient. Therefore, the obtained NMI score of 0.871 confirmed a high efficiency of clustering samples based on density, thus establishing that the optimised BNAF protocol could fractionate the root proteome in a density-dependent, highly-reproducible manner (Figure 5.3.1.1.1). This analysis also confirmed the proteomic profile of fractions was density dependent, as clusters representative of lower densities showed greater similarity to each other than to fractions obtained at greater densities.

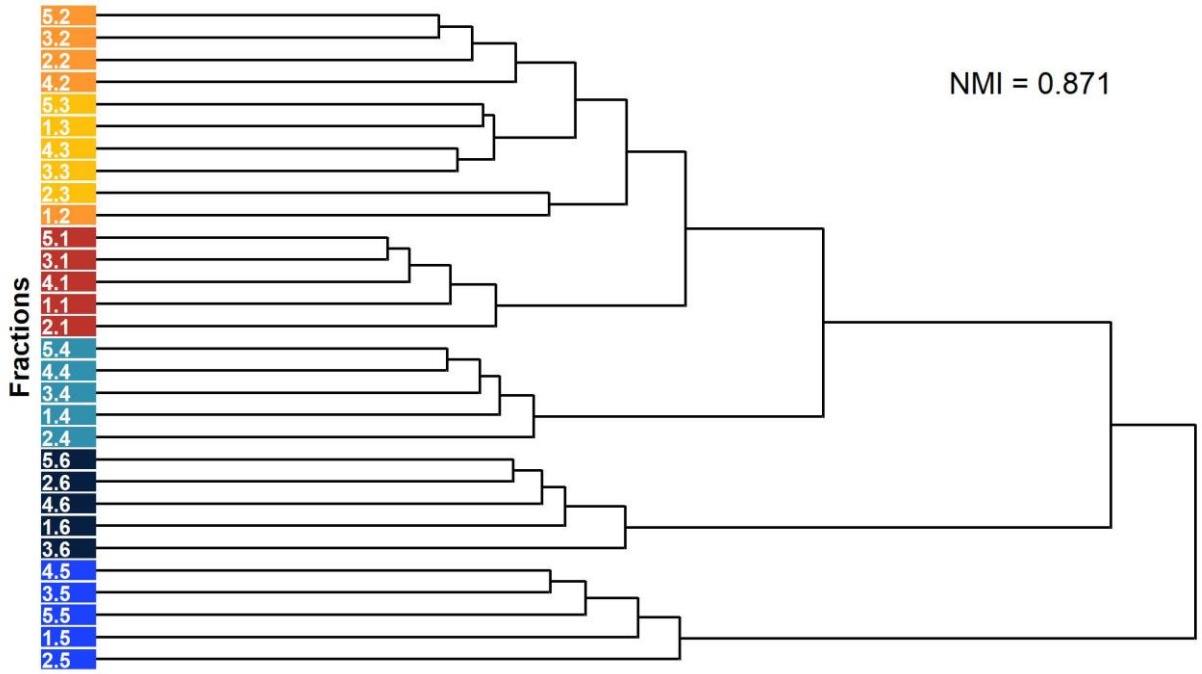


**Figure 5.3.1.1.1: Hierarchical clustering of BNAF fractions based on similarities in proteomic profiles.** Analysis was based on similarities in relative protein abundance between samples. Numeric labels correspond to the biological replicate and the density the sample was acquired at respectively, with density 1 representing $\rho$ = 1.47 g cm$^{-3}$ and density 6 representing $\rho$ < 1.3 g cm$^{-3}$. An NMI score of 0.871 confirmed highly efficient clustering of samples based on density.

### 5.3.1.2 Spatial allocation of root proteome

As proteomic profiles of replicate fractions were confirmed to be suitably similar (Figure 5.3.1.1.1), the distribution profiles of marker enzymes for each subcellular compartment were then compared. This analysis aimed to identify whether the major subcellular compartments within the root cell showed distinct distribution profiles across the density gradient. Hierarchical cluster analysis identified that subcellular compartments could be grouped into five clusters based on marker enzyme distribution profiles (Figure 5.3.1.2.1A). Cluster 1 comprised the vacuole, plasma membrane, and the extracellular space which includes the apoplast. This cluster showed an enrichment within the first fraction ($\rho$ > 1.47 g cm$^{-3}$) with a linear-like decrease in abundance with lowest levels detected within fraction 6 ($\rho$ < 1.3 g cm$^{-3}$) (Figure 5.3.1.2.1B). Cluster 2 represented the peroxisome, and exhibited a minor enrichment within the first fraction with abundance decreasing marginally across the density gradient (Figure 5.3.1.2.1C). Cluster 3 comprised the cytosol, ER and the golgi, and was characterized by equal distribution across the density gradient (Figure 5.3.1.2.1D). Cluster 4 represented the nucleus, with

protein abundance in this cluster presenting a linear increase with density peaking at fraction 5 ($\rho$> 1.3 g $cm^{-3}$) (Figure 5.3.1.2.1E). Finally, Cluster 5 comprised mitochondria and plastids. Similar to cluster 4, this group of proteins had the lowest abundance within the first fraction but displayed an enrichment in fraction 5 which was sharper than displayed for nuclear marker proteins (Figure 5.3.1.2.1F).

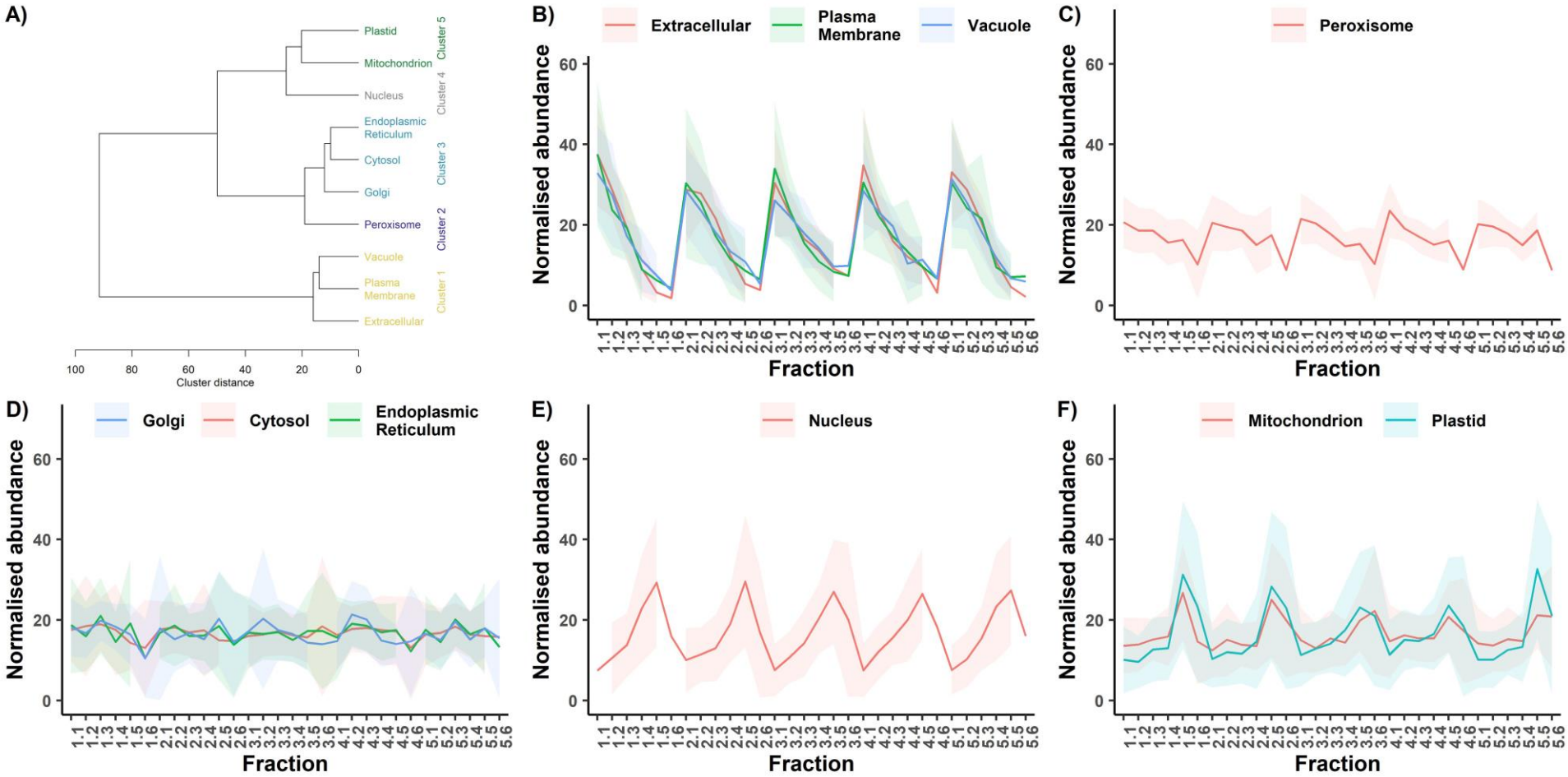


**Figure 5.3.1.2.1: Clustering of subcellular compartments based on density-distribution profiles of marker enzymes. A)** Hierarchical clustering of subcellular compartments based on marker enzyme distributions across the density gradient. **B)** Distribution profiles of the vacuole, plasma membrane and extracellular marker proteins. Solid lines represent mean abundance of marker proteins whilst shaded regions represent ± SD. The first number of fraction label refers to the biological replicate whilst the second number refers to fraction

density, with 1 representing $\rho$ = 1.47 g $cm^{-3}$ and 6 representing $\rho$ < 1.3 g $cm^{-3}$. **C)** Distribution profile of peroxisome marker proteins. **D)** Distributions profiles of cytosol, ER and golgi marker proteins. **E)** Distribution of nuclear marker proteins. **F)** Distribution profiles of mitochondria and plastid marker proteins.

As several subcellular compartments showed high similarity in distribution profiles, the impact of reducing spatial resolution to five compartmental clusters, on spatial allocation by machine learning, was investigated. This analysis compared the ten-cluster model, with each cluster representing a single subcellular compartment, against the five-cluster model for their ability to obtain distinguishable clusters from proteomic data. The resolution of clustering was quantified by calculating cluster normalised distances (CNDs), these represent the ratio of between-cluster to within-cluster average distances with larger CNDs indicative of greater distinction between clusters. The CND values obtained from both models ranged between 0.85 and 2.0 (Figure 5.3.1.2.2A&C), indicative of large within cluster average distances. This result was verified visually through the overlay of clusters onto PCA plots of protein distributions (Figure 5.3.1.2.2B&D). The use of a five-cluster model, relative to the ten-cluster model, resulted in a minor decrease in CND values that was shown not to be significant (Students T Test, $p > 0.05$). Therefore, though the five-cluster model increased the size of individual clusters it did not negatively impact the ability to distinguish between these clusters.

Following on from resolution analysis, the impact each model had on the confidence of protein spatial allocation was assessed through comparison of SVM scores. The SVM scores are a measure of the probability that the protein allocation to a cluster is correct. In respect to subcellular localisation, higher SVM scores suggest that the protein is most likely found within that compartment, with marker proteins having a SVM score of 1. Both the five-cluster and ten-cluster model allocated spatial identities to 49.9 % of the unknown proteins detected, 2385 and 2389 proteins respectively. However, the SVM scores obtained with the five-cluster model were significantly higher, with a median score of 0.62 compared to 0.39 obtained by the ten-cluster model (Mann Whitney U test, $p < 0.0001$). It was also interesting to note that when the ten-cluster model was used, no proteins were allocated to the ER, golgi or vacuole (Figure 5.3.1.2.3A). These were compartments that had highly similar distributions to other subcellular compartments but were represented by fewer marker enzymes. A final point to note was that the use of a five-cluster model resulted in allocation of proteins to different compartments, shown by the decrease in the number of proteins allocated to the peroxisome and nucleus (Clusters 2 and 4 respectively) and correspondingly, an increase within the vacuole, cytosol and plastid clusters (Clusters 1,3 and 5 respectively; Figure 5.3.1.2.3B). These results confirmed that the use of a five-cluster model greatly improved the confidence in cluster allocation of proteins with unknown spatial identity.

As the five-cluster model, when compared to the ten-cluster model, exhibited improved cluster allocation confidence whilst not impacting clustering resolution, it was chosen as the most suitable way

to present the spatial data obtained from the proteomic investigation. Therefore, the use of proteomics has confirmed that the currently optimised BNAF technique is able to obtain a greater compartmental resolution than identifiable with spectrophotometric enzyme assays; however, it is only able to obtain uniquely distinct distributions for two of the ten major subcellular compartments.

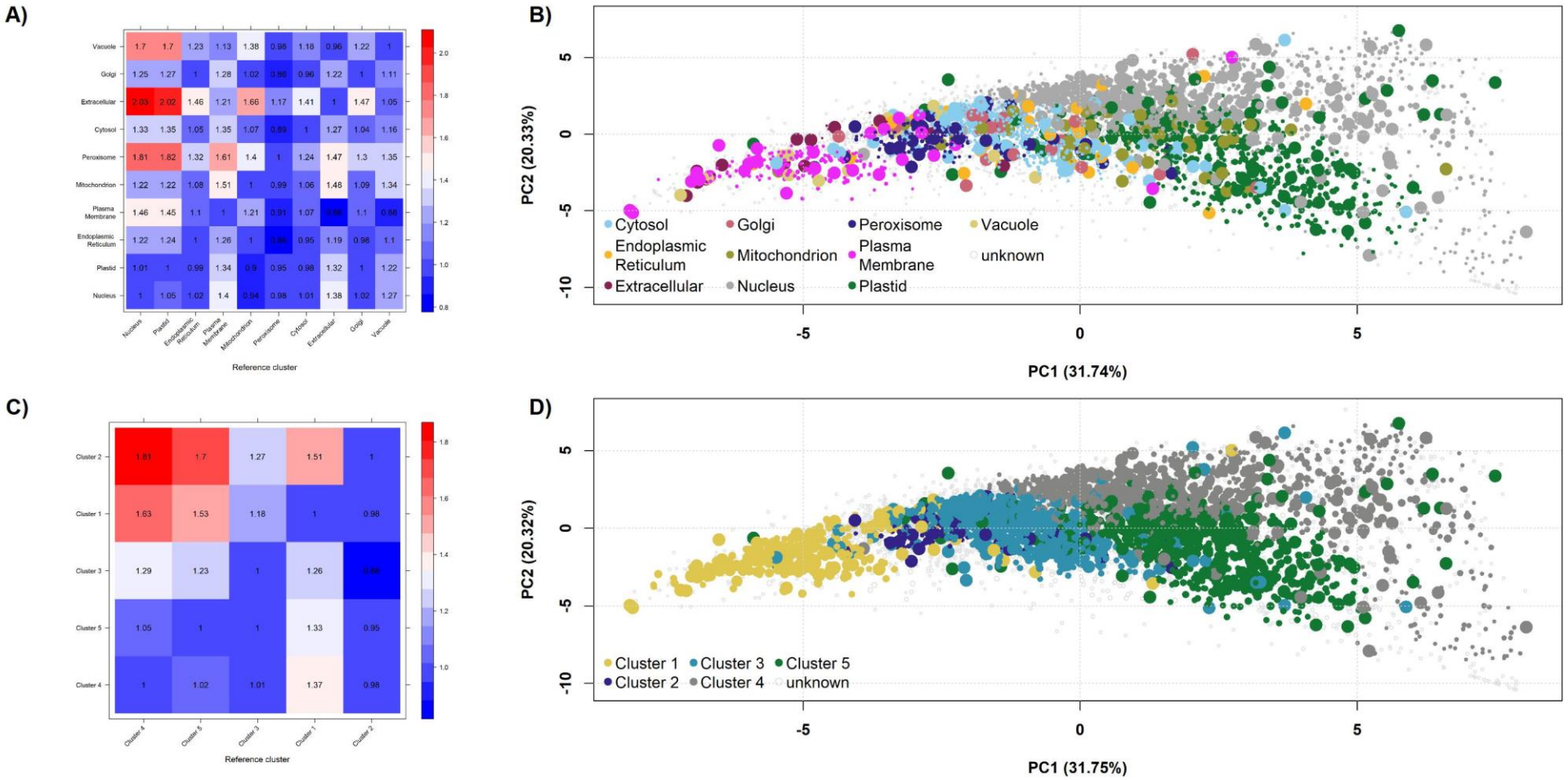


**Figure 5.3.1.2.2: Comparison of impact of ten-cluster and five-cluster models on cluster resolution using CNDs. A)** The CND scores obtained for cluster generated using the ten-cluster model. The larger the ratio the more distinguishable the compartments, the greatest separation was seen between the extracellular and the nucleus/plastid compartments. **B)** Variation of detected proteomes SVM scores for organelle classifications from ten-cluster model projected onto two principal components. Size of points are proportional to SVM scores of proteins allocated classification. Uncoloured points did not pass the score threshold for cluster classification. **C)** The CND scores obtained for cluster generated using the

five-cluster model. Whilst marginally lower ratios were obtained, there was no significant difference in the mean CND score (Two Sample T-test, $p > 0.05$). The greatest differences were seen between Cluster 2 and clusters 4 and 5. **D)** Variation of detected proteomes SVM scores for organelle-cluster classifications from five-cluster model projected onto two principal components.

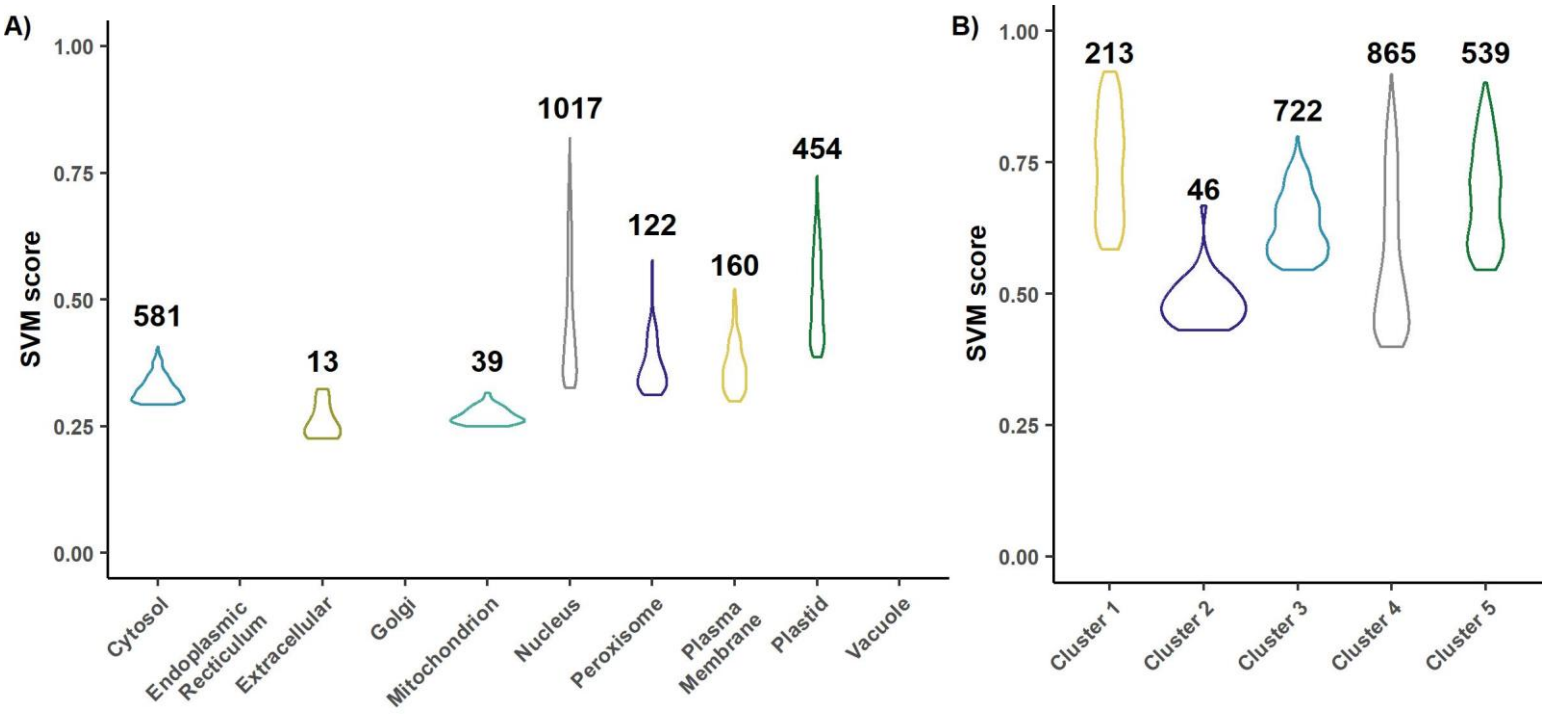


**Figure 5.3.1.2.3: Comparison of ten-cluster and five-cluster models on confidence in spatial allocation of proteins. A)** SVM score distribution of proteins allocated using ten-cluster model. The majority of compartmental allocations were of low confidence shown by a median SVM score of 0.39. No proteins were allocated to the ER, golgi or vacuole compartments. **B)** SVM score distribution of proteins allocated using the five-cluster model.

Performing proteomic analysis on fractions obtained from BNAF allows spatial localisation of metabolites to be inferred from the use of multiple compartmental markers. This analysis can provide a deep understanding of the compartmentalised cell when complete metabolomics is performed but can still be useful when investigating only a handful of metabolites. The spatial allocation of TNT metabolites, identified within previous chapters, was investigated using the five-cluster model. All metabolites were allocated to Cluster 1 which comprises the vacuole, plasma membrane and extracellular space (Figure 5.3.1.2.4). SVM scores for each metabolite are found in Table 5.3.1.2.1. These findings confirm those inferred from colorimetric enzyme assays i.e., that detoxified metabolites are sequestered from the cytosol.

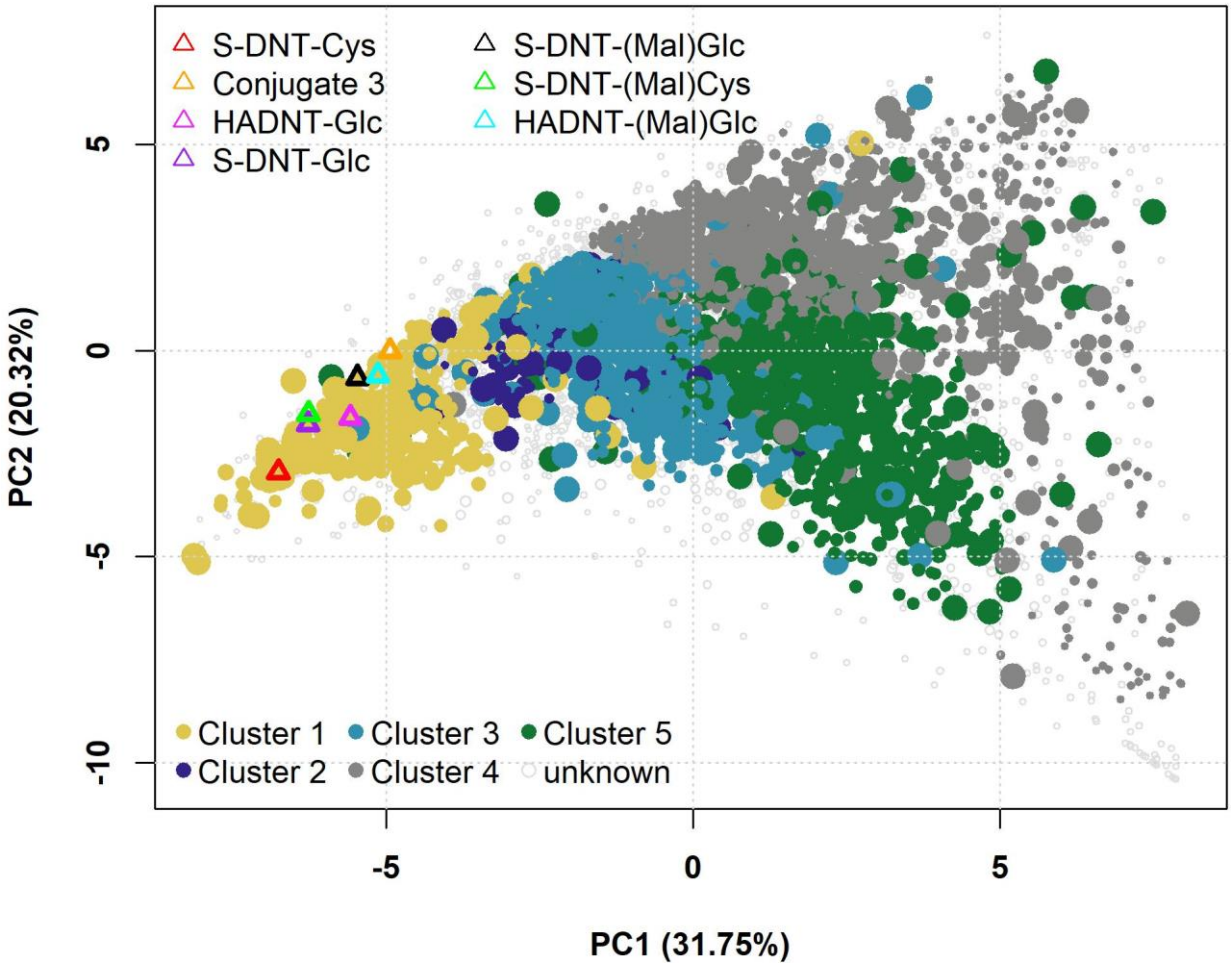


**Figure 5.3.1.2.4: Compartmentalisation of detoxified TNT-metabolites validated by machine-learning techniques.** All metabolites generated by TNT-detoxification were allocated to Cluster 1 which comprises the vacuole, plasma membrane and extracellular space.

**Table 5.3.1.2.1: Spatial allocation of metabolites generated from TNT-detoxification using five-cluster SVM model.** Numbers within brackets are the SVM scores of spatial allocation for each metabolite.

| Metabolite | Cluster Prediction |
|---|---|
| Conjugate 3 | Cluster 1 (0.56) |
| S-DNT-Cys | Cluster 1 (0.48) |
| S-DNT-(Mal)Cys | Cluster 1 (0.36) |
| S-DNT-Glc | Cluster 1 (0.70) |
| S-DNT-(Mal)Glc | Cluster 1 (0.58) |
| HADNT-Glc | Cluster 1 (0.71) |
| HADNT-(Mal)Glc | Cluster 1 (0.68) |

## 5.3.2 Proteomic response within whole-root tissue to the presence of *Dm*GST and TNT exposure

### 5.3.2.1 Investigating the interactions of proteomic responses

To identify proteins that were differentially expressed in response to TNT exposure and enhanced Conjugate 3 production, a two-by-two condition study was performed. This study comprised analysing the root proteome from WT and *Dm*GST plant lines following 20-hour exposure to either 250 µM TNT in DMSO (+TNT) or to an equivalent volume of DMSO only (-TNT). In total, 6381 proteins were detected within each sample and the changes in relative abundance of proteins between each condition was calculated. Hierarchical analysis of protein abundance changes compared to the control condition, WT (-TNT), revealed similarities between the endogenous and *Dm*GST-enhanced response to TNT (Figure 5.3.2.1.1A). Interestingly, this analysis also revealed similarities between the responses to the presence of *Dm*GST and TNT exposure. The PCA of protein abundance confirmed TNT exposure and *Dm*GST presence were responsible for the largest proportion of sample variation, 30% of the total variation, with samples clustering into their respective conditions (Figure 5.3.2.1.1B). The individual and additive impacts of *Dm*GST presence and TNT exposure was then investigated through pair-wise comparison of conditions at the individual protein level. Comparison between plant lines, WT vs *Dm*GST, revealed that the presence of TNT reduced the number of differentially-expressed proteins from 63 to 11 (Figure 5.3.2.1.1C&D). Comparison within plant lines, -TNT vs +TNT, revealed a slightly greater response to TNT within WT than within *Dm*GST, 87 compared to 73, though in both lines the majority of proteins were induced (Figure 5.3.2.1.1E&F). Interestingly, the greatest response was between WT (-TNT) vs *Dm*GST (+TNT), with 237 proteins differentially expressed (Figure 5.3.2.1.1G). As this response was larger than the sum of individual responses to either *Dm*GST presence or TNT exposure, it is evidence for the additive effect of these two factors on the root proteome.

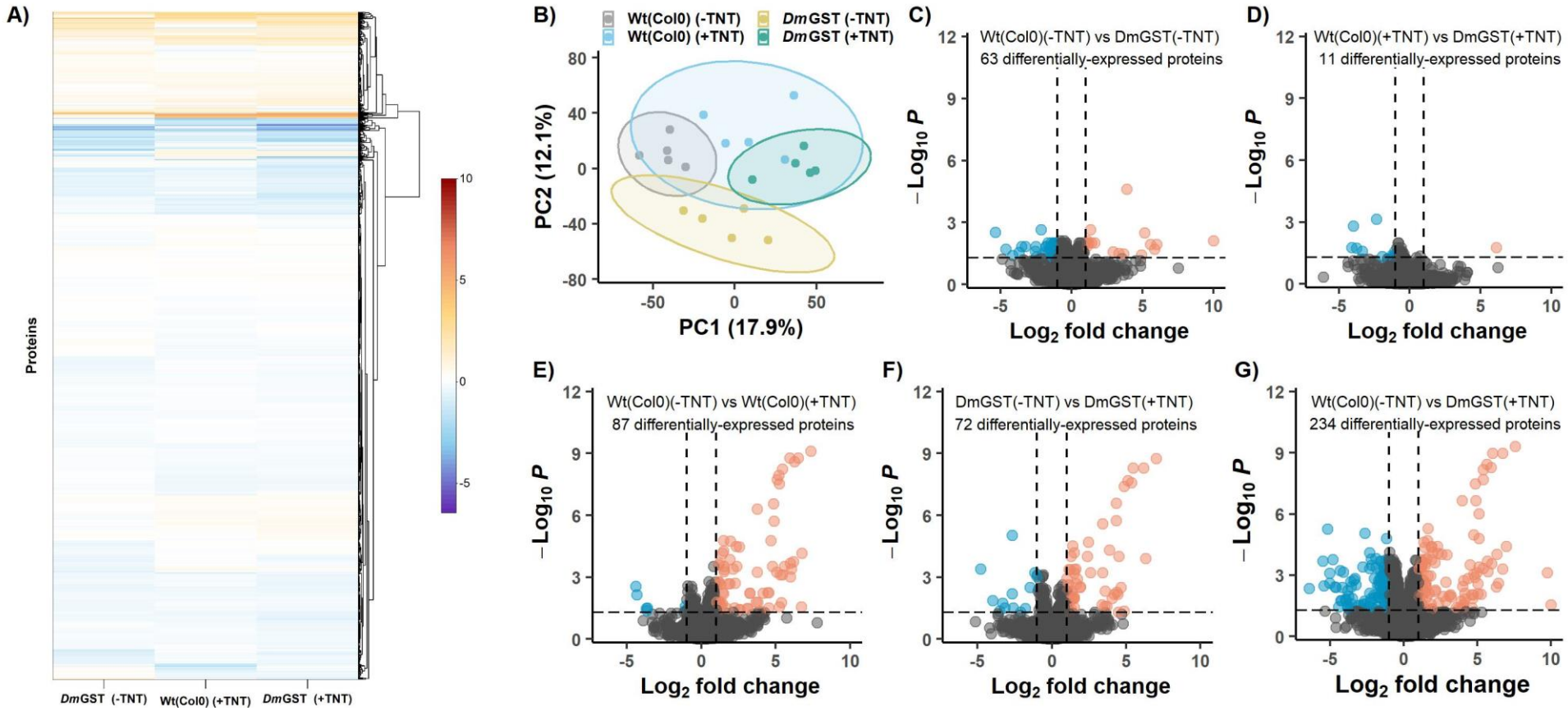


**Figure 5.3.2.1.1: *Dm*GST presence and TNT exposure generate similar proteomic responses whilst also having an additive effect. A)** Hierachical analysis of proteomic response to *Dm*GST presence, TNT exposure and the combination of both, measured as $\log_2$ fold change in respect to WT (-TNT) control. **B)** PCA analysis of relative protein abundance within the four experimental conditions. The four experimental conditions separate, mostly, into distinct groups. **C)** Protein response to the presence of *Dm*GST in the absence of TNT. Dashed lines indicate thresholds for both $\log_2$ fold change and FDR values. Red points represent significantly induced proteins, blue points represent significantly repressed proteins. **D)** Protein response to the presence of *Dm*GST in the copresence of TNT. **E)** Endogenous response to TNT. **F)** *Dm*GST-enhanced response to TNT. **G)** Protein response to the combination of *Dm*GST presence and TNT exposure.

To further understand the interactions between the proteomic responses to the presence of *Dm*GST and TNT exposure, the number of differentially-expressed proteins shared across different pair-wise comparisons was investigated. This analysis identified five categories of proteins and is shown in Figure 5.3.2.1.2 A & B for induced and repressed proteins respectively.

The first category consisted of proteins that were differentially expressed in response to TNT, irrespective of *Dm*GST presence, referred to as *Dm*GST-independent TNT-responsive proteins. Overall, 51 proteins across the proteomic experiment fitted this description with 50 of these being found within the induced population, the haloacid dehalogenase-like hydrolase AT3G62040 was the only repressed member of this group.

The second category contained proteins that were only differentially expressed within the WT(-TNT): WT(+TNT) comparison, indicating that *Dm*GST activity reduces the induction/repression of these proteins within the detoxification response, these were referred to as *Dm*GST-impacted TNT-responsive proteins. Only eight proteins matched this description, with five of this within the induced population.

The third category, referred to as *Dm*GST-related TNT-responsive proteins, showed the overlap in responses to *Dm*GST presence and TNT exposure. These proteins were characterised by either being differentially expressed to both TNT treatment and the presence of *Dm*GST, differentially expressed in response to TNT but not when compared to a *Dm*GST(-TNT) control or differentially expressed in response to *Dm*GST presence except when in combination with TNT exposure. These characteristics of expression indicated that the proteins within this group were impacted by both TNT exposure and *Dm*GST presence but not in a manner that required their combination. This group contained 80 proteins, which was 53% of the combined protein response to *Dm*GST presence and TNT exposure, highlighting the large overlap in the response to these two stimuli.

The fourth category of proteins were referred to as *Dm*GST-dependent TNT-responsive proteins and were identified by only being differentially expressed in response to the combination of TNT exposure and the presence of *Dm*GST. These are the proteins that are most likely involved in the response to enhanced Conjugate 3 production, as this was assumed to be the sole product of the combination of TNT-exposure and the presence of *Dm*GST within root tissue. There was a total of 120 proteins within this category, with 81 being found within the repressed population. The majority of *Dm*GST-dependent TNT-responsive proteins, 99 of the 120, were identified within the WT(-TNT): *Dm*GST(+TNT) comparison only. As these 99 proteins were not differentially expressed within the WT(+TNT): *Dm*GST(+TNT) and

*Dm*GST(-TNT): *Dm*GST(+TNT) comparisons, it suggests that they respond in a similar manner to *Dm*GST presence and TNT exposure separately, and that the combination of these stimuli has a subtle, additive effect.

The final category of proteins was labelled *Dm*GST-responsive TNT-independent proteins as they were differentially expressed in response to the presence of *Dm*GST, irrespective of TNT exposure. This was the smallest group, containing just five proteins, with four of these being repressed. Overall, these results confirm the extensive overlap between the proteomic responses to *Dm*GST presence and TNT exposure, and through the identification of *Dm*GST-dependent TNT-responsive proteins, distinguished a pool of candidates with putative involvement in Conjugate 3 metabolism.

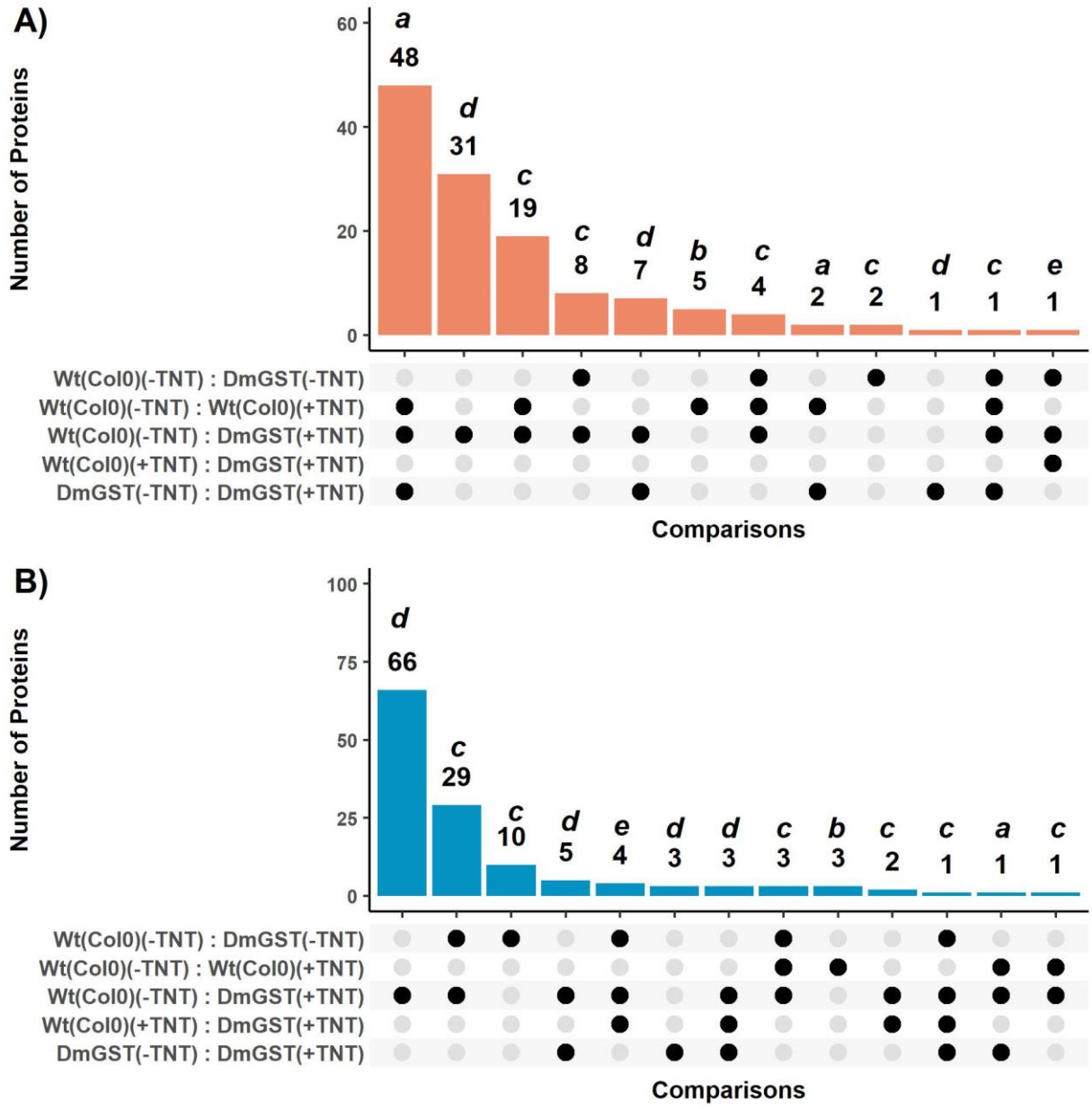


**Figure 5.3.2.1.2: Categorising proteins within induced and repressed populations by their response to the presence of *Dm*GST and TNT exposure. A)** Upset plot of the induced proteomic response identified across the experiment. Bars represent the number of proteins whilst matrix indicates which comparisons those proteins were significantly induced in. Letters indicate the identified category that the proteins belong to: *Dm*GST-independent TNT responsive proteins (*a*), *Dm*GST-impacted TNT-responsive proteins (*b*), *Dm*GST-related TNT-responsive proteins (*c*), *Dm*GST-dependent TNT-responsive proteins(*d*), and *Dm*GST-responsive TNT-independent proteins (*e*). **B)** Upset plot of the repressed proteomic response identified across the experiment.

#### 5.3.2.2 Characterising the endogenous response to TNT exposure.

To aid in the generation of testable models, the biological processes enriched within the response to TNT and the presence of *Dm*GST were investigated, along with the molecular functions and spatial localisation of the proteins comprised within these responses. Analysis of the endogenous response to TNT focused on the 87 proteins differentially expressed within the WT (-TNT): WT (+TNT) comparison. Within this group of proteins, 50 were identified as *Dm*GST-independent, 8 were *Dm*GST-impacted and 29 were *Dm*GST-related TNT-responsive proteins.

Biological process enrichment was performed through cluster analysis and subsequent KEGG pathway and GO term enrichment. In total 57 proteins met the conditions of clustering, from which three clusters with enrichment of biological processes/pathways were identified (Figure 5.3.2.2.1A). Both Cluster 1 and Cluster 2 were enriched with the *Response to chemical* (GO:0042221) GO term (Figure 5.3.2.2.1B). The other terms enriched within these clusters suggest that they are involved in different aspects of the response to chemical stress. Cluster 1 was also enriched with the molecular function GO term *Transferase activity* (GO:0016740) and contained several GSTs and UGTs including GSTU24, GSTU25, UGT73B4 and UGT74E2, enzymes known to directly conjugate TNT or its transformed derivatives [104,106]. In comparison, Cluster 2 was enriched with GO terms associated with amino acid metabolism and contained enzymes such as methionine gamma lyase (MGL), which functions within methionine metabolism [285]. This analysis indicates that proteins within Cluster 2 are associated with the primary metabolic response to TNT, which enables the detoxification of the xenobiotic, and related oxidative stress, through the activity of proteins within Cluster 1. Cluster 3 comprised seven proteins and was enriched with the *Suberin biosynthetic process* (GO:0010345) GO term. These results imply that TNT induces responses in both primary and secondary metabolism, as well as minor physiological alterations to the root cell.

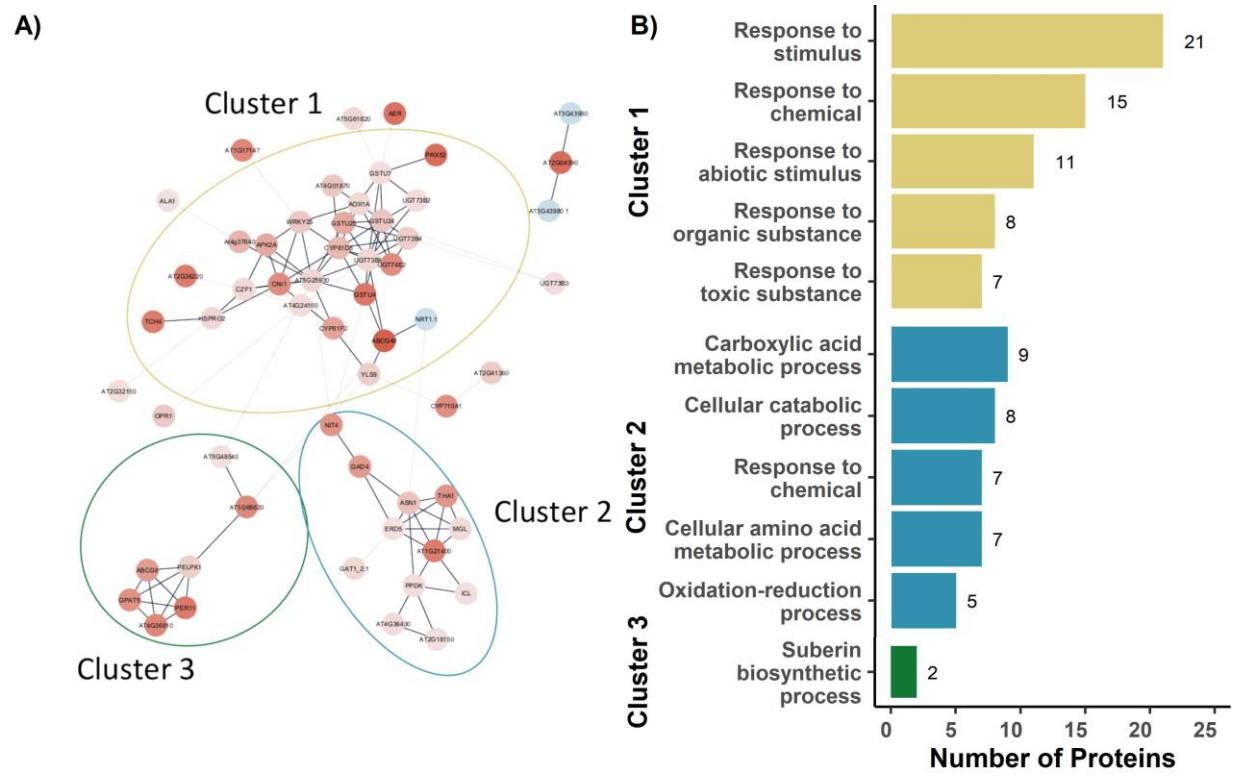


**Figure 5.3.2.2.1: Analysis of biological pathways within the endogenous response to TNT. A)** Network analysis of proteins differentially expressed in endogenous response to TNT. Protein clustering was based on STRING scores, with 57 of the 89 proteins passing the threshold for analysis. Three distinct clusters containing enriched biological processes and/or pathways were identified. Nodes represent individual proteins and are coloured in accordance with $\log_2$ fold-change compared to WT (-TNT) control, blue is repressed and red is induced. Edges represent protein interactions; bold edges represent interactions that were above the STRING score threshold of 0.5. **B)** Top 5 enriched biological process GO terms within each cluster and the number of proteins to which they encompass.

An overview of the molecular functions was generated by grouping the GO terms of proteins into functionally-related categories. Within the induced response, there were 14 proteins which did not have an allocated molecular function. Of the remaining 65, 48 (74% of the total) were covered by eight categories which in order of size were: *Oxidoreductases & Peroxidases*, *UGTs & GSTs*, *Transporters*, *Transcription/Translation*, *Protein inhibition/modification*, *Amino acid metabolism*, *Methyl- & Acyltransferases* and *Glycosyl hydrolases* (Figure 5.3.2.2.2A). These allocations are consistent with the results from biological process enrichment as the largest three categories correspond to the transformation, conjugation, and compartmentalisation steps of xenobiotic detoxification (Cluster 1) whilst the next three correspond to gene expression and biological compound synthesis (Cluster 2). The eight proteins comprising the downregulated population could be encompassed by four categories:

*Transcription/Translation*, *Transporter/Ion Channel*, *Haloacid dehydrogenase-like protein* and *C1-domain proteins* (Figure 5.3.2.2.2B).

Proteins encompassed by the *Oxidoreductases & Peroxidases*, *UGTs & GSTs*, *Transporters*, *Methyl- & Acyltransferases* and *Glycosyl hydrolases* categories of the induced protein population are putative candidates involved in metabolism of the TNT-molecule during detoxification. The *Oxidoreductases & Peroxidases* category contained within it OPR1, a protein known to reduce TNT, as well as three cytochrome P450 monooxygenases (CYPs) and four peroxidases. Whilst CYPs have been shown to be involved in xenobiotic metabolism within plants [286], they are also upregulated to a variety of abiotic and biotic stresses [287–289]. The CYPs upregulated in response to TNT have been identified to function within oxidative stress response and glucosinolate metabolism [290–292] thus are most likely not involved in directly modifying the TNT-molecule. Peroxidases have been shown to function within lignin biosynthesis [293] and are thus candidates for incorporation of TNT-derived metabolites into the lignocellulosic material. Of the four peroxidases upregulated in response to TNT only PER52 has been linked with lignin biosynthesis [294]. Proteins within the *UGTs & GSTs* category, including GSTU24 and UGT74E2, had been shown to be induced at the transcript level in previous serial analysis of gene expression (SAGE) and microarray analyses [104,248,250]. In respect to the four GSTs induced in response to TNT, all have been assessed *in vitro* for their activity towards TNT which confirmed only GSTU24 and GSTU25 were able to conjugate the xenobiotic [106]. Four of the five UGTs induced belonged to the UGT73B subfamily, suggesting that this family has overlapping or integrated functions. The *Transporters* category contained three proteins belonging to families with links to xenobiotic detoxification: ABCG6, ABCG40 and zinc induced facilitator-like 1 (ZIFL1). Of these three proteins, only the major facilitator transporter ZIFL1 is localised to the tonoplast within Arabidopsis roots [295]. The ABC-transporters, ABCG6 and ABCG40, are located to the plasma membrane [296,297]. Proteins within the *Methyl- & Acyltransferases* category could function within TNT metabolism, as this body of work has detected putative malonyl-conjugates. The two induced acyltransferases upregulated were GPAT5 and AT4G24160, both of which are involved in lipid metabolism [298,299] and thus unlikely to function in the malonylation of xenobiotic glucosides. The detected methyltransferase was uncharacterised. Finally, due to the production of glucosyl-conjugates within TNT-detoxification, glycosyl hydrolases may function in the hydrolysis of the glucosidic bond found within these conjugates. The three proteins allocated to the *Glycosyl hydrolases* category are all in the xyloglucan endotransglucosylase/hydrolase (XTH) family. As this family of proteins function in the remodeling of cell wall hemicellulose [300], it is unlikely they are involved in metabolism of small molecules such as xenobiotic glucosides.

The spatial allocation of proteins, within categories that are potentially involved in TNT metabolism, were then identified using the proteomic dataset generated from the analysis of BNAF fractions (Figure 5.3.2.2.2C). As xenobiotic metabolism is believed to occur within the cytosol, vacuole, and potentially the apoplast, proteins localised to their corresponding clusters, Cluster 3 and Cluster 1 respectively, are commented on here. Most proteins within the *Oxidoreductases & Peroxidases* and *UGTs & GSTs* categories fell within the cytosolic Cluster 3. These proteins included OPR1, GSTU24, and GSTU25 which supports the current model that the identified transformation and conjugation reactions for TNT do occur within the cytosol. The proteins localised to the vacuolar and apoplastic Cluster 1 were the transporter ABCG40, the uncharacterised methyltransferase AT2G41380 and UGT73B3. As ABCG40 is a known plasma membrane-localised transporter [297], it was used as a compartmental marker and thus had an SVM score of 1 for this allocation. However, the confidence of AT2G41380 and UGT73B3 allocations was low, with SVM scores of 0.32 and 0.35 respectively, suggesting their allocation to Cluster 1 most likely resulted from limited compartmental resolution and thus should not be included in predictive metabolic models. As expected, the two glycosyl-hydrolases detected within this dataset, XTH23 and XTH24, were also allocated to Cluster 1 which aligns with their function in modifying cell wall hemicellulose. Five proteins with unknown molecular function were also allocated to Clusters 1 and 3 and are thus putative candidates to further investigate in the context of TNT metabolism, there were: CRRSP55, AT3G27880, MAC9.6, MXH1.3 and PELPK1.

The subcellular-cluster allocations of proteins differentially expressed in the endogenous response to TNT alongside their molecular function, the biological processes they are linked with, and their fold-change can be found in Tables 5.3.2.2.1 - 5.3.2.2.3. These tables list the *Dm*GST-independent TNT responsive proteins, *Dm*GST-impacted TNT responsive proteins and *Dm*GST-related TNT responsive proteins respectively.

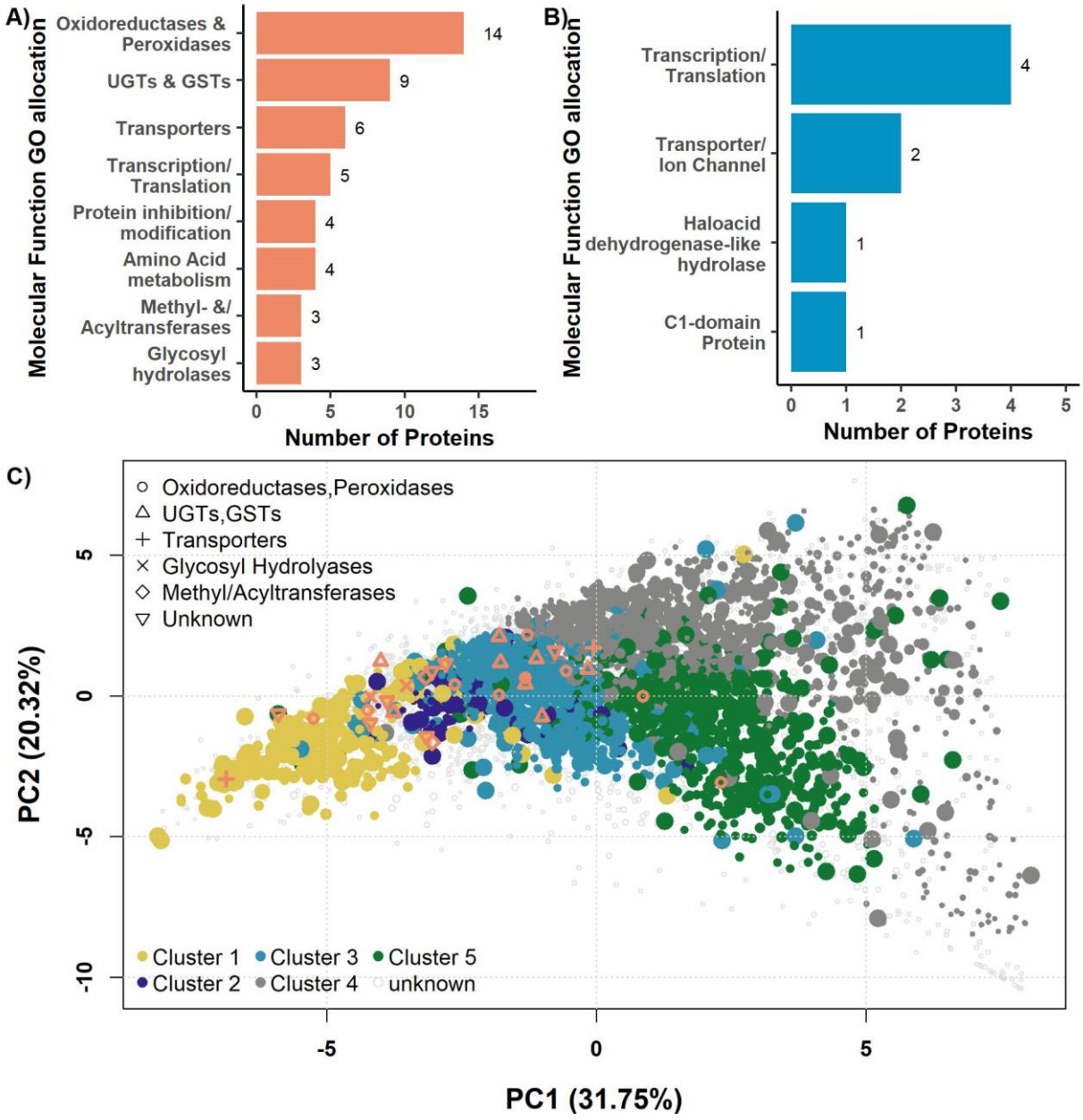


**Figure 5.3.2.2.2: Endogenous Response to TNT requires a diversity of molecular functions though not all proteins with functions relating to TNT metabolism show the required sub-cellular localisation. A)** Eight molecular-function GO-term categories represent 48 out of the 79 proteins induced in the endogenous response to TNT. **B)** Four molecular-function GO-term categories represent the entirety of the repressed in the endogenous response to TNT. **C)** Subcellular-cluster allocations of induced proteins within molecular-function categories with links to xenobiotic metabolism.

**Table 5.3.2.2.1: *Dm*GST-independent TNT-responsive proteins within the endogenous response to TNT.** Protein UniProt identifiers and their Arabidopsis Gene ID, log2 fold change and its significance level, the molecular function and biological processes GO terms allocated to the protein and the spatial information obtained from proteomics on BNAF fractions. FDR values represented by * < 0.05, ** < 0.01, *** <0.001.

| Protein | Arabidopsis Gene ID | WT(-TNT) : WT(+TNT) | Molecular Function | Biological Processes | Compartmental Prediction | Cluster Prediction |
|---|---|---|---|---|---|---|
| ABCG40 | At1g15520 | 7.36 *** | ABC-type transporter activity | Response to abscisic acid. Abscisic acid-activated signalling pathway. Transmembrane transport. Response to abiotic stress. Defence response to oomycetes. Intercellular transport. Negative regulation of post-embryonic development. Abscisic acid transport. Import into cell. Lead ion transport. Terpenoid transport. Stomatal closure. Import across plasma membrane | Plasma Membrane (1.00) | Cluster 1 (1.00) |
| ABCG6 | At5g13580 | 4.45 ** | ABC-type transporter activity | Response to nematode. Suberin biosynthetic process. Organic acid transmembrane transport | Data not obtained | Data not obtained |
| GPAT5 | At3g11430 | 4.88 *** | Acyltransferase activity | Suberin biosynthetic process | Data not obtained | Data not obtained |
| AT4G24160 | At4g24160 | 1.16 * | Acyltransferase activity | Cellular response to hypoxia. Lipid homeostasis | Peroxisome (0.35) | Cluster 3 (0.42) |
| ASN1 | At3g47340 | 2.56 *** | Asparagine synthase (glutamine-hydrolyzing) activity | Asparagine biosynthetic process. Response to sucrose. Response to glucose. Response to fructose. Cellular response to sucrose starvation | Nucleus (0.44) | Cluster 4 (0.49) |
| CXE6 | At1g68620 | 5.32 *** | Carboxylesterase | Cellular response to hypoxia | Nucleus (0.32) | Cluster 4 (0.37) |
| SAP9 | At4g22820 | 4.67 *** | DNA binding | Proteasome-mediated ubiquitin-dependent protein catabolic process. Defence response to other organism | Data not obtained | Data not obtained |
| AT2G40140 | At2g40140 | 1.4 *** | DNA binding | Response to abiotic stress. Defence response to other organism. Cellular response to hypoxia | Data not obtained | Data not obtained |
| GAT1_2.1 | At1g15040 | 1.52 *** | Glutamine amidotransferase | Regulation of secondary shoot formation | Nucleus (0.32) | Cluster 4 (0.37) |
| GSTU4 | At2g29460 | 6.19 *** | Glutathione transferase activity | Positive regulation of defence response to insect | Nucleus (0.30) | Cluster 5 (0.34) |

| Protein | Arabidopsis Gene ID | WT(-TNT) : WT(+TNT) | Molecular Function | Biological Processes | Compartmental Prediction | Cluster Prediction |
|---|---|---|---|---|---|---|
| GSTU25 | At1g17180 | 3.75 *** | Glutathione transferase activity | 2,4,6-trinitrotoluene catabolic process | Cytosol (0.27) | Cluster 3 (0.49) |
| GSTU24 | At1g17170 | 2.36 *** | Glutathione transferase activity | 2,4,6-trinitrotoluene catabolic process | Cytosol (0.31) | Cluster 3 (0.59) |
| GSTU7 | At2g29420 | 1.2 *** | Glutathione transferase activity | Response to salicylic acid | Cytosol (1.00) | Cluster 3 (1.00) |
| UGT73B4 | At2g15490 | 1.91 *** | Glycosyltransferase activity | Response to other organism | Cytosol (0.31) | Cluster 3 (0.72) |
| UGT73B5 | At2g15480 | 1.48 *** | Glycosyltransferase activity | Response to other organism | Data not obtained | Data not obtained |
| UGT73B2 | At4g34135 | 1.22 * | Glycosyltransferase activity | Response to other organism. Flavonol biosynthetic process | Cytosol (0.27) | Cluster 3 (0.49) |
| UGT73B3 | At4g34131 | 1.1 ** | Glycosyltransferase activity | Cellular response to hypoxia. Response to other organism | Peroxisome (0.21) | Cluster 1 (0.35) |
| PSK3 | At3g49780 | 6.27 *** | Growth factor activity | Cellular response to hypoxia | Nucleus (0.32) | Cluster 4 (0.38) |
| HSPRO2 | At2g40000 | 1.49 *** | Heme binding | Defence response to other organism. Response to oxidative stress. Cellular response to hypoxia. Response to salicylic acid | Cytosol (0.27) | Cluster 3 (0.51) |
| XTH23 | At4g25810 | 5.97 *** | Hydrolase activity | Response to abiotic stress. Response to auxin. Cellular response to hypoxia. Response to mechanical stimulus. Response to brassinosteroid | Plasma Membrane (0.25) | Cluster 1 (0.52) |
| XTH24 | At4g30270 | 1.81 ** | Hydrolase activity | Plant-type cell wall organization or biogenesis | Plasma Membrane (0.29) | Cluster 1 (0.63) |
| AT3G62040 | At3g62040 | -4.36 ** | Hydrolase activity | Data not obtained | Data not obtained | Data not obtained |
| MGL | At1g64660 | 1.4 * | Methionine gamma-lyase activity | Response to abiotic stress. Cellular response to sulfate starvation. Protein homotetramerisation | Nucleus (0.45) | Cluster 4 (0.52) |

| Protein | Arabidopsis Gene ID | WT(-TNT) : WT(+TNT) | Molecular Function | Biological Processes | Compartmental Prediction | Cluster Prediction |
|---|---|---|---|---|---|---|
| AT2G41380 | At2g41380 | 2.12 *** | Methyltransferase activity | Data not obtained | Plasma Membrane (0.20) | Cluster 1 (0.32) |
| AT2G36220 | At2g36220 | 5.93 *** | Unknown | Cellular response to hypoxia. Anaerobic respiration | Data not obtained | Data not obtained |
| C7A10.750 | At4g36610 | 5.45 *** | Unknown | Data not obtained | Data not obtained | Data not obtained |
| VQ1 | At1g17147 | 5.43 *** | Unknown | Data not obtained | Data not obtained | Data not obtained |
| ATJ11 | At4g36040 | 5.21 *** | Unknown | Data not obtained | Nucleus (0.31) | Cluster 4 (0.36) |
| AT3G27880 | At3g27880 | 3.74 *** | Unknown | Data not obtained | Nucleus (0.23) | Cluster 1 (0.30) |
| NHL10 | At2g35980 | 1.95 *** | Unknown | Leaf senescence. Defence response to virus | Plastid (1.00) | Cluster 5 (1.00) |
| PELPK1 | At5g09530 | 1.91 ** | Unknown | Post-embryonic development. Regulation of photoperiodism, flowering. Positive regulation of seed germination | Cytosol (0.16) | Cluster 3 (0.34) |
| MXH1.3 | At5g35690 | 1.16 ** | Unknown | Data not obtained | Cytosol (0.27) | Cluster 3 (0.50) |
| NAS1 | At5g04950 | 1.24 * | Nicotianamine synthase activity | Pollen development. Pollen tube growth. Phloem transport | Plasma Membrane (0.32) | Cluster 1 (0.74) |
| NIT4 | At5g22300 | 4.85 *** | Nitrilase | Cyanide metabolic process. Detoxification of nitrogen compound | Data not obtained | Data not obtained |
| PER52 | At5g05340 | 6.76 *** | Oxidoreductase activity | Lignin biosynthetic process. Xylem development. Positive regulation of syringal lignin biosynthetic process | Nucleus (0.30) | Cluster 4 (0.34) |
| AER | At5g16970 | 6.51 *** | Oxidoreductase activity | Response to oxidative stress | Nucleus (0.30) | Cluster 4 (0.34) |

| Protein | Arabidopsis Gene ID | WT(-TNT) : WT(+TNT) | Molecular Function | Biological Processes | Compartmental Prediction | Cluster Prediction |
|---|---|---|---|---|---|---|
| PER11 | At1g68850 | 6.03 *** | Oxidoreductase activity | Data not obtained | Cytosol (0.30) | Cluster 3 (0.59) |
| CYP710A1 | At2g34500 | 5.08 *** | Oxidoreductase activity | Data not obtained | Data not obtained | Data not obtained |
| OPR1 | At1g76680 | 2.26 ** | Oxidoreductase activity | Response to wounding. Cellular response to hypoxia. Response to salicylic acid. Oxylipin metabolic process | Cytosol (0.33) | Cluster 3 (0.67) |
| AOX1A | At3g22370 | 1.52 *** | Oxidoreductase activity | Response to abiotic stress. Mitochondria-nucleus signalling pathway. Cellular respiration | Data not obtained | Data not obtained |
| AT5G22140 | At5g22140 | 1.29 ** | Oxidoreductase activity | Data not obtained | Cytosol (0.33) | Cluster 3 (0.66) |
| JOX2 | At5g05600 | 1.06 * | Oxidoreductase activity | Regulation of defence response to fungus. Regulation of jasmonic acid mediated signalling pathway. Cellular response to toxic substance. Negative regulation of defence response to insect | Nucleus (0.32) | Cluster 4 (0.37) |
| POX1 | At3g30775 | 1 * | Oxidoreductase activity | Response to abiotic stress. Defence response to other organism. Response to oxidative stress. Cellular response to hypoxia | Cytosol (0.24) | Cluster 3 (0.47) |
| UPI | At5g43580 | 1.43 ** | Peptidase inhibitor activity | Defence response to other organism | Plastid (0.31) | Cluster 5 (0.39) |
| AT2G32150 | At2g32150 | 1.17 *** | Phosphatase | Response to abiotic stress. Response to abscisic acid. Purine nucleoside catabolic process. Xanthosine biosynthetic process | Cytosol (0.27) | Cluster 3 (0.53) |
| T1N24.22 | At5g25930 | 1.53 *** | Protein kinase activity | Data not obtained | Nucleus (0.26) | Cluster 5 (0.30) |
| AT4G01870 | At4g01870 | 2.34 *** | Proteolysis | Data not obtained | Cytosol (0.34) | Cluster 3 (0.69) |
| THA1 | At1g08630 | 4.78 *** | Threonine aldolase activity | Threonine catabolic process | Nucleus (0.32) | Cluster 4 (0.37) |
| PPDK | At4g15530 | 1.16 * | Transferase activity, transferring phosphorus-containing groups | Data not obtained | Cytosol (0.33) | Cluster 3 (0.65) |

| Protein | Arabidopsis Gene ID | WT(-TNT) : WT(+TNT) | Molecular Function | Biological Processes | Compartmental Prediction | Cluster Prediction |
|---|---|---|---|---|---|---|
| ZIFL1 | At5g13750 | 4.53 ** | Transmembrane transporter activity | Response to abiotic stress. Root development. Gravitropism. Basipetal auxin transport. Regulation of stomatal closure | Data not obtained | Data not obtained |
| ATL31 | At5g27420 | 5.23 * | Ubiquitin ligase | Response to abscisic acid. Defence response to other organism. Cellular response to hypoxia. Cellular response to nitrogen levels | Data not obtained | Data not obtained |

**Table 5.3.2.2.2: *Dm*GST-impacted TNT-responsive proteins within the endogenous response to TNT**. Protein UniProt identifiers and their Arabidopsis Gene ID, log2 fold change and its significance level, the molecular function and biological processes GO terms allocated to the protein and the spatial information obtained from proteomics on BNAF fractions. FDR values represented by * < 0.05, ** < 0.01, *** <0.001.

| Protein | Arabidopsis Gene ID | WT(-TNT) : WT(+TNT) | Molecular Function | Biological Processes | Compartmental Prediction | Cluster Prediction |
|---|---|---|---|---|---|---|
| ALA1 | At5g04930 | 1.05 * | ATPase-coupled intramembrane lipid transporter activity | Data not obtained | Data not obtained | Data not obtained |
| AT1G78830 | At1g78830 | 1.02 * | Carbohydrate binding | Data not obtained | Cytosol (0.23) | Cluster 3 (0.41) |
| GLR2.2 | At2g24720 | -3.66 * | Ligand-gated ion channel activity | Data not obtained | Data not obtained | Data not obtained |
| GH3.2 | At4g37390 | 1.3 * | Ligase activity | Data not obtained | Plastid (0.21) | Cluster 1 (0.38) |
| CRRSP55 | At5g48540 | 1.12 * | Unknown | Data not obtained | Plasma Membrane (0.28) | Cluster 1 (0.62) |
| AT4G01920 | At4g01920 | -3.64 * | C1-domain Protein | Data not obtained | Data not obtained | Data not obtained |
| WNK4 | At5g58350 | 1.7 * | Protein kinase activity | Protein autophosphorylation. Photoperiodism, flowering | Plasma Membrane (0.36) | Cluster 1 (0.78) |
| NPF6.3 | At1g12110 | -1.01 * | Symporter activity | Response to water deprivation. Lateral root development. Photoperiodism, flowering. Response to nitrate. Basipetal auxin transport. Nitrate transmembrane transport | Data not obtained | Data not obtained |

**Table 5.3.2.2.3: *Dm*GST-related TNT-responsive proteins within the endogenous response to TNT.** Protein UniProt identifiers and their Arabidopsis Gene ID, log2 fold change and its significance level, the molecular function and biological processes GO terms allocated to the protein and the spatial information obtained from proteomics on BNAF fractions. FDR values represented by * < 0.05, ** < 0.01, *** <0.001.

| Protein | Arabidopsis Gene ID | WT(-TNT) : WT(+TNT) | Molecular Function | Biological Processes | Compartmental Prediction | Cluster Prediction |
|---|---|---|---|---|---|---|
| ALPHACA2 | At2g28210 | 3.24 ** | Carbonate dehydratase activity | Data not obtained | Data not obtained | Data not obtained |
| NAC001 | At1g01010 | 4.15 ** | DNA binding | Data not obtained | Data not obtained | Data not obtained |
| WRKY25 | At2g30250 | 2.22 * | DNA binding | Response to abiotic stress. Response to salt stress. Response to osmotic stress. Cellular heat acclimation. Cellular response to heat | Data not obtained | Data not obtained |
| GAD4 | At2g02010 | 4.51 * | Glutamate decarboxylase activity | Data not obtained | Plasma Membrane (0.17) | Cluster 1 (0.43) |
| UGT74E2 | At1g05680 | 5.23 *** | Glycosyltransferase activity | Cellular response to abscisic acid stimulus. Shoot system morphogenesis. Response to abiotic stress. Indole butyric acid metabolic process. Cellular response to hydrogen peroxide. Cellular hyperosmotic salinity response | Nucleus (0.25) | Cluster 4 (0.29) |
| XTH22 | At5g57560 | 5.38 * | Hydrolase activity | Response to abiotic stress. Response to auxin. Cellular response to hypoxia. Response to mechanical stimulus. Response to brassinosteroid | Data not obtained | Data not obtained |
| ICL | At3g21720 | 1.1 * | Isocitrate lyase activity | Data not obtained | Peroxisome (1.00) | Cluster 2 (1.00) |
| GH3.3 | At2g23170 | 5.6 *** | Ligase activity | Data not obtained | Nucleus (0.26) | Cluster 4 (0.30) |
| AT3G09925 | At3g09925 | 5.06 *** | Unknown | Data not obtained | Data not obtained | Data not obtained |
| AT2G37110 | At2g37110 | 3.68 * | Unknown | Data not obtained | Data not obtained | Data not obtained |
| AT1G22930 | At1g22930 | 2.57 * | Unknown | Data not obtained | Data not obtained | Data not obtained |
| AT1G69890 | At1g69890 | 2.54 * | Unknown | Cellular response to hypoxia. Response to nitric oxide | Data not obtained | Data not obtained |

| Protein | Arabidopsis Gene ID | WT(-TNT) : WT(+TNT) | Molecular Function | Biological Processes | Compartmental Prediction | Cluster Prediction |
|---|---|---|---|---|---|---|
| MAC9.6 | At5g61820 | 1.48 ** | Unknown | Data not obtained | Plasma Membrane (0.32) | Cluster 1 (0.68) |
| STP13 | At5g26340 | 1.12 ** | Monosaccharide transmembrane transporter activity | Response to abiotic stress. Response to salt stress. Response to abscisic acid. Monosaccharide transmembrane transport | Data not obtained | Data not obtained |
| MORF9 | At1g11430 | -1.09 * | mRNA binding | Chloroplast RNA modification | Plastid (0.37) | Cluster 5 (0.57) |
| NAS2 | At5g56080 | 1.21 * | Nicotianamine synthase activity | Pollen development. Pollen tube growth. Response to zinc ion. Phloem transport | Plasma Membrane (0.33) | Cluster 1 (0.67) |
| AT1G21400 | At1g21400 | 5.97 *** | Oxidoreductase activity | Response to sucrose. Branched-chain amino acid catabolic process. Response to absence of light. Cellular response to sucrose starvation | Data not obtained | Data not obtained |
| CYP81F2 | At5g57220 | 3.99 * | Oxidoreductase activity | Defence response to other organism. Response to bacterium. Cellular response to hypoxia. Glucosinolate metabolic process. Induced systemic resistance. Defence response by callose deposition in cell wall. Indole glucosinolate biosynthetic process. Indole glucosinolate metabolic process | Data not obtained | Data not obtained |
| CYP81D8 | At4g37370 | 3.06 * | Oxidoreductase activity | Data not obtained | Data not obtained | Data not obtained |
| PER49 | At4g36430 | 1.31 * | Oxidoreductase activity | Data not obtained | Plastid (0.21) | Cluster 5 (0.43) |
| PER15 | At2g18150 | 1.18 * | Oxidoreductase activity | Data not obtained | Plastid (0.39) | Cluster 5 (0.55) |
| ACA2 | At4g37640 | 3.24 ** | P-type calcium transporter activity | Calcium ion transmembrane transport | Endoplasmic Reticulum (1.00) | Cluster 3 (1.00) |
| PBL2 | At1g14370 | 3.8 * | Protein kinase activity | Positive regulation of defence response to bacterium | Data not obtained | Data not obtained |
| RPS17C | At3g10610 | 6.73 * | Structural constituent of Ribosome | Data not obtained | Nucleus (0.32) | Cluster 4 (0.37) |
| RPS29A | At3g43980 | -1.09 * | Structural constituent of Ribosome | Data not obtained | Nucleus (0.38) | Cluster 4 (0.44) |

| Protein | Arabidopsis Gene ID | WT(-TNT) : WT(+TNT) | Molecular Function | Biological Processes | Compartmental Prediction | Cluster Prediction |
|---|---|---|---|---|---|---|
| AT4G07950 | At4g07950 | -4.41 ** | Termination of RNA polymerase III transcription | Data not obtained | Data not obtained | Data not obtained |
| AT1G72090 | At1g72090 | -3.71 * | tRNA methylthiolation | Data not obtained | Data not obtained | Data not obtained |
| SEC1B | At4g12120 | 3.1 * | Vesicle-mediated transport | Data not obtained | Nucleus (0.32) | Cluster 4 (0.37) |

### 5.3.2.3 Characterising the response to *Dm*GST presence

To characterise the response to the presence of *Dm*GST *in planta*, the 63 proteins differentially expressed within the WT (-TNT): *Dm*GST (-TNT) comparison were analysed. Within this group of proteins there were 58 (92% of the total) that were identified as *Dm*GST-related TNT-responsive proteins, highlighting the substantial overlap in the plant response to these stimuli. For cluster analysis and biological pathway enrichment, 32 proteins passed the clustering criteria. This analysis generated two distinct clusters (Figure 5.3.2.3.1A). In Cluster 1, the majority of proteins were repressed, and enrichment analysis of biological process GO-terms revealed these proteins to be associated with gene expression, with enriched terms including *Translation* (GO:0006412) and *Nucleobase biosynthetic process* (GO:0046112; Figure 5.3.2.3.1B). No GO terms were enriched within Cluster 2, however a KEGG pathway corresponding to oxidative phosphorylation was enriched with four of the five proteins within the cluster being mitochondrial membrane acyl carrier proteins or found within the cytochrome C complex (Figure 5.3.2.3.1C), all of which were repressed. From this analysis it can be concluded that a substantial portion of the response to the presence of *Dm*GST *in planta* is related to diversion of resources, evidenced by repression of processes related to gene expression and oxidative phosphorylation.

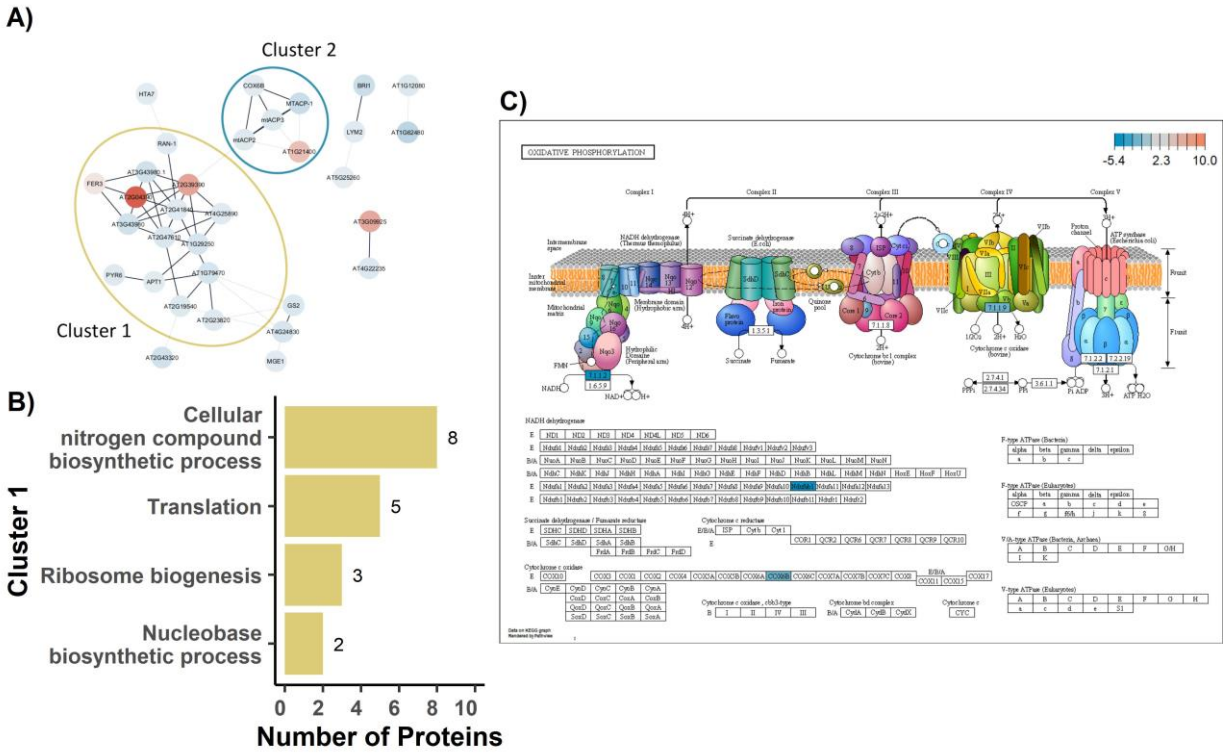

**Figure 5.3.2.3.1: Analysis of biological processes involved in the response to presence of *Dm*GST *in planta*. A)** Network analysis of differentially-expressed proteins, two distinct clusters were identified within the 32 proteins that passed clustering criteria. Nodes represent individual proteins and are coloured in accordance with $\log_2$ fold-change compared to WT (-TNT) control, blue is repressed and red is induced. Edges represent protein interactions; bold edges represent interactions that were above the STRING score threshold of 0.5. **B)** Enriched biological process GO terms within Cluster 1. **C)** Location of proteins within the oxidative-phosphorylation KEGG biological pathway enriched within Cluster 2. Proteins are highlighted in respect to their level of repression.

Analysis of molecular functions revealed that 9 of the 63 differentially-expressed proteins did not have an allocated function. Of the remaining 52, 14 had molecular functions that could be grouped under *Transcription/Translation*, supporting results obtained from biological pathway analysis that gene expression was a substantial response to the presence of *Dm*GST

5.3.2.3.2A & B). Similar categories, as those identified for the response to TNT, were identified for the response to the presence of *Dm*GST, these were: *Oxidoreductases & Peroxidases*, *UGTs & GSTs*, *Transporters*, *Glycosyl hydrolases* and *Methly- & Acyltransferases*. Within the protein population induced by *Dm*GST presence were several proteins linked to oxidative stress responses, this included FER3 and UGT74E2 [301,302]. To investigate the breadth of impact that *Dm*GST presence has on cellular processes the spatial localisation of differentially-expressed proteins was investigated. This analysis revealed that proteins responding to *Dm*GST presence were allocated to all five compartmental clusters suggesting that there is a whole cell response to the *Dm*GST presence *in planta* (

5.3.2.3.2C).

The complete list of proteins differentially expressed in response to the presence of *Dm*GST *in planta*, alongside their fold change, and respective GO-term and subcellular-cluster allocations are listed in Tables 5.3.2.3.1 - 5.3.2.3.2. These tables list the *Dm*GST-related TNT-responsive and the *Dm*GST-responsive TNT-independent proteins respectively.

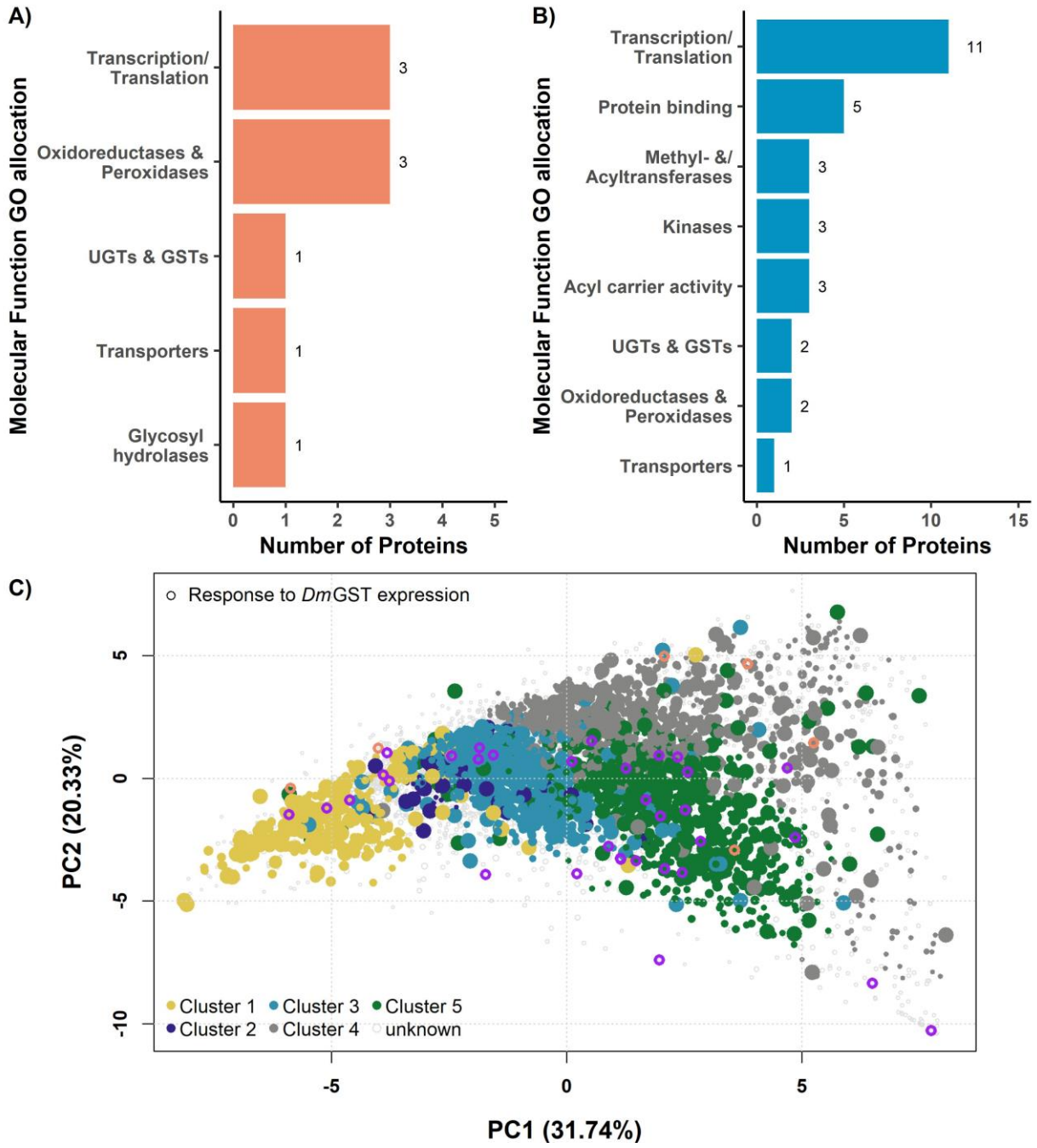


**5.3.2.3.2: Molecular and spatial analysis of the proteomic response to the presence of *Dm*GST *in planta*. A)** Molecular Function GO term categories for proteins induced in response to *Dm*GST presence, these categories represent 50% of the total response. *Dm*GST presence results in similar molecular functions being upregulated as exposure to TNT. **B)** Molecular Function GO term categories for proteins repressed in response to *Dm*GST presence, these categories represent 61% of the response. **C)** Subcellular compartment allocations of differential-expressed proteins detected within spatial proteomics dataset. Red circles represent induced proteins, purple represents repressed proteins.

**Table 5.3.2.3.1: *Dm*GST-related TNT-responsive proteins within the response to *Dm*GST presence.** Protein UniProt identifiers and their Arabidopsis Gene ID, log2 fold change and its significance level, the molecular function and biological processes GO terms allocated to the protein and the spatial information obtained from proteomics on BNAF fractions. FDR values represented by * < 0.05, ** < 0.01, *** < 0.001.

| Protein | Arabidopsis Gene ID | WT(-TNT): *Dm*GST(-TNT) | Molecular Function | Biological Processes | Compartmental Prediction | Cluster Prediction |
|---|---|---|---|---|---|---|
| AT2G23820 | At2g23820 | -1.27 * | 5'-deoxynucleotidase activity | Data not obtained | Plastid (0.49) | Cluster 5 (0.69) |
| MTACP2 | At1g65290 | -1.31 * | Acyl carrier activity | Mitochondrial electron transport, NADH to ubiquinone | Plastid (0.34) | Cluster 5 (0.55) |
| MTACP1 | At2g44620 | -2.57 * | Acyl carrier activity | Fatty acid biosynthetic process. Mitochondrial electron transport, NADH to ubiquinone | Data not obtained | Data not obtained |
| AIG2A | At3g28930 | -4.13 * | Acyltransferase activity | Response to bacterium | Data not obtained | Data not obtained |
| MGE1 | At5g55200 | -1.24 ** | Adenyl-nucleotide exchange factor activity | Response to UV | Plastid (0.29) | Cluster 5 (0.59) |
| AT4G24830 | At4g24830 | -1.78 * | Argininosuccinate synthase activity | Data not obtained | Plastid (0.29) | Cluster 5 (0.56) |
| AT5G16940.F2K13_90 | At5g16940 | -1.02 * | Carbon-sulfur lyase activity | Data not obtained | Data not obtained | Data not obtained |
| LYM2 | At2g17120 | -1.16 * | Chitin binding | Data not obtained | Nucleus (0.30) | Cluster 5 (0.36) |
| AT5G27670 | At5g27670 | -1.09 * | DNA binding | Response to wounding. Response to bacterium. DNA-mediated transformation | Nucleus (0.44) | Cluster 4 (0.52) |
| AT1G72230 | At1g72230 | -1.65 ** | Electron transfer activity | Data not obtained | Plastid (0.21) | Cluster 1 (0.35) |
| GSTU21 | At1g78360 | -1.26 * | Glutathione transferase activity | Data not obtained | Data not obtained | Data not obtained |
| UGT74E2 | At1g05680 | 3.9 *** | Glycosyltransferase activity | Cellular response to abscisic acid stimulus. Shoot system morphogenesis. Cellular response to water deprivation. | Nucleus (0.25) | Cluster 4 (0.29) |

| Protein | Arabidopsis Gene ID | WT(-TNT): *Dm*GST(-TNT) | Molecular Function | Biological Processes | Compartmental Prediction | Cluster Prediction |
|---|---|---|---|---|---|---|
| | | | | Indolebutyric acid metabolic process. Cellular response to hydrogen peroxide. Cellular hyperosmotic salinity response | | |
| APT1 | At1g27450 | -1.12 * | Glycosyltransferase activity | Circadian rhythm. Cytokinin metabolic process | Cytosol (0.28) | Cluster 3 (0.55) |
| RABG3E | At1g49300 | -1.34 * | GTPase activity | Response to salt stress. Response to oxidative stress | Cytosol (0.21) | Cluster 5 (0.43) |
| BGAL9 | At2g32810 | 1.39 ** | Hydrolase activity | Data not obtained | Cytosol (0.29) | Cluster 3 (0.59) |
| AT3G46270 | At3g46270 | -1 * | Kinase activity | Data not obtained | Nucleus (0.28) | Cluster 4 (0.33) |
| AT1G67325 | At1g67325 | -4.62 * | Metal ion binding | Data not obtained | Cytosol (0.23) | Cluster 3 (0.45) |
| AT2G43320 | At2g43320 | -2.08 * | Methyltransferase activity | Data not obtained | Cytosol (0.20) | Cluster 1 (0.39) |
| MORF9 | At1g11430 | -1.07 * | mRNA binding | Chloroplast RNA modification | Plastid (0.37) | Cluster 5 (0.57) |
| RAN1 | At5g20010 | -1.21 ** | mRNA binding | Defence response to bacterium. Defence response to fungus | Nucleus (0.24) | Cluster 5 (0.39) |
| AT3G02650 | At3g02650 | -1.36 * | mRNA binding | Data not obtained | Mitochondrion (0.32) | Cluster 5 (0.72) |
| GLN2 | At5g35630 | -1.51 * | mRNA binding | Response to cadmium ion | Plastid (0.23) | Cluster 5 (0.34) |
| RPL7AA | At2g47610 | -1.55 * | mRNA binding | Data not obtained | Plastid (0.37) | Cluster 5 (0.58) |
| AT4G07950 | At4g07950 | -5.38 ** | Nucleic acid binding | Data not obtained | Data not obtained | Data not obtained |

| Protein | Arabidopsis Gene ID | WT(-TNT): *Dm*GST(-TNT) | Molecular Function | Biological Processes | Compartmental Prediction | Cluster Prediction |
|---|---|---|---|---|---|---|
| UMK3 | At5g26667 | -1.35 * | Nucleobase-containing compound kinase activity | Pyrimidine nucleotide biosynthetic process | Plastid (0.27) | Cluster 5 (0.37) |
| AT1G21400 | At1g21400 | 3.65 * | Oxidoreductase activity | Response to sucrose. Branched-chain amino acid catabolic process. Response to abiotic stress. Cellular response to sucrose starvation | Data not obtained | Data not obtained |
| KO | At5g25900 | 1.33 ** | Oxidoreductase activity | Gibberellin biosynthetic process. Ent-kaurene oxidation to kaurenoic acid | Data not obtained | Data not obtained |
| FER3 | At3g56090 | 1.21 ** | Oxidoreductase activity | Photosynthesis. Response to reactive oxygen species. Leaf development. Flower development. Response to iron ion. Iron ion transport | Nucleus (0.47) | Cluster 4 (0.58) |
| LIGB | At4g15093 | -1.01 ** | Oxidoreductase activity | Data not obtained | Plasma Membrane (0.37) | Cluster 1 (0.85) |
| IMPDH | At1g79470 | -1.8 * | Oxidoreductase activity | Data not obtained | Nucleus (0.53) | Cluster 4 (0.64) |
| RAN1.1 | At5g44790 | -1.21 ** | P-type monovalent copper transporter activity | Regulation of stomatal movement. Response to ethylene | Data not obtained | Data not obtained |
| HSP17.8 | At1g07400 | 5.83 * | Protein binding | Response to abiotic stress. Response to oxidative stress. Cellular response to hypoxia. Response to osmotic stress. Protein folding. Protein complex oligomerisation | Data not obtained | Data not obtained |
| PBL2 | At1g14370 | 3.33 * | Protein binding | Positive regulation of defence response to bacterium | Data not obtained | Data not obtained |
| AT4G20300 | At4g20300 | 2.94 * | Protein binding | Data not obtained | Data not obtained | Data not obtained |
| FLOT2 | At5g25260 | -1.09 * | Protein binding | Data not obtained | Data not obtained | Data not obtained |
| SEC5A | At1g76850 | -1.09 * | Protein binding | Acceptance of pollen | Cytosol (0.28) | Cluster 3 (0.54) |

| Protein | Arabidopsis Gene ID | WT(-TNT): *Dm*GST(-TNT) | Molecular Function | Biological Processes | Compartmental Prediction | Cluster Prediction |
|---|---|---|---|---|---|---|
| PP2AB2 | At1g17720 | -1.1 ** | Protein binding | Data not obtained | Cytosol (0.34) | Cluster 3 (0.60) |
| HTD1 | At2g19540 | -1.34 * | Protein binding | Response to heat. Negative regulation of cellular response to heat | Plastid (0.38) | Cluster 5 (0.60) |
| KTN80.2 | At1g61210 | -3.5 * | Protein binding | Microtubule severing. Regulation of unidimensional cell growth. Response to salt stress. Response to abscisic acid | Nucleus (0.31) | Cluster 4 (0.36) |
| BRI1 | At4g39400 | -2.46 * | Protein serine kinase activity | Response to UV-b. Positive regulation of flower development. Leaf development. Brassinosteroid mediated signaling pathway. Pollen exine formation. Detection of brassinosteroid stimulus. Brassinosteroid homeostasis. Anther wall tapetum cell differentiation. Seedling development | Data not obtained | Data not obtained |
| PDX11 | At2g38230 | -3.69 * | Pyridoxal 5'-phosphate synthase (glutamine hydrolysing) activity | Data not obtained | Data not obtained | Data not obtained |
| COX6B.1 | At1g22450 | -1.06 * | Respiratory chain complex IV | Data not obtained | Data not obtained | Data not obtained |
| RRC1 | At5g25060 | 1.63 ** | RNA binding | Data not obtained | Nucleus (0.33) | Cluster 4 (0.39) |
| RPS17C | At3g10610 | 9.99 ** | Structural constituent of Ribosome | Data not obtained | Nucleus (0.32) | Cluster 4 (0.37) |
| RPS2C | At2g41840 | -1.16 * | Structural constituent of Ribosome | Data not obtained | Nucleus (0.43) | Cluster 5 (0.45) |
| RPP3A | At4g25890 | -1.27 * | Structural constituent of Ribosome | Data not obtained | Nucleus (0.32) | Cluster 4 (0.37) |
| RPS29A | At3g43980 | -2.13 ** | Structural constituent of Ribosome | Data not obtained | Nucleus (0.38) | Cluster 4 (0.44) |
| UDP.GALT1 | At1g77610 | 5.99 * | UDP-glucose transmembrane transporter activity | UDP-galactose transmembrane transport. GDP-fucose transmembrane transport. UDP-glucose transmembrane transport | Data not obtained | Data not obtained |

| Protein | Arabidopsis Gene ID | WT(-TNT): *Dm*GST(-TNT) | Molecular Function | Biological Processes | Compartmental Prediction | Cluster Prediction |
|---|---|---|---|---|---|---|
| AT3G09925 | At3g09925 | 5.15 ** | Unknown | Data not obtained | Data not obtained | Data not obtained |
| NOI4 | At5g55850 | 4.92 * | Unknown | Defence response to other organism | Data not obtained | Data not obtained |
| RTNLB8 | At3g10260 | 1.12 ** | Unknown | Defence response to other organism | Nucleus (0.32) | Cluster 4 (0.37) |
| AT3G06390 | At3g06390 | 1.11 * | Unknown | Data not obtained | Data not obtained | Data not obtained |
| F25L23_230 | At3g59370 | -1.1 * | Unknown | Data not obtained | Data not obtained | Data not obtained |
| AT4G22235 | At4g22235 | -1.44 ** | Unknown | Data not obtained | Data not obtained | Data not obtained |
| AT1G12080 | At1g12080 | -1.46 * | Unknown | Data not obtained | Plastid (0.44) | Cluster 5 (0.56) |
| GASA7 | At2g14900 | -2.5 * | Unknown | Data not obtained | Cytosol (0.23) | Cluster 1 (0.44) |
| AT1G62480 | At1g62480 | -3.27 * | Unknown | Data not obtained | Nucleus (0.33) | Cluster 4 (0.39) |

**Table 5.3.2.3.2: *Dm*GST-responsive TNT-independent proteins within the response to *Dm*GST presence.** Protein UniProt identifiers and their Arabidopsis Gene ID, log2 fold change and its significance level, the molecular function and biological processes GO terms allocated to the protein and the spatial information obtained from proteomics on BNAF fractions. FDR values represented by * < 0.05, ** < 0.01, *** <0.001.

| Protein | Arabidopsis Gene ID | WT(-TNT): *Dm*GST(-TNT) | Molecular Function | Biological Processes | Compartmental Prediction | Cluster Prediction |
|---|---|---|---|---|---|---|
| AIG2B | At3g28940 | -1.13 * | Acyltransferase activity | Data not obtained | Plastid (0.21) | Cluster 3 (0.44) |
| AT1G29250 | At1g29250 | -1.8 * | mRNA binding | rRNA processing | Plastid (0.26) | Cluster 5 (0.55) |
| RPL35B | At2g39390 | 5.55 * | Structural constituent of Ribosome | Data not obtained | Plastid (0.40) | Cluster 5 (0.52) |
| UXS5 | At3g46440 | -1.17 * | UDP-glucuronate decarboxylase activity | Xylan biosynthetic process | Cytosol (1.00) | Cluster 3 (1.00) |
| AT3G22845 | At3g22845 | -1.07 * | Vesicle-mediated transport | Data not obtained | Plastid (0.36) | Cluster 5 (0.58) |

#### 5.3.2.4 Characterising the additive response to the combination of *Dm*GST presence and TNT exposure

The product of the additive effect of *Dm*GST presence *in planta* and TNT exposure is a significant enhancement of Conjugate 3 production, thus the biological processes enriched in this response were investigated. For this, the 239 differentially-expressed proteins identified within the WT (-TNT): *Dm*GST (+TNT) and *Dm*GST (-TNT): *Dm*GST (+TNT) comparisons were analysed. Of the 239 proteins, 182 met the criteria for clustering from which seven clusters, enriched with biological processes, were identified (Figure 5.3.2.4.1A). Analysis of these clusters further supports a subtle additive effect of combining *Dm*GST presence and TNT exposure, with the enriched biological responses reflecting for the most part a combination of those generated to each stimulus individually (Figure 5.3.2.4.1B). However, the additive effect did result in an increase in gene expression and amino acid metabolism, with the representative Clusters 1 and 4 containing a total of 51 proteins, compared to 27 across the homologous clusters identified within the separate responses to each stimulus. This increase predominantly resulted from a greater number of repressed proteins. However, KEGG pathway analysis revealed that both glutamate (ath00250) and cysteine metabolic pathways (ath00270) were significantly enriched within cluster 5 (FDR <0.001 and FDR <0.05, respectively). This enrichment was not detected in the homologous cluster identified within the endogenous response to TNT, suggesting a specific response to the increased glutathione consumption resulting from Conjugate 3 production. This analysis also suggests that enhanced Conjugate 3 production requires a suppression of mitochondrial metabolism as the novel Cluster 3, enriched in mitochondrial biological processes, contained mostly repressed proteins. These findings imply that enhanced Conjugate 3 production builds on endogenous biological processes responding to TNT exposure rather than inducing novel routes.

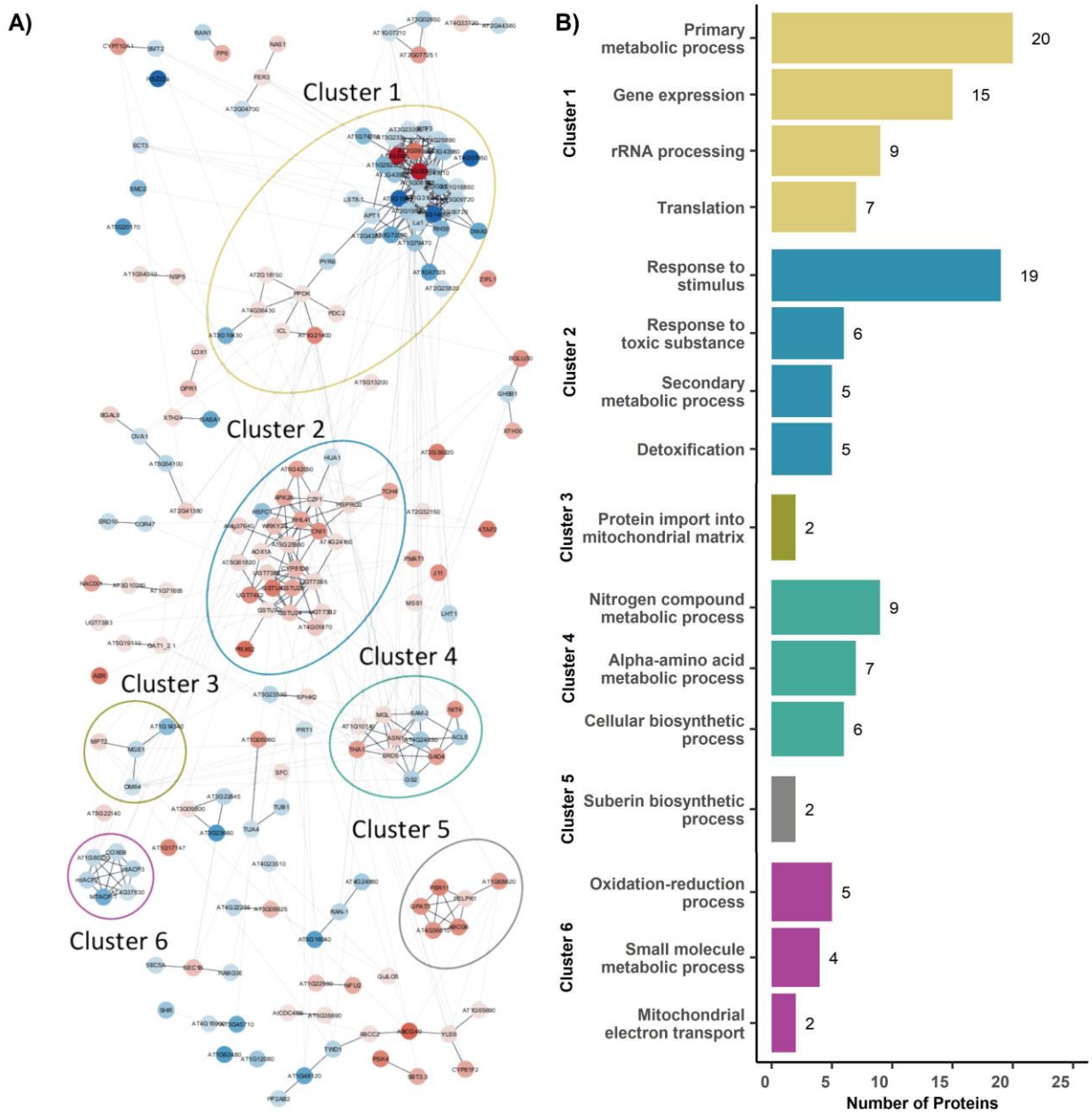


**Figure 5.3.2.4.1: Analysis of the biological responses to enhanced Conjugate 3 production, resulting from the combination of *Dm*GST presence *in planta* and TNT exposure. A)** Network analysis of differently expressed proteins. The analysis comprised 182 of the 239 proteins differentially expressed in response to the combination of *Dm*GST presence *in planta* and TNT exposure when compared to WT (-TNT) control. Seven distinct clusters enriched with biological processes were identified. Nodes represent individual proteins and are coloured in accordance with $\log_2$ fold change compared to WT (-TNT) control, blue is repressed and red is induced. Edges represent protein interactions; bold edges represent interactions that were above the STRING score threshold of 0.5. Protein clustering was based on STRING scores. **B)** Biological GO term enrichment within each cluster. All terms were significantly enriched with an FDR < 0.05.

As *Dm*GST-dependent TNT-response proteins were assumed to be the proteomic response to enhanced Conjugate 3 production, the molecular functions of the proteins were investigated. This category contained 114 proteins, 28 of which did not have an allocated molecular function. Analysis of the remaining 86 proteins identified that 28 have functions involved in gene expression, being allocated to the *Transcription/Translation* category, with the majority being downregulated. The main molecular function categories were similar for induced and repressed proteins with *Oxidoreductases & Peroxidases*, *Glycosyl hydrolases*, *Transporters* and *Methyl- & Acyltransferases* present in both. (Figure 5.3.2.4.2A & B). Based on the metabolomic profile generated by Conjugate 3 metabolism, the induced proteins within these categories have putative function in the metabolism of Conjugate 3. Two peroxidases, PER12 and PER37, were within the *Oxidoreductases & Peroxidases* category. Fourier transform infrared spectrometry analysis identified PER37 overexpression lines contained enhanced phenolic profile within cell walls compared to WT [303], this result signposts PER37 as a putative candidate for TNT-metabolite incorporation to the cell wall. The induced proteins within the *Glycosyl hydrolases* category were XTH30 and, of particular interest, the atypical myrosinase BGLU30 due to its capabilities to hydrolyse the S-glucoside bonds within glucosinolates [304]. The *Transporter* and *Methyl- & Acyltransferases* categories contained the ABC-transporter ABCC2 and the malonyltransferase PMAT1 respectively, these proteins have been linked to *in planta* metabolism of CDNB and naphthol-glucosides respectively [168,251]. Only a fraction of the induced proteins within these categories were detected within the spatial proteomic dataset; however, this analysis did support the cytosolic localisation of PMAT1. Additionally, two proteins with unknown functions, AT5G13200 and VUP1, were allocated to vacuolar/apoplastic Cluster 1 (Figure 5.3.2.4.2C) and thus could play a role in Conjugate 3 metabolism.

The complete list of *Dm*GST-dependent TNT-response proteins, alongside their fold change, and respective GO-term and subcellular-cluster allocations are listed in Table **5.3.2.4.1**.

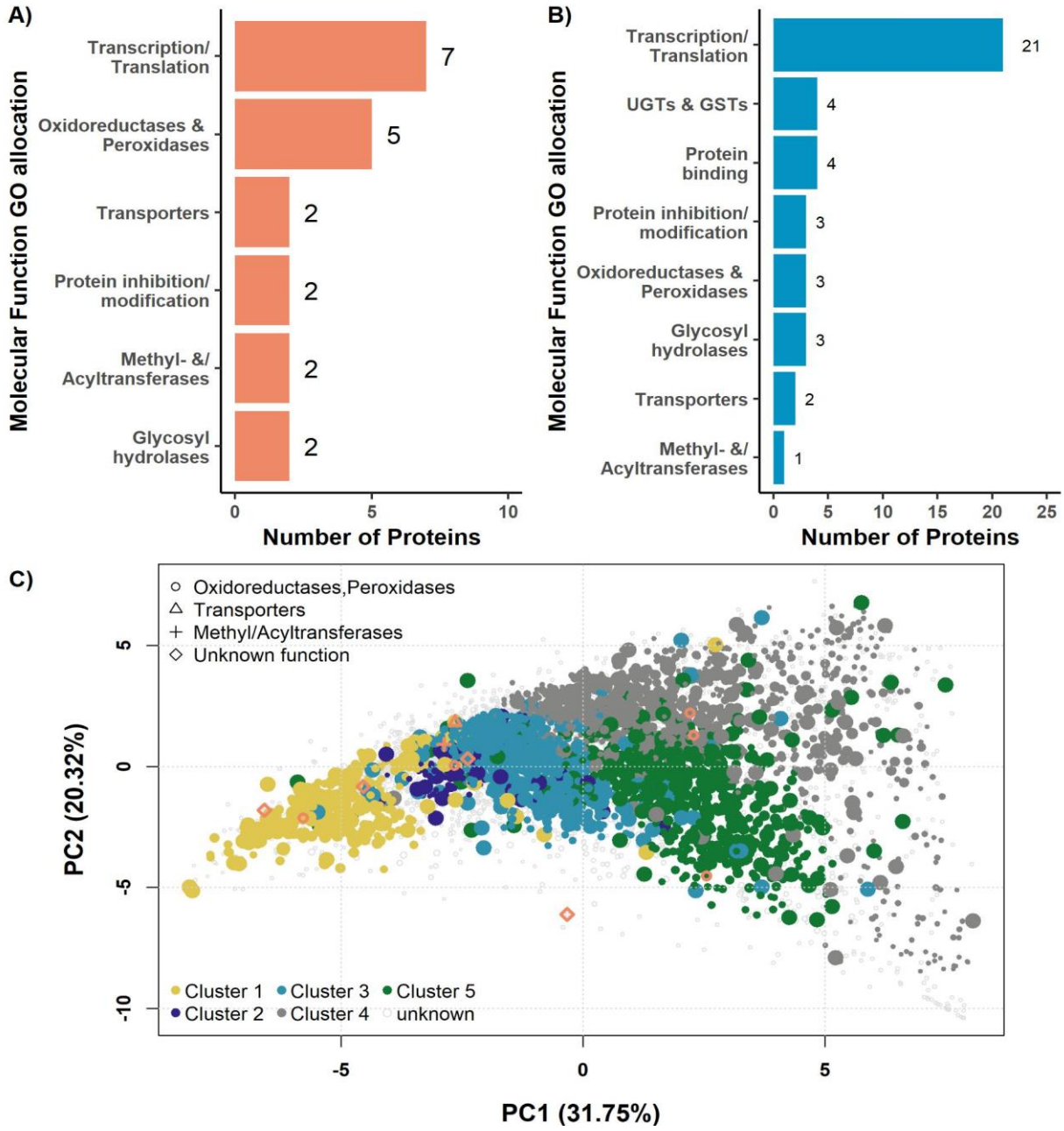


**Figure 5.3.2.4.2**: **Molecular function and spatial analysis of *Dm*GST-dependent TNT-responsive proteins. A)** Top six categories of assigned molecular-function GO terms cover 21 of the 39 induced *Dm*GST-dependent TNT-responsive proteins. **B)** Top eight categories of assigned molecular function GO terms cover 41 of the 77 repressed *Dm*GST-dependent TNT-responsive proteins. **C)** Compartmental allocations of induced *Dm*GST-dependent TNT-responsive proteins, detected within spatial proteomic datasets, and within molecular function categories that imply putative function in Conjugate 3 metabolism. Spatial allocations of induced proteins with unknown molecular functions were investigated as those allocated to cytostol (Cluster 3), vacuole or the apoplast (Clusters 1) are candidates of interest in respect to Conjugate 3 metabolism.

**Table 5.3.2.4.1: *Dm*GST-dependent TNT-responsive proteins, these are proteins assumed to respond to enhanced Conjugate 3 production.** Protein UniProt identifiers and their Arabidopsis Gene ID, log2 fold change and its significance level, the molecular function and biological processes GO terms allocated to the protein and the spatial information obtained from proteomics on BNAF fractions. FDR values represented by * < 0.05, ** < 0.01, *** < 0.001.

| Protein | Arabidopsis Gene ID | WT(-TNT): *Dm*GST(+TNT) | *Dm*GST(-TNT): *Dm*GST(+TNT) | Molecular Function | Biological Processes | Compartmental Prediction | Cluster Prediction |
|---|---|---|---|---|---|---|---|
| ABCC2 | At2g34660 | 1.22 ** | 0.852 * | ABC-type transporter activity | (+)-Abscisic acid D-glucopyranosyl ester transmembrane transport | Vacuole (1.00) | Cluster 1 (1.00) |
| PMAT1 | At5g39050 | 3.89 * | 3.52 | Acyltransferase activity | Data not obtained | Cytosol (0.29) | Cluster 3 (0.59) |
| AT2G16900 | At2g16900 | 1.03 * | 0.607 | Chromatin binding | Data not obtained | Cytosol (0.22) | Cluster 3 (0.40) |
| ASK4 | At1g20140 | -6.44 ** | -1.57 | Cullin family protein binding | Jasmonic acid mediated signaling pathway. Response to jasmonic acid | Data not obtained | Data not obtained |
| NAC081 | At5g08790 | 6.26 ** | 4.67 | DNA binding | Positive regulation of DNA-templated transcription. Negative regulation of DNA-templated transcription. Response to sucrose. Response to wounding. Embryo development ending in seed dormancy. Response to salicylic acid. Defence response to other organism. Response to jasmonic acid. Response to abiotic stress. Leaf senescence. Regulation of cell size. Regulation of photomorphogenesis | Data not obtained | Data not obtained |
| SAP3 | At2g27580 | 2.15 ** | 0.446 | DNA binding | Response to abiotic stress | Nucleus (0.32) | Cluster 4 (0.37) |
| SHR | At4g37650 | -2.24 * | -2.14 | DNA-binding transcription factor activity | Leaf development. Asymmetric cell division. Radial pattern formation. Negative regulation of mitotic cell cycle | Data not obtained | Data not obtained |
| HSFC1 | At3g24520 | -2.41 * | -3.3 * | DNA-binding transcription factor activity | Data not obtained | Data not obtained | Data not obtained |
| GSTF14 | At1g49860 | -0.864 ** | -1.16 *** | Glutathione transferase activity | Data not obtained | Data not obtained | Data not obtained |

| Protein | Arabidopsis Gene ID | WT(-TNT): *Dm*GST(+TNT) | *Dm*GST(-TNT): *Dm*GST(+TNT) | Molecular Function | Biological Processes | Compartmental Prediction | Cluster Prediction |
|---|---|---|---|---|---|---|---|
| CSLA2 | At5g22740 | -1.04 *** | -1.02 *** | Glycosyltransferase activity | Mucilage biosynthetic process. Mucilage metabolic process involved in seed coat development | Data not obtained | Data not obtained |
| AT4G25870 | At4g25870 | -3.84 * | -0.906 | Glycosyltransferase activity | Data not obtained | Data not obtained | Data not obtained |
| AT4G30060 | At4g30060 | -4.42 * | -2.98 | Glycosyltransferase activity | Data not obtained | Data not obtained | Data not obtained |
| BGLU30 | At3g60140 | 5.03 ** | 4.48 * | Hydrolase activity | Data not obtained | Data not obtained | Data not obtained |
| XTH30 | At1g32170 | 3.66 * | 3.1 | Hydrolase activity | Data not obtained | Data not obtained | Data not obtained |
| CDC48D | At3g53230 | 0.934 ** | 1.03 ** | Hydrolase activity | Positive regulation of protein catabolic process | Cytosol (0.25) | Cluster 3 (0.51) |
| AT1G06720 | At1g06720 | -1.09 * | -0.682 | Hydrolase activity | Data not obtained | Nucleus (0.41) | Cluster 4 (0.49) |
| TUBA1 | At1g64740 | -1.14 *** | -0.506 | Hydrolase activity | Microtubule cytoskeleton organization. Cellular response to gravity | Plastid (0.27) | Cluster 5 (0.53) |
| CEL1 | At1g70710 | -1.35 * | -0.509 | Hydrolase activity | Cell wall modification involved in multidimensional cell growth | Data not obtained | Data not obtained |
| AT5G52882 | At5g52882 | -1.79 ** | -1.03 | Hydrolase activity | Data not obtained | Nucleus (0.32) | Cluster 4 (0.37) |
| GLL23 | At1g54010 | 1.41 *** | 1.05 ** | Hydrolase activity, acting on ester bonds | Data not obtained | Plasma Membrane (0.49) | Cluster 1 (0.81) |
| MPT2 | At3g48850 | 1.84 * | 1.12 | Inorganic phosphate transmembrane transporter activity | Response to abiotic stress | Data not obtained | Data not obtained |
| SPHK2 | At4g21534 | 1.06 * | 0.68 | Kinase activity | Sphingolipid metabolic process. Response to abscisic acid. Cellular response to abscisic acid stimulus | Data not obtained | Data not obtained |

| Protein | Arabidopsis Gene ID | WT(-TNT): *Dm*GST(+TNT) | *Dm*GST(-TNT): *Dm*GST(+TNT) | Molecular Function | Biological Processes | Compartmental Prediction | Cluster Prediction |
|---|---|---|---|---|---|---|---|
| GH3.15 | At5g13370 | 5.01 ** | 3.22 | Ligase activity | Auxin conjugate metabolic process | Data not obtained | Data not obtained |
| ZAT12 | At5g59820 | 4.13 ** | 3.57 | Metal ion binding | Response to abiotic stress. Response to wounding. Response to chitin. Response to oxidative stress. Cellular response to hypoxia. Cold acclimation. Hyperosmotic salinity response. Photosynthetic acclimation | Nucleus (0.32) | Cluster 4 (0.37) |
| NIFU2 | At5g49940 | 3.93 * | 3.38 | Metal ion binding | Chloroplast organization. Iron-sulfur cluster assembly | Plastid (0.44) | Cluster 5 (0.57) |
| HIPP26 | At4g38580 | 3.56 * | 0.405 | Metal ion binding | Heat acclimation | Nucleus (0.27) | Cluster 4 (0.32) |
| PDC2 | At5g54960 | 1.37 ** | 1.5 * | Metal ion binding | Response to hypoxia. Cellular response to hypoxia | Cytosol (0.29) | Cluster 3 (0.54) |
| CAR7 | At1g70810 | 1.25 ** | 1.01 * | Metal ion binding | Data not obtained | Plasma Membrane (0.34) | Cluster 1 (0.49) |
| COR47 | At1g20440 | -1.14 ** | -0.552 | Metal ion binding | Response to cold. Response to water deprivation. Response to osmotic stress. Heat acclimation. Defence response to fungus. Response to heat. Response to abscisic acid. Cold acclimation | Cytosol (0.30) | Cluster 3 (0.53) |
| COX5B.2 | At1g80230 | -1.28 ** | -0.309 | Metal ion binding | Data not obtained | Data not obtained | Data not obtained |
| AT3G26730 | At3g26730 | -2.95 * | -0.332 | Metal ion binding | Data not obtained | Nucleus (0.61) | Cluster 4 (0.72) |
| MAIL3 | At1g48120 | -3.64 * | -1.89 | Metal ion binding | Data not obtained | Data not obtained | Data not obtained |
| SAM2 | At4g01850 | -1.32 * | -0.689 | Methionine adenosyltransferase activity | Data not obtained | Plastid (0.48) | Cluster 5 (0.53) |
| OVA1 | At3g55400 | -1.11 ** | -0.159 | Methionine-tRNA ligase activity | Plant ovule development | Plastid (0.39) | Cluster 5 (0.53) |

| Protein | Arabidopsis Gene ID | WT(-TNT): *Dm*GST(+TNT) | *Dm*GST(-TNT): *Dm*GST(+TNT) | Molecular Function | Biological Processes | Compartmental Prediction | Cluster Prediction |
|---|---|---|---|---|---|---|---|
| AT3G05100 | At3g05100 | 4.04 * | 3.81 | Methyltransferase activity | Data not obtained | Data not obtained | Data not obtained |
| SMT2 | At1g20330 | -1.19 *** | -0.678 | Methyltransferase activity | Multidimensional cell growth. Negative regulation of DNA endoreduplication. Xylem and phloem pattern formation. Sterol biosynthetic process. Pattern specification process | Nucleus (0.38) | Cluster 4 (0.46) |
| AT1G12830 | At1g12830 | -2.16 * | -1.34 | Mitochondrial respiratory chain complex iii | Data not obtained | Nucleus (0.41) | Cluster 4 (0.51) |
| AT1G05060 | At1g05060 | 4.67 * | 2.55 | Unknown | Data not obtained | Data not obtained | Data not obtained |
| NRP | At5g42050 | 4.06 ** | 3.38 * | Unknown | Cellular response to hypoxia. Response to endoplasmic reticulum stress. Response to abiotic stress. Regulation of cell death. Regulation of protein catabolic process in the vacuole | Data not obtained | Data not obtained |
| VUP1 | At3g21710 | 1.9 * | 0.649 | Unknown | Xylem development | Plastid (0.23) | Cluster 1 (0.32) |
| T16L1.210 | At4g33720 | 1.71 ** | 1.34 | Unknown | Data not obtained | Plastid (0.31) | Cluster 5 (0.41) |
| AT1G10140 | At1g10140 | 1.16 *** | 0.775 * | Unknown | Cellular response to hypoxia | Cytosol (0.29) | Cluster 3 (0.60) |
| AT5G13200 | At5g13200 | 1.12 ** | 0.972 * | Unknown | Seed germination. Embryo development ending in seed dormancy. Regulation of seed germination. Maintenance of seed dormancy by abscisic acid | Plasma Membrane (0.27) | Cluster 1 (0.55) |
| NHL6 | At1g65690 | 1.1 ** | 1.15 ** | Unknown | Response to osmotic stress. Response to abscisic acid. Response to abiotic stress. Positive regulation of abscisic acid biosynthetic process | Data not obtained | Data not obtained |

| Protein | Arabidopsis Gene ID | WT(-TNT): *Dm*GST(+TNT) | *Dm*GST(-TNT): *Dm*GST(+TNT) | Molecular Function | Biological Processes | Compartmental Prediction | Cluster Prediction |
|---|---|---|---|---|---|---|---|
| AT4G23510 | At4g23510 | -1.06 *** | -0.159 | Unknown | Data not obtained | Data not obtained | Data not obtained |
| AT5G66090 | At5g66090 | -1.17 *** | -0.402 | Unknown | Data not obtained | Plastid (0.44) | Cluster 5 (0.71) |
| AT2G44380 | At2g44380 | -1.26 ** | -0.455 | Unknown | Data not obtained | Plastid (0.27) | Cluster 5 (0.35) |
| MHF15.13 | At5g06350 | -1.4 | -2.11 * | Unknown | Data not obtained | Nucleus (0.46) | Cluster 4 (0.55) |
| MJP23.8 | At5g54100 | -1.5 ** | -0.484 | Unknown | Data not obtained | Nucleus (0.31) | Cluster 5 (0.36) |
| AT2G20820.F5H14.21 | At2g20820 | -1.73 * | -1.25 | Unknown | Data not obtained | Data not obtained | Data not obtained |
| MNF13.11 | At5g40590 | -1.9 *** | -1.47 ** | Unknown | Data not obtained | Nucleus (0.32) | Cluster 4 (0.37) |
| AT3G14172 | At3g14172 | -2.01 * | -1.01 | Unknown | Data not obtained | Data not obtained | Data not obtained |
| AT2G27090 | At2g27090 | -2.26 * | -0.737 | Unknown | Data not obtained | Data not obtained | Data not obtained |
| AT2G18990 | At2g18990 | -2.7 * | -1.52 | Unknown | Data not obtained | Nucleus (0.32) | Cluster 4 (0.37) |
| AT1G74280 | At1g74280 | -2.78 * | -2.07 | Unknown | Data not obtained | Data not obtained | Data not obtained |
| DL4930W | At4g17790 | -3.06 * | -2.35 | Unknown | Data not obtained | Data not obtained | Data not obtained |
| AT3G19430 | At3g19430 | -3.27 ** | -1.37 | Unknown | Data not obtained | Nucleus (0.30) | Cluster 4 (0.35) |
| AT3G03150 | At3g03150 | -3.59 ** | -1.9 | Unknown | Data not obtained | Data not obtained | Data not obtained |

| Protein | Arabidopsis Gene ID | WT(-TNT): *Dm*GST(+TNT) | *Dm*GST(-TNT): *Dm*GST(+TNT) | Molecular Function | Biological Processes | Compartmental Prediction | Cluster Prediction |
|---|---|---|---|---|---|---|---|
| GASA1 | At1g75750 | -3.59 * | -0.447 | Unknown | Response to abscisic acid. Response to gibberellin. Response to brassinosteroid | Cytosol (0.23) | Cluster 1 (0.45) |
| AT5G16040 | At5g16040 | -3.94 * | -3.61 | Unknown | Data not obtained | Plastid (0.50) | Cluster 5 (0.62) |
| AT1G72480 | At1g72480 | -4.19 ** | -2.19 | Unknown | Data not obtained | Data not obtained | Data not obtained |
| DL4016C | At4g15960 | -4.2 * | -2.83 | Unknown | Data not obtained | Nucleus (0.32) | Cluster 4 (0.37) |
| AT1G73390 | At1g73390 | -4.28 * | -2.99 | Unknown | Data not obtained | Data not obtained | Data not obtained |
| AT1G14820 | At1g14820 | -4.69 ** | -1.28 | Unknown | Data not obtained | Data not obtained | Data not obtained |
| HUA1 | At3g12680 | -1.03 ** | -0.593 | mRNA binding | Data not obtained | Nucleus (0.32) | Cluster 4 (0.37) |
| ECT3 | At5g61020 | -1.18 *** | -0.725 ** | mRNA binding | Data not obtained | Nucleus (0.42) | Cluster 4 (0.46) |
| BTF3 | At1g17880 | -1.25 ** | -0.205 | mRNA binding | Data not obtained | Plastid (0.39) | Cluster 5 (0.50) |
| TUBB1 | At1g75780 | -1.39 *** | -0.535 | mRNA binding | Unidimensional cell growth. Response to light stimulus | Data not obtained | Data not obtained |
| LA1 | At4g32720 | -1.41 *** | -0.7 | mRNA binding | Embryo development ending in seed dormancy. rRNA processing. Ribosome biogenesis. ncRNA processing | Nucleus (0.66) | Cluster 4 (0.77) |
| AT5G08180 | At5g08180 | -1.78 * | -0.769 | mRNA binding | Data not obtained | Nucleus (0.45) | Cluster 4 (0.54) |
| RH39 | At4g09730 | -2.77 * | -2.48 | mRNA binding | Ribulose bisphosphate carboxylase complex assembly. Chloroplast rRNA processing | Data not obtained | Data not obtained |

| Protein | Arabidopsis Gene ID | WT(-TNT): *Dm*GST(+TNT) | *Dm*GST(-TNT): *Dm*GST(+TNT) | Molecular Function | Biological Processes | Compartmental Prediction | Cluster Prediction |
|---|---|---|---|---|---|---|---|
| RSZ22A | At2g24590 | -5.43 ** | -3.26 | mRNA binding | Data not obtained | Plastid (0.47) | Cluster 5 (0.48) |
| PER37 | At4g08770 | 1.54 * | 1.26 | Oxidoreductase activity | Negative regulation of growth | Plastid (0.41) | Cluster 5 (0.56) |
| LOX1 | At1g55020 | 1.52 * | 0.947 | Oxidoreductase activity | Response to abscisic acid. Response to jasmonic acid. Root development. Lateral root formation. Lipid oxidation | Peroxisome (0.30) | Cluster 3 (0.53) |
| GULLO5 | At2g46740 | 1.16 *** | 0.805 ** | Oxidoreductase activity | L-Ascorbic acid biosynthetic process | Plasma Membrane (0.37) | Cluster 1 (0.91) |
| PER12 | At1g71695 | 1.05 ** | 0.626 | Oxidoreductase activity | Data not obtained | Nucleus (0.43) | Cluster 4 (0.50) |
| FTRC | At2g04700 | -1.13 ** | -0.353 | Oxidoreductase activity | Data not obtained | Plastid (0.66) | Cluster 5 (0.82) |
| AT3G23530 | At3g23530 | -1.55 * | -1.4 | Oxidoreductase activity | Data not obtained | Data not obtained | Data not obtained |
| CYP712A1 | At2g42250 | -1.84 | -3.51 * | Oxidoreductase activity | Data not obtained | Data not obtained | Data not obtained |
| AT1G31020 | At1g31020 | 4.08 * | 2 | Oxidoreductase activity, acting on a sulfur group of donors, disulfide as acceptor | Data not obtained | Nucleus (0.32) | Cluster 4 (0.37) |
| SBT3.3 | At1g32960 | 3.87 * | 3.31 | Peptidase activity | Induced systemic resistance | Data not obtained | Data not obtained |
| AT5G19110 | At5g19110 | 1.16 * | 0.458 | Peptidase activity | Data not obtained | Nucleus (0.28) | Cluster 4 (0.32) |
| AT2G01710 | At2g01710 | 1.32 * | 0.375 | Positive regulation of transcription by RNA polymerase II | Data not obtained | Nucleus (0.59) | Cluster 4 (0.72) |

| Protein | Arabidopsis Gene ID | WT(-TNT): *Dm*GST(+TNT) | *Dm*GST(-TNT): *Dm*GST(+TNT) | Molecular Function | Biological Processes | Compartmental Prediction | Cluster Prediction |
|---|---|---|---|---|---|---|---|
| LST8.1 | At3g18140 | -1.01 ** | -0.151 | Protein binding | Long-day photoperiodism. Regulation of inositol biosynthetic process. Regulation of raffinose biosynthetic process | Data not obtained | Data not obtained |
| OM64 | At5g09420 | -1.06 ** | -0.407 | Protein binding | Protein targeting to mitochondrion. Protein import into mitochondrial matrix | Data not obtained | Data not obtained |
| FKBP42 | At3g21640 | -1.7 * | -0.544 | Protein binding | Leaf development | Data not obtained | Data not obtained |
| AT5G14050 | At5g14050 | -4.6 ** | -2.2 | Protein binding | Data not obtained | Nucleus (0.33) | Cluster 4 (0.39) |
| AT3G51270 | At3g51270 | -2.26 * | -2.26 | Protein kinase activity | Data not obtained | Data not obtained | Data not obtained |
| LECRK11 | At3g45330 | -3.83 * | -0.14 | Protein kinase activity | Defence response to fungus | Data not obtained | Data not obtained |
| NSP5 | At5g48180 | 1.36 *** | 1.39 *** | Regulation of catalytic activity | Glucosinolate catabolic process. Nitrile biosynthetic process | Plastid (0.29) | Cluster 5 (0.53) |
| AGD3 | At5g13300 | 1.34 * | 0.627 | Regulation of catalytic activity | Leaf morphogenesis. Response to auxin. Phloem or xylem histogenesis. Endocytosis. Xylem and phloem pattern formation | Nucleus (0.23) | Cluster 1 (0.29) |
| COX6A | At4g37830 | -1.04 * | -0.193 | Regulation of catalytic activity | Data not obtained | Mitochondrion (0.24) | Cluster 5 (0.50) |
| RH57 | At3g09720 | -1.36 * | -1.22 | RNA binding | Data not obtained | Nucleus (0.64) | Cluster 4 (0.75) |
| AT4G24880 | At4g24880 | -2.04 ** | -1.16 | RNA binding | Data not obtained | Nucleus (0.43) | Cluster 4 (0.52) |
| AT1G14340 | At1g14340 | -2.67 * | -3.18 * | RNA binding | Data not obtained | Nucleus (0.30) | Cluster 4 (0.34) |
| BRIX1.1 | At3g15460 | -5.05 ** | -3.61 | rRNA binding | rRNA processing. Ribosomal large subunit assembly | Data not obtained | Data not obtained |

| Protein | Arabidopsis Gene ID | WT(-TNT): *Dm*GST(+TNT) | *Dm*GST(-TNT): *Dm*GST(+TNT) | Molecular Function | Biological Processes | Compartmental Prediction | Cluster Prediction |
|---|---|---|---|---|---|---|---|
| AT1G18850 | At1g18850 | -1 *** | -0.59 | rRNA processing | rRNA processing | Nucleus (0.36) | Cluster 4 (0.43) |
| ENP1 | At1g31660 | -1.12 ** | -0.567 | rRNA processing | Embryo sac development. Pollen development. rRNA processing | Nucleus (0.54) | Cluster 4 (0.64) |
| RPL4D | At5g02870 | 10 * | 2.48 | Structural constituent of Ribosome | Data not obtained | Nucleus (0.61) | Cluster 4 (0.71) |
| RPL5 | At4g01310 | 4.65 * | 1.5 | Structural constituent of Ribosome | Data not obtained | Nucleus (0.38) | Cluster 4 (0.45) |
| RPP2A | At2g27720 | 2.13 ** | 0.651 | Structural constituent of Ribosome | Data not obtained | Plastid (0.22) | Cluster 5 (0.49) |
| AT1G07210 | At1g07210 | -1.02 ** | -0.393 | Structural constituent of Ribosome | Data not obtained | Plastid (0.51) | Cluster 5 (0.56) |
| RPL36AA | At4g14320 | -1.08 ** | -0.424 | Structural constituent of Ribosome | Data not obtained | Plastid (0.33) | Cluster 5 (0.38) |
| LHT1 | At5g40780 | -1.56 ** | -0.536 | Symporter activity | Defence response. Amino acid import | Data not obtained | Data not obtained |
| ACL5 | At5g19530 | -1.77 * | -1.8 * | Thermospermine synthase activity | Phloem or xylem histogenesis. Auxin polar transport. Xylem vessel member cell differentiation | Data not obtained | Data not obtained |
| MDC12.25 | At5g63280 | -1.98 * | -0.89 | Transcription cis-regulatory region binding | Data not obtained | Data not obtained | Data not obtained |
| MED17 | At5g20170 | -3.82 ** | -1.01 | Transcription coregulator activity | miRNA processing | Nucleus (0.32) | Cluster 4 (0.37) |
| PRT1 | At3g24800 | -1.07 *** | -0.633 * | Transferase activity | Ubiquitin-dependent protein catabolic process via the n-end rule pathway. Defence response to fungus | Nucleus (0.32) | Cluster 4 (0.37) |
| HAKAI | At5g01160 | -3.63 * | -0.307 | Transferase activity | mRNA methylation | Data not obtained | Data not obtained |

| Protein | Arabidopsis Gene ID | WT(-TNT): *Dm*GST(+TNT) | *Dm*GST(-TNT): *Dm*GST(+TNT) | Molecular Function | Biological Processes | Compartmental Prediction | Cluster Prediction |
|---|---|---|---|---|---|---|---|
| NPF2.5 | At3g45710 | -3.52 * | -1.13 | Transmembrane transporter activity | Chloride transport. Cellular response to salt | Data not obtained | Data not obtained |
| AT3G09800 | At3g09800 | 1.08 *** | 0.0936 | Vesicle-mediated transport | Data not obtained | Nucleus (0.32) | Cluster 4 (0.37) |
| SEC23E | At3g23660 | -1.15 * | -0.0714 | Vesicle-mediated transport | Data not obtained | Data not obtained | Data not obtained |
| AT1G15370.F9L1_32 | At1g15370 | -1.35 ** | -0.523 | Vesicle-mediated transport | Data not obtained | Data not obtained | Data not obtained |

## 5.4 Discussion

Proteomic analysis of fractionated and whole root tissue has provided resources that can aid in the development of detailed, testable models relating to the TNT detoxification response and metabolism of Conjugate 3. Analysis of BNAF fractions identified that the optimised technique yields a five-cluster resolution from the ten main subcellular compartments, and from this, a level of spatial identity has been provided to over 2300 proteins within root tissue. Proteomic analysis of whole-root tissue identified that the protein response to *Dm*GST presence has substantial overlap with the response to TNT, as well as showing subtle additivity from the combination of the two stimuli. The identification of *Dm*GST-dependent TNT-responsive proteins provides a pool of candidates with putative involvement in the glutathione-detoxification pathway for TNT. Analysis of this group of proteins has already identified obvious candidates for future research. The combination of the two proteomic datasets, alongside the biological- and molecular-function analysis performed, can aid in generating models relating to TNT-, and more specifically, Conjugate 3.

### 5.4.1 Reproducibility and compartmental resolution of BNAF

Proteomic analysis of BNAF fractions confirmed the technique optimised within this body of work is highly reproducible but limited in its ability to distinguish subcellular compartments. A possible weakness of BNAF, compared to conventional NAF-techniques that use a continuous linear gradient, is that the iterative fractionation process may result in high variability between gradients due to accumulative human-error. However, the density-dependent clustering of samples, within hierarchical analysis of protein distributions, confirmed the capability of BNAF to be of comparable reproducibility to conventional NAF techniques [191,192]. Proteomics also allowed the compartmental resolution of the optimised BNAF technique to be investigated, revealing a five-cluster model, based on the ten main subcellular compartments, was most suitable for data analysis. Obtaining distinct distribution profiles for the peroxisome and nucleus has not been previously achieved within published examples of NAF-based proteomics [191,194]. The inclusion of sonication during the iterative fractionation process of BNAF has been suggested to improve compartmental separation [193], a hypothesis supported by the presented data. The high similarity of distribution profiles between the different subcellular compartments could reflect the functionality or the evolutionary origin of these compartments. In the case of mitochondria and plastids, previous studies have also shown the difficulty in obtaining a plastid-enriched fraction from Arabidopsis root cells without mitochondrial co-enrichment [264,269]. A potential explanation for the co-enrichment is that mitochondria and plastids are both evolutionarily

derived from the endosymbiosis of prokaryotes, this possibly distinguishes them compositionally from other organelles. The presence of a double membrane within the mitochondria, plastids and nucleus may also explain the close relationship between the respective clusters of these subcellular compartments. The finding that the ER has a diffuse distribution across the gradient, comparable to the cytosol, aligns with results obtained using conventional NAF-techniques which could not distinguish these compartments based on density-distribution patterns [191]. The discovery that the distribution of the golgi is highly similar to that of the ER could reflect the close functional relationship between these compartments. This relationship has been demonstrated by the collapse of the golgi into the ER following inhibition of the golgi-localised nucleotide exchange factor GBF1 [305]. The clustering of the vacuole, plasma membrane and the extracellular compartments confirms that the currently optimised BNAF technique is unable to identify the exact compartmental fate of TNT-metabolites within root tissue. A potential alteration to the current technique that could improve the compartmental resolution is an increase in the number of fractions. Both previously published NAF-proteomic studies, and the majority of LOPIT studies, have used more than nine fractions within their gradients to increase the compartmental resolution [191,194,306]. However, there are trade-offs to increasing the number of fractions, with one being the loss of distinct distribution profiles for subcellular compartments, which prevents the allocation of spatial information to proteins and metabolites. The optimised BNAF method may be particularly sensitive to the effects caused by increasing the number of fractions, due to the limited density range available for root tissue. Whilst the compartmental resolution is lower than achieved in other investigations [306], these results provide the first spatial analysis of the Arabidopsis root proteome using BNAF, as well as demonstrate how this technique can be used to integrate proteomic and metabolomic spatial information to provide a greater understanding of compartmentalised metabolism.

Due to the time constraints, characterisation of the compartmentalised proteome beyond the proteins differentially expressed in response to TNT and *Dm*GST presence was not performed. As protein localisation can differ between tissue-specific isoforms [295], investigating proteins with unexpected spatial allocations might allow for the identification of novel biological functions. One method to achieve this could be via the *phenoDisco* algorithm [268] which can detect novel clusters for which no prior knowledge has been provided i.e., no marker protein input. This approach could identify protein clustering, unique to the roots, that is unidentifiable if analysis is based solely on elucidating compartmental identity through identified marker enzyme distributions.

### 5.4.2 Overlap of proteomic responses to *Dm*GST presence and TNT-exposure

A surprising finding from this proteomic investigation was the overlap in the responses to *Dm*GST presence and TNT exposure. This overlap was evidenced by results from hierarchical clustering of the proteomic responses, as well as the identification that the presence of TNT reduced the response to *Dm*GST presence, and that *Dm*GST lines showed a reduced response to TNT. A potential reason for this overlap is that transgene expression induces oxidative stress, with the presence of *Dm*GST impacting the cellular balance of glutathione, and thus the redox state within plant cells. However, as *Dm*GST lines showed comparable growth to respective WT controls in the absence of TNT [236], it indicates any oxidative stress induced by *Dm*GST presence occurs at a low, manageable level. Another interesting finding from this analysis was that proteins involved in the oxidative phosphorylation pathway were repressed in response to *Dm*GST presence. This repression is surprising as oxidative phosphorylation is expected to be the most efficient pathway to address the increased energy demand resulting from enhanced gene expression. A potential explanation for this discrepancy is that the oxygen concentration required for efficient oxidative phosphorylation is not provided by the static hydroponic system used to grow and dose plants. The repression of oxidative phosphorylation in static hydroponics might only be identifiable under greater energy requirement, such as those driven by increased gene expression, a hypothesis supported by the finding that the identified proteins are also repressed in response to TNT exposure, though not significantly.

### 5.4.3 Putative proteins involved in TNT metabolism

Analysis of the endogenous proteomic response to TNT identified proteins previously confirmed to modify the xenobiotic; putative candidates that may offer alternative pathways; and proteins that could facilitate downstream metabolic processes. In respect to TNT transformation, despite all three functional OPRs being capable of reducing TNT *in vitro* [99], this analysis identified that only OPR1 was significantly upregulated, suggesting it to be the primary enzyme for TNT reduction within the root. Interestingly, alongside OPR1 induction, the dioxygenase JOX2 was also induced in response to TNT. While JOX2 has a confirmed role in oxidising jasmonic acid to 12-hydroxyjasmonate [307,308], and thus may be involved in the complex hormonal response to TNT, it is also linked to *in planta* metabolism of the polyaromatic hydrocarbon pheanthrene [307], these findings suggest JOX2 could have catalytic activity towards aliphatic and aromatic structures found within TNT. Currently only oxidation of the methyl functional group within TNT has been indicated to occur *in planta* [309], generating a methoxy-derivative, investigating *in vitro* JOX2 activity towards TNT would identify whether this enzyme can

directly catalyse this reaction. In relation to conjugation of TNT and its derivatives, this analysis did not identify any novel enzymes capable of catalysing this step. Interestingly, GSTU24 and GSTU25 were identified as *Dm*GST-independent TNT-responsive proteins with the magnitude of their induction unchanged by enhanced Conjugate 3 production. As enhanced Conjugate 3 production is assumed to result in greater depletion of cellular glutathione, these results indicate GSTU24 and GSTU25 expression is independent of glutathione availability. The quantification of glutathione levels between WT and *Dm*GST lines following TNT exposure would allow this to be confirmed. Regarding GSTU4 and GSTU7, the other GSTs induced by TNT exposure, these proteins have little activity towards TNT [106], thus they are most likely involved in the response to induced oxidative stress; glutathione peroxidase activity of GSTU7 supports this hypothesis [127]. Alongside GSTs, several UGTs were induced, including the majority of the UGT73B subfamily. Simultaneous induction of multiple UGT73B subfamily members has been identified for a variety of chemical stressors including, but not limited to, environmental pollutants, pharmaceuticals and allelochemicals [288]. The promiscuity of the UGT73B subfamily could have evolved to respond to allelochemicals, which are a group of highly diverse plant-derived compounds [310]. The vacuolar uptake of glucosyl-conjugates, like HADNT-Glc and ADNT-Glc, has been shown to be energised through proton gradients [112,218], with MATE-transporters capable of facilitating this process identified [173,174]. Within the analysis presented here, MATE-transporters were not induced however, the vacuolar major-facilitator protein ZIFL1 was. A homolog of the fungal Drug/$H^+$ antiporter Tpo1, ZIFL1 is capable of enhancing 2,4-D tolerance within yeast [311]. Alongside this finding, the induction of ZIFL1 in response to *Pseudomonas syringae pv*.tomato infection is strongly correlated with glucosyl- and malonyltransferase expression [312]. Together, these findings present ZIFL1 as a strong candidate for the vacuolar import of glucosyl/malonylglucosyl conjugates generated during TNT-metabolism.

### 5.4.4 Putative proteins involved in Conjugate 3 metabolism

Despite generating significant metabolic changes, the additive effects of *Dm*GST presence and TNT exposure were subtle at the proteomic level requiring comparison to the WT (-TNT) control to detect. This conclusion is supported by network analysis identifying minimal change to the biological processes enriched in the response to the combination of *Dm*GST and TNT, when compared to the endogenous response to TNT. Despite this subtle effect, proteins with putative functions in the metabolism of Conjugate 3 were identified by their significant induction in response to greater concentrations of the metabolite, this included the ABC-transporter ABCC2 and the malonyltransferase PMAT1. As ABCC2 is

localised to the tonoplast and transports glutathione-conjugates [313], it is predicted to facilitate the vacuolar sequestration of Conjugate 3. The confirmed O-malonyltransferase activity of PMAT1 [251,252,314] implies a function in the malonylation of the S-glucoside generated during Conjugate 3 metabolism. The atypical myrosinase BGLU30 was also induced by enhanced Conjugate 3 production. Due to its ability to hydrolyse S-glucosidic bonds, induction of BGLU30 signposts its involvement in the further metabolism of the S-malonylglucoside derivative of Conjugate 3. Surprisingly, enzymatic candidates involved in the formation of S-glucoside and N-malonyl conjugates, derived from Conjugate 3, were not identified within the induced protein population. An explanation for these findings is that the respective S-glucosyltransferase and N-malonyltransferase are within the population of proteins with unknown molecular functions induced in response to either TNT or Conjugate 3. However, an alternative explanation for the inability to identify induced S-glucosyltransferases and N-malonyltransferases is that these enzymes are constitutively expressed and have promiscuous activity towards cysteinyl-conjugate derivatives of TNT. Promiscuous activity of constitutively expressed enzymes is the most likely case in respect to S-glucoside formation, as the activity of an unidentified UGT is unlikely as the enzymatic family have well defined signature sequences [105], and *in vitro* investigations revealed the UGT73B subfamily and UGT74E2 to have little or no conjugating activity towards thiol-containing compounds [287]. Therefore, the opportunistic activity of a UGT involved within a constitutively active cellular pathway provides a better explanation for S-glucoside formation, with glucosinolate biosynthesis being an obvious source due to the characteristic S-glucoside linkage within these compounds.

### 5.4.5 Biological responses to TNT exposure

Part of the biological response to TNT, and influenced by enhanced production of Conjugate 3, was the adaptation of primary metabolism. Within the amino-acid metabolising proteins induced by TNT were glutamine amidotransferase 1_2.1 and MGL, enzymes involved in the synthesis of glutathione constituents' glutamate and cysteine respectively [285,315]. This finding suggests that the availability of amino acids comprising glutathione could limit the role of the molecule in TNT detoxification, a hypothesis supported by the discovery that exogenous glutathione enhances TNT uptake both in WT and *Dm*GST lines (see Tzafestas *et al*. (2017) [236]), as well as by the presented proteomics data identifying the induction of enzymes involved in glucosinolate catabolism i.e., BGLU30. Glucosinolate content within plants responds to a variety of abiotic stressors [316], the catabolism of these sulfur-rich metabolites to aid glutathione synthesis, via increasing sulfur availability within the cell, offers a

mechanism to explain these findings. This theory is supported by the discovery that the activity of BGLU30, alongside BGLU28, is involved in the use of glucosinolates as a sulfur reservoir within nutrient-deficient plants [304,317,318]. As well as BGLU30, proteomic analysis identified that the nitrile-specifier NSP5 was also induced in response to enhanced Conjugate 3 production. The sequential activity of BGLU30 and NSP5 offers an enzymatic pathway for the catabolism of glucosinolates to nitrile-derivatives, thus allowing the sulfur within glucosinolates to be released for use in primary metabolism. Investigating the TNT uptake and tolerance capabilities of *bglu28bglu30* knockout lines, in combination with quantifying glucosinolates and thiol-containing compounds such as cysteine and glutathione content *in planta*, would offer insight into whether glucosinolate catabolism can provide a source of sulfur during enhanced periods of glutathione-mediated detoxification. Further elucidating the adjustments of primary metabolism in response to enhanced detoxification could identify enzymatic steps which limit resource availability.

Alongside adjustments to primary metabolism, cell wall modification was indicated as another important response to TNT treatment, evidenced by the induction of proteins involved in suberin biosynthesis and hemicellulose modification. Suberin is a lipophilic polyester that comprises the suberin lamellae, the waxy coating on the surface of endodermal cells within the roots, which controls the transport of water and nutrients from the apoplastic to the symplastic environments within the root endodermis [319]. In respect to TNT-detoxification, increased suberin biosynthesis may act as a physical barrier to reduce the flux of the xenobiotic into the endodermal cells. As TNT is a hydrophobic molecule, the aromatic layer that suberin provides could decrease the mobility of TNT, reducing its flux and reducing TNT phytotoxicity. This hypothesis assumes that the induction of suberin-biosynthesis proteins translates to increased root suberisation. While directed suberin deposition has been identified as a response to cadmium exposure [320], such a relationship has not yet been observed for TNT. Additionally, the induction of several XTHs in response to TNT is potentially related to enhanced suberin biosynthesis. In response to abiotic stress, such as salt and temperature, XTHs are thought to control cell wall elasticity to maintain symplastic volume and/or cell turgor [321–323]. In respect to TNT-detoxification, XTH activity might therefore enable a thickening of the suberin lamellae via cell wall expansion.

### 5.4.6 Limitations of proteomic analysis

A limitation of this study, in elucidating metabolic processes occurring in plants grown in TNT-contaminated soil, was its sole focus on the root-localised proteomic response. This focus resulted from

prior studies, using plants grown within TNT-contaminated soil, confirming roots to be the primary location of TNT-detoxification and sequestration [78,85,86,92]. However, the significant resource requirement of detoxification most likely induces responses across the whole organism. This effect has been confirmed in tomato plants grown in soil contaminated by the pesticide dichlorodiphenyltrichloroethane (DDT). Despite the vast majority of DDT being found within the root tissue, antioxidant enzyme activities within shoots and leaves were significantly increased, whilst in roots they decreased or did not respond [324]. Though whether this organ specific response resulted from transport of DDT metabolites to aerial tissues was not investigated, the results suggest differential responses across the plant to a tissue-localised xenobiotic stress. Therefore, identifying the response of aerial tissues to root-localised TNT exposure is likely to elucidate further mechanisms of metabolic adaptation that could aid in a systems-based approach to developing plants with enhanced xenobiotic-tolerance.

It is also important to note that due to the generation of superoxide radicals via the toxic metabolism of TNT, it cannot be assumed that proteins whose abundance increased in response to the xenobiotic are involved in its direct metabolism. Rather these proteins may have roles involved in the complex response to oxidative stress caused by these radicals. It is for this reason that it is vital to perform functional analysis through either substrate specificity characterisation of recombinant proteins or via metabolic analysis of respective knockout lines to confirm a role for putative proteins in the direct metabolism of TNT.

### 5.4.7 Conclusions

In conclusion, the research described within this chapter has provided valuable resources for the further investigation of TNT and Conjugate 3 metabolism within the root tissue of plants. It has identified multiple candidates with putative roles in TNT-detoxification, both related to and independent of Conjugate 3 metabolism. The spatial information provided by analysis of BNAF will be of interest to a broader research community, aiding in the investigation of cellular processes not restricted to xenobiotic detoxification. The combination of these proteomic resources will aid in the development of testable metabolic models for the further advancement in the phytoremediation of xenobiotics.

# Chapter 6: Final Discussion

Prior to this study, the understanding of TNT-metabolism within plants was limited to the transformation and conjugation steps [90]. The presented research has investigated the molecular processes that occur following conjugation within plant TNT-detoxification pathways. A focus was placed on the nitro-substituted product of glutathionylation, Conjugate 3, due to its potential in respect to TNT-phytoremediation. Through *Dm*GST expression, Conjugate 3 production *in planta* was enhanced; this allowed the significance of GGT-initiated metabolism within roots to be confirmed, and multiple downstream metabolites to be putatively identified. This analysis indicated that both O-linked and N-linked malonyl conjugates were downstream metabolites of Conjugate 3, with the former also being putatively generated within HADNT and ADNT metabolism. The use of BNAF with Arabidopsis root tissue, provided the first *in planta* evidence for the sequestration of these downstream metabolites from the cytosol. Finally, putative protein candidates involved in the metabolism of these molecules, within Arabidopsis root tissue, have been identified though compartmental analysis of the root proteome and investigation of its response to TNT and enhanced Conjugate 3 production. From this combination of metabolomic and proteomic analysis a testable metabolic model of TNT-detoxification within Arabidopsis roots has been generated (Figure 6.1).

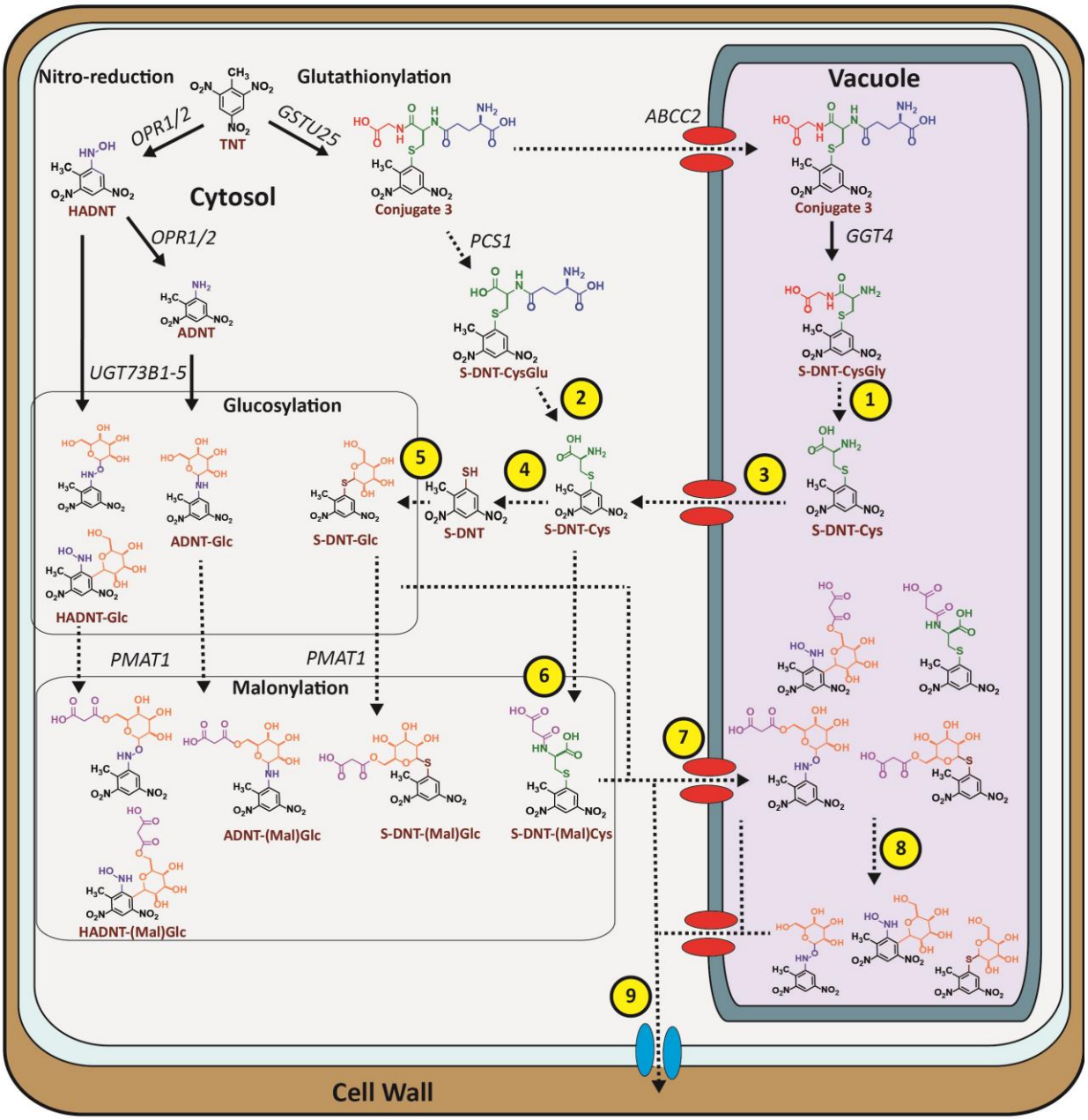


**Figure 6.1: Model for TNT-metabolism within Arabidopsis based on metabolomic and proteomic data obtained within this body of work and supported by information from the literature.** Hydroxyamino-derivatives of TNT generated from nitro-reduction are rapidly glucosylated and subsequently malonylated. Nitro-substituted glutathione conjugates of TNT are metabolised to a cysteinyl conjugate, which undergoes malonylation either directly or through a glucosylated 2-thiol-4,6-dinitrotoluene (S-DNT) intermediate. Except for S-DNT all conjugates have been detected to 2 ppm accuracy by LC-MS/MS analysis. Confirmed pathways represented by solid arrows whilst putative pathways represented by segmented arrows. Proteins with confirmed activities or whose activity is strongly indicated by proteomics and the literature are labelled next to the metabolic step they catalyse. Numbers represent metabolic steps in which putative candidate proteins have been identified but the evidence within the literature for the predicted role is not of sufficient strength.

## 6.1 Vacuolar metabolism of Conjugate 3 to cysteinyl conjugate derivatives

Metabolite subcellular localisation confirmed Conjugate 3 is sequestered from the cytosol in root tissue. The assumed destination is the vacuole, as prior studies have shown the accumulation of fluorescent glutathione-conjugates within the organelle [114,115]. This assumption is supported by proteomic analysis, which identified the vacuolar transporter ABCC2 is significantly induced in response to enhanced Conjugate 3 production. As ABCC2 has been shown to transport a variety of glutathione-conjugates [109], and respective knockout lines are less tolerant to the model GST-substrate CDNB [168], the protein is a likely candidate for transporting Conjugate 3 across the tonoplast. Confirmation of this function *in planta* can be ascertained by investigating Conjugate 3 compartmental association within *abcc2* knockout lines using BNAF. As ABCC1 has been shown to provide redundancy in ABCC2 functions [130], respective single and double knockout lines should be included within *in planta* studies. Once within the vacuole, Conjugate 3 is metabolised to S-DNT-Cys via sequential enzymatic reactions initiated by GGT activity. The allocation of this activity, to either GGT1 or GGT4, was not achieved in this study due to time restraints. However, as prior work has shown GGT4 to be the only vacuolar localised GGT [115,121], it is reasonable to assume that it is responsible for initiating Conjugate 3 metabolism. Surprisingly, proteomic analysis did not detect a change in the abundance of GGT4, or GGT1, in response to either TNT exposure or enhanced Conjugate 3 production. This suggests either GGT4 has a high capacity, which allows endogenous expression levels to cope with enhanced fluxes, or that the metabolic recycling of glutathione-conjugates following sequestration is not vital for xenobiotic tolerance. The importance of glutathione-conjugate recycling may not have been detected in this study as plant tissue was grown and exposed to TNT in nutritionally complete media. Quantifying GGT4 response to TNT and enhanced Conjugate 3 production, either at the protein or transcript level, within tissue grown in a nutrient-restricted system would confirm whether nutrient availability underpins the response of GGT4 shown in this study. The GGT4 response also suggests the peptidase responsible for hydrolysing S-DNT-CysGly is unlikely to be induced in response to either TNT or enhanced Conjugate 3 production. Currently only the leucine aminopeptidase (LAP) protein family within plants has been associated with cysteinylglycine dipeptidase activity [124,325]. The two induced peptidases identified by proteomic analysis, AT5G19110 and SBT3.3, are not members of this family. The Arabidopsis genome contains three LAPs, with LAP1 and LAP3 having confirmed cysteinylglycine peptidase activity *in vitro* [124]. Interestingly, LAP2 is a component of the tonoplast [326] and respective knockout lines have significant reductions in the free glycine content of aerial tissue [327]. Based on these results, and its constitutive expression, LAP2 is a putative candidate to investigate in the metabolism of xenobiotic

cysteinylglycine conjugates (Figure 6.1, Metabolic Step 1). The assessment of S-DNT-CysGly and S-DNT-Cys content within the root tissue of *Dm*GST-*lap2* plant lines could provide evidence for this function *in planta*.

## 6.2 Cytosolic metabolism of Conjugate 3 to cysteinyl conjugate derivatives

Investigations using *Dm*GST-*ggt1ggt4* lines confirmed the presence of a GGT-independent pathway for Conjugate 3 metabolism. A pathway for glutathione-conjugate metabolism within the cytosol is initiated through the activity of PCS1 [227], however an enzyme responsible for hydrolysis of S-DNT-CysGlu remains unidentified (Figure 6.1, Metabolic Step 2). As PCS1 abundance was not altered after TNT exposure, or enhanced Conjugate 3 production, it is unlikely the enzyme responsible for S-DNT-CysGlu hydrolysis is within the induced protein population. As mentioned in previous chapters, the cytosolic GGP1 and GGP3 have been shown to release glutamate from glutathione-conjugates during glucosinolate biosynthesis [126]. Alternative cytosolic enzymes that may hydrolyse S-DNT-CysGlu are the GGCT family due to their function in glutamate recycling from glutathione and $\gamma$-glutamyl-peptides [124,328]. As GGPs and GGCTs are currently the only identified plant proteins, alongside GGTs, capable of hydrolysing the $\gamma$-glutamyl bond, it would be prudent to investigate the *in vitro* activity of these proteins towards $\gamma$-glutamatylcysteine conjugates. Though *in vitro* studies have shown GGPs and GGCTs to have low activity towards $\gamma$-glutamatylcysteine [124,125], this may be a metabolic adaption to stop recycling mechanisms from degrading the non-conjugated metabolite prior to its incorporation into glutathione. However, it is important to note, that due to the co-elution of S-DNT-CysGlu with the more abundant HADNT-Glc conjugates, the metabolites subcellular localisation could not be verified; therefore, sequestration of S-DNT-CysGlu is still a possibility. Optimisation of the chromatography gradient used in plant extract analysis may allow a distinct S-DNT-CysGlu peak to be obtained, enabling the metabolites cytosolic localisation to be verified.

## 6.3 Vacuolar export of cysteinyl conjugate-derivatives of Conjugate 3

The significant association of S-DNT-Cys with the vacuole supports the model that the vast majority of cysteinyl-conjugate production, from respective glutathione conjugates, occurs within this compartment as previously indicated [114,115]. However, the further metabolism of S-DNT-Cys suggests a requirement of cytosolic import by a vacuolar exporter (Figure 6.1, Metabolic Step 3). No induced protein with this activity, hypothesised or confirmed, was identified by proteomic analysis. A finding that further supports prior hypotheses relating to the capacity/importance of glutathione-conjugate

recycling within Arabidopsis vacuoles. The chemical properties of S-DNT-Cys, such as pKa and pKb, have not been identified due to an absence of purified compound. However, as cysteine is a neutral amino acid and the nitro-groups within DNT provide a high electronegativity, it can be assumed that S-DNT-Cys is a neutral/basic molecule. Protein families, previously mentioned, that could transport such a compound are the AAAP and APC superfamilies. The AVT3 subfamily of AAAP transporters are localised to the tonoplast and have been shown to function in neutral amino acid export from the vacuole [329]. The CAT subfamily of APC transporters contains CAT2 and CAT4 which are both localised to the tonoplast of Arabidopsis root cells, though only CAT2 has shown vacuolar export activity to both neutral and basic amino acids [261]. Preliminary data into the activity of these transporters, in respect to S-DNT-Cys vacuolar export, could be obtained through the reduction/loss of metabolite production within respective knockout lines transformed with *Dm*GST.

## 6.4 Further metabolism of cysteinyl conjugate-derivatives of Conjugate 3

The low-association of S-DNT-Cys with the cytosolic compartment and the inability to detect S-DNT indicate that cytosolic S-DNT-Cys is rapidly metabolised to S-DNT-Glc. Proteomic analysis was unable to identify protein candidates involved in the formation of S-DNT-Glc (Figure 6.1, Metabolic Steps 4 and 5), this suggests that the enzymes responsible are constitutively expressed. A potential source of these enzymes is the constitutively active glucosinolate biosynthesis pathway. Within glucosinolate biosynthesis thiohydroximates are produced from cysteinylglycine- or cysteine-conjugate precursors through the activity of SUR1 [330]. Currently, SUR1 is the only identified cysteine conjugate $\beta$-lyase within Arabidopsis, the near-complete loss of glucosinolate production in *sur1* knockout lines confirms limited redundancy in the activity of the enzyme [330]. Whilst prior work has shown an inducible cysteine conjugate $\beta$-lyase activity in response to xenobiotics, this activity was SAM-dependent resulting in the production of a methylthiol-conjugate [224]. As no such metabolite was identified in metabolomic analysis of either WT or *Dm*GST plant lines, it is unlikely this inducible enzyme is involved in Conjugate 3 metabolism. Once generated S-DNT is rapidly glucosylated to an S-glucoside, a biochemical step identical to what occurs to thiohydroximates generated by SUR1 activity. Within glucosinolate biosynthesis this step is catalysed by the glucosyltransferase UGT74B1 [331]. As UGT74B1 has high expression within the roots and has been shown to conjugate a variety of thiophenols *in vitro* [287], it is a putative candidate in the formation of S-DNT-Glc. Whilst the function of SUR1 is largely non-redundant, allowing its role in S-DNT-Cys metabolism to be investigated *in planta* via *Dm*GST expression

within knockout lines, the activity of UGT74B1 is partially redundant [331] and will require *in vitro* analysis to confirm a possibility of this enzymes function in S-DNT-Glc production.

The cytosolic metabolism of S-DNT-Cys is also indicated to produce O-malonyl and N-malonyl conjugates, though proteomics only identified putative enzyme candidates involved in production of the former. Proteomic analysis identified the O-malonyltransferase PMAT1 as a *Dm*GST-dependent TNT-responsive protein, this alongside the broad substrate specificity of the enzyme [251,252,314] make it a strong candidate for involvement in S-DNT-(Mal)Glc production. In respect to the formation of S-DNT-(Mal)Cys (Figure 6.1, Metabolic Step 6), an enzymatic candidate was not identified within the induced population. Currently, a genetic locus encoding a functional N-malonyltransferase remains unidentified within Arabidopsis. This is despite N-malonyltransferase activity being induced within the organism in response to xenobiotic exposure [224]. As the only induced malonyltransferase identified by proteomics, assessing the substrate specificity of PMAT1 *in vitro* would identify whether it can perform N-malonylation alongside O-malonylation. Similar studies investigating the UGT superfamily have shown numerous members to catalyse the formation of various glycosidic bonds i.e., S-, N-, O- and C-linked [287]. Additionally, investigating the degree of N-malonyltransferase activity induction by TNT, within WT and *Dm*GST plant lines, would provide an indication as to whether the respective enzyme is found within the proteomics dataset presented in this body of work. This is important as currently xenobiotic induction of N-malonyltransferase activity has only been shown in cell-culture; thus, there is potential that within whole tissue the N-malonyltransferase of interest is constitutively expressed. This may explain the difficulty in identifying plant N-malonyltransferases despite N-malonyl conjugates being identified for a variety of xenobiotics [224,225,232].

## 6.5 Compartmentalisation of Conjugate 3 metabolites

The Conjugate 3 metabolites derived from the hypothesised cytosolic metabolism of S-DNT-Cys were all shown to be sequestered from the cytosol. As *in vitro* studies have shown transport of glucosyl- and malonyl-conjugates across the tonoplast [112,173,174,218,332], vacuolar import is a likely fate for S-DNT-Cys metabolites (Figure 6.1, Metabolic Step 7). This transport can either be directly energised through the ATP-hydrolysing activity of an ABC-transporter or be passively energised via a proton gradient antiporter [333]. Two proteins representative of each transportation mechanism were identified by proteomic analysis as putative candidates involved in vacuolar import of TNT-metabolites. In respect to directly-energised transport, ABCC2 may function in transporting more than just Conjugate

3. Alongside transportation of glutathione conjugates, ABCC2 has shown the capability to facilitate the movement of glucosyl- and acylglucosyl-conjugates *in vitro* [112,334,335]. Interestingly, ABCC2 has the capability to simultaneously transport glutathione and a glucosyl conjugate, with the rate of co-transport being significantly greater than transport of the glucosyl-conjugate alone [334]. This boost in ABCC2-facilitated transport has also been seen in the co-transport of a dinitrophenol-glutathione conjugate with either malonyl or glucoronide conjugates [109,313]. This suggests an exciting possibility that ABCC2 could co-transport Conjugate 3 with either glucosyl or malonyl-conjugates derivatives of TNT during the detoxification process. Preliminary investigations could assess the activity of ABCC2 in the co-transport of HADNT-Glc and Conjugate 3 using methods identical to those described in Behrens *et al*., (2019)[334], which quantified the removal of conjugates from media by vacuolar membrane-enriched vesicles. Enzymes capable of generating these conjugates have been identified and successfully expressed *in vitro* [104,236], thus overcoming the issue of substrate commercial availability. The protein candidate in respect to proton-gradient energised transport is the tonoplast-localised isoform of ZIFL1 [295]. The $H^+$-antiporter activity of this protein has been indicated by enhanced acidification of the vacuole in *zifl1* knockout lines [295]. In respect to transport of S-DNT-Cys metabolites, ZIFL1 is hypothesised to function in the transport of malonyl- and glucosyl-conjugates for multiple reasons. Firstly, the transgenic expression of this transporter enhanced tolerance within yeast to 2,4-D, a xenobiotic indicated to undergo glucosylation [295,311,336]. Secondly, the transporter has been shown to have a strong positive correlation in co-expression with UGT73B proteins and PMAT1 during chemical and pathogen-induced stress responses [288,312]. As UGTs and PMAT1 are thought to work in sequence to generate malonylglucosides, ZIFL1 may function in sequestering these conjugates. A function of ZIFL1 in malate transport has also been indicated, with expression of the protein in yeast enhancing malate tolerance [295]; as N-malonyl conjugates have been shown to competitively inhibit malate uptake by plant vacuoles [337], these findings suggest a possible ability of ZIFL1 to transport N-malonyl derivatives of TNT. As the ability of ZIFL1 to transport conjugated-compounds has not been investigated, confirming this *in vitro* should be the aim of preliminary work alongside the identification of detectable TNT-induced phenotypes within respective knockout lines.

## 6.6 Insights into the reduction-initiated glucosylation pathway of TNT-metabolism

Although the focus of this research was the characterisation of Conjugate 3 metabolism, it has offered new insights into the reduction-initiated glucosylation pathway of TNT detoxification. Firstly, spatial

proteomics confirmed the co-localisation of OPR1 and OPR2 to the cytosolic Cluster 3. This finding, alongside *in vitro* evidence of OPR2 activity towards TNT [99], supports a hypothesis of functional redundancy between these proteins in reducing TNT, despite proteomic analysis confirming only OPR1 to be induced. The metabolic analysis of TNT-dosed root tissues also indicated that O-malonylation of HADNT and ADNT glucosides occurs. It is important to note that the evidence for this metabolic reaction is preliminary at this point due to the absence of a no-TNT control within the LC-MS/MS analysis. However, there are multiple pieces of evidence within this research that suggests this identification to be valid. Firstly, HPLC analysis of no-TNT controls did not detect any peaks at the retention times at which these conjugates eluted. Secondly, PMAT1 is upregulated to a similar degree in both the endogenous and *Dm*GST-enhanced proteomic responses to TNT, therefore indicating a need for this enzyme in the absence of S-DNT-Glc. Finally, MS/MS spectra of the putative metabolites revealed fragmentation patterns indicative of HADNT and ADNT conjugates, these included an ADNT fragment of *m/z* 196 and HADNT fragments of *m/z* 212 and 254 [104]. The distinction between N-linked and C-linked glucosyl conjugates, and their malonylated products, was not possible as MS/MS spectra indicated co-elution of the isomers. Optimisation of chromatography gradient may improve isomer separation, though this was beyond the scope of the research.

## 6.7 Putative functions of malonylation in xenobiotic metabolism

The commonality of malonylation within TNT metabolic pathways suggests this modification may have a conserved role within detoxification, as indicated by the presence of xenobiotic malonyl-conjugates within both monocot and eudicot species [87,174,224–226,233,253]. Aside from preventing the reactivation of glucosides by promiscuous $\beta$-glucosidases, the role of malonylation in xenobiotic detoxification remains obscure. However, research into endogenous plant compounds suggests potential functions. One such function being that malonylation enables/enhances vacuolar import. This putative function was suggested by studies which identified the requirement of malonylation for vacuolar uptake of 1-aminocyclopropane-1-carboxylic acid and flavonoid glucosides [169,332]. This function is further supported by the *in vitro* characterisation of a vacuolar MATE transporter, which showed greater specificity and activity to flavonoid glucosides following O-malonylation [174]. Evidence for this function has also been provided *in planta*, with glucosyl-conjugates accumulating to a greater degree in the growth medium of Arabidopsis seedlings unable to perform malonylation due to the elimination of PMAT1 expression [251,314]. Whilst this work confirmed the sequestration of TNT malonyl-conjugates, it also confirmed the sequestration of unmodified glucoside derivatives of TNT, thus

indicating malonylation is not essential for compartmentalisation. This hypothesis is supported by studies confirming the transport of glucosides across the tonoplast, as well as their detection within isolated vacuoles [112,113,173,218,334]. However, these findings could also indicate that malonyl-conjugates undergo further metabolism following sequestration. Post-sequestration metabolism of malonyl-conjugates has been identified in isoflavonoids metabolism. Isoflavonoids are a legume specific class of flavonoid, which are found predominantly as inactive malonylglucosides within the plant but are converted to aglycon derivatives when their activity is required [338,339]. Researchers have identified a putative vacuolar isoflavone malonylesterase within *Cicer arietinum* L. that releases glucoside-derivatives from respective malonylglucosides [254,340]. Interestingly, proteomic analysis identified that the GDSL-like esterase GLL23 was induced in response to enhanced Conjugate 3 production. GDSL esterases are hydrolytic enzymes identified by a N-terminal GDSL motif, GDSxxDxG, these proteins have broad substrate specificity with some identified as acylesterases [341]. Previous studies identified GLL23 as a constituent of both the tonoplast and apoplast [326,342,343], these findings are supported by results from the spatial proteomics performed in this research, with GLL23 allocated to the vacuolar/apoplastic Cluster 1 (See Chapter 5 Section 4.1 and Table 4.2.3.1) Currently the substrate specificity of GLL23 has not been investigated and therefore *in vitro* analysis against commercially available malonyl conjugates could provide useful preliminary data relating to its function in Conjugate 3 metabolism. The activity of a vacuolar/apoplastic malonylesterase offers a route for glucoside sequestration via a malonylglucoside intermediate (Figure 6.1, Metabolic Step 8); therefore, malonylation may act as a reversible-modification that enhances conjugate compartmentalisation by increasing the variety of transporters involved in sequestration. It is important to note however, that due to the limitations of BNAF compartmental resolution there is a possibility that glucosides and malonylglucoside products of TNT-detoxification are localised separately between the apoplast and vacuole. Therefore, identifying the exact subcellular localisation of metabolites will aid in the further characterisation of malonylations function within detoxification.

## 6.8 Enhancing the subcellular resolution of Conjugate 3 metabolite localisation

As well as aiding in the further characterisation of metabolic pathways, improving the compartmental resolution in respect to TNT-metabolite subcellular localisation may identify the state of the xenobiotic prior to lignocellulosic incorporation (Figure 6.1, Metabolic Step 9). Proteomic analysis confirmed that the currently optimised BNAF technique is unable to distinguish between the apoplastic and vacuolar compartments. Whilst there is potential that further optimisation of the BNAF gradient can obtain

greater distinction between these compartments, alternative approaches may be required. One such approach is BNAF analysis of both protoplasts and whole root tissue following TNT exposure. As protoplasts do not contain an apoplast, they could be used in a subtractive manner to confirm which metabolites are localised to the vacuole. Another approach is the combination of MALDI-MSI and BNAF. Currently, MALDI resolution is commonly limited by sampling dot size, with even the combination of oversampling techniques and secondary ionisation obtaining a resolution greater than 5 µm [344]. Whilst using MALDI-MSI alone at this resolution would not provide a clear distinction between apoplast and vacuole within Arabidopsis root tissue, combining these results with the findings from BNAF potentially could. The detection of signal around the periphery of root cells by high-resolution MALDI-MSI, that is absent within the center of the cell, would be indicative of apoplastic localisation; results obtained with BNAF would confirm that the peripheral signal is not due to cytosolic localisation of metabolites. Very recent advancements in MALDI-MSI may make this approach obsolete with reductions in sampling dot size, achieved through the use of microlensed fibres, obtaining submicron level resolution [345,346]. However, due to requiring modifications to the mass spectrometry equipment, wide-spread use of this approach may be limited by manufacturer incorporation. A currently existing IMS approach capable of submicron resolution of plant material is nanoscale secondary-ion mass spectrometry (NanoSIMS). This technique uses a beam of high-energy ions to ablate secondary-ion fragments from a biological section. Unlike MALDI-IMS, NanoSIMS can only identify the spatial distribution of individual isotopes, thus isotopic labelling is required for the use of NanoSIMS in characterising metabolic fate *in planta*. The use of NanoSIMS to investigate xenobioitic metabolism *in planta* has been demonstrated for the pollutant bromotoluene within common ivy (*Hedera helix*) [347]. The use of NanoSIMS could identify whether the sulfur atom retained within all putative Conjugate 3 metabolites is reclaimed by the plant. The upregulation of glucosinolate metabolism proteins, such as BGLU30, suggest this is not the case and free sulfur levels are depleted during *Dm*GST-enhanced detoxification. The high resolution of NanoSIMS, alongside its ability to simultaneously detect multiple isotopes, could identify if sulfur, provided in the form of $^{35}$S-labelled glutathione, co-localises to the cell wall with $^{13}$C/$^{15}$N-labelled TNT following exposure. The identification of this fate would provide greater understanding as to whether sulfur availability may limit Conjugate 3 production in plant lines used for phytoremediation.

## 6.9 Application of research to phytoremediation

Though Arabidopsis provides an excellent platform in which to elucidate biological processes and molecular mechanisms relating to detoxification, it is in no way suitable for in-field phytoremediation of TNT. Plant traits that are desirable for phytoremediation of contaminated land are fast growth, dense phreatophytic root systems and low maintenance requirements [90]. These traits allow for effective remediation of polluted land at a low-economic cost. Species that fit these descriptions include poplar and perennial grasses such as switchgrass (*Panicum virgatum*), creeping bentgrass (*Agrostis stolonifera*) and vetiver grass (*Chrysopogon zizanioides*), all of which have been investigated in respect to TNT tolerance and uptake [14,80,348,349]. The sequestration of TNT within the root system has been confirmed for both poplar (*Populus deltoides* x *nigra*) and switchgrass [78,348], therefore the induced proteins identified by the proteomic analysis performed in this work, may provide a resource to identify functional homologs within these species. This has already been demonstrated in poplar within which homologs of *GSTU24* and *GSTU25* were identified and shown to be upregulated in response to TNT, with subsequent *in vitro* assays confirming activity towards the xenobiotic [350]. One of these homologs, *Pt*GSTU16, contained several key residues that have been linked to the ability of GSTU25 to generate Conjugate 3 [107,351]. These findings suggest that the ability to generate Conjugate 3 may be found across a wide variety of plants. Despite this however, the detection of TNT glutathione-conjugates has only been achieved within Arabidopsis. This may reflect the rapid turnover of glutathione-conjugates within plants, a hypothesis supported by the requirement of enhanced glutathionylation to detect conjugates within Arabidopsis plant extract [106]. Therefore, it would be useful to express the *Dm*GST enzyme within a species such as switchgrass and perform metabolic analysis following TNT exposure, this would confirm whether the downstream metabolic pathways described in this body of work are found within other plant species. Prior studies in which switchgrass has been transformed with bacterial genes provide a template as to how this could be achieved [80,352].

Alongside confirming the presence of metabolic pathways within species relevant to phytoremediation, genetic methods may also be required to allow these species to cope with the levels of TNT found at military training ranges. Studies have shown TNT contamination of soil to be heterogenous with the presence of hot spots in which the concentrations can reach over 1000 mg/kg [353]. These concentrations are far higher than endogenous detoxification mechanisms within plants can tolerate [14]. Whilst classical breeding approaches, such as mutagenesis screens, can generate plants with improved traits relating to xenobiotic detoxification and tolerance, the use of genome-editing

techniques provides a more targeted and powerful approach. The introduction of transgenes is one such way genome-editing techniques can be used to generate plants with superior ability to remediate contaminated land. Transgenic transformation of plants can introduce novel activities relating to xenobiotic metabolism, as demonstrated in the case of the XplAB system from *Rhodococcus rhodochrous* 11Y providing RDX-degrading capabilities to switchgrass [80,81]. This work has demonstrated an alternative transgenic approach in which existing detoxification steps within plants are significantly enhanced. This approach has also been demonstrated within switchgrass, with the expression of a bacterial nitroreductase increasing plant uptake and tolerance to DNT [352]. Alongside introducing and enhancing detoxification steps, transgenics could also be used to redirect primary metabolism within plants to support detoxification reactions. This has been demonstrated within poplar, with transgenics lines expressing a bacterial $\gamma$-ECS showing enhanced tolerance to xenobiotic chloroacetanilide herbicides [354]. As proteomic analysis suggested sulfur availability may be limiting detoxification, in the form of cysteine and not glutathione, genetic techniques may offer a way in which to address this. Growing proficiency in synthetic approaches may soon allow the specific induction of transgene expression by a particular stressor, thus mitigating any metabolic fatigue or disadvantage resulting from constitutive transgene expression [355]. Whilst there are currently federal regulations that restrict the use of genetically engineered plants in-the-field, the use of genetic-use restriction technologies [356] and changes in public perception of genetic editing [357] may soon change that, at least in respect to non-food applications.

## 6.10 Final conclusions

In conclusion, the research presented in this body of work has further enhanced the understanding of TNT metabolism with Arabidopsis, particularly in respect to the nitro-substituted glutathionylation product Conjugate 3. It has also optimised and demonstrated a BNAF protocol that can provide an integrated understanding of root metabolism within Arabidopsis. The proteomic datasets provided alongside this research offer resources to aid in the generation of future hypothesises in respect to TNT-metabolism and xenobiotic-induced stress more broadly. This is demonstrated by the presented metabolic model of TNT-metabolism within which multiple enzymatic candidates for future research have been identified based on their proteomic response, spatial localisation and previously described activity. The combination of *Dm*GST-expression within respective knockout lines, alongside BNAF, provides a platform in which hypothesised functions of enzymes, within Conjugate 3 metabolism, can be investigated within Arabidopsis and other plant species. The further characterisation of TNT metabolism

*in planta* will elucidate the molecular processes that limit plant detoxification of the xenobiotic, and thus allow for the targeted improvement of phytoremediation-relevant species for the treatment of contaminated land.

# References

[1] D. Kumar, A.J. Elias, The explosive chemistry of nitrogen, Resonance. 24 (2019) 1253–1271.

[2] F. Zapata, C. García-Ruiz, Chemical classification of explosives, Crit. Rev. Anal. Chem. 51 (2021) 656–673.

[3] J.J. Sabatini, K.D. Oyler, Recent advances in the synthesis of high explosive materials, Crystals. 6 (2015) 5.

[4] H. Sprengel, XXXII.—On a new class of explosives which are non-explosive during their manufacture, storage, and transport, J. Chem. Soc. 26 (1873) 796–808.

[5] P.O.K. Krehl, History of shock waves, explosions and impact: A chronological and biographical reference, Springer Science & Business Media, 2008.

[6] Z. Snellinx, A. Nepovím, S. Taghavi, J. Vangronsveld, T. Vanek, D. van der Lelie, Biological remediation of explosives and related nitroaromatic compounds, Environ. Sci. Pollut. Res. Int. 9 (2002) 48–61.

[7] P.J. Davies, A. Provatas, DEFENCE SCIENCE AND TECHNOLOGY ORGANISATION EDINBURGH (AUSTRALIA) WEAPONS SYSTEMS DIV, Characterisation of 2,4-dinitroanisole: An ingredient for use in low sensitivity melt cast formulations, DEFENCE SCIENCE AND TECHNOLOGY ORGANISATION EDINBURGH (AUSTRALIA) WEAPONS SYSTEMS DIV, 2006.

[8] Technavio, Trinitrotoluene (TNT) Market by Application, Product and Geography - Forecast and Analysis 2023-2027. <https://www.technavio.com/report/trinitrotoluene-market-analysis> 2023, (accessed 22.09.2023)

[9] T.M. Mallon, P.G. Matos, W.S.M. Mpas, R.A. Mirza, D.T. Bodeau, EXPLOSIVES AND PROPELLANTS, (n.d.). <https://medcoeckapwstorprd01.blob.core.usgovcloudapi.net/pfw-images/dbimages/OH%20ch%2028.pdf>, (accessed 24.09.2023)

[10] J.W. Bennett, Prospects for fungal bioremediation of TNT munition waste, Int. Biodeterior. Biodegradation. 34 (1994) 21–34.

[11] Y. Li, Q.G. Jiang, S.Q. Yao, W. Liu, G.J. Tian, J.W. Cui, Effects of exposure to trinitrotoluene on male reproduction, Biomed. Environ. Sci. 6 (1993) 154–160.

[12] Agency for Toxic Substances and Disease Registry, Complete toxicological profile: 2,4,6-trinitrotoluene (TNT). <https://www.atsdr.cdc.gov/ToxProfiles/tp81.pdf>, 1995 (accessed 04.03.2019)

[13] E.P.H. Best, H.E. Tatem, K.N. Geter, M.L. Wells, B.K. Lane, Effects, uptake, and fate of 2,4,6-trinitrotoluene aged in soil in plants and worms, Environ. Toxicol. Chem. 27 (2008) 2539–2547.

[14] G. Krishnan, G.L. Horst, P.J. Shea, Differential tolerance of cool- and W arm-season grasses to TNT -contaminated soil, Int. J. Phytoremediation. 2 (2000) 369–382.

[15] R.G. Kuperman, R.T. Checkai, M. Simini, C.T. Phillips, J.E. Kolakowski, C.W. Kurnas, Weathering and aging of 2,4,6-trinitrotoluene in soil increases toxicity to potworm enchytraeus crypticus, Environ. Toxicol. Chem. 24 (2005) 2509–2518.

[16] E.R. Travis, N.C. Bruce, S.J. Rosser, Short term exposure to elevated trinitrotoluene concentrations induced structural and functional changes in the soil bacterial community, Environ. Pollut. 153 (2008) 432–439.

[17] H.C. Bailey, R.J. Spanggord, H.S. Javitz, D.H.W. Liu, others, Toxicity of TNT wastewaters to aquatic organisms. Volume 3. Chronic toxicity of LAP wastewater and 2, 4, 6-trinitrotoluene, (1985).

[18] D.T. Burton, S.D. Turley, G.T. Peters, MARYLAND UNIV COLLEGE PARK AGRICULTURAL EXPERIMENT STATION, Toxicity of nitroguanidine, nitroglycerin, hexahydro-1,3,5-trinitro-1,3,5-triazine (RDX), and 2,4,6-trinitrotoluene (TNT) to selected freshwater aquatic organisms, MARYLAND UNIV COLLEGE PARK AGRICULTURAL EXPERIMENT STATION, 1993.

[19] W.D. Won, L.H. DiSalvo, J. Ng, Toxicity and mutagenicity of 2,4,-6-trinitrotoluene and its microbial metabolites, Appl. Environ. Microbiol. 31 (1976) 576–580.

[20] R.W. Millar, A.W. Arber, R.M. Endsor, J. Hamid, M.E. Colclough, Clean manufacture of 2,4,6-trinitrotoluene (TNT) via improved regioselectivity in the nitration of toluene, J. Energ. Mater. 29 (2011) 88–114.

[21] M.A. Major, J.C. Amos, A.B. Research, D.L.F.D. Md, Incineration of explosive contaminated soil as a means of site remediation, US Army Medical Research; Development Command, Fort Detrick, 1992.

[22] R. Martel, T.J. Robertson, M.Q. Doan, S. Thiboutot, G. Ampleman, A. Provatas, T. Jenkins, 2,4,6-trinitrotoluene in soil and groundwater under a waste lagoon at the former explosives factory maribyrnong (EFM), victoria, australia, Environ. Geol. 53 (2008) 1249–1259.

[23] National Academies of Sciences, Engineering, and Medicine, Division on Engineering and Physical Sciences, Board on Army Science and Technology, Committee on Alternatives for the Demilitarization of Conventional Munitions, Alternatives for the demilitarization of conventional munitions, National Academies Press, 2019.

[24] T.F. Jenkins, A.D. Hewitt, C.L. Grant, S. Thiboutot, G. Ampleman, M.E. Walsh, T.A. Ranney, C.A. Ramsey, A.J. Palazzo, J.C. Pennington, Identity and distribution of residues of energetic compounds at army live-fire training ranges, Chemosphere. 63 (2006) 1280–1290.

[25] United States General Accounting Office. Department of defense operational ranges, more reliable cleanup cost estimates and a proactive approach to identifying contamination are needed (report to congressional requesters). <https://www.gao.gov/assets/gao-04-601.pdf>, 2004 (accessed 30.10.2019)

[26] Strategic Environmental Research and Development Program, Elimination of redwater from TNT manufacture, (. <https://serdp-estcp.org/projects/details/453fe6a6-19f6-4792-9da3-8c01dc868f15>, 2010). (accessed 25.09.2023)

[27] United States Government Accountability Office, Defense infrastructure: Risk assessment needed to identify if foreign encroachment threatens test and training ranges. <https://www.gao.gov/products/gao-15-149>, 2014 (accessed 25.09.2023)

[28] P.-G. Rieger, H.-J. Knackmuss, Basic knowledge and perspectives on biodegradation of 2,4,6-trinitrotoluene and related nitroaromatic compounds in contaminated soil, in: J.C. Spain (Ed.), Biodegradation of Nitroaromatic Compounds, Springer US, Boston, MA, 1995: pp. 1–18.

[29] K.W. Weissmahr, S.B. Haderlein, R.P. Schwarzenbach, R. Hany, R. Nüesch, In situ spectroscopic investigations of adsorption mechanisms of nitroaromatic compounds at clay minerals, Environ. Sci. Technol. 31 (1997) 240–247.

[30] T.F. Jenkins, C.L. Grant, G.S. Brar, others, Sampling error associated with collection and analysis of soil samples at TNT-contaminated sites, Field Anal. Chem. Technol. (1997).

[31] S.B. Haderlein, K.W. Weissmahr, others, Specific adsorption of nitroaromatic explosives and pesticides to clay minerals, Sci. Technol. China. (1996).

[32] S. Im, J.-W. Jung, E.H. Jho, K. Nam, Effect of soil conditions on natural attenuation of 2,4,6-trinitrotoluene (TNT) by UV photolysis in soils at an active firing range in south korea, J. Soils Sediments. 15 (2015) 1455–1462.

[33] A. Gerth, A. Hebner, H. Thomas, Natural remediation of TNT-contaminated water and soil, Acta Biotechnol. 23 (2003) 143–150.

[34] G. Bordeleau, R. Martel, G. Ampleman, S. Thiboutot, Environmental impacts of training activities at an air weapons range, J. Environ. Qual. 37 (2008) 308–317.

[35] K.A. Thorn, 13C and 15N NMR identification of product compound classes from aqueous and solid phase photodegradation of 2,4,6-trinitrotoluene, PLoS One. 14 (2019) e0224112.

[36] J.C. Pennington, K.A. Thorn, L. Cox, D.K. MacMillan, others, Photochemical degradation of composition B and its components, (2007).

[37] T.F. Jenkins, J.C. Pennington, T.A. Ranney, T.E. Berry, P.H. Miyares, M.E. Walsh, A.D.(alan.D. Hewitt, N.M. Perron, L.V.(louise.V.). Parker, C.A. Hayes, E.G. Wahlgren, Characterization of explosives contamination at military firing ranges, (2001).

[38] J. Klausen, S.P. Troeber, S.B. Haderlein, R.P. Schwarzenbach, Reduction of substituted nitrobenzenes by Fe(II) in aqueous mineral suspensions, Environ. Sci. Technol. 29 (1995) 2396–2404.

[39] T.B. Hofstetter, C.G. Heijman, S.B. Haderlein, C. Holliger, R.P. Schwarzenbach, Complete reduction of TNT and other (poly)nitroaromatic compounds under Iron-Reducing subsurface conditions, Environ. Sci. Technol. 33 (1999) 1479–1487.

[40] T.B. Hofstetter, A. Neumann, R.P. Schwarzenbach, Reduction of nitroaromatic compounds by Fe(II) species associated with iron-rich smectites, Environ. Sci. Technol. 40 (2006) 235–242.

[41] M.Y. Serrano-González, R. Chandra, C. Castillo-Zacarias, F. Robledo-Padilla, M. de J. Rostro-Alanis, R. Parra-Saldivar, Biotransformation and degradation of 2,4,6-trinitrotoluene by microbial metabolism and their interaction, Defence Technology. 14 (2018) 151–164.

[42] C.K. Chua, M. Pumera, L. Rulíšek, Reduction pathways of 2,4,6-trinitrotoluene: An electrochemical and theoretical study, J. Phys. Chem. C. 116 (2012) 4243–4251.

[43] A. Esteve-Núñez, A. Caballero, J.L. Ramos, Biological degradation of 2,4,6-trinitrotoluene, Microbiol. Mol. Biol. Rev. 65 (2001) 335–52, table of contents.

[44] M.I. Khan, J. Lee, J. Park, A toxicological review on potential microbial degradation intermediates of 2,4,6-trinitrotoluene, and its implications in bioremediation, KSCE Journal of Civil Engineering. 17 (2013) 1223–1231.

[45] R.-M. Wittich, J.L. Ramos, P. van Dillewijn, Microorganisms and explosives: Mechanisms of nitrogen release from TNT for use as an n-source for growth, Environ. Sci. Technol. 43 (2009) 2773–2776.

[46] R.E. Williams, D.A. Rathbone, N.S. Scrutton, N.C. Bruce, Biotransformation of explosives by the old yellow enzyme family of flavoproteins, Appl. Environ. Microbiol. 70 (2004) 3566–3574.

[47] C.E. French, S. Nicklin, N.C. Bruce, Aerobic degradation of 2,4,6-trinitrotoluene by enterobacter cloacae PB2 and by pentaerythritol tetranitrate reductase, Appl. Environ. Microbiol. 64 (1998) 2864–2868.

[48] S.F. Nishino, G.C. Paoli, J.C. Spain, Aerobic degradation of dinitrotoluenes and pathway for bacterial degradation of 2,6-dinitrotoluene, Appl. Environ. Microbiol. 66 (2000) 2139–2147.

[49] S.B. Funk, D.J. Roberts, D.L. Crawford, R.L. Crawford, Initial-phase optimization for bioremediation of munition compound-contaminated soils, Appl. Environ. Microbiol. 59 (1993) 2171–2177.

[50] C.D. Silva, L. Beristain-Montiel, F. de Maria Cuervo-López, A.-C. Texier, P-cresol mineralization and bacterial population dynamics in a nitrifying sequential batch reactor, J. Environ. Sci. 26 (2014) 1885–1893.

[51] J. Hawari, A. Halasz, L. Paquet, E. Zhou, B. Spencer, G. Ampleman, S. Thiboutot, Characterization of metabolites in the biotransformation of 2,4,6-trinitrotoluene with anaerobic sludge: Role of triaminotoluene, Appl. Environ. Microbiol. 64 (1998) 2200–2206.

[52] F.W. Parrish, Fungal transformation of 2,4-dinitrotoluene and 2,4,6-trinitrotoluene, Appl. Environ. Microbiol. 34 (1977) 232–233.

[53] M.W. Perkins, S. De, L. Frederick, S.K. Dutta, Ligninolytic and nonligninolytic mineralization of trinitrotoluene by several white rot basidiomycetes, Bioremediat. J. 9 (2005) 77–85.

[54] J. Michels, G. Gottschalk, Inhibition of the lignin peroxidase of phanerochaete chrysosporium by hydroxylamino-dinitrotoluene, an early intermediate in the degradation of 2,4,6-trinitrotoluene, Appl. Environ. Microbiol. 60 (1994) 187–194.

[55] L. Kutateladze, N. Zakariashvili, I. Khokhashvili, M. Jobava, T. Alexidze, T. Urushadze, E. Kvesitadze, Fungal elimination of 2,4,6-trinitrotoluene (TNT) from the soils, The EuroBiotech Journal. 2 (2018) 39–46.

[56] J.C. Pennington, C.A. Hayes, K.F. Myers, M. Ochman, D. Gunnison, D.R. Felt, E.F. McCormick, Fate of 2,4,6-trinitrotoluene in a simulated compost system, Chemosphere. 30 (1995) 429–438.

[57] D.A. Newcombe, R.L. Crawford, Transformation and fate of 2,4,6-trinitrotoluene (TNT) in anaerobic bioslurry reactors under various aeration schemes: Implications for the decontamination of soils, Biodegradation. 18 (2007) 741–754.

[58] J.C. Pennington, M.E. Honeycutt, A.S. Jarvis, V.A. McFarland, D. Gunnison, ARMY ENGINEER WATERWAYS EXPERIMENT STATION VICKSBURG MS, Explosives conjugation products in remediation matrices: Interim report, ARMY ENGINEER WATERWAYS EXPERIMENT STATION VICKSBURG MS, 1997.

[59] K.A. Thorn, K.R. Kennedy, 15N NMR investigation of the covalent binding of reduced TNT amines to soil humic acid, model compounds, and lignocellulose, Environ. Sci. Technol. 36 (2002) 3787–3796.

[60] G.S. Nyanhongo, A. Erlacher, M. Schroeder, G.M. Gübitz, Enzymatic immobilization of 2,4,6-trinitrotoluene (TNT) biodegradation products onto model humic substances, Enzyme Microb. Technol. 39 (2006) 1197–1204.

[61] A. HaÏdour, J.L. Ramos, Identification of products resulting from the biological reduction of 2,4,6-trinitrotoluene, 2,4-dinitrotoluene, and 2,6-dinitrotoluene by pseudomonas sp, Environ. Sci. Technol. 30 (1996) 2365–2370.

[62] S.E. George, G. Huggins-Clark, L.R. Brooks, Use of a salmonella microsuspension bioassay to detect the mutagenicity of munitions compounds at low concentrations, Mutat. Res. 490 (2001) 45–56.

[63] A. Eisentraeger, G. Reifferscheid, F. Dardenne, R. Blust, A. Schofer, Hazard characterization and identification of a former ammunition site using microarrays, bioassays, and chemical analysis, Environ. Toxicol. Chem. 26 (2007) 634–646.

[64] B. Gumuscu, D. Cekmecelioglu, T. Tekinay, Complete dissipation of 2,4,6-trinitrotoluene by in-vessel composting, RSC Adv. 5 (2015) 51812–51819.

[65] C. Karasch, M. Popovic, M. Qasim, R.K. Bajpai, Alkali hydrolysis of trinitrotoluene, Appl. Biochem. Biotechnol. 98-100 (2002) 1173–1185.

[66] D.R. Felt, S.L. Larson, L.D. Hansen, ENGINEER RESEARCH AND DEVELOPMENT CENTER VICKSBURG MS, Kinetics of Base-Catalyzed 2,4,6-trinitrotoluene transformation, ENGINEER RESEARCH AND DEVELOPMENT CENTER VICKSBURG MS, 2001.

[67] D.R. Felt, C.C. Nestler, J.L. Davis, S.L. Larson, ENGINEER RESEARCH AND DEVELOPMENT CENTER VICKSBURG MS, Potential for biodegradation of the alkaline hydrolysis end products of TNT and RDX, ENGINEER RESEARCH AND DEVELOPMENT CENTER VICKSBURG MS, 2007.

[68] M. Arienzo, Degradation of 2,4,6-trinitrotoluene in water and soil slurry utilizing a calcium peroxide compound, Chemosphere. 40 (2000) 331–337.

[69] J.L. Davis, M.C. Brooks, S.L. Larson, C.C. Nestler, D.R. Felt, Lime treatment of Explosives-Contaminated soil from munitions plants and firing ranges, Soil and Sediment Contamination: An International Journal. 15 (2006) 565–580.

[70] L.D. Hansen, S.L. Larson, J.L. Davis, J.M. Cullinane, C.C. Nestler, ENGINEER RESEARCH AND DEVELOPMENT CENTER VICKSBURG MS ENVIRONMENTAL LAB, Lime treatment of 2,4,6-trinitrotoluene contaminated soils: Proof of concept study, ENGINEER RESEARCH AND DEVELOPMENT CENTER VICKSBURG MS ENVIRONMENTAL LAB, 2003.

[71] A. Laveglia, L. Sambataro, N. Ukrainczyk, N. De Belie, E. Koenders, Hydrated lime life-cycle assessment: Current and future scenarios in four EU countries, J. Clean. Prod. 369 (2022) 133224.

[72] S. Krishnasamy, R. Lakshmanan, M. Ravichandran, Phytoremediatiation of metal and metalloid pollutants from farmland: An in-situ soil conservation, in: K.F. Mendes, R.N. de Sousa, K.C. Mielke (Eds.), Biodegradation Technology of Organic and Inorganic Pollutants, IntechOpen, Rijeka, 2021. https://doi.org/10.5772/intechopen.98659.

[73] E. Pilon-Smits, Phytoremediation, Annu. Rev. Plant Biol. 56 (2005) 15–39.

[74] N. Terry, C. Carlson, T.K. Raab, A.M. Zayed, Rates of selenium volatilization among crop species, J. Environ. Qual. 21 (1992) 341–344.

[75] R.R. Brooks, M.F. Chambers, L.J. Nicks, B.H. Robinson, Phytomining, Trends Plant Sci. 3 (1998) 359–362.

[76] S. Singh, D.P. Fulzele, Phytoextraction of arsenic using a weed plant calotropis procera from contaminated water and soil: Growth and biochemical response, Int. J. Phytoremediation. 23 (2021) 1310–1318.

[77] M. Salinitro, S. Montanari, A. Simoni, C. Ciavatta, A. Tassoni, Phytoextraction of arsenic, nickel, selenium and zinc from sewage sludge: From laboratory to pilot scale, Plant Soil. 481 (2022) 195–212.

[78] L.B. Brentner, S.T. Mukherji, S.A. Walsh, J.L. Schnoor, Localization of hexahydro-1,3,5-trinitro-1,3,5-triazine (RDX) and 2,4,6-trinitrotoluene (TNT) in poplar and switchgrass plants using phosphor imager autoradiography, Environ. Pollut. 158 (2010) 470–475.

[79] E.L. Rylott, M.V. Budarina, A. Barker, A. Lorenz, S.E. Strand, N.C. Bruce, Engineering plants for the phytoremediation of RDX in the presence of the co-contaminating explosive TNT, New Phytol. 192 (2011) 405–413.

[80] L. Zhang, R. Routsong, Q. Nguyen, E.L. Rylott, N.C. Bruce, S.E. Strand, Expression in grasses of multiple transgenes for degradation of munitions compounds on live-fire training ranges, Plant Biotechnol. J. 15 (2017) 624–633.

[81] T.J. Cary, E.L. Rylott, L. Zhang, R.M. Routsong, A.J. Palazzo, S.E. Strand, N.C. Bruce, Field trial demonstrating phytoremediation of the military explosive RDX by XplA/XplB-expressing switchgrass, Nat. Biotechnol. 39 (2021) 1216–1219.

[82] S.L. Doty, J.L. Freeman, C.M. Cohu, J.G. Burken, A. Firrincieli, A. Simon, Z. Khan, J.G. Isebrands, J. Lukas, M.J. Blaylock, Enhanced degradation of TCE on a superfund site using Endophyte-Assisted poplar tree phytoremediation, Environ. Sci. Technol. 51 (2017) 10050–10058.

[83] C.-G. Ren, C.-C. Kong, B. Bian, W. Liu, Y. Li, Y.-M. Luo, Z.-H. Xie, Enhanced phytoremediation of soils contaminated with PAHs by arbuscular mycorrhiza and rhizobium, Int. J. Phytoremediation. 19 (2017) 789–797.

[84] A. Barra Caracciolo, V. Terenzi, Rhizosphere microbial communities and heavy metals, Microorganisms. 9 (2021).

[85] C. Sens, P. Scheidemann, A. Klunk, D. Werner, Distribution of 14C-TNT and derivatives in different biochemical compartments of phaseolus vulgaris, Environ. Sci. Pollut. Res. Int. 5 (1998) 202–208.

[86] C. Sens, P. Scheidemann, D. Werner, The distribution of 14C-TNT in different biochemical compartments of the monocotyledonous triticum aestivum, Environ. Pollut. 104 (1999) 113–119.

[87] Q. Zhang, W. Kong, L. Wei, X. Hou, Q. Ma, Y. Liu, Y. Luo, C. Liao, J. Liu, J.L. Schnoor, G. Jiang, Compartmentalization and excretion of 2,4,6-tribromophenol sulfation and glycosylation conjugates in rice plants, Environ. Sci. Technol. 55 (2021) 2980–2990.

[88] A. Jerbi, N.J.B. Brereton, E. Sas, S. Amiot, X. Lachapelle-T, Y. Comeau, F.E. Pitre, M. Labrecque, High biomass yield increases in a primary effluent wastewater phytofiltration are associated to altered leaf morphology and stomatal size in salix miyabeana, Sci. Total Environ. 738 (2020) 139728.

[89] Y. Bai, M.F. Cotrufo, Grassland soil carbon sequestration: Current understanding, challenges, and solutions, Science. 377 (2022) 603–608.

[90] E.L. Rylott, N.C. Bruce, Right on target: Using plants and microbes to remediate explosives, Int. J. Phytoremediation. 21 (2019) 1051–1064.

[91] C.J. Rhodes, Applications of bioremediation and phytoremediation, Sci. Prog. 96 (2013) 417–427.

[92] B.W. Schoenmuth, W. Pestemer, Dendroremediation of trinitrotoluene (TNT). Part 2: Fate of radio-labelled TNT in trees, Environ. Sci. Pollut. Res. Int. 11 (2004) 331–339.

[93] E.J. Johnston, E.L. Rylott, E. Beynon, A. Lorenz, V. Chechik, N.C. Bruce, Monodehydroascorbate reductase mediates TNT toxicity in plants, Science. 349 (2015) 1072–1075.

[94] K. Obara, K. Sumi, H. Fukuda, The use of multiple transcription starts causes the dual targeting of arabidopsis putative monodehydroascorbate reductase to both mitochondria and chloroplasts, Plant Cell Physiol. 43 (2002) 697–705.

[95] M. Tanaka, R. Takahashi, A. Hamada, Y. Terai, T. Ogawa, Y. Sawa, T. Ishikawa, T. Maruta, Distribution and functions of monodehydroascorbate reductases in plants: Comprehensive reverse genetic analysis of arabidopsis thaliana enzymes, Antioxidants (Basel). 10 (2021).

[96] H. Sandermann Jr, Plant metabolism of xenobiotics, Trends Biochem. Sci. 17 (1992) 82–84.

[97] J.J. Zhang, H. Yang, Metabolism and detoxification of pesticides in plants, Sci. Total Environ. 790 (2021) 148034.

[98] W. Dekant, S. Vamvakas, M.W. Anders, Formation and fate of nephrotoxic and cytotoxic glutathione s-conjugates: Cysteine conjugate beta-lyase pathway, Adv. Pharmacol. 27 (1994) 115–162.

[99] E.R. Beynon, Z.C. Symons, R.G. Jackson, A. Lorenz, E.L. Rylott, N.C. Bruce, The role of oxophytodienoate reductases in the detoxification of the explosive 2,4,6-trinitrotoluene by arabidopsis, Plant Physiol. 151 (2009) 253–261.

[100] F. Schaller, C. Biesgen, C. Müssig, T. Altmann, E.W. Weiler, 12-oxophytodienoate reductase 3 (OPR3) is the isoenzyme involved in jasmonate biosynthesis, Planta. 210 (2000) 979–984.

[101] T. Tani, H. Sobajima, K. Okada, T. Chujo, S.-I. Arimura, N. Tsutsumi, M. Nishimura, H. Seto, H. Nojiri, H. Yamane, Identification of the OsOPR7 gene encoding 12-oxophytodienoate reductase involved in the biosynthesis of jasmonic acid in rice, Planta. 227 (2008) 517–526.

[102] Y. Wang, G. Yuan, S. Yuan, W. Duan, P. Wang, J. Bai, F. Zhang, S. Gao, L. Zhang, C. Zhao, TaOPR2 encodes a 12-oxo-phytodienoic acid reductase involved in the biosynthesis of jasmonic acid in wheat (triticum aestivum l.), Biochem. Biophys. Res. Commun. 470 (2016) 233–238.

[103] N. Hannink, S.J. Rosser, C.E. French, A. Basran, J.A. Murray, S. Nicklin, N.C. Bruce, Phytodetoxification of TNT by transgenic plants expressing a bacterial nitroreductase, Nat. Biotechnol. 19 (2001) 1168–1172.

[104] F. Gandia-Herrero, A. Lorenz, T. Larson, I.A. Graham, D.J. Bowles, E.L. Rylott, N.C. Bruce, Detoxification of the explosive 2,4,6-trinitrotoluene in arabidopsis: Discovery of bifunctional O- and c-glucosyltransferases, Plant J. 56 (2008) 963–974.

[105] J. Ross, Y. Li, E. Lim, D.J. Bowles, Higher plant glycosyltransferases, Genome Biol. 2 (2001) REVIEWS3004.

[106] V. Gunning, K. Tzafestas, H. Sparrow, E.J. Johnston, A.S. Brentnall, J.R. Potts, E.L. Rylott, N.C. Bruce, Arabidopsis glutathione transferases U24 and U25 exhibit a range of detoxification activities with the environmental pollutant and explosive, 2,4,6-trinitrotoluene, Plant Physiol. 165 (2014) 854–865.

[107] K. Tzafestas, L. Ahmad, M.P. Dani, G. Grogan, E.L. Rylott, N.C. Bruce, Structure-Guided mechanisms behind the metabolism of 2,4,6-trinitrotoluene by glutathione transferases U25 and U24 that lead to alternate product distribution, Front. Plant Sci. 9 (2018) 1846.

[108] J.O.D. Coleman, R. Randall, M.M.A. Blake-Kalff, Detoxification of xenobiotics in plant cells by glutathione conjugation and vacuolar compartmentalization: A fluorescent assay using monochlorobimane, Plant Cell Environ. 20 (1997) 449–460.

[109] Y.P. Lu, Z.S. Li, Y.M. Drozdowicz, S. Hortensteiner, E. Martinoia, P.A. Rea, AtMRP2, an arabidopsis ATP binding cassette transporter able to transport glutathione s-conjugates and chlorophyll catabolites: Functional comparisons with Atmrp1, Plant Cell. 10 (1998) 267–282.

[110] T.H.T. Do, E. Martinoia, Y. Lee, J.-U. Hwang, 2021 update on ATP-binding cassette (ABC) transporters: How they meet the needs of plants, Plant Physiol. 187 (2021) 1876–1892.

[111] C. Gaillard, A. Dufaud, R. Tommasini, K. Kreuz, N. Amrhein, E. Martinoia, A herbicide antidote (safener) induces the activity of both the herbicide detoxifying enzyme and of a vacuolar transporter for the detoxified herbicide, FEBS Lett. 352 (1994) 219–221.

[112] B. Burla, S. Pfrunder, R. Nagy, R.M. Francisco, Y. Lee, E. Martinoia, Vacuolar transport of abscisic acid glucosyl ester is mediated by ATP-binding cassette and proton-antiport mechanisms in arabidopsis, Plant Physiol. 163 (2013) 1446–1458.

[113] O. Dima, K. Morreel, B. Vanholme, H. Kim, J. Ralph, W. Boerjan, Small glycosylated lignin oligomers are stored in arabidopsis leaf vacuoles, Plant Cell. 27 (2015) 695–710.

[114] A. Grzam, P. Tennstedt, S. Clemens, R. Hell, A.J. Meyer, Vacuolar sequestration of glutathione s-conjugates outcompetes a possible degradation of the glutathione moiety by phytochelatin synthase, FEBS Lett. 580 (2006) 6384–6390.

[115] N. Ohkama-Ohtsu, P. Zhao, C. Xiang, D.J. Oliver, Glutathione conjugates in the vacuole are degraded by $\gamma$-glutamyl transpeptidase GGT3 in arabidopsis: GGT3 degrades GSH conjugates in the vacuole, Plant J. 49 (2007) 878–888.

[116] M. Arjmand, H. Sandermann jr, Plant biochemistry of xenobiotics. Mineralization of Chloroaniline/Lignin metabolites from wheat by the White-Rot fungus, phanerochaete chrysosporium, Zeitschrift für Naturforschung C. 41 (1986) 206–214.

[117] G. Noctor, A. Mhamdi, S. Chaouch, Y. Han, J. Neukermans, B. Marquez-Garcia, G. Queval, C.H. Foyer, Glutathione in plants: An integrated overview, Plant Cell Environ. 35 (2012) 454–484.

[118] D. Mendoza-Cózatl, H. Loza-Tavera, A. Hernández-Navarro, R. Moreno-Sánchez, Sulfur assimilation and glutathione metabolism under cadmium stress in yeast, protists and plants, FEMS Microbiol. Rev. 29 (2005) 653–671.

[119] A. Wachter, S. Wolf, H. Steininger, J. Bogs, T. Rausch, Differential targeting of GSH1 and GSH2 is achieved by multiple transcription initiation: Implications for the compartmentation of glutathione biosynthesis in the brassicaceae, Plant J. 41 (2005) 15–30.

[120] G. Noctor, L. Gomez, H. Vanacker, C.H. Foyer, Interactions between biosynthesis, compartmentation and transport in the control of glutathione homeostasis and signalling, J. Exp. Bot. 53 (2002) 1283–1304.

[121] N. Ohkama-Ohtsu, S. Radwan, A. Peterson, P. Zhao, A.F. Badr, C. Xiang, D.J. Oliver, Characterization of the extracellular $\gamma$-glutamyl transpeptidases, GGT1 and GGT2, in arabidopsis: Apoplastic glutathione degradation in arabidopsis, Plant J. 49 (2007) 865–877.

[122] N. Ohkama-Ohtsu, Y. Sasaki-Sekimoto, A. Oikawa, Y. Jikumaru, S. Shinoda, E. Inoue, Y. Kamide, T. Yokoyama, M.Y. Hirai, K. Shirasu, Y. Kamiya, D.J. Oliver, K. Saito, 12-oxo-phytodienoic acid-glutathione conjugate is transported into the vacuole in arabidopsis, Plant Cell Physiol. 52 (2011) 205–209.

[123] N. Ohkama-Ohtsu, A. Oikawa, P. Zhao, C. Xiang, K. Saito, D.J. Oliver, A gamma-glutamyl transpeptidase-independent pathway of glutathione catabolism to glutamate via 5-oxoproline in arabidopsis, Plant Physiol. 148 (2008) 1603–1613.

[124] S. Kumar, A. Kaur, B. Chattopadhyay, A.K. Bachhawat, Defining the cytosolic pathway of glutathione degradation in arabidopsis thaliana: Role of the ChaC/GCG family of $\gamma$-glutamyl cyclotransferases as glutathione-degrading enzymes and AtLAP1 as the Cys-Gly peptidase, Biochem. J. 468 (2015) 73–85.

[125] T. Ito, T. Kitaiwa, K. Nishizono, M. Umahashi, S. Miyaji, S.-I. Agake, K. Kuwahara, T. Yokoyama, S. Fushinobu, A. Maruyama-Nakashita, R. Sugiyama, M. Sato, J. Inaba, M.Y. Hirai, N. Ohkama-Ohtsu, Glutathione degradation activity of $\gamma$-glutamyl peptidase 1 manifests its dual roles in primary and secondary sulfur metabolism in arabidopsis, Plant J. 111 (2022) 1626–1642.

[126] F. Geu-Flores, M.E. Møldrup, C. Böttcher, C.E. Olsen, D. Scheel, B.A. Halkier, Cytosolic $\gamma$-glutamyl peptidases process glutathione conjugates in the biosynthesis of glucosinolates and camalexin in arabidopsis, Plant Cell. 23 (2011) 2456–2469.

[127] J.M. Ugalde, L. Lamig, A. Herrera-Vásquez, P. Fuchs, M. Homagk, S. Kopriva, S.J. Müller-Schüssele, L. Holuigue, A.J. Meyer, A dual role for glutathione transferase U7 in plant growth and protection from methyl viologen-induced oxidative stress, Plant Physiol. 187 (2021) 2451–2468.

[128] P. Pandey, J. Singh, V.M.M. Achary, M.K. Reddy, Redox homeostasis via gene families of ascorbate-glutathione pathway, Front. Environ. Sci. Eng. China. 3 (2015).

[129] S.B. Ha, A.P. Smith, R. Howden, W.M. Dietrich, S. Bugg, M.J. O'Connell, P.B. Goldsbrough, C.S. Cobbett, Phytochelatin synthase genes from arabidopsis and the yeast schizosaccharomyces pombe, Plant Cell. 11 (1999) 1153–1164.

[130] W.-Y. Song, J. Park, D.G. Mendoza-Cózatl, M. Suter-Grotemeyer, D. Shim, S. Hörtensteiner, M. Geisler, B. Weder, P.A. Rea, D. Rentsch, J.I. Schroeder, Y. Lee, E. Martinoia, Arsenic tolerance in arabidopsis is mediated by two ABCC-type phytochelatin transporters, Proc. Natl. Acad. Sci. U. S. A. 107 (2010) 21187–21192.

[131] M. Wójcik, A. Tukiendorf, Glutathione in adaptation of arabidopsis thaliana to cadmium stress, Biol. Plant. 55 (2011) 125–132.

[132] S. Dorion, J.C. Ouellet, J. Rivoal, Glutathione metabolism in plants under stress: Beyond reactive oxygen species detoxification, Metabolites. 11 (2021).

[133] I. Cummins, D.J. Wortley, F. Sabbadin, Z. He, C.R. Coxon, H.E. Straker, J.D. Sellars, K. Knight, L. Edwards, D. Hughes, S.S. Kaundun, S.-J. Hutchings, P.G. Steel, R. Edwards, Key role for a glutathione transferase in multiple-herbicide resistance in grass weeds, Proc. Natl. Acad. Sci. U. S. A. 110 (2013) 5812–5817.

[134] C. Huber, B. Bartha, R. Harpaintner, P. Schröder, Metabolism of acetaminophen (paracetamol) in plants—two independent pathways result in the formation of a glutathione and a glucose conjugate, Environ. Sci. Pollut. Res. 16 (2009) 206–213.

[135] M.H. Farkas, J.O. Berry, D.S. Aga, Chlortetracycline detoxification in maize via induction of glutathione s-transferases after antibiotic exposure, Environ. Sci. Technol. 41 (2007) 1450–1456.

[136] D.P. Dixon, R. Edwards, Glutathione transferases, Arabidopsis Book. 8 (2010) e0131.

[137] P.J. Jakobsson, R. Morgenstern, J. Mancini, A. Ford-Hutchinson, B. Persson, Common structural features of MAPEG – a widespread superfamily of membrane associated proteins with highly divergent functions in eicosanoid and glutathione metabolism, Protein Sci. 8 (1999) 689–692.

[138] R. Edwards, D.P. Dixon, Plant glutathione transferases, in: H. Sies, L. Packer (Eds.), Methods in Enzymology, Academic Press, 2005: pp. 169–186.

[139] D.P. Dixon, T. Hawkins, P.J. Hussey, R. Edwards, Enzyme activities and subcellular localization of members of the arabidopsis glutathione transferase superfamily, J. Exp. Bot. 60 (2009) 1207–1218.

[140] D.P. Dixon, D.J. Cole, R. Edwards, Characterisation of a zeta class glutathione transferase from arabidopsis thaliana with a putative role in tyrosine catabolism, Arch. Biochem. Biophys. 384 (2000) 407–412.

[141] D.P. Dixon, R. Edwards, Enzymes of tyrosine catabolism in arabidopsis thaliana, Plant Sci. 171 (2006) 360–366.

[142] Z.Z. Banday, A.K. Nandi, Arabidopsis thaliana GLUTATHIONE-S-TRANSFERASE THETA 2 interacts with RSI1/FLD to activate systemic acquired resistance, Mol. Plant Pathol. 19 (2018) 464–475.

[143] D.P. Dixon, B.G. Davis, R. Edwards, Functional divergence in the glutathione transferase superfamily in plants: IDENTIFICATION OF TWO CLASSES WITH PUTATIVE FUNCTIONS IN REDOX HOMEOSTASIS IN ARABIDOPSIS THALIANA*, J. Biol. Chem. 277 (2002) 30859–30869.

[144] D.P. Dixon, R. Edwards, Roles for stress-inducible lambda glutathione transferases in flavonoid metabolism in plants as identified by ligand fishing*, J. Biol. Chem. 285 (2010) 36322–36329.

[145] D.R. Gallie, The role of l-ascorbic acid recycling in responding to environmental stress and in promoting plant growth, J. Exp. Bot. 64 (2013) 433–443.

[146] M.-S. Rahantaniaina, S. Li, G. Chatel-Innocenti, A. Tuzet, E. Issakidis-Bourguet, A. Mhamdi, G. Noctor, Cytosolic and chloroplastic DHARs cooperate in oxidative Stress-Driven activation of the salicylic acid pathway, Plant Physiol. 174 (2017) 956–971.

[147] P.G. Sappl, A.J. Carroll, R. Clifton, R. Lister, J. Whelan, A. Harvey Millar, K.B. Singh, The arabidopsis glutathione transferase gene family displays complex stress regulation and co-silencing multiple genes results in altered metabolic sensitivity to oxidative stress, Plant J. 58 (2009) 53–68.

[148] E. Horváth, K. Bela, B. Holinka, R. Riyazuddin, Á. Gallé, Á. Hajnal, Á. Hurton, A. Fehér, J. Csiszár, The arabidopsis glutathione transferases, AtGSTF8 and AtGSTU19 are involved in the maintenance of root redox homeostasis affecting meristem size and salt stress sensitivity, Plant Sci. 283 (2019) 366–374.

[149] E. Horváth, K. Bela, C. Papdi, Á. Gallé, L. Szabados, I. Tari, J. Csiszár, The role of arabidopsis glutathione transferase F9 gene under oxidative stress in seedlings, Acta Biol. Hung. 66 (2015) 406–418.

[150] Y. Sun, H. Li, J.-R. Huang, Arabidopsis TT19 functions as a carrier to transport anthocyanin from the cytosol to tonoplasts, Mol. Plant. 5 (2012) 387–400.

[151] L. Ahmad, E.L. Rylott, N.C. Bruce, R. Edwards, G. Grogan, Structural evidence for arabidopsis glutathione transferase AtGSTF2 functioning as a transporter of small organic ligands, FEBS Open Bio. 7 (2017) 122–132.

[152] D.P. Dixon, R. Edwards, Selective binding of glutathione conjugates of fatty acid derivatives by plant glutathione transferases, J. Biol. Chem. 284 (2009) 21249–21256.

[153] M. Piślewska-Bednarek, R.T. Nakano, K. Hiruma, M. Pastorczyk, A. Sanchez-Vallet, S. Singkaravanit-Ogawa, D. Ciesiołka, Y. Takano, A. Molina, P. Schulze-Lefert, P. Bednarek, Glutathione transferase U13 functions in Pathogen-Triggered glucosinolate metabolism, Plant Physiol. 176 (2018) 538–551.

[154] J. Xu, Y.-S. Tian, X.-J. Xing, R.-H. Peng, B. Zhu, J.-J. Gao, Q.-H. Yao, Over-expression of AtGSTU19 provides tolerance to salt, drought and methyl viologen stresses in arabidopsis, Physiol. Plant. 156 (2016) 164–175.

[155] A. Zhang, R. Luo, J. Li, R. Miao, H. An, X. Yan, Q. Pang, Arabidopsis Glutathione-S-Transferases GSTF11 and GSTU20 function in aliphatic glucosinolate biosynthesis, Front. Plant Sci. 12 (2021) 816233.

[156] R Core Team, R: A language and environment for statistical computing, R Foundation for Statistical Computing, Vienna, Austria, 2022. https://www.R-project.org/.

[157] RStudio Team, RStudio: Integrated development environment for r, RStudio, PBC., Boston, MA, 2020. http://www.rstudio.com/.

[158] T.K. Kim, T test as a parametric statistic, Korean J. Anesthesiol. 68 (2015) 540–546.

[159] L. St»hle, S. Wold, Analysis of variance (ANOVA), Chemometrics Intellig. Lab. Syst. 6 (1989) 259–272.

[160] H. Abdi, L.J. Williams, Tukey's honestly significant difference (HSD) test, Encyclopedia of Research Design. 3 (2010) 1–5.

[161] A. Kassambara, Rstatix: Pipe-friendly framework for basic statistical tests, 2023. https://CRAN.R-project.org/package=rstatix.

[162] H. Wickham, M. Averick, J. Bryan, W. Chang, L.D. McGowan, R. François, G. Grolemund, A. Hayes, L. Henry, J. Hester, M. Kuhn, T.L. Pedersen, E. Miller, S.M. Bache, K. Müller, J. Ooms, D. Robinson, D.P. Seidel, V. Spinu, K. Takahashi, D. Vaughan, C. Wilke, K. Woo, H. Yutani, Welcome to the tidyverse, Journal of Open Source Software. 4 (2019) 1686. https://doi.org/10.21105/joss.01686.

[163] B. Hou, E.-K. Lim, G.S. Higgins, D.J. Bowles, N-glucosylation of cytokinins by glycosyltransferases of arabidopsis thaliana, J. Biol. Chem. 279 (2004) 47822–47832.

[164] Z. Liu, J.-P. Yan, D.-K. Li, Q. Luo, Q. Yan, Z.-B. Liu, L.-M. Ye, J.-M. Wang, X.-F. Li, Y. Yang, UDP-glucosyltransferase71c5, a major glucosyltransferase, mediates abscisic acid homeostasis in arabidopsis, Plant Physiol. 167 (2015) 1659–1670.

[165] P. Ding, Y. Ding, Stories of salicylic acid: A plant defense hormone, Trends Plant Sci. 25 (2020) 549–565.

[166] J. Coleman, M. Blake-Kalff, E. Davies, Detoxification of xenobiotics by plants: Chemical modification and vacuolar compartmentation, Trends Plant Sci. 2 (1997) 144–151.

[167] Q.-Y. Lv, M.-L. Han, Y.-Q. Gao, C.-Y. Zhang, Y.-L. Wang, Z.-F. Chao, L.-Y. Zhong, D.-Y. Chao, Sec24C mediates a golgi-independent trafficking pathway that is required for tonoplast localization of ABCC1 and ABCC2, New Phytol. (2022).

[168] A. Frelet-Barrand, H.Ü. Kolukisaoglu, S. Plaza, M. Rüffer, L. Azevedo, S. Hörtensteiner, K. Marinova, B. Weder, B. Schulz, M. Klein, Comparative mutant analysis of arabidopsis ABCC-Type ABC transporters: AtMRP2 contributes to detoxification, vacuolar organic anion transport and chlorophyll degradation, Plant Cell Physiol. 49 (2008) 557–569.

[169] U. Matern, C. Reichenbach, W. Heller, Efficient uptake of flavonoids into parsley (petroselinum hortense) vacuoles requires acylated glycosides, Planta. 167 (1986) 183–189.

[170] A.E. Wolf, K.J. Dietz, P. Schröder, Degradation of glutathione s-conjugates by a carboxypeptidase in the plant vacuole, FEBS Lett. 384 (1996) 31–34.

[171] Y.P. Lu, Z.S. Li, P.A. Rea, AtMRP1 gene of arabidopsis encodes a glutathione s-conjugate pump: Isolation and functional definition of a plant ATP-binding cassette transporter gene, Proc. Natl. Acad. Sci. U. S. A. 94 (1997) 8243–8248.

[172] H.A. Walczak, J.V. Dean, Vacuolar transport of the glutathione conjugate of trans-cinnamic acid, Phytochemistry. 53 (2000) 441–446.

[173] J. Zhao, R.A. Dixon, MATE transporters facilitate vacuolar uptake of epicatechin 3'-o-glucoside for proanthocyanidin biosynthesis in medicago truncatula and arabidopsis, Plant Cell. 21 (2009) 2323–2340.

[174] J. Zhao, D. Huhman, G. Shadle, X.-Z. He, L.W. Sumner, Y. Tang, R.A. Dixon, MATE2 mediates vacuolar sequestration of flavonoid glycosides and glycoside malonates in medicago truncatula, Plant Cell. 23 (2011) 1536–1555.

[175] M.D. Fricker, A.J. Meyer, Confocal imaging of metabolism in vivo: Pitfalls and possibilities, J. Exp. Bot. 52 (2001) 631–640.

[176] F. Hu, L. Shi, W. Min, Biological imaging of chemical bonds by stimulated raman scattering microscopy, Nat. Methods. 16 (2019) 830–842.

[177] C. Lima, H. Muhamadali, R. Goodacre, The role of raman spectroscopy within quantitative metabolomics, Annu. Rev. Anal. Chem. 14 (2021) 323–345.

[178] T. Iino, K. Hashimoto, T. Asai, K. Kuchitsu, Y. Ozeki, Multicolour chemical imaging of plant tissues with hyperspectral stimulated raman scattering microscopy, Analyst. 146 (2021) 1234–1238.

[179] D. Tsikritsis, E.J. Legge, N.A. Belsey, Practical considerations for quantitative and reproducible measurements with stimulated raman scattering microscopy, Analyst. 147 (2022) 4642–4656.

[180] A.R. Buchberger, K. DeLaney, J. Johnson, L. Li, Mass spectrometry imaging: A review of emerging advancements and future insights, Anal. Chem. 90 (2018) 240–265.

[181] J. Soltwisch, H. Kettling, S. Vens-Cappell, M. Wiegelmann, J. Müthing, K. Dreisewerd, Mass spectrometry imaging with laser-induced postionization, Science. 348 (2015) 211–215.

[182] X. Zhu, T. Xu, C. Peng, S. Wu, Advances in MALDI mass spectrometry imaging single cell and tissues, Front Chem. 9 (2021) 782432.

[183] T. Fujii, S. Matsuda, M.L. Tejedor, T. Esaki, I. Sakane, H. Mizuno, N. Tsuyama, T. Masujima, Direct metabolomics for plant cells by live single-cell mass spectrometry, Nat. Protoc. 10 (2015) 1445–1456.

[184] K. Yamamoto, K. Takahashi, H. Mizuno, A. Anegawa, K. Ishizaki, H. Fukaki, M. Ohnishi, M. Yamazaki, T. Masujima, T. Mimura, Cell-specific localization of alkaloids in *catharanthus roseus* stem tissue measured with imaging MS and single-cell MS, Proceedings of the National Academy of Sciences. 113 (2016) 3891–3896.

[185] M. Tanaka, T. Esaki, H. Kenmoku, T. Koeduka, Y. Kiyoyama, T. Masujima, Y. Asakawa, K. Matsui, Direct evidence of specific localization of sesquiterpenes and marchantin a in oil body cells of marchantia polymorpha L, Phytochemistry. 130 (2016) 77–84.

[186] K. Yamamoto, K. Takahashi, L. Caputi, H. Mizuno, C.E. Rodriguez-Lopez, T. Iwasaki, K. Ishizaki, H. Fukaki, M. Ohnishi, M. Yamazaki, T. Masujima, S.E. O'Connor, T. Mimura, The complexity of intercellular localisation of alkaloids revealed by single-cell metabolomics, New Phytol. 224 (2019) 848–859.

[187] S.J. Swanson, W.-G. Choi, A. Chanoca, S. Gilroy, In vivo imaging of Ca2+, pH, and reactive oxygen species using fluorescent probes in plants, Annu. Rev. Plant Biol. 62 (2011) 273–297.

[188] K. Yahata, H. Mizuno, E. Sugiyama, K. Todoroki, Analysis of the intracellular localization of amiodarone using live single-cell mass spectrometry, J. Pharm. Biomed. Anal. 205 (2021) 114318.

[189] R. Gerhardt, H.W. Heldt, Measurement of subcellular metabolite levels in leaves by fractionation of freeze-stopped material in nonaqueous media, Plant Physiol. 75 (1984) 542–547.

[190] D. Riewe, L. Grosman, A.R. Fernie, C. Wucke, P. Geigenberger, The potato-specific apyrase is apoplastically localized and has influence on gene expression, growth, and development, Plant Physiol. 147 (2008) 1092–1109.

[191] S. Arrivault, M. Guenther, A. Florian, B. Encke, R. Feil, D. Vosloh, J.E. Lunn, R. Sulpice, A.R. Fernie, M. Stitt, W.X. Schulze, Dissecting the subcellular compartmentation of proteins and metabolites in arabidopsis leaves using non-aqueous fractionation, Mol. Cell. Proteomics. 13 (2014) 2246–2259.

[192] W.F. Beshir, T. Tohge, M. Watanabe, M.L.A.T.M. Hertog, R. Hoefgen, A.R. Fernie, B.M. Nicolaï, Non-aqueous fractionation revealed changing subcellular metabolite distribution during apple fruit development, Hortic Res. 6 (2019) 98.

[193] L. Fürtauer, W. Weckwerth, T. Nägele, A benchtop fractionation procedure for subcellular analysis of the plant metabolome, Front. Plant Sci. 7 (2016) 1912.

[194] L. Fürtauer, L. Küstner, W. Weckwerth, A.G. Heyer, T. Nägele, Resolving subcellular plant metabolism, Plant J. 100 (2019) 438–455.

[195] T. Boller, H. Kende, Hydrolytic enzymes in the central vacuole of plant cells, Plant Physiol. 63 (1979) 1123–1132.

[196] T. Jelitto, U. Sonnewald, L. Willmitzer, M. Hajirezeai, M. Stitt, Inorganic pyrophosphate content and metabolites in potato and tobacco plants expressing e. Coli pyrophosphatase in their cytosol, Planta. 188 (1992) 238–244.

[197] R. Zrenner, L. Willmitzer, U. Sonnewald, Analysis of the expression of potato uridinediphosphate-glucose pyrophosphorylase and its inhibition by antisense RNA, Planta. 190 (1993) 247–252.

[198] J. Murphy, J.P. Riley, A modified single solution method for the determination of phosphate in natural waters, Anal. Chim. Acta. 27 (1962) 31–36.

[199] H.P. Price, L. MacLean, J. Marrison, P.J. O'Toole, D.F. Smith, Validation of a new method for immobilising kinetoplastid parasites for live cell imaging, Mol. Biochem. Parasitol. 169 (2010) 66.

[200] M. Morsch, R.A.W. Radford, E.K. Don, A. Lee, E. Hortle, N.J. Cole, R.S. Chung, Triggering cell stress and death using conventional UV laser confocal microscopy, J. Vis. Exp. (2017).

[201] D.P. Vu, C. Martins Rodrigues, B. Jung, G. Meissner, P.A.W. Klemens, D. Holtgräwe, L. Fürtauer, T. Nägele, P. Nieberl, B. Pommerrenig, H.E. Neuhaus, Vacuolar sucrose homeostasis is critical for plant development, seed properties, and night-time survival in arabidopsis, J. Exp. Bot. 71 (2020) 4930–4943.

[202] A. Khan, J. Cheng, A. Kitashova, L. Fürtauer, T. Nägele, C. Picco, J. Scholz-Starke, I. Keller, H.E. Neuhaus, B. Pommerrenig, Vacuolar sugar transporter EARLY RESPONSE TO DEHYDRATION 6-LIKE4 affects fructose signaling and plant growth, Plant Physiol. (2023).

[203] S. Krueger, D. Steinhauser, J. Lisec, P. Giavalisco, Analysis of subcellular metabolite distributions within arabidopsis thaliana leaf tissue: A primer for subcellular metabolomics, in: J.J. Sanchez-Serrano, J. Salinas (Eds.), Arabidopsis Protocols, Humana Press, Totowa, NJ, 2014: pp. 575–596.

[204] D.B. Medeiros, S. Arrivault, J. Alpers, A.R. Fernie, F. Aarabi, Non-aqueous fractionation (NAF) for metabolite analysis in subcellular compartments of arabidopsis leaf tissues, Bio Protoc. 9 (2019) e3399.

[205] P.J. Taylor, Matrix effects: The achilles heel of quantitative high-performance liquid chromatography-electrospray-tandem mass spectrometry, Clin. Biochem. 38 (2005) 328–334.

[206] Alconox Inc., Detergent residue testing using a pH meter, pH indicator, or test kit, (2014).

[207] S.M. Patel, T. Doen, M.J. Pikal, Determination of end point of primary drying in freeze-drying process control, AAPS PharmSciTech. 11 (2010) 73–84.

[208] O.B. Polivanova, V.A. Bedarev, Hyperhydricity in plant tissue culture, Plants. 11 (2022).

[209] V. Jausoro, B.E. Llorente, N.M. Apóstolo, Structural differences between hyperhydric and normal in vitro shoots of handroanthus impetiginosus (mart. Ex DC) mattos (bignoniaceae), Plant Cell Tissue Organ Cult. 101 (2010) 183–191.

[210] H. Gao, J. Li, H. Ji, L. An, X. Xia, Hyperhydricity-induced ultrastructural and physiological changes in blueberry (vaccinium spp.), Plant Cell Tissue Organ Cult. 133 (2018) 65–76.

[211] A. Endler, S. Meyer, S. Schelbert, T. Schneider, W. Weschke, S.W. Peters, F. Keller, S. Baginsky, E. Martinoia, U.G. Schmidt, Identification of a vacuolar sucrose transporter in barley and arabidopsis mesophyll cells by a tonoplast proteomic approach, Plant Physiol. 141 (2006) 196–207.

[212] L. Carmona-Salazar, R.E. Cahoon, J. Gasca-Pineda, A. González-Solís, R. Vera-Estrella, V. Treviño, E.B. Cahoon, M. Gavilanes-Ruiz, Plasma and vacuolar membrane sphingolipidomes: Composition and insights on the role of main molecular species, Plant Physiol. 186 (2021) 624–639.

[213] A.V. Morant, K. Jørgensen, C. Jørgensen, S.M. Paquette, R. Sánchez-Pérez, B.L. Møller, S. Bak, Beta-glucosidases as detonators of plant chemical defense, Phytochemistry. 69 (2008) 1795–1813.

[214] Y. Miyagawa, Y. Tobimatsu, P.Y. Lam, T. Mizukami, S. Sakurai, H. Kamitakahara, T. Takano, Possible mechanisms for the generation of phenyl glycoside-type lignin-carbohydrate linkages in lignification with monolignol glucosides, Plant J. 104 (2020) 156–170.

[215] C.M. Mulvey, L.M. Breckels, A. Geladaki, N.K. Britovšek, D.J.H. Nightingale, A. Christoforou, M. Elzek, M.J. Deery, L. Gatto, K.S. Lilley, Using hyperLOPIT to perform high-resolution mapping of the spatial proteome, Nat. Protoc. 12 (2017) 1110–1135.

[216] M. Knaupp, K.B. Mishra, L. Nedbal, A.G. Heyer, Evidence for a role of raffinose in stabilizing photosystem II during freeze-thaw cycles, Planta. 234 (2011) 477–486.

[217] L. Fürtauer, A. Pschenitschnigg, H. Scharkosi, W. Weckwerth, T. Nägele, Combined multivariate analysis and machine learning reveals a predictive module of metabolic stress response in arabidopsis thaliana, Mol Omics. 14 (2018) 437–449.

[218] D.M. Bartholomew, D.E. Van Dyk, S.-M.C. Lau, D.P. O'Keefe, P.A. Rea, P.V. Viitanen, Alternate energy-dependent pathways for the vacuolar uptake of glucose and glutathione conjugates, Plant Physiol. 130 (2002) 1562–1572.

[219] S.C. Lu, Glutathione synthesis, Biochim. Biophys. Acta. 1830 (2013) 3143–3153.

[220] M.H.H. A. J. L. Cooper, Metabolism of glutathione S-Conjugates: Multiple pathways, Comprehensive Toxicology. (2018) 363.

[221] T. Ito, N. Ohkama-Ohtsu, Degradation of glutathione and glutathione conjugates in plants, J. Exp. Bot. 74 (2023) 3313–3327.

[222] A. Grzam, M.N. Martin, R. Hell, A.J. Meyer, Gamma-glutamyl transpeptidase GGT4 initiates vacuolar degradation of glutathione s-conjugates in arabidopsis, FEBS Lett. 581 (2007) 3131–3138.

[223] D.E. Riechers, E.P. Fuerst, K.D. Miller, Initial metabolism of dimethenamid in safened and unsafened wheat shoots, J. Agric. Food Chem. 44 (1996) 1558–1564.

[224] M. Brazier-Hicks, K.M. Evans, O.D. Cunningham, D.R.W. Hodgson, P.G. Steel, R. Edwards, Catabolism of glutathione conjugates in arabidopsis thaliana. Role in metabolic reactivation of the herbicide safener fenclorim, J. Biol. Chem. 283 (2008) 21102–21112.

[225] I. Cummins, D.N. Bryant, R. Edwards, Safener responsiveness and multiple herbicide resistance in the weed black-grass (alopecurus myosuroides), Plant Biotechnol. J. 7 (2009) 807–820.

[226] J.J. Zhang, J.Y. Xu, F.F. Lu, S.F. Jin, H. Yang, Detoxification of atrazine by low molecular weight thiols in alfalfa (medicago sativa), Chem. Res. Toxicol. 30 (2017) 1835–1846.

[227] R. Blum, A. Beck, A. Korte, A. Stengel, T. Letzel, K. Lendzian, E. Grill, Function of phytochelatin synthase in catabolism of glutathione-conjugates, Plant J. 49 (2007) 740–749.

[228] R. Blum, K.C. Meyer, J. Wünschmann, K.J. Lendzian, E. Grill, Cytosolic action of phytochelatin synthase, Plant Physiol. 153 (2010) 159–169.

[229] N.M. Mozier, J.L. Hoffman, Biosynthesis and urinary excretion of methyl sulfonium derivatives of the sulfur mustard analog, 2-chloroethyl ethyl sulfide, and other thioethers, FASEB J. 4 (1990) 3329–3333.

[230] P.I. Mathias, C. B'hymer, Mercapturic acids: Recent advances in their determination by liquid chromatography/mass spectrometry and their use in toxicant metabolism studies and in occupational and environmental exposure studies, Biomarkers. 21 (2016) 293–315.

[231] Y. Jarrar, S.-J. Lee, The functionality of UDP-Glucuronosyltransferase genetic variants and their association with drug responses and human diseases, J Pers Med. 11 (2021).

[232] G.L. Lamoureux, J.M. Gouot, D.G. Davis, D.G. Rusness, Pentachloronitrobenzene metabolism in peanut. 3. Metabolism in peanut cell suspension cultures, J. Agric. Food Chem. 29 (1981) 996–1002.

[233] G.L. Lamoureux, D.G. Rusness, P. Schroder, Metabolism of a diphenylether herbicide to a volatile thioanisole and a polar sulfonic acid metabolite in spruce (picea), Pestic. Biochem. Physiol. 47 (1993) 8–20.

[234] R. Dücker, P. Zöllner, E. Parcharidou, S. Ries, L. Lorentz, R. Beffa, Enhanced metabolism causes reduced flufenacet sensitivity in black-grass (alopecurus myosuroides huds.) field populations, Pest Manag. Sci. 75 (2019) 2996–3004.

[235] A.M.A. Mazari, B. Mannervik, Drosophila GSTs display outstanding catalytic efficiencies with the environmental pollutants 2,4,6-trinitrotoluene and 2,4-dinitrotoluene, Biochemistry and Biophysics Reports. 5 (2016) 141–145.

[236] K. Tzafestas, M.M. Razalan, I. Gyulev, A.M.A. Mazari, B. Mannervik, E.L. Rylott, N.C. Bruce, Expression of a drosophila glutathione transferase in arabidopsis confers the ability to detoxify the environmental pollutant, and explosive, 2,4,6-trinitrotoluene, New Phytol. 214 (2017) 294–303.

[237] S. Parinov, M. Sevugan, D. Ye, W.C. Yang, M. Kumaran, V. Sundaresan, Analysis of flanking sequences from dissociation insertion lines: A database for reverse genetics in arabidopsis, Plant Cell. 11 (1999) 2263–2270.

[238] D. Kessner, M. Chambers, R. Burke, D. Agus, P. Mallick, ProteoWizard: Open source software for rapid proteomics tools development, Bioinformatics. 24 (2008) 2534–2536.

[239] K. Dührkop, M. Fleischauer, M. Ludwig, A.A. Aksenov, A.V. Melnik, M. Meusel, P.C. Dorrestein, J. Rousu, S. Böcker, SIRIUS 4: A rapid tool for turning tandem mass spectra into metabolite structure information, Nat. Methods. 16 (2019) 299–302.

[240] C.J. Thompson, N.R. Movva, R. Tizard, R. Crameri, J.E. Davies, M. Lauwereys, J. Botterman, Characterization of the herbicide-resistance gene bar from streptomyces hygroscopicus, EMBO J. 6 (1987) 2519–2523.

[241] C.E. French, S.J. Rosser, G.J. Davies, S. Nicklin, N.C. Bruce, Biodegradation of explosives by transgenic plants expressing pentaerythritol tetranitrate reductase, Nat. Biotechnol. 17 (1999) 491–494.

[242] J. Robak, E. Marcinkiewicz, Z. Michalska, R.J. Gryglewski, Nitric oxide donation and nitrite assays in the presence of thiols and albumin as determined by griess' and werringloer's methods, Pol. J. Pharmacol. 49 (1997) 255–262.

[243] D. Tsikas, Analysis of nitrite and nitrate in biological fluids by assays based on the griess reaction: Appraisal of the griess reaction in the l-arginine/nitric oxide area of research, J. Chromatogr. B Analyt. Technol. Biomed. Life Sci. 851 (2007) 51–70.

[244] N.E. Savin, The bonferroni and the scheffe multiple comparison procedures, Rev. Econ. Stud. 47 (1980) 255.

[245] J. Attieh, K.F. Kleppinger-Sparace, C. Nunes, S.A. Sparace, H.S. Saini, Evidence implicating a novel thiol methyltransferase in the detoxification of glucosinolate hydrolysis products inBrassica oleraceaL, Plant Cell Environ. 23 (2000) 165–174.

[246] S. Ma, Q. Gong, H.J. Bohnert, Dissecting salt stress pathways, J. Exp. Bot. 57 (2006) 1097–1107.

[247] E. García-Cano, H. Hak, S. Magori, S.G. Lazarowitz, V. Citovsky, The agrobacterium F-Box protein effector VirF destabilizes the arabidopsis GLABROUS1 Enhancer/Binding Protein-Like transcription factor VFP4, a transcriptional activator of defense response genes, Mol. Plant. Microbe. Interact. 31 (2018) 576–586.

[248] D.R. Ekman, W.W. Lorenz, A.E. Przybyla, N.L. Wolfe, J.F.D. Dean, SAGE analysis of transcriptome responses in arabidopsis roots exposed to 2,4,6-trinitrotoluene, Plant Physiol. 133 (2003) 1397–1406.

[249] A. Mentewab, V. Cardoza, C.N. Stewart, Genomic analysis of the response of arabidopsis thaliana to trinitrotoluene as revealed by cDNA microarrays, Plant Sci. 168 (2005) 1409–1424.

[250] M.R. Rao, M.D. Halfhill, L.G. Abercrombie, P. Ranjan, J.M. Abercrombie, J.S. Gouffon, A.M. Saxton, C.N. Stewart Jr, Phytoremediation and phytosensing of chemical contaminants, RDX and TNT: Identification of the required target genes, Funct. Integr. Genomics. 9 (2009) 537–547.

[251] G. Taguchi, T. Ubukata, H. Nozue, Y. Kobayashi, M. Takahi, H. Yamamoto, N. Hayashida, Malonylation is a key reaction in the metabolism of xenobiotic phenolic glucosides in arabidopsis and tobacco, Plant J. 63 (2010) 1031–1041.

[252] S. Gan, W. Rozhon, E. Varga, J. Halder, F. Berthiller, B. Poppenberger, The acyltransferase PMAT1 malonylates brassinolide glucoside, J. Biol. Chem. 296 (2021) 100424.

[253] G.L. Lamoureux, D.G. Rusness, MALONYLCYSTEINE CONJUGATES AS END-PRODUCTS OF GLUTATHIONE CONJUGATE METABOLISM IN PLANTS, in: S. Matsunaka, D.H. Hutson, S.D. Murphy (Eds.), Mode of Action, Metabolism and Toxicology, Pergamon, 1983: pp. 295–300.

[254] W. Hinderer, J. Köster, W. Barz, Purfication and properties of a specific isoflavone 7-o-glucoside-6”-malonate malonyestrase from roots of chickpea (cicer arietinum l.), Arch. Biochem. Biophys. 248 (1986) 570–578.

[255] E. Martinoia, E. Grill, R. Tommasini, K. Kreuz, N. Amrhein, ATP-dependent glutathione s-conjugate ’export’ pump in the vacuolar membrane of plants, Nature. 364 (1993) 247–249.

[256] P. Ranocha, O. Dima, R. Nagy, J. Felten, C. Corratgé-Faillie, O. Novák, K. Morreel, B. Lacombe, Y. Martinez, S. Pfrunder, X. Jin, J.-P. Renou, J.-B. Thibaud, K. Ljung, U. Fischer, E. Martinoia, W. Boerjan, D. Goffner, Arabidopsis WAT1 is a vacuolar auxin transport facilitator required for auxin homoeostasis, Nat. Commun. 4 (2013) 2625.

[257] Z. Yin, H. Jiang, T. Syversen, J.B.T. Rocha, M. Farina, M. Aschner, The methylmercury-l-cysteine conjugate is a substrate for the l-type large neutral amino acid transporter, J. Neurochem. 107 (2008) 1083–1090.

[258] M. Kawano-Kawada, Y. Kakinuma, T. Sekito, Transport of amino acids across the vacuolar membrane of yeast: Its mechanism and physiological role, Biol. Pharm. Bull. 41 (2018) 1496–1501.

[259] V. Kalatzis, S. Cherqui, C. Antignac, B. Gasnier, Cystinosin, the protein defective in cystinosis, is a h(+)-driven lysosomal cystine transporter, EMBO J. 20 (2001) 5940–5949.

[260] Y.-H. Su, W.B. Frommer, U. Ludewig, Molecular and functional characterization of a family of amino acid transporters from arabidopsis, Plant Physiol. 136 (2004) 3104–3113.

[261] H. Yang, M. Krebs, Y.-D. Stierhof, U. Ludewig, Characterization of the putative amino acid transporter genes AtCAT2, 3 & 4: The tonoplast localized AtCAT2 regulates soluble leaf amino acids, J. Plant Physiol. 171 (2014) 594–601.

[262] H.T. Parsons, K. Christiansen, B. Knierim, A. Carroll, J. Ito, T.S. Batth, A.M. Smith-Moritz, S. Morrison, P. McInerney, M.Z. Hadi, M. Auer, A. Mukhopadhyay, C.J. Petzold, H.V. Scheller, D. Loqué, J.L. Heazlewood, Isolation and proteomic characterization of the arabidopsis golgi defines functional and novel components involved in plant cell wall biosynthesis, Plant Physiol. 159 (2012) 12–26.

[263] C. Goto, S. Hashizume, Y. Fukao, I. Hara-Nishimura, K. Tamura, Comprehensive nuclear proteome of arabidopsis obtained by sequential extraction, Nucleus. 10 (2019) 81–92.

[264] M. Grabsztunowicz, A. Rokka, I. Farooq, E.-M. Aro, P. Mulo, Gel-based proteomic map of arabidopsis thaliana root plastids and mitochondria, BMC Plant Biol. 20 (2020) 413.

[265] J.S. Andersen, C.J. Wilkinson, T. Mayor, P. Mortensen, E.A. Nigg, M. Mann, Proteomic characterization of the human centrosome by protein correlation profiling, Nature. 426 (2003) 570–574.

[266] T.P.J. Dunkley, R. Watson, J.L. Griffin, P. Dupree, K.S. Lilley, Localization of organelle proteins by isotope tagging (LOPIT), Mol. Cell. Proteomics. 3 (2004) 1128–1134.

[267] A. Geladaki, N. Kočevar Britovšek, L.M. Breckels, T.S. Smith, O.L. Vennard, C.M. Mulvey, O.M. Crook, L. Gatto, K.S. Lilley, Combining LOPIT with differential ultracentrifugation for high-resolution spatial proteomics, Nat. Commun. 10 (2019) 331.

[268] A.J. Groen, G. Sancho-Andrés, L.M. Breckels, L. Gatto, F. Aniento, K.S. Lilley, Identification of trans-golgi network proteins in arabidopsis thaliana root tissue, J. Proteome Res. 13 (2014) 763–776.

[269] T.P.J. Dunkley, S. Hester, I.P. Shadforth, J. Runions, T. Weimar, S.L. Hanton, J.L. Griffin, C. Bessant, F. Brandizzi, C. Hawes, R.B. Watson, P. Dupree, K.S. Lilley, Mapping the *arabidopsis* organelle proteome, Proc. Natl. Acad. Sci. U. S. A. 103 (2006) 6518–6523.

[270] V. Demichev, C.B. Messner, S.I. Vernardis, K.S. Lilley, M. Ralser, DIA-NN: Neural networks and interference correction enable deep proteome coverage in high throughput, Nat. Methods. 17 (2020) 41–44.

[271] L.M. Breckels, C.M. Mulvey, K.S. Lilley, L. Gatto, A bioconductor workflow for processing and analysing spatial proteomics data, F1000Res. 5 (2016) 2926.

[272] C.M. Hooper, I.R. Castleden, S.K. Tanz, N. Aryamanesh, A.H. Millar, SUBA4: The interactive data analysis centre for arabidopsis subcellular protein locations, Nucleic Acids Res. 45 (2016) D1064–D1074.

[273] Y. Benjamini, Y. Hochberg, Controlling the false discovery rate: A practical and powerful approach to multiple testing, J. R. Stat. Soc. Series B Stat. Methodol. 57 (1995) 289–300.

[274] F. Yu, G.C. Teo, A.T. Kong, K. Fröhlich, G.X. Li, V. Demichev, A.I. Nesvizhskii, Analysis of DIA proteomics data using MSFragger-DIA and FragPipe computational platform, Nat. Commun. 14 (2023) 4154.

[275] T. Galili, Dendextend: An r package for visualizing, adjusting, and comparing trees of hierarchical clustering, Bioinformatics. (2015). https://doi.org/10.1093/bioinformatics/btv428.

[276] J. Chiquet, G. Rigaill, M. Sundqvist, Aricode: Efficient computations of standard clustering comparison measures, 2022. https://CRAN.R-project.org/package=aricode.

[277] A. de Vries, B.D. Ripley, Ggdendro: Create dendrograms and tree diagrams using 'ggplot2', 2022. https://CRAN.R-project.org/package=ggdendro.

[278] D. Hammill, HeatmapR: Create heatmaps using base graphics, 2022. https://github.com/DillonHammill/HeatmapR.

[279] P. Shannon, A. Markiel, O. Ozier, N.S. Baliga, J.T. Wang, D. Ramage, N. Amin, B. Schwikowski, T. Ideker, Cytoscape: A software environment for integrated models of biomolecular interaction networks, Genome Res. 13 (2003) 2498–2504.

[280] M. Utriainen, J.H. Morris, clusterMaker2: A major update to clusterMaker, a multi-algorithm clustering app for cytoscape, BMC Bioinformatics. 24 (2023) 134.

[281] D. Szklarczyk, A.L. Gable, D. Lyon, A. Junge, S. Wyder, J. Huerta-Cepas, M. Simonovic, N.T. Doncheva, J.H. Morris, P. Bork, L.J. Jensen, C. von Mering, STRING v11: Protein-protein association

networks with increased coverage, supporting functional discovery in genome-wide experimental datasets, Nucleic Acids Res. 47 (2019) D607–D613.

[282] S. Van Dongen, Graph clustering via a discrete uncoupling process, SIAM J. Matrix Anal. Appl. 30 (2008) 121–141.

[283] H. Pagès, M. Carlson, S. Falcon, N. Li, AnnotationDbi: Manipulation of SQLite-based annotations in bioconductor, 2023. https://bioconductor.org/packages/AnnotationDbi.

[284] N.T. Doncheva, J.H. Morris, J. Gorodkin, L.J. Jensen, Cytoscape StringApp: Network analysis and visualization of proteomics data, J. Proteome Res. 18 (2019) 623–632.

[285] A. Goyer, E. Collakova, Y. Shachar-Hill, A.D. Hanson, Functional characterization of a methionine gamma-lyase in arabidopsis and its implication in an alternative to the reverse trans-sulfuration pathway, Plant Cell Physiol. 48 (2007) 232–242.

[286] N.G. Dimaano, T. Yamaguchi, K. Fukunishi, T. Tominaga, S. Iwakami, Functional characterization of cytochrome P450 CYP81A subfamily to disclose the pattern of cross-resistance in echinochloa phyllopogon, Plant Mol. Biol. 102 (2020) 403–416.

[287] M. Brazier-Hicks, M. Gershater, D. Dixon, R. Edwards, Substrate specificity and safener inducibility of the plant UDP-glucose-dependent family 1 glycosyltransferase super-family, Plant Biotechnol. J. 16 (2018) 337–348.

[288] S.R. Baerson, A. Sánchez-Moreiras, N. Pedrol-Bonjoch, M. Schulz, I.A. Kagan, A.K. Agarwal, M.J. Reigosa, S.O. Duke, Detoxification and transcriptome response in arabidopsis seedlings exposed to the allelochemical benzoxazolin-2(3H)-one, J. Biol. Chem. 280 (2005) 21867–21881.

[289] C.C. Hansen, D.R. Nelson, B.L. Møller, D. Werck-Reichhart, Plant cytochrome P450 plasticity and evolution, Mol. Plant. 14 (2021) 1244–1265.

[290] A. Baruah, K. Simková, K. Apel, C. Laloi, Arabidopsis mutants reveal multiple singlet oxygen signaling pathways involved in stress response and development, Plant Mol. Biol. 70 (2009) 547–563.

[291] M. Pfalz, H. Vogel, J. Kroymann, The gene controlling the indole glucosinolate modifier1 quantitative trait locus alters indole glucosinolate structures and aphid resistance in arabidopsis, Plant Cell. 21 (2009) 985–999.

[292] T. Griebel, J. Zeier, A role for beta-sitosterol to stigmasterol conversion in plant-pathogen interactions, Plant J. 63 (2010) 254–268.

[293] C. Gabaldón, M. López-Serrano, F. Pomar, F. Merino, J. Cuello, M.A. Pedreño, A.R. Barceló, Characterization of the last step of lignin biosynthesis in zinnia elegans suspension cell cultures, FEBS Lett. 580 (2006) 4311–4316.

[294] J. Herrero, A. Esteban-Carrasco, J.M. Zapata, Looking for arabidopsis thaliana peroxidases involved in lignin biosynthesis, Plant Physiol. Biochem. 67 (2013) 77–86.

[295] E. Remy, T.R. Cabrito, P. Baster, R.A. Batista, M.C. Teixeira, J. Friml, I. Sá-Correia, P. Duque, A major facilitator superfamily transporter plays a dual role in polar auxin transport and drought stress tolerance in arabidopsis, Plant Cell. 25 (2013) 901–926.

[296] V. Yadav, I. Molina, K. Ranathunge, I.Q. Castillo, S.J. Rothstein, J.W. Reed, ABCG transporters are required for suberin and pollen wall extracellular barriers in arabidopsis, Plant Cell. 26 (2014) 3569–3588.

[297] M. Lee, K. Lee, J. Lee, E.W. Noh, Y. Lee, AtPDR12 contributes to lead resistance in arabidopsis, Plant Physiol. 138 (2005) 827–836.

[298] F. Beisson, Y. Li, G. Bonaventure, M. Pollard, J.B. Ohlrogge, The acyltransferase GPAT5 is required for the synthesis of suberin in seed coat and root of arabidopsis, Plant Cell. 19 (2007) 351–368.

[299] A.K. Ghosh, N. Chauhan, S. Rajakumari, G. Daum, R. Rajasekharan, At4g24160, a soluble acyl-coenzyme a-dependent lysophosphatidic acid acyltransferase, Plant Physiol. 151 (2009) 869–881.

[300] K. Ishida, R. Yokoyama, Reconsidering the function of the xyloglucan endotransglucosylase/hydrolase family, J. Plant Res. 135 (2022) 145–156.

[301] K. Ravet, B. Touraine, J. Boucherez, J.-F. Briat, F. Gaymard, F. Cellier, Ferritins control interaction between iron homeostasis and oxidative stress in arabidopsis, Plant J. 57 (2009) 400–412.

[302] V.B. Tognetti, O. Van Aken, K. Morreel, K. Vandenbroucke, B. van de Cotte, I. De Clercq, S. Chiwocha, R. Fenske, E. Prinsen, W. Boerjan, B. Genty, K.A. Stubbs, D. Inzé, F. Van Breusegem, Perturbation of Indole-3-Butyric acid homeostasis by the UDP-Glucosyltransferase UGT74E2 modulates arabidopsis architecture and water stress tolerance, Plant Cell. 22 (2012) 2660–2679.

[303] J. Pedreira, M.T. Herrera, I. Zarra, G. Revilla, The overexpression of AtPrx37, an apoplastic peroxidase, reduces growth in arabidopsis, Physiol. Plant. 141 (2011) 177–187.

[304] L. Zhang, R. Kawaguchi, T. Morikawa-Ichinose, A. Allahham, S.-J. Kim, A. Maruyama-Nakashita, Sulfur Deficiency-Induced glucosinolate catabolism attributed to two $\beta$-Glucosidases, BGLU28 and BGLU30, is required for plant growth maintenance under sulfur deficiency, Plant Cell Physiol. 61 (2020) 803–813.

[305] J. Smirle, C.E. Au, M. Jain, K. Dejgaard, T. Nilsson, J. Bergeron, Cell biology of the endoplasmic reticulum and the golgi apparatus through proteomics, Cold Spring Harb. Perspect. Biol. 5 (2013) a015073.

[306] L. Gatto, L.M. Breckels, K.S. Lilley, Assessing sub-cellular resolution in spatial proteomics experiments, Curr. Opin. Chem. Biol. 48 (2019) 123–149.

[307] J.C. Hernández-Vega, B. Cady, G. Kayanja, A. Mauriello, N. Cervantes, A. Gillespie, L. Lavia, J. Trujillo, M. Alkio, A. Colón-Carmona, Detoxification of polycyclic aromatic hydrocarbons (PAHs) in arabidopsis thaliana involves a putative flavonol synthase, J. Hazard. Mater. 321 (2017) 268–280.

[308] E. Smirnova, V. Marquis, L. Poirier, Y. Aubert, J. Zumsteg, R. Ménard, L. Miesch, T. Heitz, Jasmonic acid oxidase 2 hydroxylates jasmonic acid and represses basal defense and resistance responses against botrytis cinerea infection, Mol. Plant. 10 (2017) 1159–1173.

[309] G. Adamia, M. Ghoghoberidze, D. Graves, G. Khatisashvili, G. Kvesitadze, E. Lomidze, D. Ugrekhelidze, G. Zaalishvili, Absorption, distribution, and transformation of TNT in higher plants, Ecotoxicol. Environ. Saf. 64 (2006) 136–145.

[310] C.-H. Kong, T.D. Xuan, T.D. Khanh, H.-D. Tran, N.T. Trung, Allelochemicals and signaling chemicals in plants, Molecules. 24 (2019).

[311] T.R. Cabrito, M.C. Teixeira, A.A. Duarte, P. Duque, I. Sá-Correia, Heterologous expression of a Tpo1 homolog from arabidopsis thaliana confers resistance to the herbicide 2,4-d and other chemical stresses in yeast, Appl. Microbiol. Biotechnol. 84 (2009) 927–936.

[312] C. Simon, M. Langlois-Meurinne, L. Didierlaurent, S. Chaouch, F. Bellvert, K. Massoud, M. Garmier, V. Thareau, G. Comte, G. Noctor, P. Saindrenan, The secondary metabolism

glycosyltransferases UGT73B3 and UGT73B5 are components of redox status in resistance of arabidopsis to pseudomonas syringae pv. tomato, Plant Cell Environ. 37 (2014) 1114–1129.

[313] G. Liu, R. Sánchez-Fernández, Z.S. Li, P.A. Rea, Enhanced multispecificity of arabidopsis vacuolar multidrug resistance-associated protein-type ATP-binding cassette transporter, AtMRP2, J. Biol. Chem. 276 (2001) 8648–8656.

[314] B.R. Khan, D.J. Wherritt, D. Huhman, L.W. Sumner, K.D. Chapman, E.B. Blancaflor, Malonylation of glucosylated N-Lauroylethanolamine a NEW PATHWAY THAT DETERMINES N-ACYLETHANOLAMINE METABOLIC FATE IN PLANTS*, J. Biol. Chem. 291 (2016) 27112–27121.

[315] S. Kambhampati, A. Pajak, F. Marsolais, Evidence that class I glutamine amidotransferase, GAT1_2.1, acts as a glutaminase in roots of arabidopsis thaliana, Plant Sci. 312 (2021) 111033.

[316] M. Del Carmen Martínez-Ballesta, D.A. Moreno, M. Carvajal, The physiological importance of glucosinolates on plant response to abiotic stress in brassica, Int. J. Mol. Sci. 14 (2013) 11607–11625.

[317] R. Sugiyama, R. Li, A. Kuwahara, R. Nakabayashi, N. Sotta, T. Mori, T. Ito, N. Ohkama-Ohtsu, T. Fujiwara, K. Saito, R.T. Nakano, P. Bednarek, M.Y. Hirai, Retrograde sulfur flow from glucosinolates to cysteine in *arabidopsis thaliana*, Proc. Natl. Acad. Sci. U. S. A. 118 (2021).

[318] L. Zhang, R. Kawaguchi, T. Enomoto, S. Nishida, M. Burow, A. Maruyama-Nakashita, Glucosinolate catabolism maintains glucosinolate profiles and transport in sulfur-starved arabidopsis, Plant Cell Physiol. (2023).

[319] M. Barberon, The endodermis as a checkpoint for nutrients, New Phytol. 213 (2017) 1604–1610.

[320] D. Líška, M. Martinka, J. Kohanová, A. Lux, Asymmetrical development of root endodermis and exodermis in reaction to abiotic stresses, Ann. Bot. 118 (2016) 667–674.

[321] H. Le Gall, F. Philippe, J.-M. Domon, F. Gillet, J. Pelloux, C. Rayon, Cell wall metabolism in response to abiotic stress, Plants. 4 (2015) 112–166.

[322] M.M. Purugganan, J. Braam, S.C. Fry, The arabidopsis TCH4 xyloglucan endotransglycosylase. Substrate specificity, pH optimum, and cold tolerance, Plant Physiol. 115 (1997) 181–190.

[323] P. Xu, S. Fang, H. Chen, W. Cai, The brassinosteroid-responsive xyloglucan endotransglucosylase/hydrolase 19 (XTH19) and XTH23 genes are involved in lateral root development under salt stress in arabidopsis, Plant J. 104 (2020) 59–75.

[324] F.M. Mitton, M. Gonzalez, J.M. Monserrat, K.S.B. Miglioranza, DDTs-induced antioxidant responses in plants and their influence on phytoremediation process, Ecotoxicol. Environ. Saf. 147 (2018) 151–156.

[325] P. Panpetch, S. Sirikantaramas, Fruit ripening-associated leucylaminopeptidase with cysteinylglycine dipeptidase activity from durian suggests its involvement in glutathione recycling, BMC Plant Biol. 21 (2021) 69.

[326] T. Shimaoka, M. Ohnishi, T. Sazuka, N. Mitsuhashi, I. Hara-Nishimura, K.-I. Shimazaki, M. Maeshima, A. Yokota, K.-I. Tomizawa, T. Mimura, Isolation of intact vacuoles and proteomic analysis of tonoplast from suspension-cultured cells of arabidopsis thaliana, Plant Cell Physiol. 45 (2004) 672–683.

[327] R. Waditee-Sirisattha, J. Shibato, R. Rakwal, S. Sirisattha, A. Hattori, T. Nakano, T. Takabe, M. Tsujimoto, The arabidopsis aminopeptidase LAP2 regulates plant growth, leaf longevity and stress response, New Phytol. 191 (2011) 958–969.

[328] B. Paulose, S. Chhikara, J. Coomey, H.-I. Jung, O. Vatamaniuk, O.P. Dhankher, A $\gamma$-glutamyl cyclotransferase protects arabidopsis plants from heavy metal toxicity by recycling glutamate to maintain glutathione homeostasis, Plant Cell. 25 (2013) 4580–4595.

[329] Y. Fujiki, H. Teshima, S. Kashiwao, M. Kawano-Kawada, Y. Ohsumi, Y. Kakinuma, T. Sekito, Functional identification of AtAVT3, a family of vacuolar amino acid transporters, in arabidopsis, FEBS Lett. 591 (2017) 5–15.

[330] M.D. Mikkelsen, P. Naur, B.A. Halkier, Arabidopsis mutants in the C-S lyase of glucosinolate biosynthesis establish a critical role for indole-3-acetaldoxime in auxin homeostasis, Plant J. 37 (2004) 770–777.

[331] C.D. Grubb, B.J. Zipp, J. Ludwig-Müller, M.N. Masuno, T.F. Molinski, S. Abel, Arabidopsis glucosyltransferase UGT74B1 functions in glucosinolate biosynthesis and auxin homeostasis, Plant J. 40 (2004) 893–908.

[332] M. Bouzayen, A. Latché, G. Alibert, J.C. Pech, Intracellular sites of synthesis and storage of 1-(Malonylamino)cyclopropane-1-Carboxylic acid in acer pseudoplatanus cells, Plant Physiol. 88 (1988) 613–617.

[333] R. de Brito Francisco, E. Martinoia, The vacuolar transportome of plant specialized metabolites, Plant Cell Physiol. 59 (2018) 1326–1336.

[334] C.E. Behrens, K.E. Smith, C.V. Iancu, J.-Y. Choe, J.V. Dean, Transport of anthocyanins and other flavonoids by the arabidopsis ATP-Binding cassette transporter AtABCC2, Sci. Rep. 9 (2019) 437.

[335] J.V. Dean, M. Willis, L. Shaban, Transport of acylated anthocyanins by the arabidopsis ATP-binding cassette transporters AtABCC1, AtABCC2, and AtABCC14, Physiol. Plant. 174 (2022) e13780.

[336] C. Feung, R.H. Hamilton, R.O. Mumma, Metabolism of 2,4-dichlorophenoxyacetic acid. V. Identification of metabolites in soybean callus tissue cultures, J. Agric. Food Chem. 21 (1973) 637–640.

[337] S. Tophof, E. Martinoia, G. Kaiser, W. Hartung, N. Amrhein, Compartmentation and transport of 1-aminocyclopropane-1-carboxylic acid and n-malonyl-1-aminocyclopropane-1-carboxylic acid in barley and wheat mesophyll cells and protoplasts, Physiol. Plant. 75 (1989) 333–339.

[338] R.M. Kosslak, R. Bookland, J. Barkei, H.E. Paaren, E.R. Appelbaum, Induction of bradyrhizobium japonicum common nod genes by isoflavones isolated from glycine max, Proc. Natl. Acad. Sci. U. S. A. 84 (1987) 7428–7432.

[339] U. Mackenbrock, W. Barz, Elicitor-Induced formation of pterocarpan phytoalexins in chickpea (cicer arietinum l.) cell suspension cultures from constitutive isoflavone conjugates upon inhibition of phenylalanine ammonia lyase, Zeitschrift für Naturforschung C. 46 (1991) 43–50.

[340] U. Mackenbrock, R. Vogelsang, W. Barz, Isoflavone and pterocarpan malonylglucosides and ß - l,3 - glucan - and Chitin-Hydrolases are vacuolar constituents in chickpea (cicer arietinum l.), Zeitschrift für Naturforschung C. 47 (1992) 815–822.

[341] C.C. Akoh, G.-C. Lee, Y.-C. Liaw, T.-H. Huang, J.-F. Shaw, GDSL family of serine esterases/lipases, Prog. Lipid Res. 43 (2004) 534–552.

[342] C. Carter, S. Pan, J. Zouhar, E.L. Avila, T. Girke, N.V. Raikhel, The vegetative vacuole proteome of arabidopsis thaliana reveals predicted and unexpected proteins, Plant Cell. 16 (2004) 3285–3303.

[343] H.-K. Kwon, R. Yokoyama, K. Nishitani, A proteomic approach to apoplastic proteins involved in cell wall regeneration in protoplasts of arabidopsis suspension-cultured cells, Plant Cell Physiol. 46 (2005) 843–857.

[344] A.P. Bowman, J.F.J. Bogie, J.J.A. Hendriks, M. Haidar, M. Belov, R.M.A. Heeren, S.R. Ellis, Evaluation of lipid coverage and high spatial resolution MALDI-imaging capabilities of oversampling combined with laser post-ionisation, Anal. Bioanal. Chem. 412 (2020) 2277–2289.

[345] Y. Meng, X. Cheng, T. Wang, W. Hang, X. Li, W. Nie, R. Liu, Z. Lin, L. Hang, Z. Yin, B. Zhang, X. Yan, Micro-Lensed fiber laser desorption mass spectrometry imaging reveals subcellular distribution of drugs within single cells, Angew. Chem. Int. Ed Engl. 59 (2020) 17864–17871.

[346] Y. Meng, W. Hang, R.N. Zare, Microlensed fiber allows subcellular imaging by laser-based mass spectrometry, Nat. Protoc. (2023).

[347] R. Tartivel, R. Tatin, T. Delhaye, A. Maupas, A. Gendron, S. Gautier, O. Lavastre, Visualization and localization of bromotoluene distribution in hedera helix using NanoSIMS, Chemosphere. 89 (2012) 805–809.

[348] P.L. Thompson, L.A. Ramer, J.L. Schnoor, Uptake and transformation of TNT by hybrid poplar trees, Environ. Sci. Technol. 32 (1998) 975–980.

[349] P. Das, R. Datta, K.C. Makris, D. Sarkar, Vetiver grass is capable of removing TNT from soil in the presence of urea, Environ. Pollut. 158 (2010) 1980–1983.

[350] L.B. Brentner, S.T. Mukherji, K.M. Merchie, J.M. Yoon, J.L. Schnoor, B. Van Aken, Expression of glutathione s-transferases in poplar trees (populus trichocarpa) exposed to 2,4,6-trinitrotoluene (TNT), Chemosphere. 73 (2008) 657–662.

[351] Y. Musdal, B. Mannervik, Substrate specificities of two tau class glutathione transferases inducible by 2,4,6-trinitrotoluene in poplar, Biochimica Et Biophysica Acta (BBA) - General Subjects. 1850 (2015) 1877–1883.

[352] K. Su, Z. Wu, Y. Liu, S. Jiang, D. Ma, Y. Wang, C. Fu, Highly efficient detoxification of dinitrotoluene by transgenic switchgrass overexpressing bacterial nitroreductase, Plant Cell Environ. 44 (2021) 3173–3183.

[353] J. Pichtel, Distribution and fate of military explosives and propellants in soil: A review, Applied and Environmental Soil Science. 2012 (2012).

[354] G. Gullner, T. Kömives, H. Rennenberg, Enhanced tolerance of transgenic poplar plants overexpressing gamma-glutamylcysteine synthetase towards chloroacetanilide herbicides, J. Exp. Bot. 52 (2001) 971–979.

[355] J. Andres, T. Blomeier, M.D. Zurbriggen, Synthetic switches and regulatory circuits in plants, Plant Physiol. 179 (2019) 862–884.

[356] L. Lombardo, Genetic use restriction technologies: A review, Plant Biotechnol. J. 12 (2014) 995–1005.

[357] S. Evanega, J. Conrow, J. Adams, M. Lynas, The state of the 'GMO' debate - toward an increasingly favorable and less polarized media conversation on ag-biotech?, GM Crops Food. 13 (2022) 38–49.